National Research Council Canada
Conseil national de recherches Canada

ASSOCIATE COMMITTEE ON GEOTECHNICAL RESEARCH

PROCEEDINGS OF WORKSHOP ON THE BEARING CAPACITY OF ICE COVERS 16-17 OCTOBER 1978 WINNIPEG, MANITOBA

COMPILED BY R. FREDERKING

SPONSORED BY

SNOW AND ICE SUBCOMMITTEE
ASSOCIATE COMMITTEE ON GEOTECHNICAL RESEARCH

TECHNICAL MEMORANDUM NO. 123

MAY 1979

PRICE: $3.50

The Associate Committee on Geotechnical Research is one of about thirty special committees which assist the National Research Council in its work. Formed in 1945 to deal with an urgent wartime problem involving soil and snow, the Committee is now performing its intended task of coordinating Canadian research studies concerned with the physical and mechanical properties of Snow and Ice, Muskeg, Permafrost, Urban Engineering Terrain Problems and Soil and Rock Engineering. The Committee consists of about twenty Canadians appointed as individuals and not as representatives, each for a three-year term. Enquiries will be welcomed and should be addressed to: The Secretary, Associate Committee on Geotechnical Research, c/o Division of Building Research, National Research Council of Canada, Ottawa K1A 0R6.

****

Le Comité associé de recherches géotechniques est l'un des quelque trente comités spéciaux qui assistent le Conseil national de recherches dans ses fonctions. Créé en 1945 pour s'occuper de problèmes ayant trait aux sols et à la neige et urgents par suite de la guerre, le Comité remplit maintenant le rôle qui lui était destiné, celui de coordonner au Canada les recherches portant sur les propriétes physiques et mécaniques du sol canadien. Il s'acquitte de ses fonctions par l'intermédiaire des sous-comités de la neige et de la glace, des marécages, du pergélisol, des problèmes l'ingénierie urbaine relatifs au terrain et de génie du sol et des roches. Le Comité se compose d'environ vingt canadiens nommés à titre individuel, et répondrons avec plaisir à vos demandes de renseignement. Veuillez les adresser à:

Le Secrétaire,
Comité associé de recherches
géotechniques,
a/s Division des recherches sur le
bâtiment,
Conseil national de recherches,
Ottawa K1A 0R6.

17.50

NATIONAL RESEARCH COUNCIL OF CANADA
ASSOCIATE COMMITTEE ON GEOTECHNICAL RESEARCH

WORKSHOP ON THE BEARING CAPACITY OF ICE COVERS
16-17 OCTOBER 1978
WINNIPEG, MANITOBA

SPONSORED BY

SNOW AND ICE SUBCOMMITTEE
ASSOCIATE COMMITTEE ON GEOTECHNICAL RESEARCH

TECHNICAL MEMORANDUM NO. 123

MAY 1979

FOREWORD

The bearing capacity of ice covers has been a problem of continuing concern in Canada and now, with the heightened interest in resource exploration and development in the Arctic, the use of ice covers is being given increased attention. The last symposium of the Associate Committee on Geotechnical Research that dealt exclusively with the bearing capacity problem was held in Ottawa in 1958. That there have been important developments since that time is clear from this record of a Workshop on this subject held in Winnipeg in October 1978.

The Associate Committee wishes to express its appreciation to the authors, discussors, technical chairmen, rapporteurs, and all others who participated in the Workshop. It wishes to thank especially Dr. K. Adam and his colleagues for looking after the local arrangements; Mrs. J. Curran, Secretary of the Subcommittee, for her assistance to Dr. Frederking in the preparation of this Technical Memorandum; and the Snow and Ice Subcommittee for its initiative in organizing this review of an important Canadian problem in applied glaciology.

Lorne W. Gold,
Chairman,
Associate Committee on
Geotechnical Research.

OPENING REMARKS

On behalf of the Snow and Ice Subcommittee, I would like to welcome you to this Workshop on the Bearing Capacity of Ice Covers. I am pleased to see such a distinguished group of participants present here today. Your presence augers well for the quality and usefulness of the Workshop.

Many of you were also active participants in our last Workshop held in Calgary about 20 months ago. That Workshop was, of course, concerned with ice properties. In many ways, this Workshop on Ice Bearing Capacity is more specialized than the last. Despite some of our individual inclinations, discussions on ice forces will have no place in this Workshop, except perhaps informally. Here we are closeting ourselves away for a day and a half to talk solely about ice bearing capacity, i.e., the theory and practice of standing on, and moving over, an ice sheet.

I must confess that I admire the experts in this field. These people are indeed true entrepreneurs because, in contrast to the experts on ice forces, they have recognized the universal truth of the 2nd Ice Law, which states "Don't fight the ice, make use of it".

There is no doubt that one of the most daring and exciting uses of ice to support loads has been developed here in Canada, during the last decade, by some of the people present here today.

I am, of course, talking about the use of ice as a platform to support equipment for petroleum exploration offshore in the Arctic. This application has led to considerable interest and progress in the topic of long-term stresses in an ice sheet, a topic which I know we are going to cover at length during the Workshop. I should also add that the technique probably represents the only economic way of exploring for potential petroleum resources in the deep water high-Arctic regions of Canada.

The Snow and Ice Subcommittee, which is sponsoring this Workshop, is a Subcommittee of the Associate Committee on Geotechnical Research of the National Research Council and this, of course, is Geotechnical Week in Winnipeg, with the Annual Meeting of the Canadian Geotechnical Society taking place later.

For those of you not familiar with the National Research Council, I should point out that the Associate Committee on Geotechnical Research is one of about 25 technical committees which assist the National Research Council in the coordination of scientific research in Canada. The goals of the Subcommittees of the Associate Committee were established "to define problem areas in their assigned field, advise the Associate Committee on research needs, promote research, and assist in the publication and application of the results of research".

Within the Associate Committee on Geotechnical Research, there are Subcommittees on:

- Soil and Rock Engineering
- Muskeg
- Permafrost
- Urban Terrain, and
- Snow and Ice

The use of Workshops with invited experts has long been a method used by this Subcommittee to advance its goals. We intend to continue with these Workshops about once every 18 months and suggestions for future workshop topics would be welcomed.

Although they are Canadian events, these Workshops have traditionally been open to participants from any country. At this Workshop, there are people from the United States and the United Kingdom, to whom I extend a hearty welcome.

Today's Workshop has largely been organized by Bob Frederking and Ken Adam and for this I would like to thank them in advance.

K.R. Croasdale,
Chairman,
Snow and Ice Subcommittee

TABLE OF CONTENTS

FIELD STUDIES ON THE RESPONSE OF FLOATING ICE SHEETS TO MOVING LOADS*

S. Beltaos**
Alberta Research Council

Introduction

Under certain conditions of speed, ice thickness and water depth, the deflection under a vehicle travelling on a floating ice sheet may be amplified considerably. As suggested by Wilson (1955) and Nevel (1970), this effect is caused by a type of resonance between the structural deformation of the ice sheet and the water wave instigated by the motion of the load.

Even though this phenomenon has already been studied theoretically (Wilson, 1955; Nevel, 1970) very little experimental documentation has been obtained. Wilson (1955) presented the results of a few series of field tests with moving loads and proposed an approximate theory for predicting the critical vehicle speed, i.e. the speed at which the amplification of ice deflection is maximized. Anderson (1958) presented the results of four test runs on an ice sheet 1.37 m thick; the water depth was 15.2 m. A theoretical equation for computing the critical speed, u_c, was proposed by Assur (1961). Recently, Eyre (1977) presented experimental results on the response of a 0.5 - 0.7 m thick ice sheet, floating on a 36.4 m deep lake.

Perhaps much of the scarcity of experimental data on the problem of moving loads has been due to a lack of convenient means for measuring ice deflection-time variations at a point. The conventional deflectometers require reference to a fixed datum, usually a river or lake bed, and are thus cumbersome; occasionally they may be inaccurate as the readings can be significantly affected by minute water motions.

A deflectometer not requiring reference to a fixed datum has been developed by Eyre (1977). This is simply a pressure transducer mounted 0.3 m below the bottom of the ice

---

*Alberta Research Council, Contribution Series 938

**See List of Participants for Affiliation.

in a tube attached rigidly to the ice sheet. The response of this deflectometer includes water wave pressures in addition to purely hydrostatic effects that reflect the ice deflection. Eyre carried out a theoretical analysis which can be used to separate these effects and determine ice deflection. However, this analysis is only an approximation as it assumes a sinusoidal wave form of constant amplitude for the time-dependent deflection of the ice at a fixed point.

A research program to investigate the load bearing capacity of floating ice sheets was initiated by the Transportation and Surface Water Engineering Division of the Alberta Research Council in 1974. The results of this research to date, pertinent to moving loads, are presented briefly herein.

Experimental Procedures

To avoid some of the problems associated with conventional deflectometers, a simple deflection measurement technique has been developed; this technique is based on integration of the response of a sensitive slope transducer and does not require reference to a fixed datum.

Consider a load moving at a constant speed, u, on a floating ice sheet. If the ice sheet is sufficiently large, it can be assumed that, sometime after the beginning of motion, the ice deflection pattern caused by the load does not change in time when viewed from the load and moves along at the same speed as the load. [This assumption was adopted by Nevel (1970) and has been verified experimentally by Eyre (1977).] A slope transducer placed at a fixed point in the path of the load will record the maximum slope of the deflection pattern as a function of time. Since the slope is the gradient of the deflection form which moves past the measuring station at the constant speed, u, one could write:

$$s(t) = \frac{dw(t)}{dx} = \frac{1}{u}\frac{dw(t)}{dt} \qquad (1)$$

where s(t) is the slope recorded at time t, w(t) is the ice deflection at the time t, and x is distance measured along the direction of movement. Integrating (1) gives:

$$w(t) = u\int_{-\infty}^{t} s(t)\,dt \qquad (2)$$

Using (2) the time-deflection variation at the measuring station can be calculated if s(t) and u are measured.

For measuring the slope-time variation at a fixed point of the ice sheet, a sensitive slope indicator was utilized in conjunction with a dual channel oscillographic recorder, as shown schematically in Fig. 1. Vehicle speed was computed using fix marks established on the recorder chart and denoting the instances when the vehicle crossed the corresponding marks on the ice shown in Fig. 1. The time elapsed between such fixes was computed using the speed of the recorder chart. For any given runway, the slope-time variation was recorded for several vehicle passes so as to cover a range of speeds extending from about 4 km/h to well above the anticipated critical speed.

To test the feasibility of the slope integrating method, a series of preliminary runs were carried out at Joseph Lake which is a shallow lake located some 60 km south-east of Edmonton. Figure 2 shows ice deflection as calculated by integrating the recorded slope-time variations, plotted versus corresponding deflections measured directly[1]. Despite the considerable scatter indicated by the data points in Fig. 2, a linear relation seems to be reasonably well defined. The straight line drawn through the data points in Fig. 2 has the equation:

$$w \simeq 1.43\, w_S \qquad (3)$$

in which w is the true ice deflection and w_S the deflection determined by the slope integrating method. Ideally, (3) should read $w = w_S$. The discrepancy is thought to be due to errors in the original calibration of the transducer.

The scatter shown in Fig. 2 is attributed to errors associated with both the direct measurement of deflections smaller than 20 mm and the integration of the slope-time record. This integration was carried out manually and could thus be significantly affected by slight drift of the "zero slope" line or even by the finite thickness of the recorder pen trace. The experimental results reported herein are subject to such errors as they were based entirely on manual integration. At present, a more elaborate instrument is being built which involves integration of the slope signal prior to recording.

Experimental Results

Tests with moving loads have been carried out at Joseph Lake and Cold Lake; the latter is a large lake located on

---

[1] i.e., by observing the movement of the ice surface relative to a rod embedded in the lake bottom through a hole cut in the ice.

the Alberta-Saskatchewan boundary. These test covered a range of water depths between 2 m and 54 m. Essentially, two values of ice thickness have been tested, 0.4 m and 0.6 m.

Figure 3 shows deflection-time variations from a test series at Cold Lake. The deflection patterns can be seen to exhibit the following general trends:

i) at low vehicle speeds ($u \lesssim 0.8\ u_c$) the deflection bowl is similar to that generated by a stationary load. The bottom of the ice depression is directly under the load.

ii) at speeds near the critical speed ($u \sim u_c$) the deflection pattern becomes asymmetrical; the bottom of the depression is still located under the vehicle which, however, is now preceded by a noticeable "hump".

iii) with further increase in speed ($u \gtrsim 1.2\ u_c$) several "humps" appear in front of the vehicle, which now seems to move forward relative to the bottom of the depression. The amplitude of the deflection pattern decreases rapidly.

Integration errors are illustrated in Fig. 3 by the facts that occasionally the deflection does not seem to return to zero values at the end of a pass, and that increasing speeds seem to introduce irregularity in the observed deflection patterns. These effects are caused by increased percent errors of integration as the number of deflection "waves" increases and their amplitude decreases.

Figure 4 shows typical variations of maxium positive (downwards) deflection with vehicle speed, which demonstrate the existence of a critical speed and can be used to determine its value. If the deflection w is divided by the static deflection w_o, the experimental results can be summarized in one graph by plotting w/w_o versus u/u_c. This is illustrated in Fig. 5. The data are seen to be in fair agreement with Nevel's theoretical curve in the range $0 < u/u_c < 1.0$, but not for $u/u_c > 1.0$. This is reasonable, since the water velocity head which has been neglected by Nevel becomes more important as the vehicle speed increases.

Since the configuration of the deflection bowl changes with vehicle speed, it was thought that the amplification of the deflection may not be truly representative of the stresses generated in the ice sheet. For this reason, an attempt was made to measure the strain response by placing ordinary strain gauges near the top of the ice. These were frozen in the ice sheet about 20 mm below the surface, and connected to the second

channel of the recorder. This approach was only partially successful as the strain gauges did not seem to have been always adequately embedded in the ice sheet. Figure 6 shows maximum compressive and tensile strains plotted versus vehicle speed. Because of the substantial experimental scatter indicated in Fig. 6, the lines drawn roughly through the data points have little significance and determination of critical strain speeds is difficult. Corresponding critical speeds determined from deflection measurements are also indicated in Fig. 6 and seem to be in the neighbourhood of maximum strain. It is noted that the critical amplification of strain is not as severe as that of deflection (see also Fig. 5). This is in qualitative agreement with Nevel's theory (1970) which shows the amplification of stress to be generally lower than that of deflection[2]. Noteworthy in Fig. 6 is the behaviour of the tensile strain which seems to have a maximum well past the critical speed. The magnitude of this maximum is comparable to that of the corresponding compressive strain.

A summary of the present test results, together with published data, is presented in Table 1. The observed critical speeds are, on the average, 10 percent higher than those predicted using Nevel's (1970) theory. The critical amplification factor ranges from 1.4 to 4.6 for deflection and is about 1.4 for strain.

Discussion and Summary

The results presented herein, together with published data, give strong support to Nevel's theory concerning the response of floating ice sheets to moving loads. The available data cover a range of ice thickness between 0.28 and 1.37 m and a range of water depths between 1.8 and 54.3 m. It is noted, however, that the theory predicts an infinite critical amplification; this is in contrast with observation and the discrepancy is perhaps due to ignoring the viscosity of water in the theoretical calculation. Despite this shortcoming, it is felt that the theory could be employed profitably to study more complex problems, such as accelerated motions or effects of shoreline proximity and orientation. The latter effect is perhaps reflected by the fact that Wilson's second run (Table 1) resulted in a critical speed somewhat less than predicted, contrary to the trend exhibited by the other data.

---

[2]It is implicitly assumed that the response of the ice sheet is mostly elastic and strain is proportional to stress.

A satisfactory method for measuring the time-dependent deflection caused by a moving load, which does not require reference to a fixed datum, has been outlined. This method is based on integrating the output of a sensitive slope transducer and can be applied when the ice deflection bowl moves at constant speed. A refinement of this method is presently under way to perform the integration prior to recording.

Acknowledgments

The work presented herein is a part of a continuing research program on the load bearing capacity of floating ice sheets; this program is carried out by the Transportation and Surface Water Engineering Division of the Alberta Research Council, in cooperation with Alberta Transportation under the auspices of the Alberta Cooperative Research Program in Transportation and Surface Water Engineering.

All electronics work associated with making operational the slope transducer mentioned in this paper has been carried out by L. Chizawsky. The field tests quoted herein could not have been performed without the assistance of M. Anderson, D. McBeth, G. Childs, K. Nordin, G. Putz and J. Thompson. D. Szabo performed most of the calculations involved in integrating the slope records and determining deflection-time variations. A.W. Lipsett and B.P. Shields reviewed a draft of the manuscript. Occasional discussion with Dr. D.E. Nevel of Cold Regions Research and Engineering Laboratory is appreciated.

References

Assur, A. (1961). Traffic over frozen or crusted surfaces. Proceedings of International Conference on the Mechanics of Soil Vehicle Systems, Torino-Saint Vincent, pp. 913-923.

Anderson, D.L. (1958). Preliminary results and review of sea ice elasticity and related studies. Proceedings of Symposium on the Bearing Strength of Ice, Technical Memorandum No. 56, National Research Council of Canada, pp. 116-122.

Eyre, D. (1977). The flexural motions of a floating ice sheet induced by moving vehicles. Journal of Glaciology, Vol. 19, No. 81, pp. 555-570.

Nevel, D.E. (1970). Moving loads on a floating ice sheet. Research Report 261, United States Army Corps of Engineers, Cold Regions Research and Engineering Laboratory.

Wilson, J.T. (1955). Coupling between moving loads and flexural waves in floating ice sheets. Report 34, Snow Ice and Permafrost Establishment, United States Army Corps of Engineers.

Table 1. Summary of moving load data

Source	ice thickness (m)	water depth (m)	observed critical speed (m/s)	predicted critical speed[1] (m/s)	amplification at crit. speed for: deflection	total height[2]	strain	Comments
Wilson (1955)	0.61	3.0	6.3	5.5	1.8	2.5	-	-
	0.28	3.5	5.7	5.9	1.4	2.1	-	motion parallel to, & 60 m off, shore
Anderson (1958)	1.37	15.2	14.4	12.2	4.6	-	-	approximate
Eyre (1977)	0.72	36.4 (avg)	≈14.9	13.7	2.1	-	-	-
Writer, Joseph Lake	0.66	1.8	4.9	4.3	2.1	2.3	-	average of two runs 12 & 18 Feb. 1976
	0.37	2.0	4.9	4.5	2.1	3.1	≈1.4	21 Dec. 1976
Writer, Cold Lake 1&2 Feb., 1977	0.59	4.3	7.3	6.4	1.9	2.4	-	obs'd critical speed not as reliable as above
	0.65	11.6	11.0	10.5	1.9	2.5	≈1.4	
	0.64	27.1	13.7	12.9	2.3	3.3	-	
	0.65	54.3	15.2	13.3	2.1	2.3	≈1.4	

[1] using Nevel's theory (1970)

[2] sum of absolute values of max. downward and max. upward deflections

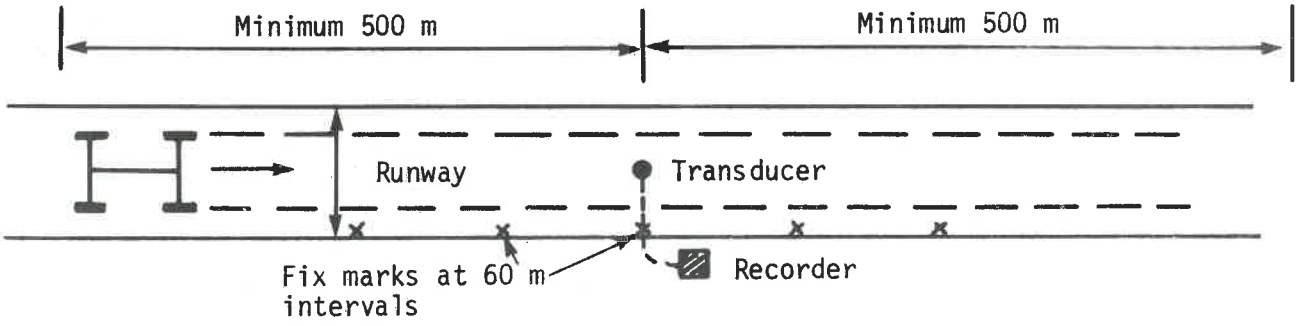

FIG. 1. Plan view of test arrangement

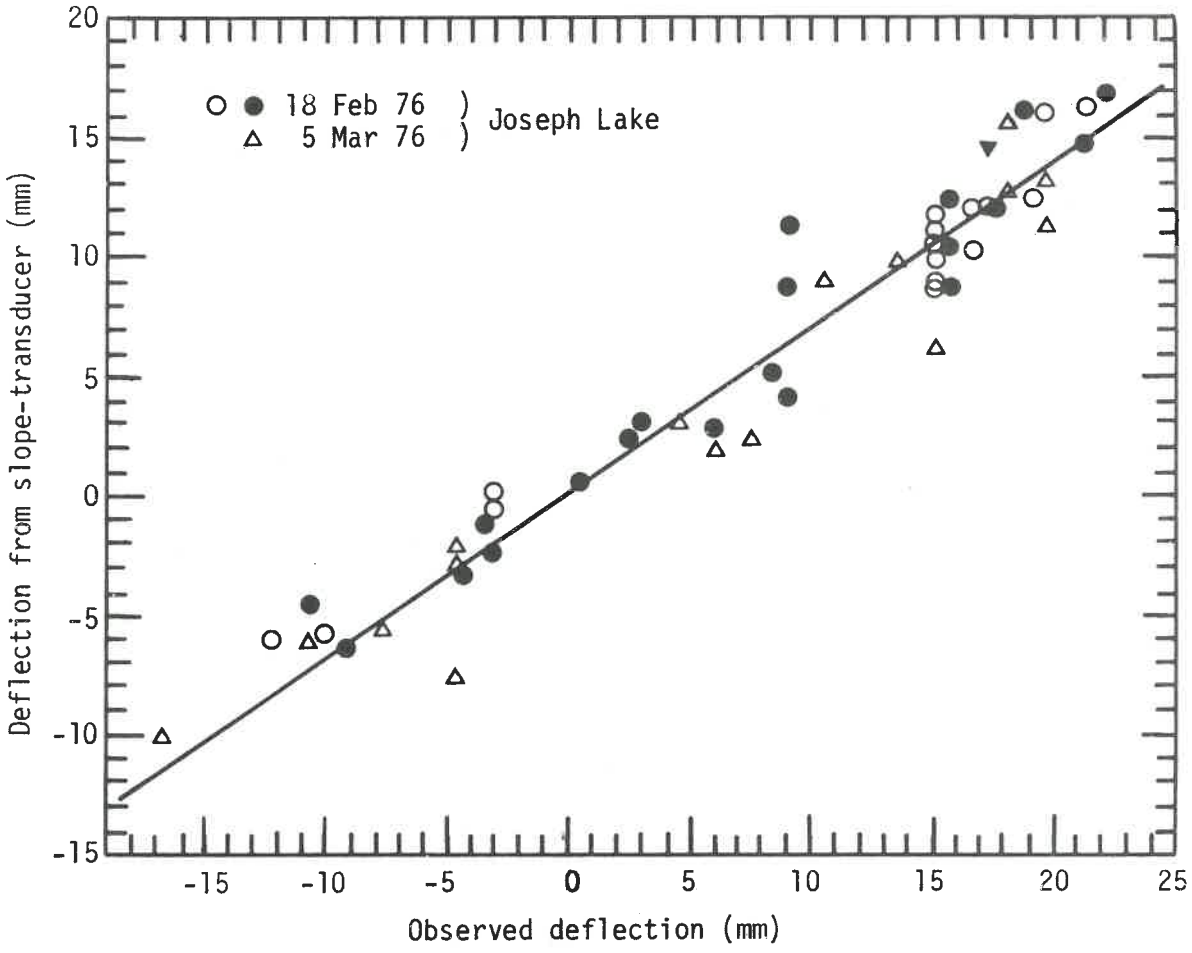

FIG. 2. Deflection from slope integrating method versus deflection measured directly

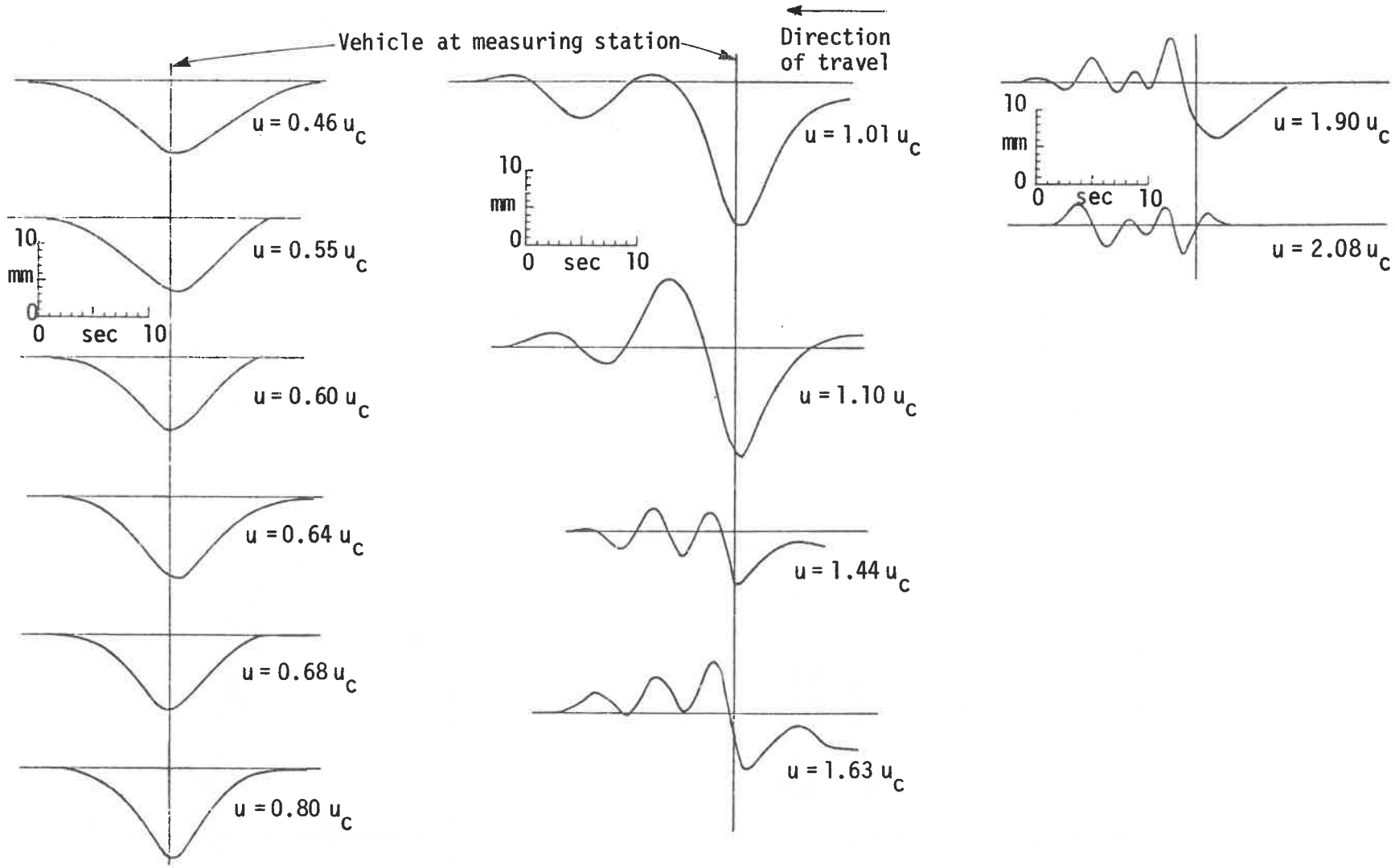

FIG. 3. Deflection-time variations at different vehicle speeds; Cold Lake, 1 Feb. 1976; Ice thickness = 0.59 m, water depth = 4.3 m, u_c = 7.3 m/s

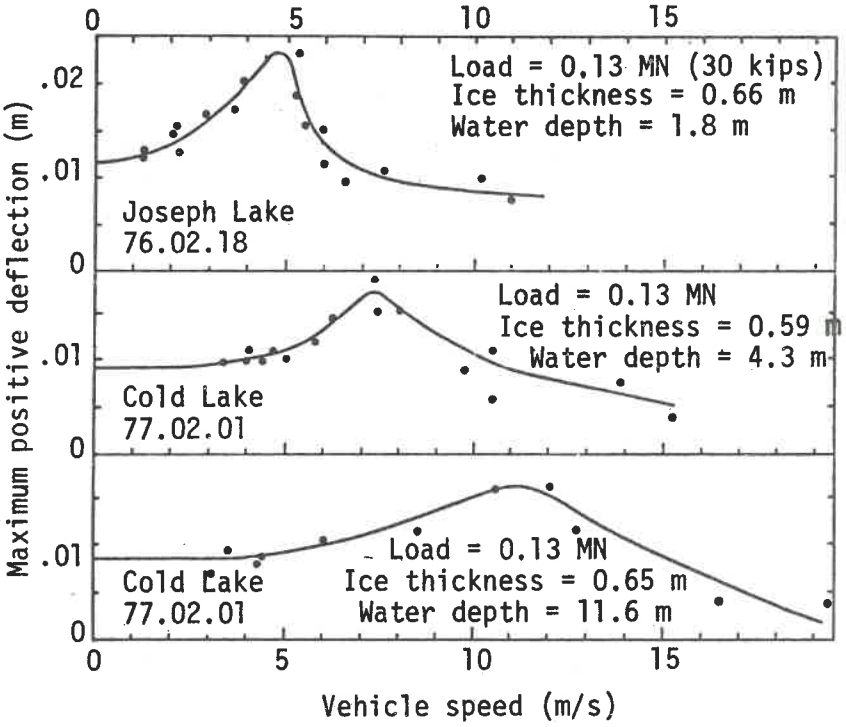

FIG. 4. Variation of maximum deflection with vehicle speed

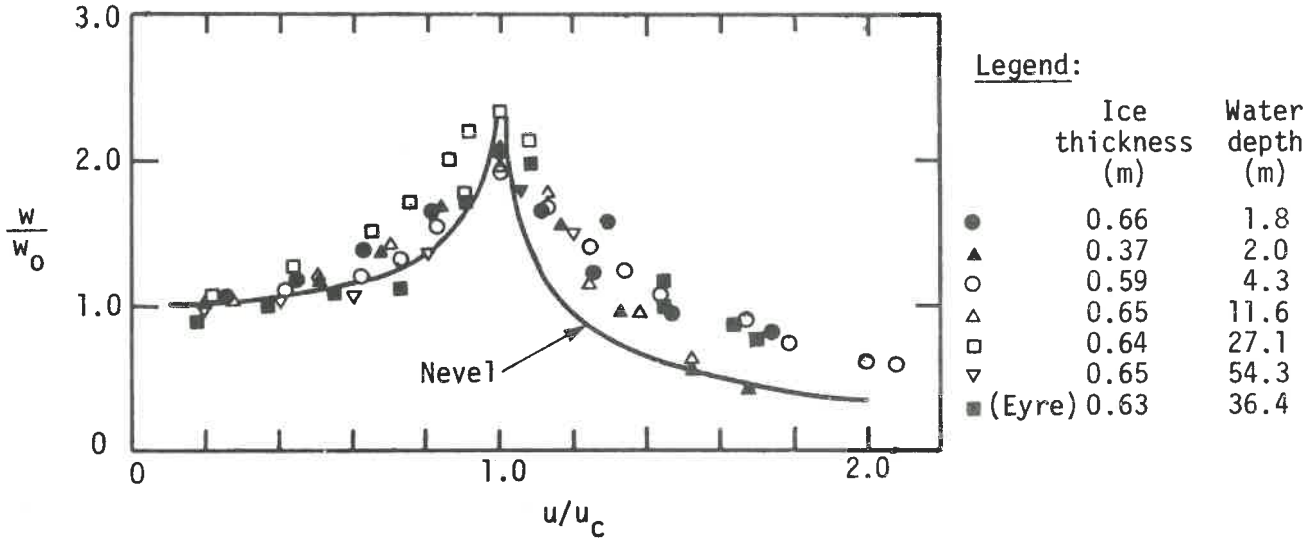

FIG. 5. Variation of deflection amplification factor with relative vehicle speed

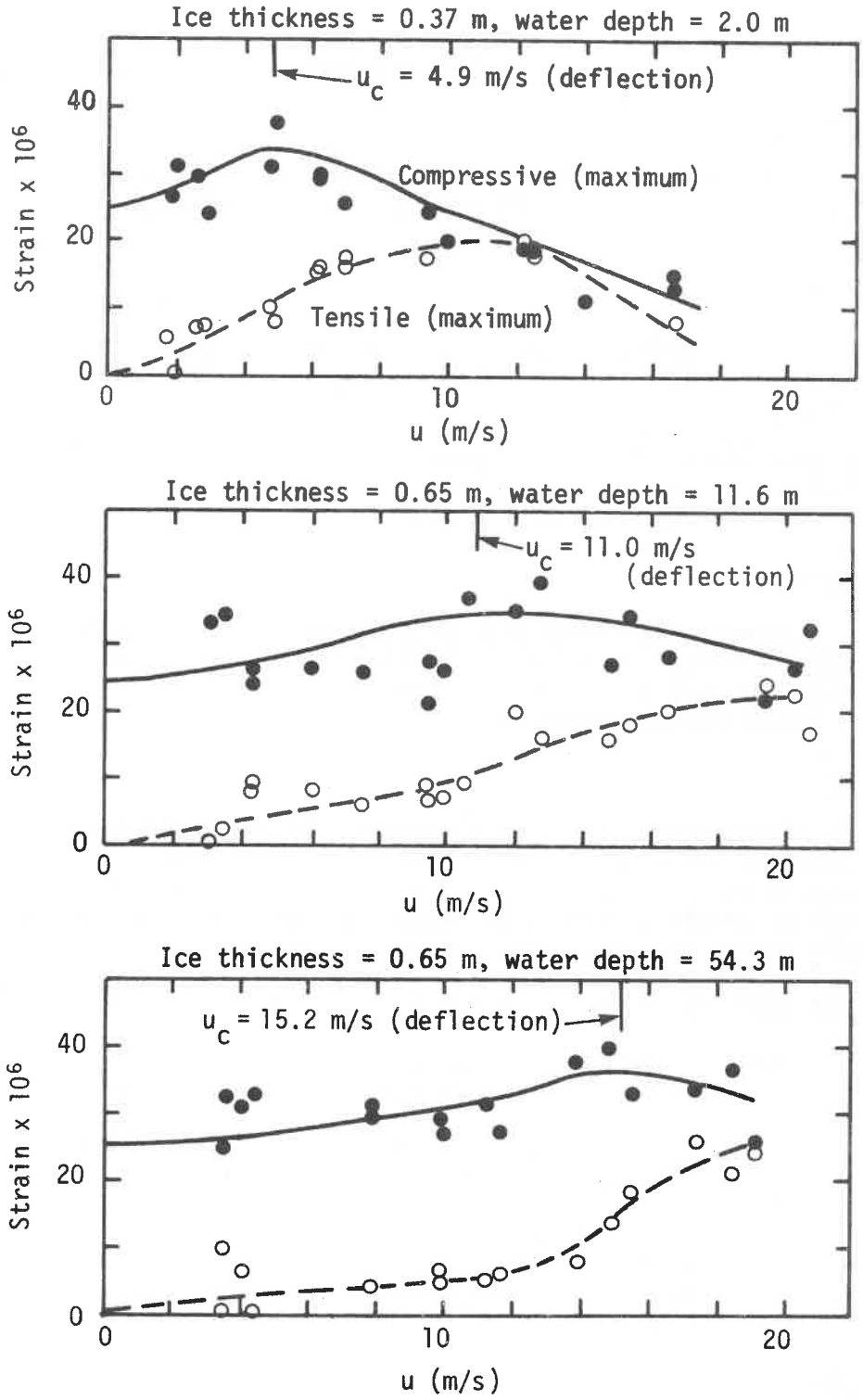

FIG. 6. Variation of maximum compressive and tensile strains with vehicle speed

Discussion

D.J. Goodman:

Could you discuss the effect of vertical acceleration of your transducer? If the slope transducer is accelerated horizontally but not tilted, will it not have an output?

S. Beltaos:

I am indebted to Dr. Goodman for pointing out this effect; some accelerations of the ice are bound to occur. As I noted during the presentation of the paper, about one-half of the discrepancy between measured and true deflections has now been accounted for. However, there still remains an error of some 15%; at least a part of this error is perhaps due to the effect indicated by Dr. Goodman.

A.W. Lipsett:

Given that the amplification of deflection is approximately 2 times and that of compressive strain is 1.4 times, what do you feel is the mode of failure for moving loads on floating ice sheets?

S. Beltaos:

Assuming that the response of an ice sheet to a moving load is mostly elastic, the critical stress amplification would seem to be about 1.4 times. In practice, a safety factor of at least 2 would be applied, so that it is difficult to explain reported failures in terms of amplification due to motion near the critical speed. The following possible explanations may be worthwhile to investigate further:

(a) Vehicles accelerating or decelerating when travelling near the critical speed;

(b) Repeated loading of the ice sheet, e.g., vehicles travelling in tandem;

(c) High amplification factors actually occurring in a very narrow range of speed which is difficult to detect with field tests due to mediocre speed control.

B. Ladanyi:

Have you tried to analyze your results in terms of maximum curvature which may give an idea on maximum strain and the proximity of failure?

S. Beltaos:

No, theoretically speaking, our measured slope-time curves could be differentiated once to give a measure of the curvature. From the practical point of view, this might have been very difficult to accomplish due to the well-known inaccuracies involved in differentiating experimentally obtained functions.

B. Michel:

Could you describe your slope transducer and tell us if it is measuring a secant slope over a distance or a punctual slope. In the former case it might explain the differences in deflections between measured and observed measurements.

S. Beltaos:

Our transducer is commercially known as a Rotary Variable Differential Transformer, Type Schaevitz R 30A. For field applications, the transducer is placed inside a stainless steel case 140 mm long, 75 mm high and 63 mm wide. Slope is measured lengthwise, i.e., over a distance of 140 mm. Considering that the minimum ice thickness tested was 0.3 m with a characteristic length of about 6.5 m, I would think our slope measurements closely approximated the corresponding punctual values.

D.M. Masterson:

Does vibration from the moving load cause distortion of strain gauge outputs?

S. Beltaos:

I would think that if any such distortion occurred, it must have been minimal because our observed strain-time curves (when the strain gauges functioned) were generally smooth and consistent with simultaneously observed slope-time variations (i.e., zero strains always occurred at the same time as maxima or minima of slope). There were a few strain records, however, for which a small fluctuation of very high frequency seemed to be superimposed on the true strain. The amplitude of this fluctuation was very small, roughly equal to the thickness of the pen trace and thus posed no difficulty in interpreting the results of these records.

SURFACE STRAIN OF ARTIFICIALLY THICKENED ICE DRILLING PLATFORMS*

A.J. Allan
C-CORE, Memorial University of Newfoundland

Introduction

The use of artificially thickened sea ice platforms for the support of drilling rigs in Arctic near-shore areas culminated this year in the successful completion of Panarctic Oil's Drake F-76 prototype production well. The platforms have been designed by FENCO Consultants Ltd. and the construction techniques are described in the literature, e.g., Masterson et al. (1975), Hood et al.,(1975). A useful review of the technology is covered by El-Tahan et al.,(1978).

The load bearing behaviour of the platforms is monitored by daily measurements of vertical deflection, which have recently been supplemented by the measurement of strain within the platform (Masterson et al., 1978). This paper presents the results from some additional strain measurements made on the Drake P-40 platform in 1977 and the Roche 0-43 platform in 1978. In both cases strains were measured using the continuous reading wire strainmeter described by Allan and Winsor (1977).

Drake P-40 Experiment

Three strainmeters were deployed on the Drake P-40 platform in a linear array along one half of the short axis of the platform; one close to the moon pool (near-rig), one 30 m out from the moon pool (mid-ice), and one at the periphery of the platform 162 m from the moon pool at the bench mark (Fig. 1). In each case the gauge length was set at 1 m and the instruments installed in shallow trenches on the surface and bolted to the ice by 10 cm tubular ice screws. The data from the three instruments together with the ice surface temperature at the mid-ice site and the recorder temperature were recorded on three inexpensive, dual-channel, galvanometric chart recorders. Chart speed was one inch per hour and the chopper bar trace activation sample the data once every four seconds. System resolution was limited to 2 microstrain by the width of the chart paper. A detailed description of the experiment is given by Allan (1977).

---

*C-Core Publication 78-17

The record commenced on January 27, 1977 after the construction of the platform but prior to spudding, which took place on February 2nd. Recording was terminated on March 11, 1977 after completion of all drilling activities. After the charts were recovered, the data were digitized, compensated for individual instrument calibration and replotted on a shortened time base. The temperature coefficient for the system has been determined at better than 0.6 apparent microstrain/°C and since the ice temperature varied only between -28°C and -34°C no temperature compensation of the data was warranted. The final plot of the data from all three instruments is shown in Fig. 2.

Unfortunately the extreme data from the important near-rig strainmeter were lost due to ice fouling the range reset mechanism following a flood of effluent shortly after installation. The mechanism was freed on February 18th. The low strain values recorded thereafter are much lower than would be expected and apart from the first few days, the record from this instrument must be considered unreliable. Intermittent flooding occurred in the immediate vicinity of the rig throughout the drilling period, but on March 4th a major flood spread as far as the mid-ice instrument, as evidenced by the ice temperature record at that point (Allan, 1977). Brine contamination of the common power supply affected all three instruments resulting in the discontinuity shown towards the end of the chart in Fig. 2. The bench-mark instrument was otherwise not affected by flooding and operated satisfactorily throughout the period.

Roche 0-43 Experiment

The susceptibility of the Drake instruments to flooding was clearly unsatisfactory. A new waterproof housing was designed utilizing a plastic tube to protect the length standard with decoupling to the end units being provided by two neoprene bellows, C-CORE (1978). The electronic part of the system was redesigned to avoid interference between channels and to eliminate any possibility of random triggering of the range reset mechanism by line transients.

Two of the redesigned strainmeters were frozen into the upper layers of the build-up ice of the Roch 0-43 platform towards the end of December 1977. The instruments were installed close to the moon pool, one parallel to the long axis, known as the long-axis instrument, and one parallel to the short axis, known as the short-axis instrument. They were positioned about 2 m apart and by the time platform construction was completed, were located 0.75 m below the ice surface. The plan layout is illustrated in Fig. 3. Ice subsurface temperature, air temperature and recorder temperature, together with the

strain information were continuously recorded on three dual-channel, galvanometric chart recorders. Sampling rate was maintained at one every four seconds, but the chart speed was reduced to 1/8 inch per hour. A detailed description of this experiment, including the temperature information is given by C-CORE (1978).

The system ran continuously for 105 days from December 22, 1977 to April 6, 1978. The data were again digitized and replotted on a shortened time base for ease of reading and are presented in Fig. 4.

Discussion

The failure to obtain a complete record from all three instruments on the Drake P-40 platform was disappointing, but the data does contain some useful and interesting information. The feature, possibly associated with the well spudding on February 2nd shows a high strain rate right across the platform surface. A similar depression of about 100 microstrain can be seen in the Roche platform data, although in this case spudding took place some weeks later, suggesting the feature may be due to relaxation of surface strain after completion of the building-up process.

As expected the near-rig channel shows generally compressive strain, while the bench-mark channel is generally tensile. The mid-ice instrument is likely situated close to the point of zero surface strain.

A number of rapid 'strain events' are evident, numbered 1-10 in Fig. 2, and A, B and C in the short-axis curve in Fig. 4. The events are typically 10 to 40 microstrain in amplitude and 10-20 seconds in period. There is no obvious pattern to the events except that they occur simultaneously on all three Drake channels and they tend to occur following a period of relative tensile strain in the Roche data. Not all the events are simple step deformations. Figure 5 is a detail from the original Drake chart showing strain event 6 where a period of rapid deformation is bracketed by two small step events.

The origin of these events is uncertain. Some of the suggested cause or causes are: instrument error, thermal cracking, shear between laminates and magnetic interference from the drill stem. Any cracking mechanism in the ice would be expected to show a Poisson's effect in the Roche record but there is no evidence of this except perhaps for a slight indication in event B, which may be circumstantial. The original charts for event B are reproduced in Fig. 6.

The Roche instruments operated well throughout the 105 day recording period and produced creep curves consistent with the theoretically expected values (Frederking, personal communication). The curves appear to be within the primary creep range with a maximum strain of 1520 microstrain along the short axis and 745 microstrain along the long axis.

Acknowledgments

These projects were initiated by Dr. Lorne Gold of the Division of Building Research of the National Research Council. Ken Butt and Terry Ridings of C-CORE were largely responsible for the design of the system and its installation. I am grateful to Panarctic Oils Ltd. for their hospitality and to the staff of FENCO for assistance in the field. The work was supported by the National Research Council under Contract Number OSQ77-00155, who permitted reproduction of the data.

References

Allan, A. (1977). Measurement of Surface Strain on Drake P-40 Artificially Thickened Sea Ice Drilling Platform. C-CORE Technical Report #77-27, 42 pp.

Allan, A. and Winsor, W. (1977). Industrial Applications of Ice Strain Measurements. In Fourth International Conference on Port and Ocean Engineering Under Arctic Conditions, September 26-30, 1977, p. 629-637.

C-CORE (1978). The Measurement of Subsurface Strain on Roche 0-43 Artificially Thickened Drilling Platform. C-CORE Contract Report, 42 pp. Publication Serial Number 78-16.

El-Tahan, H., El-Tahan, M., Swamidas, A.S.J. and Reddy, D.V. (1978). The Analysis, Design and Construction of Floating Ice Islands for Offshore Drilling: State of the Art. American Society of Civil Engineers, October 16-20, 1978, Chicago, 51 pp.

Hood, G.L., Strain, H.J. and Baudais, D.J. (1975). Offshore Drilling from Ice Platforms. Paper No. SPE 5651, 50th Annual Fall Meeting of the Society of Petroleum Engineers of AIME, Dallas, Texas, Sept. 28 - Oct. 1, 1975, 12 pp.

Masterson, D.M., Anderson, K.G., Strandberg, A.G. (1978). Strain Measurements in Ice Platforms using 3 m Long Resistance using Gauges. N.R.C. Workshop on the bearing capacity of ice covers, October 16-17, 1978, Winnipeg.

Masterson, D.M., Baudais, D.J. and Wasilewski, B.R. (1975). Experience in Ice Platform Construction for Arctic Drilling. Annual Western Meeting of the Petroleum Society of C.I.M., Edmonton, Alberta, October, 1975.

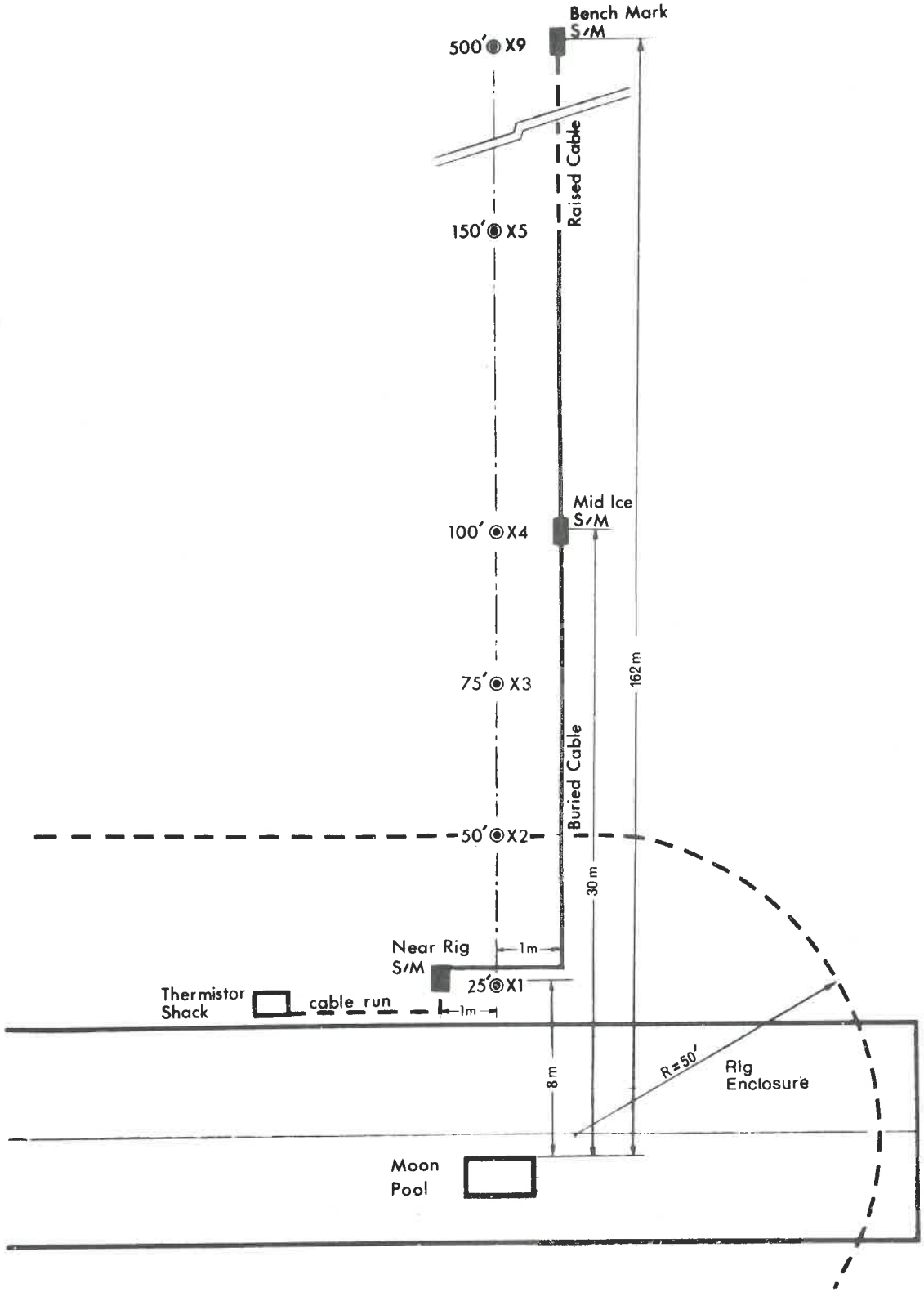

FIGURE 1

STRAINMETER SITES COMM-HI RIG NO. 2 PLATFORM, DRAKE P-40

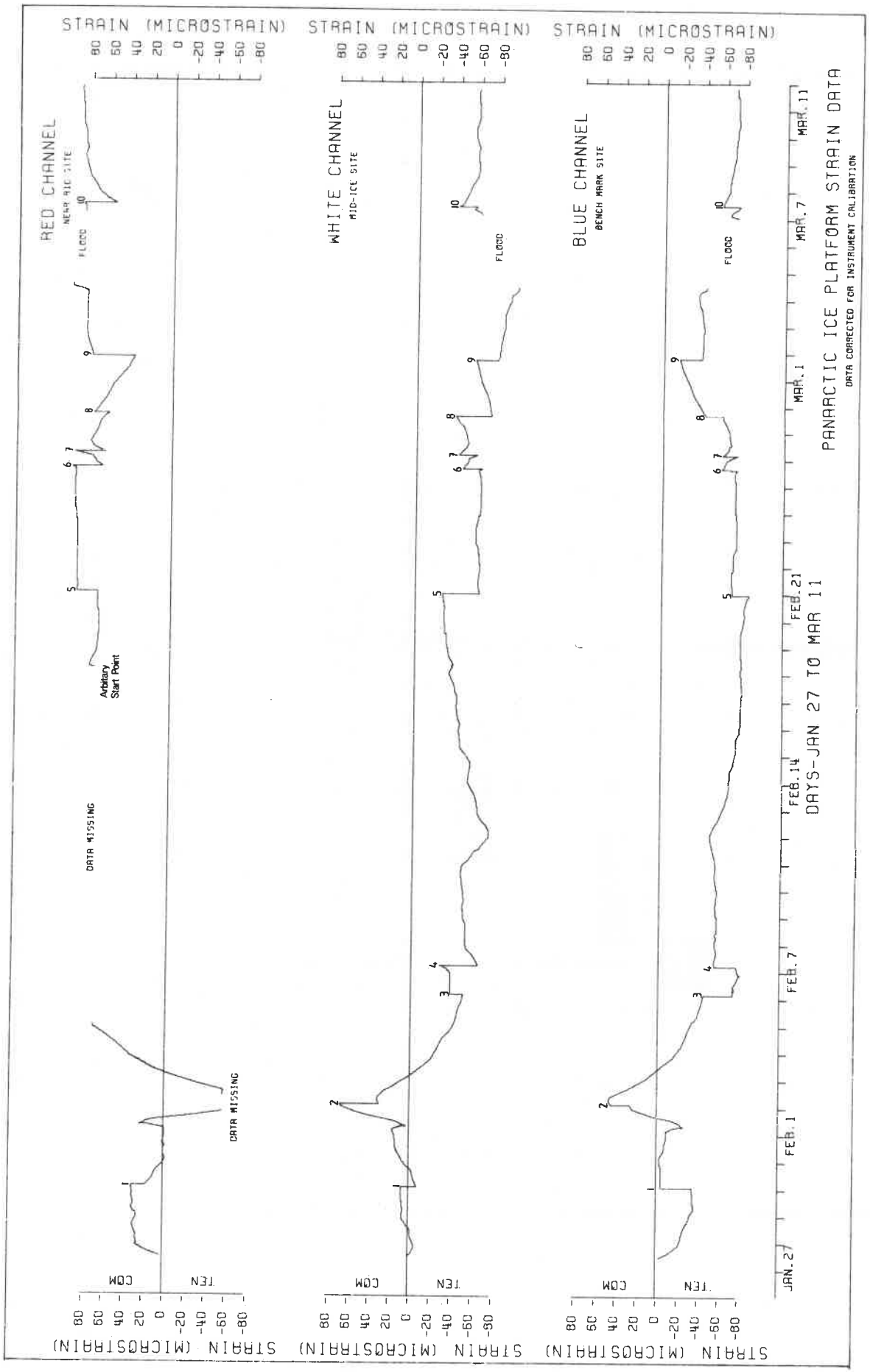

FIGURE 2

STRAIN DATA, DRAKE P-40

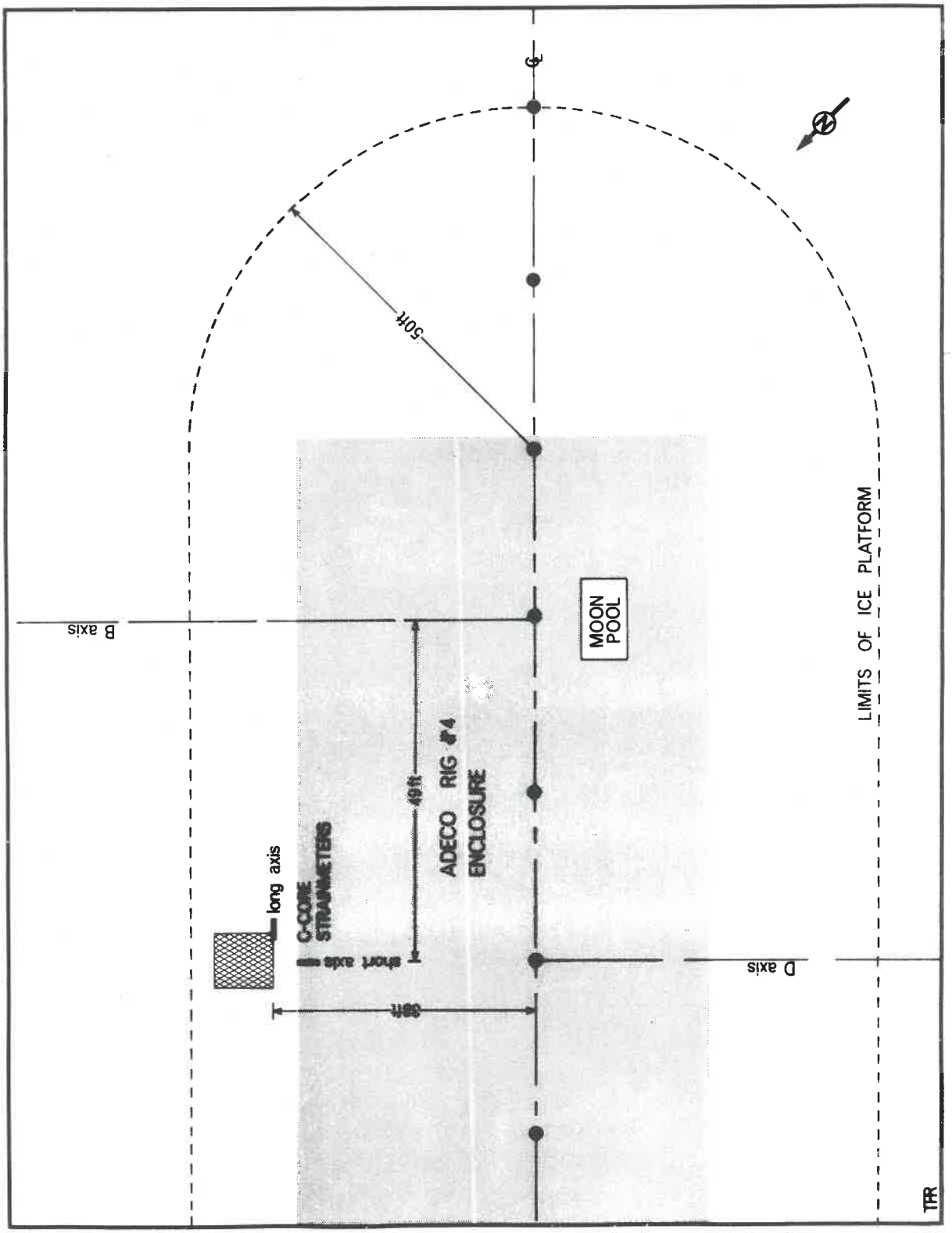

FIGURE 3

STRAINMETER LAYOUT, PLAN VIEW, ROCHE O-43

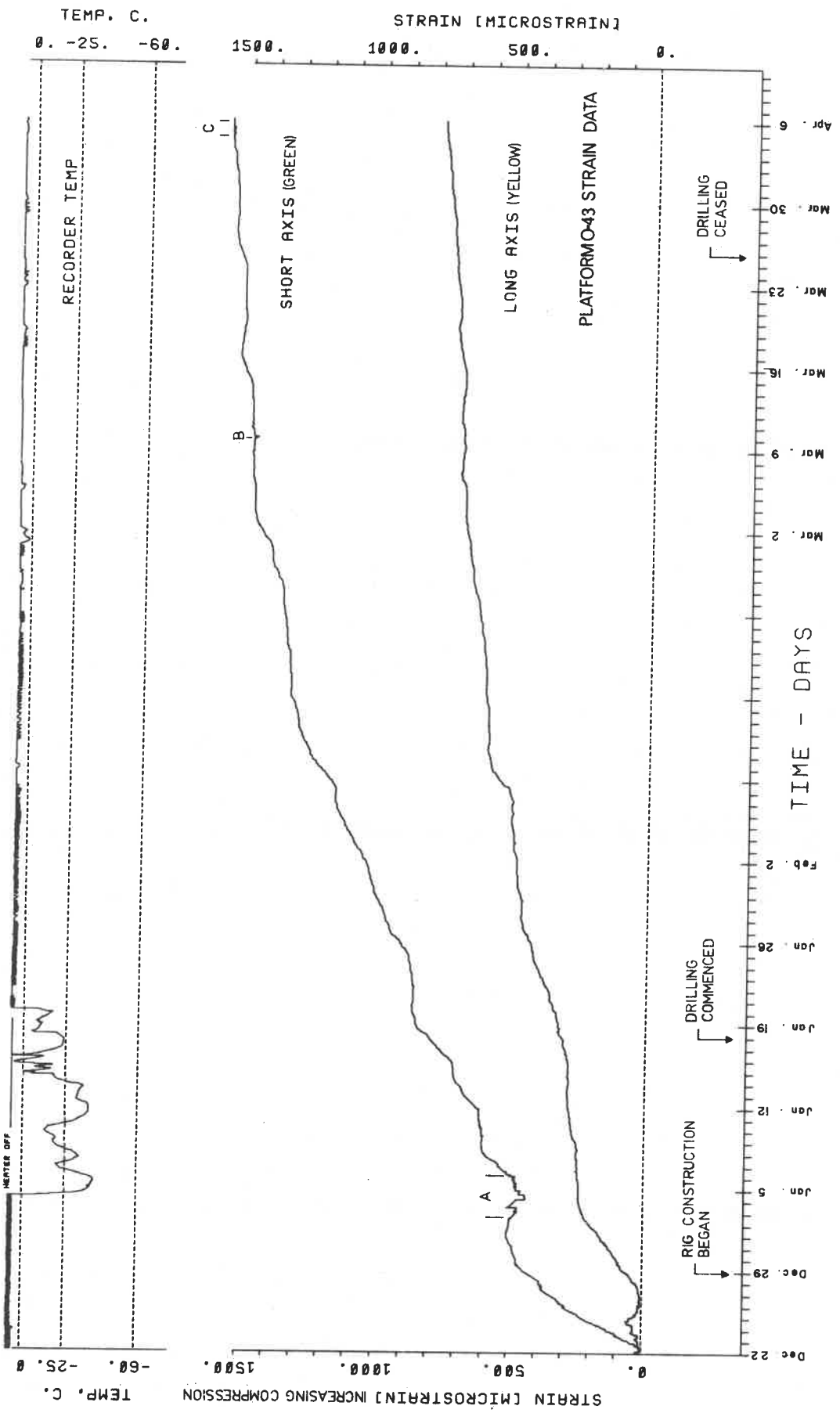

FIGURE 4

STRAIN DATA, ROCHE O-43

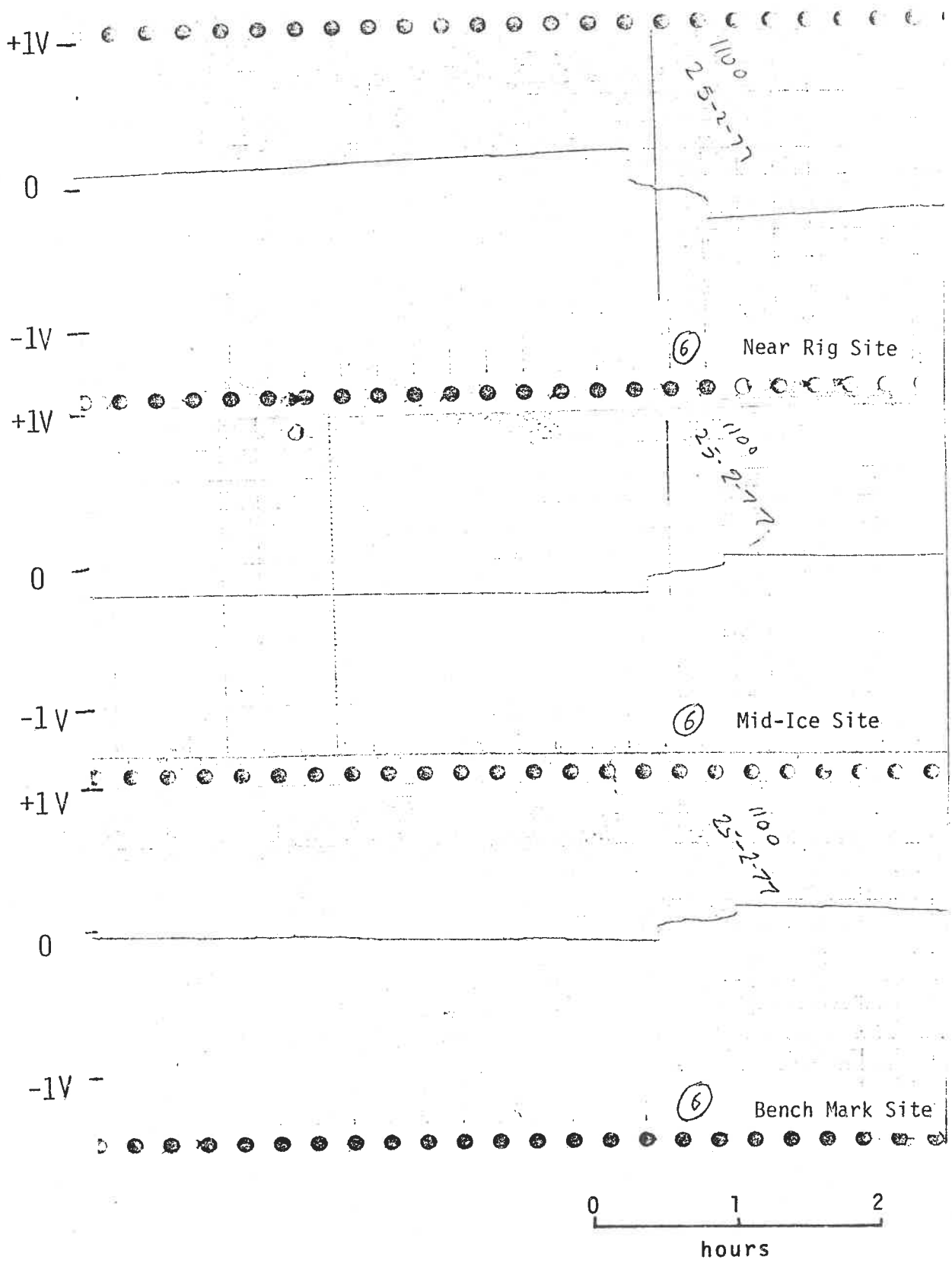

FIGURE 5

STRAIN EVENT SIX

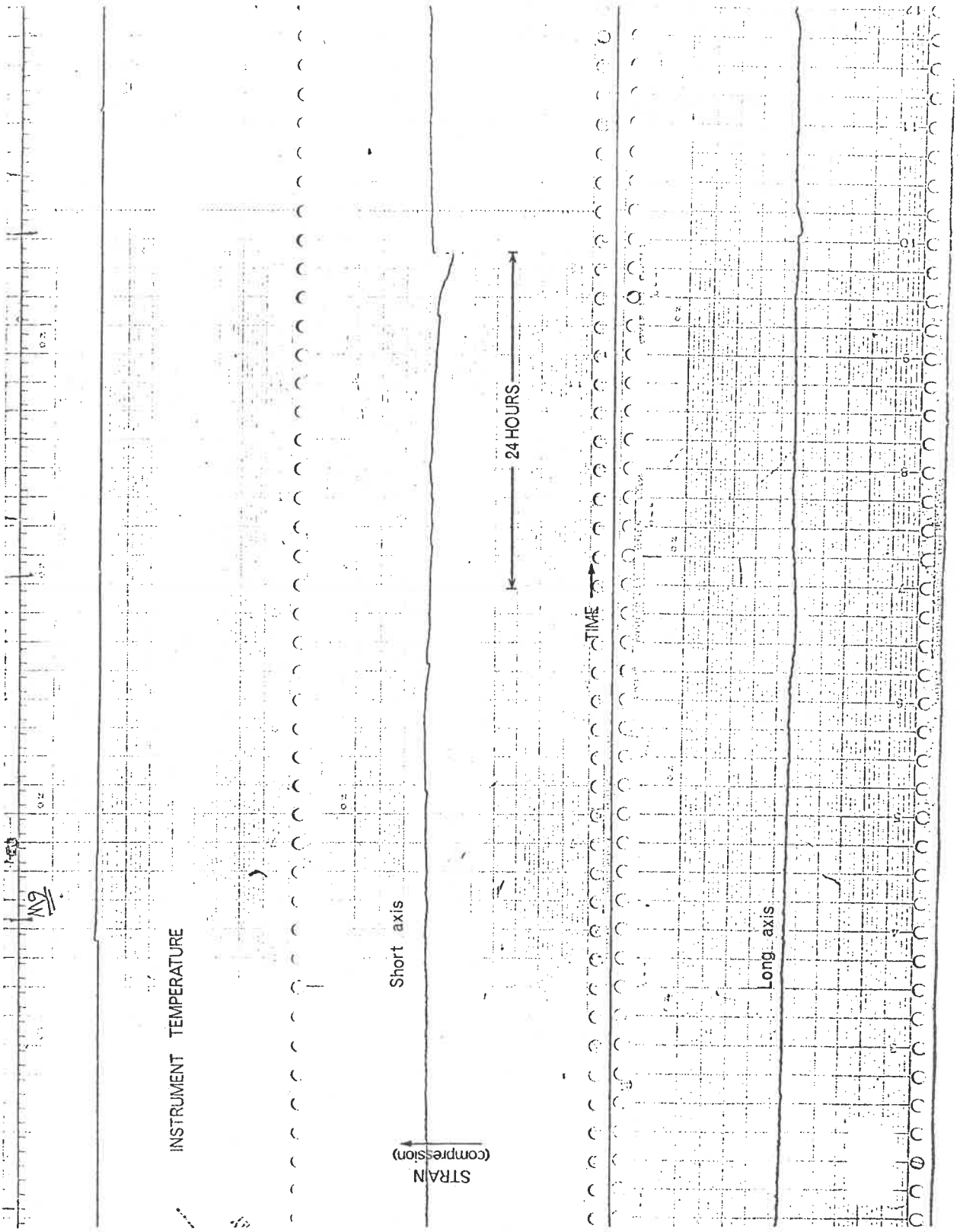

FIGURE 6

STRAIN EVENT "B"

Discussion

B. Ladanyi:

Is it possible that the anomalies you observed in strain measurement might have been produced by some outside event such as distant earthquakes resulting in disturbances in the sea surface?

A. Allan:

Yes, there is always a possibility of outside influence, particularly from ridging or cracks opening. We don't have enough strain measurements in the natural situation to know the characteristics of naturally occurring strain events. From the small amount of information we have, we tend to suspect that the platform events are not due to outside influences.

R. Tinawi:

Is that the only type of strain measuring technique available?

A. Allan:

No. Dr. Masterson will discuss in the next paper a constantan wire gauge, which has successfully been used on the thickened platforms. The literature describes other strain measuring techniques using standard strain gauges, dial gauges and optical methods.

RESULTS OF STRAIN MEASUREMENTS IN FLOATING ICE PLATFORMS USING 3 m-LONG RESISTANCE WIRE GAUGES

by D.M. Masterson, K.G. Anderson and A.G. Strandberg
FENCO Consultants Ltd.

Introduction

In the early 1970's FENCO CONSULTANTS LTD. was contracted by Panarctic Oils Ltd. to provide engineering for the design and construction of floating ice platforms to be used for offshore drilling in the Canadian High Arctic. The history of the development of this concept of support for offshore drilling is outlined in the following publications (Baudais et al, 1974, Baudais et al, 1976, Rose et al, 1975).

In the Fall of 1976 FENCO engineers designed and constructed embedded wire strain gauges which were installed that same season in two ice platforms and this past winter gauges were installed in two more platforms. The data obtained from the gauges in the ice platforms over the past two drilling seasons have verified the theories used in the design of the ice platforms and have enabled engineers to predict ice platform behaviour during the various periods of loading and unloading the ice sheet. In this paper, data obtained at Panarctic's Drake F-76 well will be presented and discussed (Fig. 1).

Design and Construction of Gauges

A strain measurement device had been used to measure the surface strains in glaciers (Warner and Cloud, 1974). The basic material used by Warner et al was also used in these gauges; this being 0.127 mm teflon coated constantan wire.

A gauge length of 3 m was chosen as the total resistance of the gauge would then be approximately 116 Ω allowing the strains to be read by conventional instrumentation. It was also felt that a 3 m gauge length would enable the measurement of strains over representative length in the ice, thus avoiding the pitfall of measuring the effects of minute cracking in the ice which were of no use in the understanding of the overall behaviour of the platforms.

Anchors

A sure means of anchoring the strain gauges was required and after many tests and failures a system of 2 small plexiglass blocks with hollow sections and holes drilled out to allow wires to pass through was used, as shown in Fig. 2.

The gauge wires were soldered to the lead wires after they were passed through the holes of the plexiglass blocks. The solder connections were cleaned in preparation for moisture proofing, sealing and glueing.

Sealers and Moistureproofers

As it was essential that all of the connections used in the gauges be kept dry and free of moisture and salt or brine, a suitable means of moisture proofing was needed. Several different types and combinations of sealants and moisture proofing compounds were tested.

The teflon coating at the end of the gauge wire was first treated with tetra-etch compound to make the coating rough and easier to bond to the moistureproofers and sealants. The cleaned soldered joint was first coated with M-LINE Accessories M-Coat D, an air drying acrylic coating. After a second thorough application of this coat, a coating of M-Coat B was applied and a coat of M-Coat C was applied.

A very fast acting joining agent was found (Methylene Chloride) to join the two half portions of each anchor block. After the two half sections were mated, sealing in the solder connections, a heavier mixture of the joining agent was injected into the anchor blocks through the lead wire holes. When this joining agent had hardened, a silicone rubber adhesive sealant was injected into the anchor block through the remaining anchor bolt hole in the back of each anchor block. The anchor bolt was then screwed into the anchor block forcing silicone into any small voids which may have been missed previously. Where the constantan wire and lead wires protrude from the anchor blocks a coating of M-Coat G was applied and followed by a final liberal coating of silicone sealant.

Dummy or Temperature Compensation Gauges

As the temperature of the strain gauge environment was expected to vary over the monitoring period, a means was needed of compensating for strains introduced by a temperature change. A temperature compensating gauge or dummy gauge was designed and constructed consisting of a 300 mm length of 150 mm diameter schedule 40 PVC pipe with two end caps with an identical gauge to those used as active gauges inside.

Lead Wires

Several types of leads were used over the past seasons with the best results being obtained from the use of a wire consisting of three twisted pairs of teflon-coated copper wire. These twisted pairs are coated with neoprene, then shielded

finally covered with a heavy rubber insulation. The lead wires were all the same length and used for both dummy gauges and active gauges alike.

Installation and Instrumentation

As flooding and construction of the ice platforms proceeds, gauges are installed on the ice surface in rosette fashion with two gauges on each arm to provide redundancy according to the plan shown in Fig. 3. The two gauges parallel to the rig's long axis were labelled G, those perpendicular to the axis were labelled F and those at 45 degrees were labelled Z. Five layers of gauges were installed as shown in the section of Fig. 3. A gauge in the Z direction at level 3 would be called Z3.

Immediately after the gauges were tensioned to a pre-determined level they were flooded over with sea water and became frozen into the ice sheet. The lead wires were kept as short as possible and were run vertically through the ice sheet to a strain reading device located in a small building on the platform surface.

Upon completion of flooding or construction of the ice platforms the strain gauges were ready to be instrumented. At Drake F-76 a B & F Instruments Inc., Type SY-161 strain gauge reader was used allowing for continuous reading and recording onto magnetic tape of 50 channels of strain gauge data. Strains were recorded at 30 minute and later 1 hour intervals.

Testing and Calibration of the Gauges

The gauge factor for this system was 2.05, gauge factor being defined as resistance change per initial resistance per unit strain. In order to confirm the accuracy of the constantan strain gauges, two tests were conducted under laboratory conditions.

The first test involved the straining of the constantan wire to over 50,000 με. The results of this experiment are plotted in Fig. 4 which presents the resistance change $\Delta R(\Omega)$ vs. strain. The test point positions were calculated using an actual ohmmeter while the theoretical line was calculated by measuring the strain with a micrometer and converting this to resistance using a gauge factor of 2.05.

The second test was similar to the first test with the exception that the constantan wire was allowed to rebound 200-300 με on various occasions. As can be seen by the results in Fig. 5, whether the wire was being extended or retracted made virtually no difference in the measured resistance at a particular strain.

Presentation of Strain Measurements Obtained

On February 27th all of the gauges were wired into the B & F strain recording system and the initial readings were taken. The final strain reading was taken on April 29th for a total of 62 days of data.

Hand readings had been taken and recorded at least once daily during the operation and these were compared with the taped values to check on the recorder. No problems were noted. During drilling of the well, the gauge readings could be seen cycling through about 50 με when the kelly and drill string were rotating or when heavy machinery was operating. Ninety percent of the time though there was no cycling or drifting. One problem noted with the B & F recorder was that interuptions in the power supply caused the recorder clock to reset. This created some difficulty with data identification.

After the raw data had been removed from the tapes and loaded into the computer memory, the principal strains and principal strain directions for each set readings were calculated (Byars and Snyder, 1963).

Strain profiles for 5 different times are plotted in Fig. 6. It can be seen that the measurements agree, in general, to what is known of laterally loaded plate behaviour. Profiles of major strains are linear. The neutral axis of the platform is at 3.1 metres, 0.4 metres above the middle plane. The tensile strains in the compression zone are of the same order of magnitude and same direction as the minor principal tensile strains in the tension zone and would indicate the effects of a uniform tensile stress field. Small ice movements were measured during this time and there could very well have been such a stress field. The average temperature strain was about 40 με tension and is indicated by line 8' in Fig. 6.

Since elastic plate theory is used to analyze ice platforms, it is encouraging to note that these measured strain profiles are linear and that the neutral axis lies close to the middle plane. Since the design stress is limited to 1/3 or less of ultimate, one would expect the strains to be small and this has proven to be true.

Analysis of Strain Data

Regression analyses on strains at level 5 showed them to vary in time according to the following equation

$$\varepsilon_5 = 212.95t^{0.47} \qquad (1)$$

Extreme fibre strain, by extrapolation, was 1.37 times ε_5.

Equation 1 was multiplied by 1.37 and differentiated to give extreme fibre strain rate. This was used in conjunction with the exponential creep equation (Glen, 1955, Gold, 1965, 1973, Masterson and Strandberg, 1978) to obtain expressions for the variation of stress and effective elastic modulus (Baudais et al, 1974, 1976, Rose et al, 1975) with time. The results are plotted in Fig. 7. From this figure, the following is evident.

Strain rate, stress and effective elastic modulus at the point of measurement which was very near the rig's heaviest loads decrease rapidly with time. Stress decreases from the initial 373 kPa and becomes nearly asymptotic to 50 kPa, approximately 1/20 the short-term failure stress.

The effective modulus used to predict long-term deflections (at approximately 50 to 60 days) corresponds quite closely to the calculated local modulus value. The modulus used in the elastic plate equations is global rather than local. Also, considering the large change in modulus with time, the agreement is good.

Stresses calculated using elastic plate theory and the 50 day elastic modulus showed these long-term values to be 56% of short-term while Fig. 7 shows them to be only 7% of short-term.

Summary and Conclusions

Strain measurements in floating ice platforms using 3 m long constantan wires as resistance gauges were carried out at Panarctic Oils' Drake F-76 well during the winter and spring of 1978. Gauges were placed at 5 different levels in the ice platform in rosette fashion during construction and during drilling readings were taken at 30 and then 60 minute intervals and recorded on magnetic tape by a B & F Type SY-161 strain gauge reader.

1. Long, fine gauge wire resistance strain gauges are well suited to the measurement of strains ranging between 1 με and 50,000 με in laterally loaded ice plates.

2. If these gauges are constructed with proper care, they can be made to withstand the rigours of installation in a harsh climate.

3. Maximum measured principal strains were 1300 με and maximum extra-polated extreme fibre strains were 2100 με.

4. Tensile strains in the compression or upper zone, of the same order of magnitude and direction as the minor principal strains in the tension zone of the platform were measured. These could be attributed to the application of an in plane tension stress field to the ice sheet.

5. Strain profiles show a linear variation of strain with depth, thus verifying that elastic plate theory can properly be used to analyze the time dependent behaviour of laterally loaded ice platforms.

6. Plots of strain rate vs time show that strain rate decreases very rapidly after initial load application.

7. The creep equation was used to calculate stress vs time and effective elastic modulus. These values also decrease rapidly in the initial loading stages.

8. Calculated effective elastic modulus values compare reasonably well with effective modulus values determined from analysis of case histories using elastic plate theory. The implication, is that long-term deflections calculated using elastic plate formula should be accurate, a fact borne out by experience.

9. Stress values over time calculated using the effective modulus and elastic plate formulas do not agree with those calculated from the measured strain data and the creep equation. Detailed long-term stress calculations very near the load area cannot be carried out using these methods as a great deal of local stress relaxation occurs.

Acknowledgment

The authors would like to thank the management of Panarctic Oils Ltd. for granting permission to publish the data contained in this paper.

References

Baudais, D.J., Masterson, D.M., and Watt, J.S. (1974). "A System for Offshore Drilling in the Arctic Islands", 25th Annual Technical Meeting of the Petroleum Society of CIM, Calgary, Paper No. 374029.

Baudais, D.J., Watts, J.S., and Masterson, D.M. (1976). "A System for Offshore Drilling in the Arctic Islands", Offshore Technology Conference, Paper No. OTC 2622, Houston, Texas.

Byars, E.F., and Snyder, R.D. (1963). "Engineering Mechanics of Deformable Bodies", Int. Textbook Co.

Glen, J.W. (1955). "The Creep of Polycrystalline Ice", Proceedings of The Royal Society, A228, pp 519-538.

Gold, L.W. (1973). "Activation Energy for Creep of Columnar-Grained Ice", Physics and Chemistry of Ice, Royal Society of Canada, pp 362-364.

Gold, L.W. (1965). "The Initial Creep of Columnar-Grained Ice", Parts I and II, Canadian Journal of Physics, Vol. 43, pp 1414-1434.

Masterson, D.M., Anderson, K.G., and Strandberg, A.G. (1979). "Strain Measurements in Floating Ice Platforms and Their Application to Platform Design", Canadian Journal of Civil Engineering (to be published).

Masterson, D.M., and Strandberg, A.G. (1979). "Long-Term Loading Analysis of Floating Ice Platforms Using Finite Element Techniques", Workshop on the Bearing Capacity of Ice Covers, NRC ACGR Tech. Memo No. 123, pp

Rose, G.D., Masterson, D.M., and Friesen, C.E. (1975). "Some Measurements of Laterally-Loaded Ice Sheets", IAHR Third International Symposium on Ice Problems, Hanover, New Hampshire, August, 1975.

Warner, G., and Cloud, G. (1974). "Measurement of Surface Strain Rates in Glaciers Using Embedded Wire Strain Gauges", Experimental Mechanics, 1974.

Symbols

E elastic modulus (MPa)

G.F. gauge factor = $\frac{dR/R}{\epsilon}$

K creep constant (strain/time/stress^n)

kPa $\times 10^{-3}$ = N/m^2, $\times$ .145 = psi

MPa $\times 10^{-6}$ = N/m^2, $\times$ 144.98 = psi

n creep exponent

R resistance (Ω)

t time in days

ε strain

$\dot{\varepsilon}$ strain rate = $\frac{d\varepsilon}{dt}$

μ micro (10^{-6})

σ stress (kPa)

Ω ohms

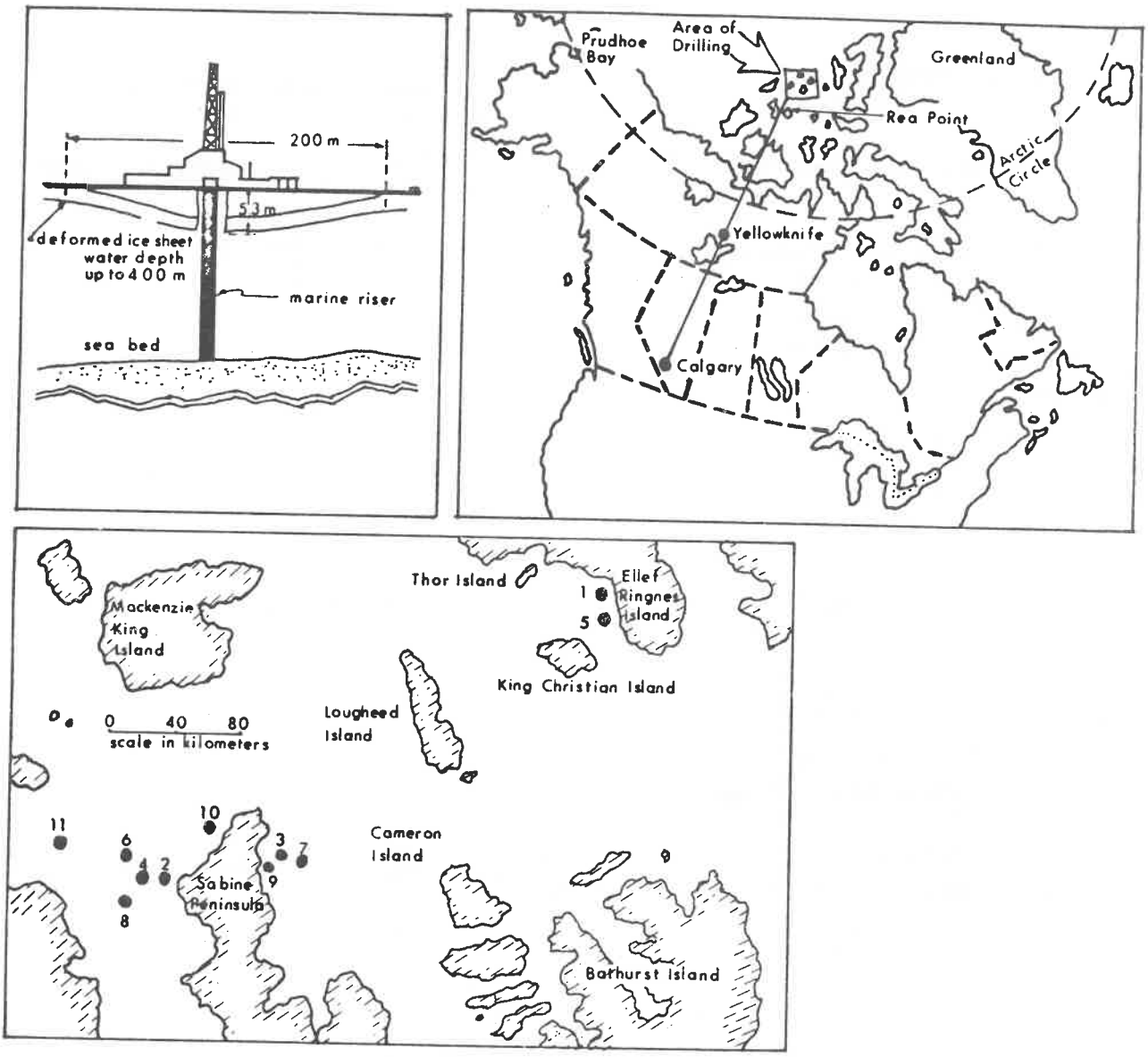

Well Name	Date Drilled	Well Name	Date Drilled
1. Panarctic Jackson Bay B-16	May 1973	7. Panarctic N.E. Drake P-40	Feb 1977
2. Panarctic W. Hecla N-52	Apr 1974	8. Panarctic S.W. Hecla C-58	Apr 1977
3. Panarctic E. Drake I-55	Apr 1975	9. Panarctic Drake F-76	Feb 1978
4. Panarctic W. Hecla P-62	Feb 1976	10. Panarctic Roche Pt. O-43	Jan 1978
5. Panarctic Jackson Bay G-16	Mar 1976	11. Panarctic Cape Grassy G-20	Mar 1978
6. Panarctic N.W. Hecla M-25	Apr 1976		

FIGURE 1 ICE PLATFORMS FOR OFFSHORE DRILLING

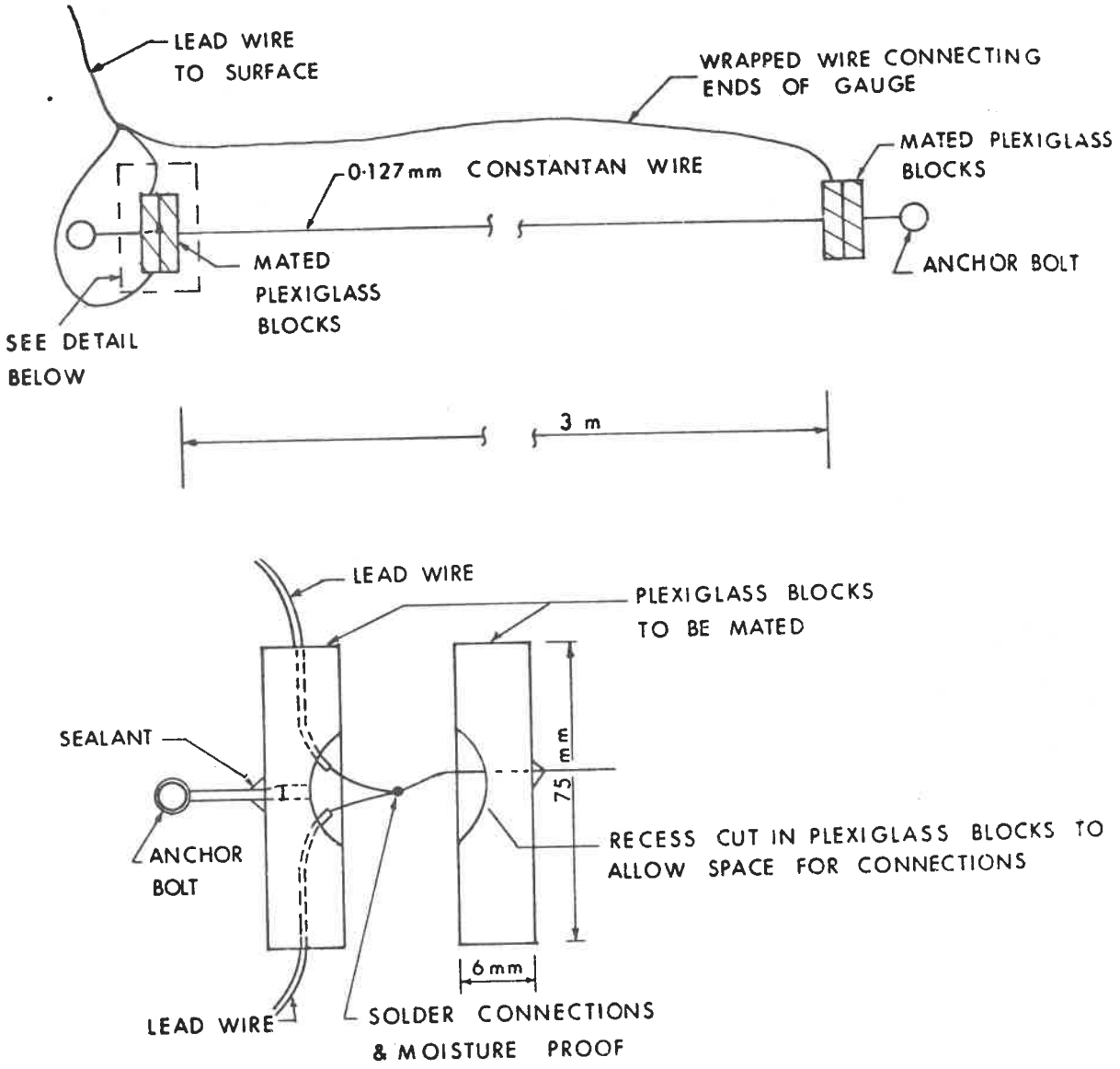

FIGURE 2 DETAILS OF 3 m WIRE RESISTANCE STRAIN GAUGE

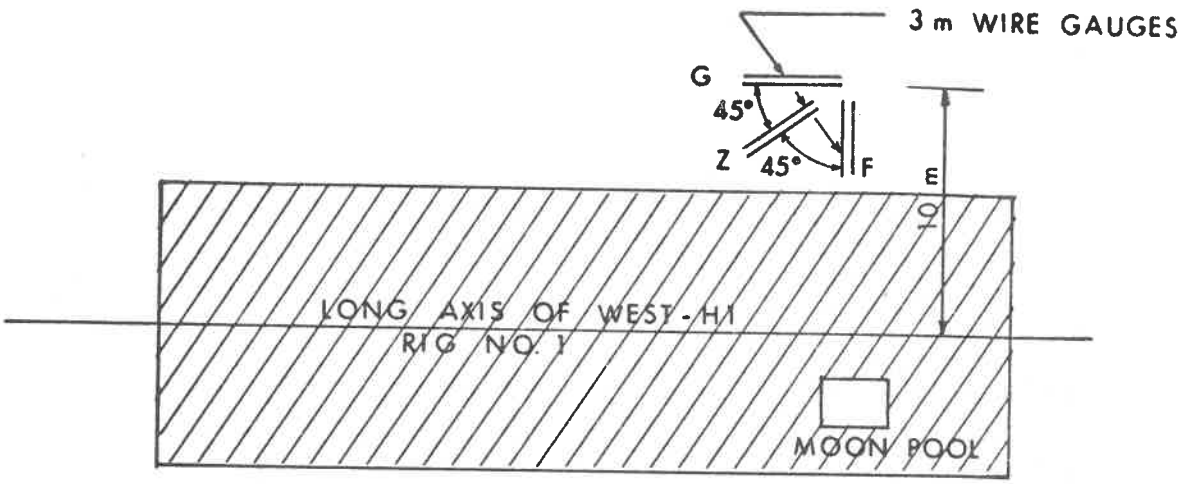

PLAN

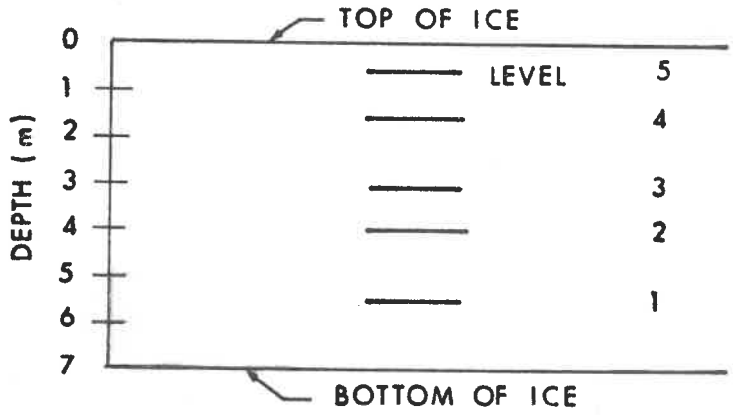

SECTION

FIGURE 3 STRAIN GAUGE INSTALLATION AT DRAKE F-76

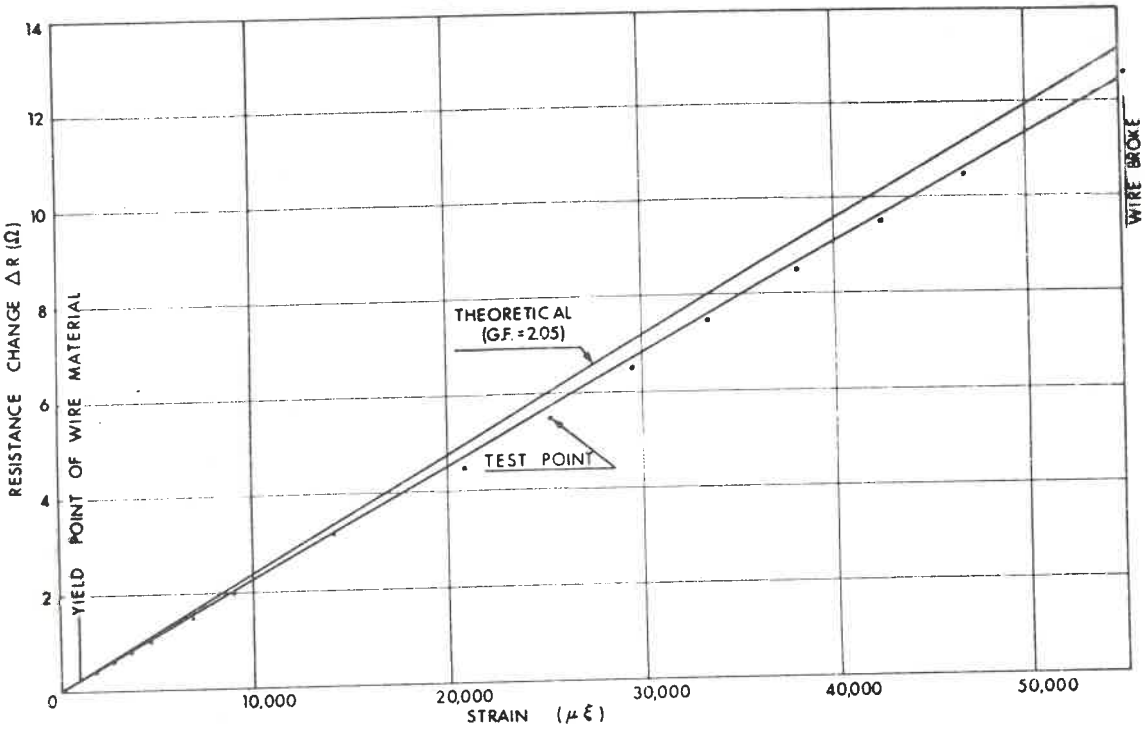

FIGURE 4 STRAIN GAUGE CALIBRATION TEST FOR RESISTANCE CHANGE VERSUS STRAIN FOR A 5 MIL CONSTANTAN WIRE

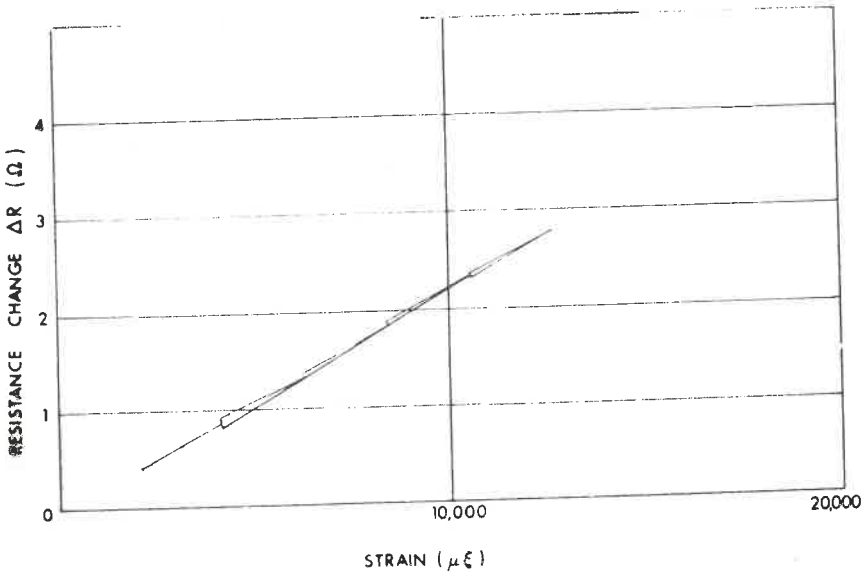

FIGURE 5 STRAIN GAUGE CALIBRATION TEST FOR RESISTANCE CHANGE VERSUS STRAIN FOR 5 MIL CONSTANTAN WIRE WITH PARTIAL REBOUND

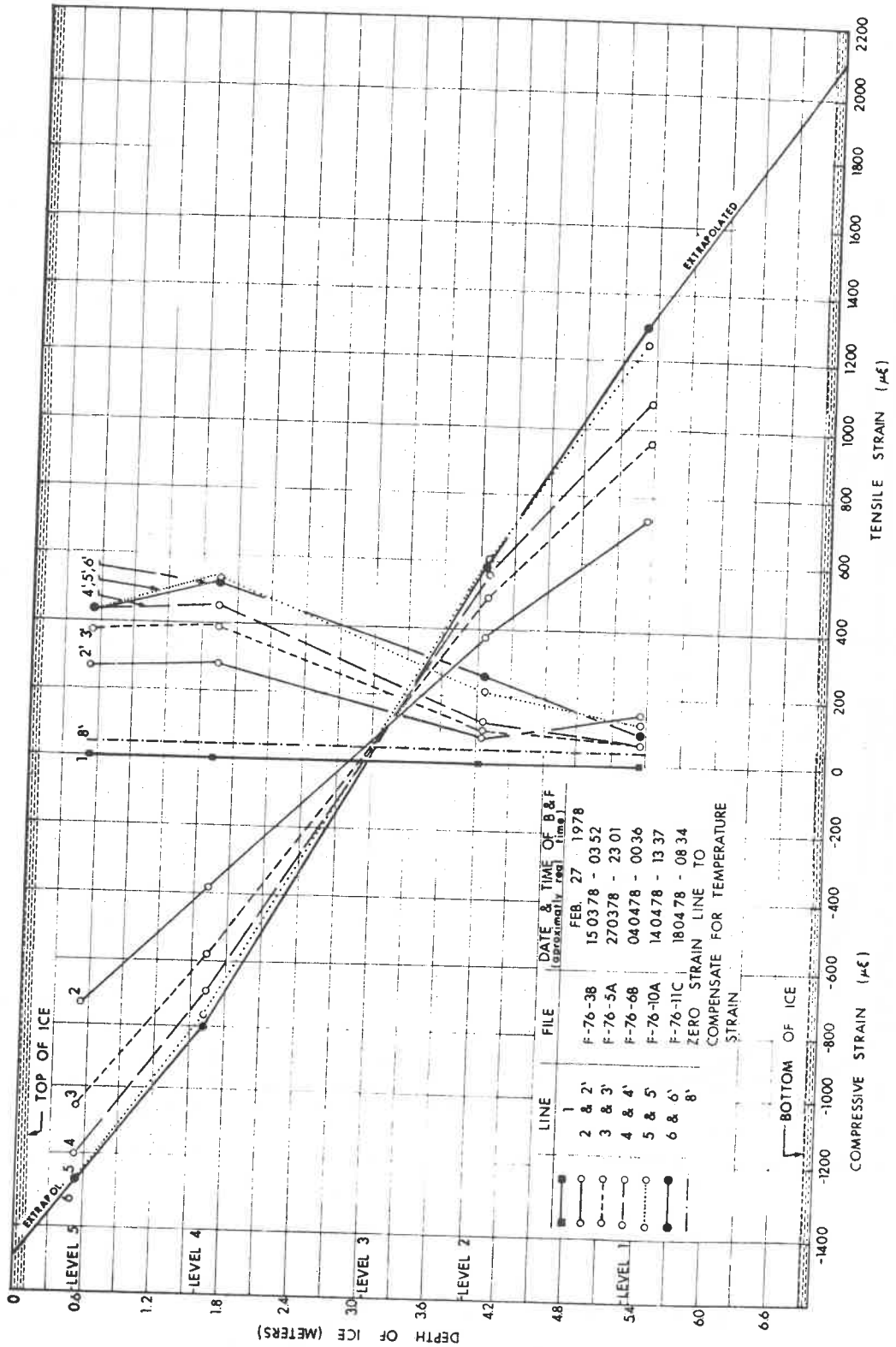

FIGURE 6 STRAIN PROFILE RECORDED AT DRAKE F-76

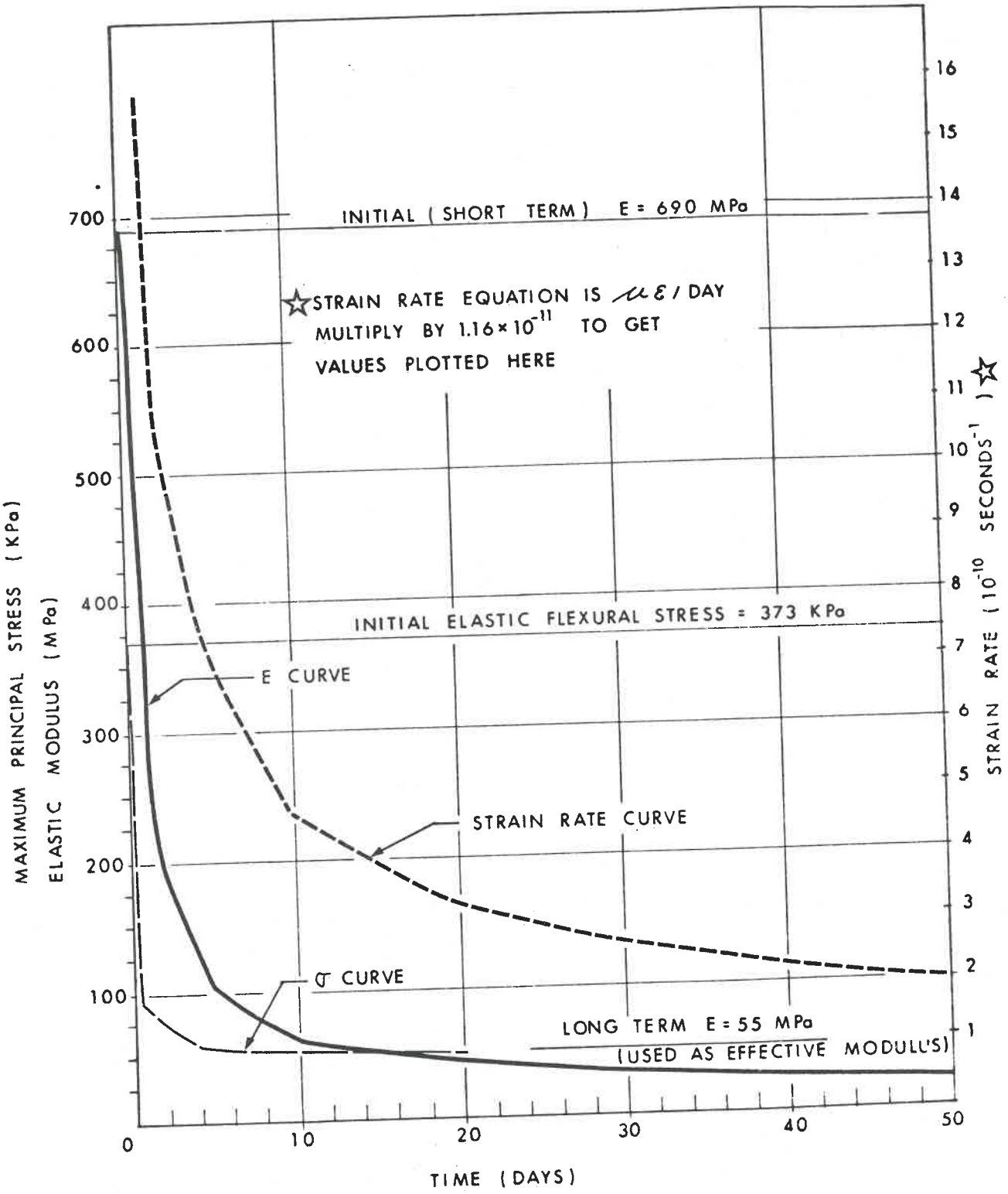

FIGURE 7 ELASTIC MODULUS & MAXIMUM PRINCIPAL STRESS VS TIME CALCULATED FROM MEASURED STRAIN RATES

Discussion

S. Beltaos:

(1) Why was a length of 3 m used as a base length over which the strain was measured? Could one use the same instrumentation to measure strain over smaller base lengths, say, in the order of 0.3 m or so?

(2) The creep law you have used, i.e., $\dot{\varepsilon} = K\sigma^n$, reflects empirical findings with uniaxial - small specimen - tests. This law applies to the so-called secondary creep range, where straight lines have been fitted to strain-time data. However, there is increasing evidence that strain-time curves are nowhere linear and that straight-line fits are only the result of a visual effect near the inflexion point which signifies the onset of tertiary creep. Could the authors comment on this?

D.M. Masterson:

(1) It was desired to measure strain over as long a gauge length as possible, for reasons discussed in the paper. Shorter gauge lengths are possible if the constantan wire is looped back and forth, as in standard gauges. Gauges of 1.5 m length are now being constructed.

(2) The creep law used in the calculations could possibly be improved but the authors had no experimental evidence to support such changes. The ratio of strain to defection has been shown to be a constant and time dependent deflection has been shown to be a proportional to initial stress to the 2.2 power. Thus, for the time being, the exponential form of the creep law is considered satisfactory. Certainly the magnitude of the strains and deflections indicate that the ice is not even approaching tertiary creep.

B. Ladanyi:

Do the curves in your last slide linearize when plotted in a log-log plot? Is that how the time exponent was determined?

D.M. Masterson:

Yes, they are linear on a log-log plot. The exponent is the slope of this curve. The expressions were derived by taking the log of both the independent variable (time) and the dependent variable (strain) and then using linear regression analysis to derive a relationship between the two.

B. Michel:

In your computation of stresses from strain distribution, did you take the temperature distribution into account?

D.M. Masterson:

No, temperature distribution was not taken into account.

D. Nevel:

If one assumes a linear viscoelastic model for the constitutive relation and solves the floating ice sheet problem for secondary creep, the deflections and strains increase as the square root of time. The constitutive relation would predict an increase proportional to time for a uniaxial problem. For the floating ice sheet problem, load from the water pressure changes its distribution as creep occurs. This changing pressure distribution causes the square root of time. In your test you obtain the strain proportional to $t^{.47}$. Hence one might conclude that a linear viscoelastic model for secondary creep would be the constitutive relation.

K.R. Croasdale:

Could you elaborate on your definition of initial stress in ice? Is this the stress at the time when the rig is moved onto the ice platform. How sensitive is the initial stress to the time of rigging up?

D.M. Masterson:

Initial stress is calculated as if the load were applied instantaneously. Normally, it takes about 7 to 10 days to move a rig onto an ice platform and thus the initial deflections are probably the result of elastic and creep deformations combined.

The initial stress would be affected by the rigging up time but observations of deflections during rig up and of load histories lead one to believe that most of the stress relaxation and creep occur after initial rig up. It should be remembered that although rig up takes 10 days, the heavier loads (substructure, drawworks and tower) are placed on the matts within a few hours of each other. The main loads to come later are the mud tanks.

R. Gerard:

Your strain distributions in depth were linear. Is this to be expected with creep taking place?

D.M. Masterson:

Strain profiles may or may not be linear. We had originally thought they would not be but had no way of being sure without measurements.

CONTINUOUS SURFACE STRAIN MEASUREMENTS ON THE SEA ICE CLOSE TO THE ANNUAL ICE RUNWAY, AND ITS ACCESS ROAD, MCMURDO SOUND, ANTARCTICA

D.J. Goodman
Cavendish Laboratory

Summary

Every year, as part of the US Antarctic Research Program, a runway is built on the sea ice close to McMurdo Station, Antarctica. The runway, and its access road, are heavily used during the short resupply months and makes an ideal site for the study of dynamic loading effects on sea ice.

In December 1977 an array of six wire strainmeters were installed next to the access road 1 Km from the runway. Two 120° arrays with 5 m gauge lengths were used. Dispersed wave trains generated by C-130 transport planes (average weight 100,000 lbs) landing and taking off were observed. Waves from passing and static vehicles were also recorded. Sea waves penetrating under the fast ice from the open water 35 Km distant could be seen on the records.

Wire strainmeters were first developed for the observation of earth tides, but have been successfully used since 1974 to measure strain changes on glaciers and sea ice. They use a length of INVAR wire held under constant tension by a lever and weight as a length standard. Rotation of the lever, which is proportional to strain, is detected with an inductive displacement transducer. The instrument has a resolution of 1 in 10^7. In this experiment the output signal was recorded on a FM tape recorder and a data logger. A rezeroing system automatically resets the instrument when it goes outside a preset range.

During the same experiment, another instrument, which is more robust and portable, and has a 1 m INVAR bar as a length standard, was used to measure spectra from waves penetrating under the sea ice at a site further North.

Discussion

P.R. Kry:

What is the order of magnitude of the strain observed due to swell?

D. Goodman:

The strain was of the order of 10^{-6}.

D. Baudais:

How far from the ice edge was swell observed?

D. Goodman:

Swell has been observed from 20 to 35 km from the ice edge. Measurements have also been made when a floe calved across one of the strain meters.

IN SITU DETERMINATION OF CREEP PROPERTIES OF ICE COVERS BY MEANS OF BOREHOLE CREEP AND RELAXATION TESTS

B. Ladanyi, E. Barthelemy and R. Saint-Pierre
Centre d'ingénierie nordique (CINEP)
Ecole Polytechnique de Montréal

Introduction

The evaluation of the bearing capacity of ice covers requires an adequate knowledge of the mechanical properties of ice under field conditions. A conventional way of getting this information consists in taking samples of ice from the cover and testing them, preferably in a field laboratory. The problems usually encountered in using such a method are related

(a) to the size effect, which sometimes requires very large samples and consequently a heavy laboratory equipment,

(b) to the anisotropy and heterogeneity of ice, which requires a large number of samples, and

(c) to the brine drainage in the case of sea ice, which makes it difficult to obtain really undisturbed samples of ice.

An alternative to a field laboratory is the use of an adequate in situ testing method. In the last five years, a number of field methods for determining elastic and short-term strength properties of ice covers have been developed and tested on the site (Croasdale, 1974; Kivisild and Iyer, 1976). As far as in situ creep properties of ice are concerned, it was found recently (Ladanyi and Saint-Pierre, 1978) that the dilatometric method, originally developed for field testing of frozen soils (Ladanyi and Johnston, 1973), can also be used for testing both short and long-term properties of ice covers.

The paper presents a critical review of the method when used for testing an ice cover, and shows some typical results obtained in sea ice. In addition to this borehole creep method using the Ménard pressuremeter, the paper describes also some preliminary results obtained in ice by means of a different type of dilatometer, and using a borehole relaxation method, which has certain interesting advantages over the earlier method, especially in the area of short-term cyclic testing and long-term creep parameter determination.

Pressuremeter Testing of Sea Ice

Ladanyi and Johnston (1973) have shown how the creep properties of ice-rich frozen soils could be determined by means of a stage-loaded creep test performed in a borehole with the Ménard pressuremeter. Essentially the same method was used recently by Ladanyi and Saint-Pierre (1978) and Saint-Pierre (1978) for evaluating the creep properties of a thick sea ice cover.

The field tests were carried out in May 1977 in a small bay close to the community of Igloolik, N.W.T. The thickness of the ice at the site varied between 135 and 155 cm. In spite of relatively large fluctuations of the air temperature during the tests, the surface temperature of the ice, which was under a 30 to 60 cm thick hardened snow cover, remained virtually constant, at about -7°C. The temperature increased linearly with the depth up to -2.1°C at the bottom of the ice.

Systematic measures of salinity on the cores and crystallographic analyses on thin sections of ice were made on the site (Murat, 1977). The analyses showed that the ice was columnar-grained of S2 type and that its salinity varied with depth following a usual pattern shown in Fig. 1.

As most of the tests were performed at a depth about 50 cm below the surface of the ice, these measurements lead to the conclusion that, at that particular level, the ice was of S2 type with the size of grains of about 1.5 cm^2, its temperature about -4°C and salinity about 4.1 ‰.

The boreholes for the tests were drilled with a gasoline driven CRREL - type ice core drill, able to make 76 mm diameter holes and to take 50 mm diameter ice cores.

As shown by Ladanyi and Johnston (1973), a pressuremeter study of mechanical properties of frozen soil requires usually the performance of three different types of tests. In the described study of the sea ice, a total of 21 tests were performed, 11 of which were short-term tests, 6 stage-loaded creep tests, and 4 one-stage long-term creep tests. In most of the stage-loaded tests, the length of each stage was 15 min, with only one exception of a test with 30 min per stage. The creep times in one-stage tests varied from 75 to 720 min.

Results

As the interpretation method for short and long-term pressuremeter tests has been described in detail in two previous papers (Ladanyi and Johnston, 1973; Ladanyi and Saint-Pierre, 1978) it will not be repeated here.

Essentially, a short-term pressuremeter test furnishes a pressuremeter curve, such as the one shown in Fig. 2, from which it is possible to determine:

(1) Short-term deformation modulus in compression,

(2) Plane-strain compression strength,

(3) Tensile strength, and

(4) Stress-strain curve in compression.

It should be noted that the final one is not very reliable in brittle materials such as ice in a short-term test, because it is strongly affected by intermittent radial cracking around the borehole.

From the short-term pressuremeter tests performed in the sea ice cover at Igloolik, the following values of the above parameters have been found:

(1) Static deformation modulus in compression:
$96 \leq E_p \leq 212$ MPa, average: 157 Mpa;

(2) Peak plane-strain compression strength:
$1.35 \leq q_{ps} \leq 3.7$ MPa, average: 2.45 Mpa;

(3) Corresponding total failure strain:
$0.70 \leq \varepsilon_f \leq 4.18\%$, average: 2%;

(4) Lateral tensile strength:
$0 \leq T_s \leq 3.52$ MPa, average: 1.19 MPa.

These values are well within the limits quoted in the literature for the same parameters of sea ice obtained under comparable conditions, as shown by Ladanyi and Saint-Pierre (1978).

As far as the creep parameters are concerned, they are the ones appearing in the general creep equation adopted for the interpretation of the pressuremeter creep tests:

$$\varepsilon_e^{(c)} = (\dot{\varepsilon}_c/b)^b \, (\sigma_e/\sigma_c)^n \, t^b \qquad (1)$$

where $\varepsilon_e^{(c)}$ and σ_e are the equivalent creep strain and the equivalent stress, $\dot{\varepsilon}_c$ is a reference strain rate, and σ_c the corresponding reference stress (also called "creep modulus"), and t is the time. The three creep parameters that can be found from a stage-loaded pressuremeter creep test are the creep modulus σ_c and the two exponents, b and n.

The values of the three parameters, determined from six stage-loaded creep tests within the pressure range of 1 to 3 MPa, lead to the following conclusions:

- The exponent b shows an increase with increasing pressure from about 0.22 to 1.00, which means that steady state creep is approached at higher pressures. In addition, b has a tendency to slightly decrease with time in long-term creep tests (Fig. 3).

If the three parameters are determined from the four most reliable stage-loaded creep tests, the following intervals and average values are obtained:

$0.706 \leq b \leq 0.805$, average: 0.785;

$2.048 \leq n \leq 2.175$, average: 2.106;

$0.184 \leq \sigma_c \leq 0.634$ MPa, average: 0.394 MPa,

for $\dot{\varepsilon}_c = 10^{-5}$ min^{-1}.

As there are very few published data on creep tests performed on the sea ice in horizontal direction, a comparison with other sources is very difficult at this moment. It should nevertheless be noted that the range of n values obtained in these tests compares well with n values found recently by Tinawi and Murat (1978) who performed a large number of flexural creep tests on beams and plates of saline ice at -10°C.

As mentioned by Ladanyi and Saint-Pierre (1978), once the creep parameters are available, one can deduce from Eq. (1) an equation of the constant-strain-rate stress vs creep-strain curve in the form

$$(\sigma_1-\sigma_3) = \sigma_c \, (\dot{\varepsilon}_1/\dot{\varepsilon}_c)^{b/n} \, \varepsilon_1^{(1-b)/n} \qquad (2)$$

to which the elastic portion of strain

$$\varepsilon_1^{(e)} = (\sigma_1-\sigma_3)/E_p \qquad (3)$$

should be added to get the complete stress-strain curve for ice. Substitution in Eqs. (2) and (3) of the average creep parameters for sea ice quoted previously, yields

$$(\sigma_1-\sigma_3) = 28.7885\ (\dot{\varepsilon}_1)^{0.3727}(\varepsilon_1)^{0.1021} \qquad (4)$$

and

$$\varepsilon_1^{(e)} = (\sigma_1-\sigma_3)/157 \qquad (5)$$

The resulting stress-strain curves for $\dot{\varepsilon}_1 = 10^{-2}$, 10^{-3} and 10^{-4} min^{-1} are shown in Fig. 4. It is clear that they remain valid only up to the creep failure strain, which was found to be about 0.7%, so that the calculated stress-strain curves have finally an approximate shape such as shown in Fig. 4 by full lines. Their peaks correspond to the strength equation

$$(\sigma_1-\sigma_3)_f = 17.347\ \dot{\varepsilon}_1^{0.3727} \qquad (6)$$

obtained by substituting $\varepsilon_1 = 0.007$ in Eq. (4), and are at 3.12, 1.32 and 0.56 MPa, respectively. The post-peak portion of the curves, which depends on the loading system, is only approximately indicated in the figure.

Dilatometer Testing of Fresh Water Ice

The experience gained up to now with the Ménard pressuremeter in frozen soils and ice has shown that the particular apparatus is quite convenient for determining the short and medium term creep properties of these materials in situ. It is a simple hydraulically operated system that can, with some minor adjustments, be used even at very low temperatures. The pressuremeter has, however, been primarily designed for performing tests with a steadily increasing load, such as in stage-loaded creep tests, and becomes quite cumbersome to operate when one wants to carry out either short-term cyclic, or long-term stress-relaxation tests. The last two types of tests are clearly quite important because the former can furnish a true static Young's modulus at any strain level, while the latter has a great potential for studying the creep properties of frozen soils and ice at low stress

levels and at long periods of time, which is not possible in pressuremeter creep tests because of limited volume increase of the cell.

For that reason it was decided to investigate the potential of another type of dilatometer for testing ice and frozen soils. The second type of dilatometer, known as the CSM cell, is a borehole device developed at the Colorado School of Mines (Hustrulid, 1973) principally for determining the modulus of rigidity of rock. Like the pressuremeter, the CSM cell is also hydraulically operated, but otherwise differs in several aspects from the former. The CSM dilatometer has only one cell, made of a 3.8 cm diameter and 16.5 cm long adiprene membrane mounted on a central steel shaft. The membrane can be extended or contracted by a manually operated high pressure generator with vernier indicator. The whole system is rated at a pressure capacity of 70 MPa, which is about 7 times higher than the conventional pressuremeter. Originally, in rock, the membrane was supposed to be extended by only one filling of the pressure cylinder, which is about 30 cm^3. This corresponds to about 7.8% increase in diameter. In the present tests, it was found that the membrane can be extended up to 2 or even 3 times that volume (i.e., up to 15 or 22% increase in diameter) without danger of bursting or loosing its cylindrical form. The whole hydraulic system is made of stainless steel tubing, and is relatively rigid (it extends about 0.12 cm^3 per 1 MPa), which makes it very convenient for borehole relaxation testing of materials much weaker than rock, such as ice and frozen soils. It is clear that, before any test is made in the borehole, the system should be calibrated to determine the volume correction, as described by Hustrulid (1973), and the membrane resistance correction, which is done by expanding the membrane outside the hole. Both of these corrections are slightly temperature dependent.

While in a pressuremeter test the pressure is usually increased in steps and kept constant at each level for a selected length of time, during which the volume increase of the cell is recorded. In a CSM test, the volume of the cell is increased in steps and, at each step, the drop of stress with time is recorded by reading a Bourdon gauge, or by a pressure transducer. Similarly as with the pressuremeter, one can then perform with the CSM cell several kinds of tests: rapid stage-strained tests, with one or two minutes per stage, slow tests with, say, 15-30 min relaxation per stage, or one-stage relaxation tests, in which the membrane is rapidly extended to a given volume, after which the stress is left to relax for a given time. The last type of test has an obvious advantage over the corresponding one-stage

constant-stress borehole creep test, because it is not limited in time by the limited membrane extension. In principle, under favorable borehole conditions, one can leave the cell in the hole and record the pressure relaxation automatically for a whole year or more.

In this investigation only some preliminary tests of that kind were made by a CSM cell in fresh water ice under laboratory conditions, (Barthélémy, 1979). For that purpose, several cylinders of ice were produced by freezing in a cold room at -5°C ordinary tap water in a 21 inch (53.54 cm) diameter steel tank. As the tests in all the cylinders gave similar results, only one of them (No. I) will be described here in some detail.

The ice cylinder I was 40 cm thick and was frozen in four layers of 10 cm within a week. After freezing, the cylinder was taken out from the tank and a vertical hole of 3.95 cm diam. was drilled through its centre.

The dilatometer test carried out in this cylinder consisted of 12 volume-increase steps, each of which was followed by a stress relaxation of 16 minutes with stress readings of 0.25, 0.5, 1, 2, 4, 8 and 16 min. The cracking noises were noted rather early in the test and the cylinder cracked in two halves at the 13th loading stage, when the total hole diameter increase attained about 3 per cent (Fig. 5). Figure 6 shows the results of this test in a plot similar to that of Fig. 2. The figure shows the determination of the contact volume V_{mo} and a set of pressure-volume curves at constant relaxation times. Figure 7 shows a set of relaxation curves in a log pressure vs log time plot with the strain measure, $\ln (V/V_o) \approx \Delta V/V \approx \gamma \approx 2\varepsilon_1$, as the parameter. Finally, Fig. 8 shows a set of isochronous stress-strain curves, deduced from the curves in Fig. 6 in the same manner as in the case of short-term pressuremeter tests.

Interpretation of Borehole Relaxation Tests

One of the simplest ways for interpreting the borehole relaxation tests is by considering the curves in Fig. 6 as a set of isochronous pressure-volume curves that can be treated in the same manner as the conventional pressuremeter curves. By using the method for short-term tests described by Ladanyi and Johnston (1973) one can then easily deduce from each of these curves (a) the initial modulus of deformation E_p, from the slope of the tangent passing through the true origin 0', and the whole stress-strain curve up and behond the peak point.

The resulting E_p-values, calculated from the formula, valid for a thick cylinder,

$$E_p = 2(1+\nu)\ \lambda\ (\Delta p_i/\Delta V)(V_o+\Delta V) \qquad (7)$$

where p_i is the internal pressure, V_o the initial volume of the cavity, and

$$\lambda = [1+(1-2\nu)(r_i/r_o)^2]/[1-(r_i/r_o)^2], \qquad (8)$$

as shown in Fig. 7. The calculation was made with the Poisson ratio $\nu = 0.5$.

Figure 8 shows the resulting isochronous stress-strain curves. The curves have a peak ($q = q_f$) at about $\varepsilon_1 = 1.5\%$, which coincides with the first cracking noise, while the total failure of the cylinder occurred at about $\varepsilon_1 = 2.6\%$. The peak strengths q_f are plotted also in Fig. 7 as a function of time, and it is found that both E_p and q_f decrease with time following approximately a power law with negative exponent of less than unity.

On the other hand, the deduction of creep parameters from a dilatometer relaxation test is much less simple than from a pressuremeter creep test. This is essentially so because, in the case of relaxation, a proper analysis of data requires also an accurate knowledge of the initial elastic state.

The solution of a relaxation problem in a kinematically determinate case can be obtained by stating that at any point the total displacement, equal to the sum of the elastic and the creep displacements at that point, should remain constant with time or, alternatively, that the sum of elastic and creep displacement rates should be zero. Using this method and a power-law creep equation such as Eq. (1), Spence and Hult (1973) have obtained exact relaxation solutions for certain kinematically determinate structures, including a hollow sphere. Corresponding solutions for a cylindrical cavity can also be found without difficulty, as will be shown in another paper.

Unfortunately, these exact solutions are not easily adaptable to the inverse problem of finding creep parameters from relaxation data. The latter problem can be solved by an approximate method, similar to that used by Vyalov and Ermakov (1966) for compression testing of ice.

According to the time hardening creep theory, a creep process can be expressed by a family of isocurves (Rabotnov, 1966), given by

$$\phi(\varepsilon) = \sigma \cdot \Psi(t) \tag{9}$$

where $\phi(\varepsilon)$ is a strain function, σ is stress and $\Psi(t)$ is a time function. For including the instantaneous response, it is required that $\Psi(0) = 1$. According to this creep theory, the stress relaxation is then given by

$$\sigma = \phi(\varepsilon)/\Psi(t) \tag{10}$$

If, however, one wants to retain the same form of the time function as that contained in Eq. (1), the condition $\Psi(0) = 1$ cannot be satisfied, but should be replaced by $\Psi(t_o) = \text{const}$, where t_o is a very short time interval in which the response of the structure is taken to be non-linear elastic. This assumption implies that, at any point and time, the total strain is equal to the sum of a pseudo-elastic strain, corresponding to t_o, and a creep strain, corresponding to t, where t is the real time. Adopting the same strain measure as in Ladanyi and Johnston (1973), one can then write Eq. (9) for a cylindrical cavity expansion case:

$$[\ln(V/V_o)]^{1/n} = [(p_c-p_o)/\sigma_c]\alpha^{1/n}\beta^{b/n}(t_o+t)^{b/n} \tag{11}$$

and the family of relaxation curves is then defined by

$$(p_c-p_o) = \sigma_c\left[\frac{\ln(V/V_o)}{\alpha\beta^b(t_o+t)^b}\right]^{1/n} \tag{12}$$

where

$$\alpha = 2(\sqrt{3}/2)^{n+1}(2/n)^n \tag{13}$$

and

$$\beta = (\dot{\varepsilon}_c/b) \tag{14}$$

while p_c and p_o denote the corrected pressure in the cavity and the original lateral stress, respectively.

If the relaxation curves are plotted against the real time t instead of (t_o+t), as in Fig. 7, they come close to Eq. (12) only when $t >> t_o$.

For example, if one takes t_o = 0.1 min, at the end of any 16 min interval, t_o is only about 0.6% of t, and the curves are sufficiently accurate for parameter determination.

It will be seen from Eq. (11) that, when such relaxation curves are plotted in a log (p_c-p_o) vs log t plot with the strain ln (V/V_o) as the parameter, their slope at the end of interval gives

$$\frac{b}{n} = -\frac{\Delta \log (p_c-p_o)}{\Delta \log\, t} = \frac{v}{h} \qquad (15)$$

On the other hand, if at the same end of interval, where $t = t_1$ = const (t_1 = 16 min in Fig. 7) one plots $\log[\ln(V/V_o)]$ vs $\log(p_c-p_o)$, as shown superimposed in Fig. 7, the slope of the line gives

$$n = \frac{\Delta \log[\ln(V/V_o)]}{\Delta(\log(p_c-p_o)} = \frac{h_1}{v_1} \qquad (16)$$

When b and n are known, one can get, for any selected reference rate $\dot{\varepsilon}_c$, the value of σ_c from any point $t = t_i$ on a relaxation line, corresponding to a strain $\ln(V/V_o)_k$, from

$$\sigma_c = (p_c-p_o)_i \left[\frac{\alpha\, \beta^b t_i^b\, \lambda_c}{\ln(V/V_o)_k}\right]^{1/n} \qquad (17)$$

The symbol λ_c in Eq. (17) denotes the correction coefficient if the test is performed in a finite cylinder, and is given by

$$\lambda_c = [1-(r_i/r_o)^{2/n}]^{-n} \qquad (18)$$

For a test in a large ice cover, $\lambda_c = 1$.

Using this type of analysis of relaxation curves in Fig. 7, it is obtained:

(a) In the low strain region, i.e. for $\ln(V/V_o) < 2.48\%$ (or $\varepsilon_1 < 1.24\%$):
b = 0.1388, n = 1.095, and
σ_c = 63.39 MPa at $\dot{\varepsilon}_c = 10^{-5}\text{min}^{-1}$.

(b) In the middle strain range, i.e. for $2.48 < \ln(V/V_o) < 3.63\%$:
b = 0.28, n = 1.75, and
σ_c = 7.49 MPa at $\dot{\varepsilon}_c = 10^{-5}\text{min}^{-1}$

(c) In the high strain region, i.e. for $\ln(V/V_o) > 3.63\%$ (or $\varepsilon_1 > 1.8\%$): $b = 0.4247$, $n = 2.40$, and $\sigma_c = 2.60$ MPa at $\dot{\varepsilon}_c = 10^{-5}\text{min}^{-1}$.

These results confirm the usual finding that in ice the exponent n tends to increase with the stress level, varying from over 1 to about 3. The values of exponent b also increase in the same sense, but remain in these relaxation tests much below the usual level found in the pressuremeter creep tests, which may be due to the much lower strain level in the former tests.

Conclusions

On the basis of a field investigation of a sea-ice cover with the pressuremeter, and a laboratory study of fresh-water ice with a borehole dilatometer, it is concluded that both of these methods show promise for field determination of deformation, strength and creep properties of ice covers. Each of the two methods has, however, its particular optimum range of application: the Ménard pressuremeter for the determination of short-term strength and medium-term creep properties, and the CSM dilatometer for performing short-term cyclic and long-term relaxation tests.

Acknowledgments

The authors wish to acknowledge the financial support of the Department of Education of Québec and the National Research Council of Canada.

References

Barthélémy, E. (1979). Utilisation du dilatomètre CSM dans la roche et dans la glace. Mémoire M.Sc.A., Dép. de génie minéral, Ecole polytechnique, Montréal.

Croasdale, K.R. (1974). Crushing strength of Arctic ice. In "The Coast and Shelf of the Beaufort Sea", Arctic Ins. of North Am., (J.C. Reed and J.E. Sater, Eds), pp. 377-399.

Hustrulid, W.A. (1975). The CSM cell - A borehole device for determining the modulus of rigidity of rock. Proc. 15th U.S. Symp. on Rock Mech., South Dakota, 1973, pp. 181-225.

Kivisild, H.R. and Iyer, S.H. (1976). In situ tests for ice strength measurements. Ocean Engrg., Pergamon Press, Vol. 3, pp. 329-342.

Ladanyi, B. and Johnston, G.H. (1973). Evaluation of in situ creep properties of frozen soils with the pressuremeter. Proc. 2nd Int. Conf. of Permafrost, Yakutsk, North Am. Contrib., Nat. Acad. of Sciences, Washington, pp. 310-318.

Ladanyi, B. and Saint-Pierre, R. (1978). Evaluation of creep properties of sea ice by means of a borehole dilatometer. Proc. IAHR Symp. on Ice Problems, Luleå, Sweden, Part I, pp. 97-115.

Murat, J.-R. (1977). Compte-rendu du voyage d'étude du CINEP à Igloolik (T.N.O.), Centre d'ing. nordique, Ecole Polytechnique, Mai 1977.

Rabotnov, Yu.N. (1966). Creep problems in structural members. Translated from Russian. North-Holland Publ. Co. 1969.

Saint-Pierre, R. (1978). Determination des propriétés mécaniques de la glace marine par l'essai pressiométrique. Mémoire M.Sc.A., Dép. de génie civil, Ecole Polytechnique, Montréal, 90 pages, 46 fig.

Spence, J. and Hult, J. (1973). Simple approximations for creep relaxation. Int. J. Mech. Sci., Pergamon Press, Vol. 15, pp. 741-755.

Tinawi, R. and Murat, J.-R. (1978). Sea Ice - Flexural Creep. Proc. 4th IAHR Symp. on Ice Problems, Luleå, Sweden.

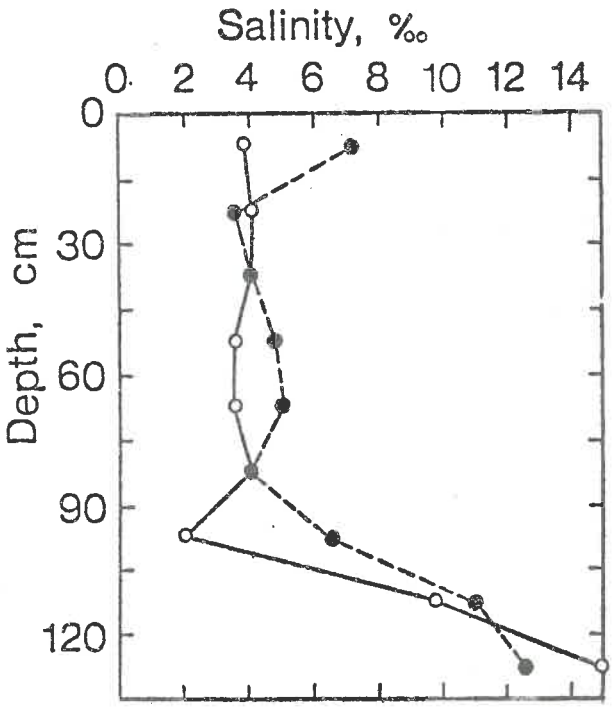

FIGURE 1. SALINITY PROFILES OF THE ICE SHEET AT THE IGLOOLIK TEST SITE. (AFTER MURAT, 1977).

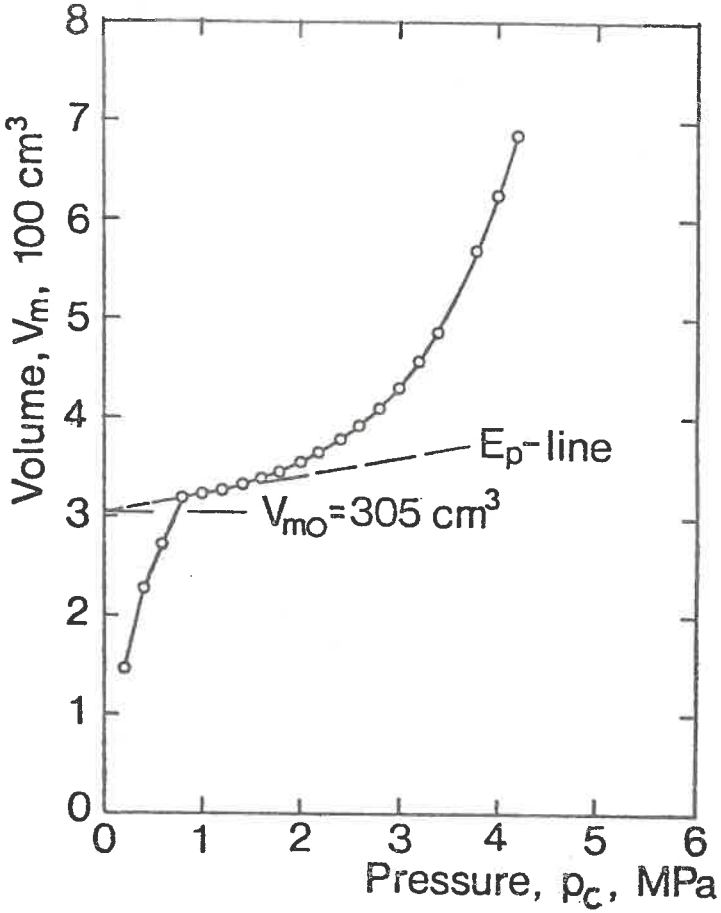

FIGURE 2. PRESSUREMETER CURVE OBTAINED IN A 1.50 M THICK SEA ICE COVER . (AFTER LADANYI AND SAINT-PIERRE, 1978).

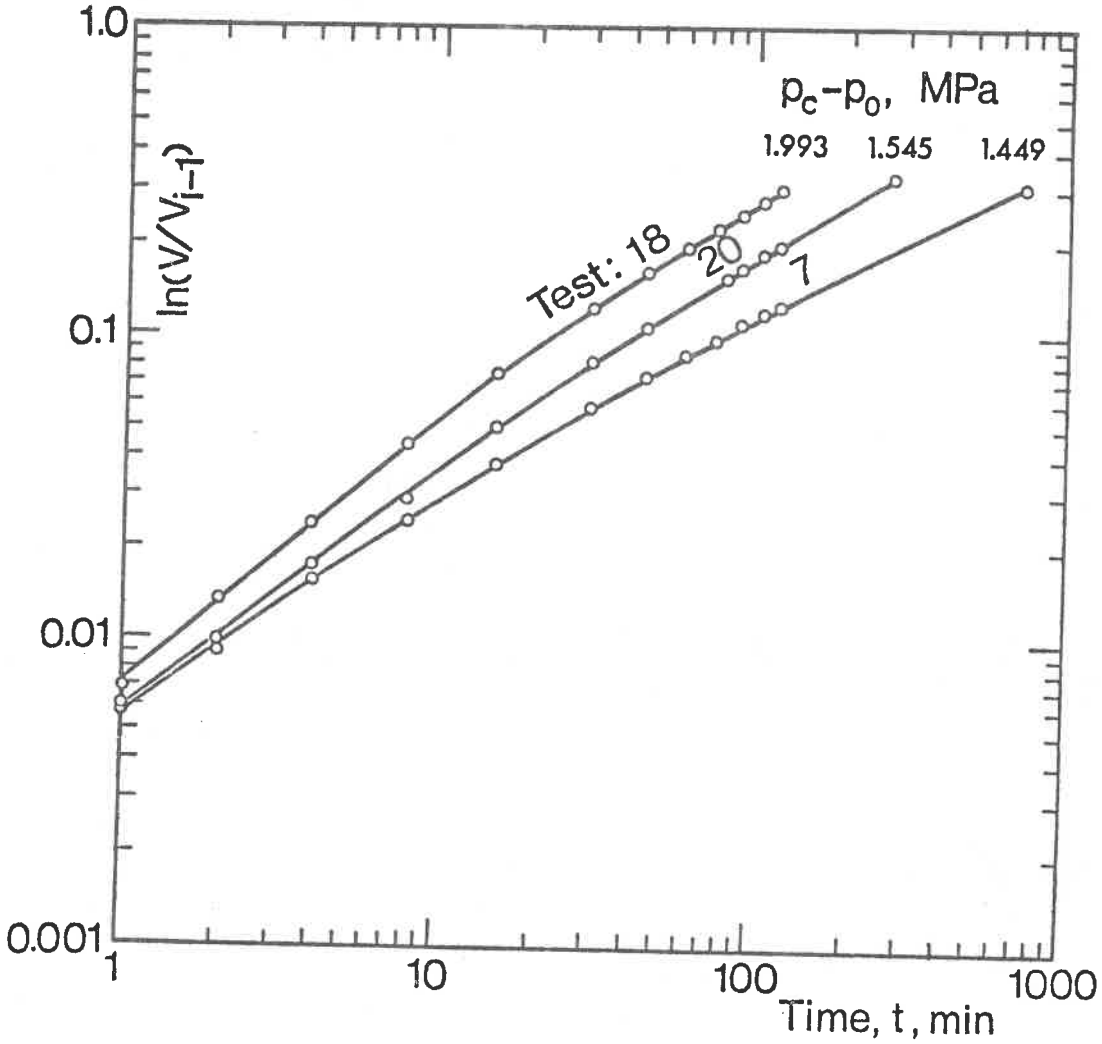

FIGURE 3. ONE-STAGE PRESSUREMETER CREEP CURVES OBTAINED IN A SEA ICE COVER. (AFTER LADANYI AND SAINT-PIERRE, 1978).

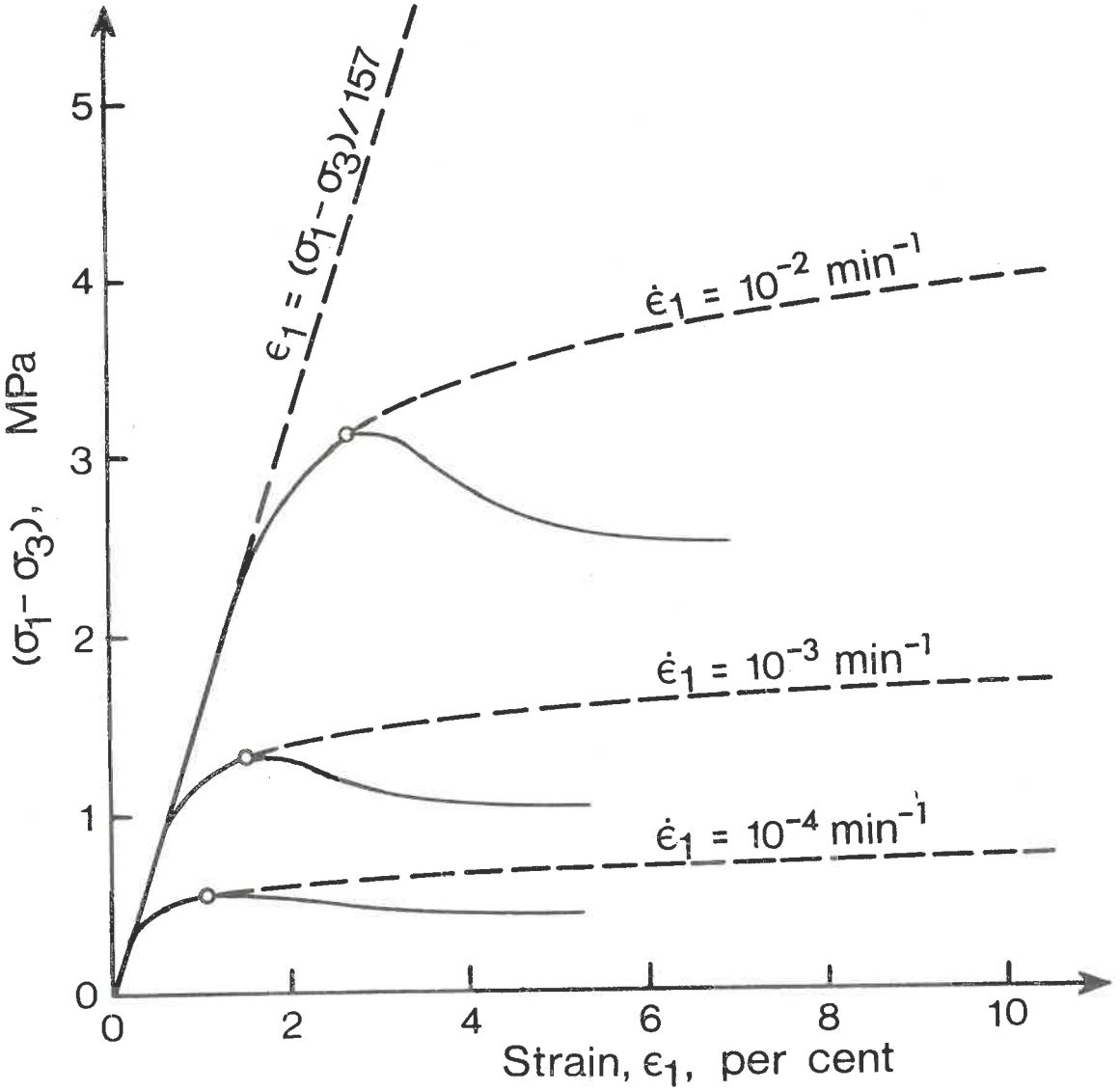

FIGURE 4. STRESS-STRAIN CURVES FOR SEA ICE CALCULATED FROM PRESSUREMETER CREEP DATA, TEMPERATURE -4° C.

FIGURE 5. FAILED FRESH WATER ICE CYLINDER AFTER A DILATOMETER TEST.

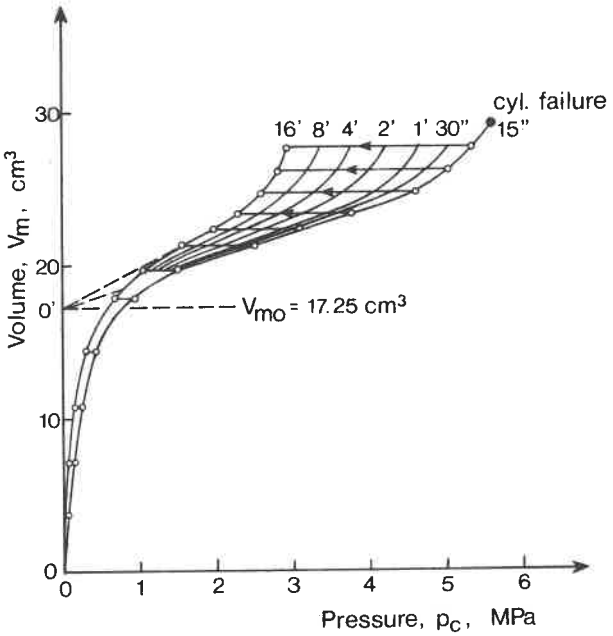

FIGURE 6. DILATOMETER RELAXATION TEST IN A FRESH WATER ICE CYLINDER: PRESSURE-VOLUME CURVES AT CONSTANT RELAXATION TIMES. TEMPERATURE -5° C.

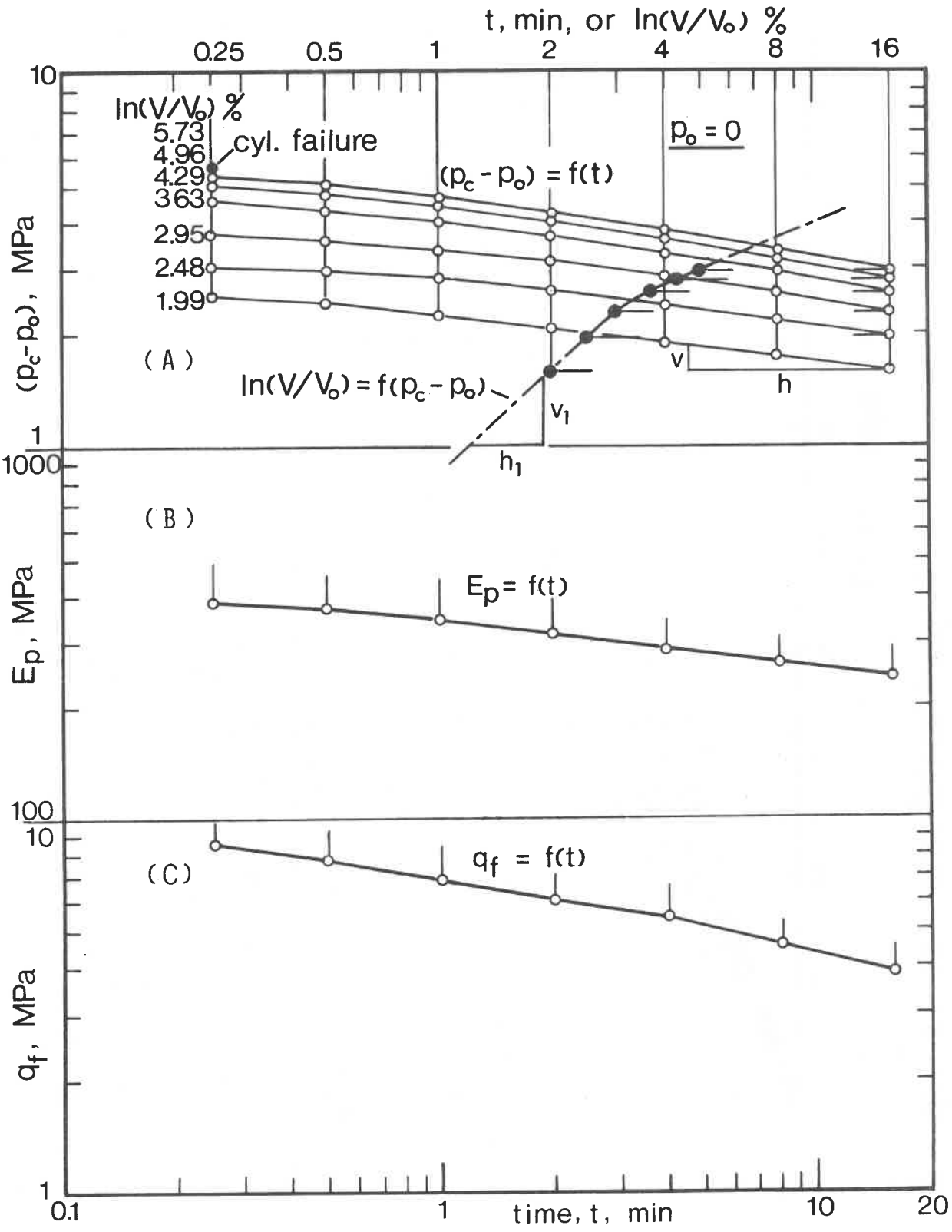

FIGURE 7. DILATOMETER TEST IN A FRESH WATER ICE CYLINDER: (A) RELAXATION CURVES, (B) AND (C) VARIATION OF DEFORMATION MODULUS E_p AND COMPRESSION STRENGTH q_f WITH TIME.

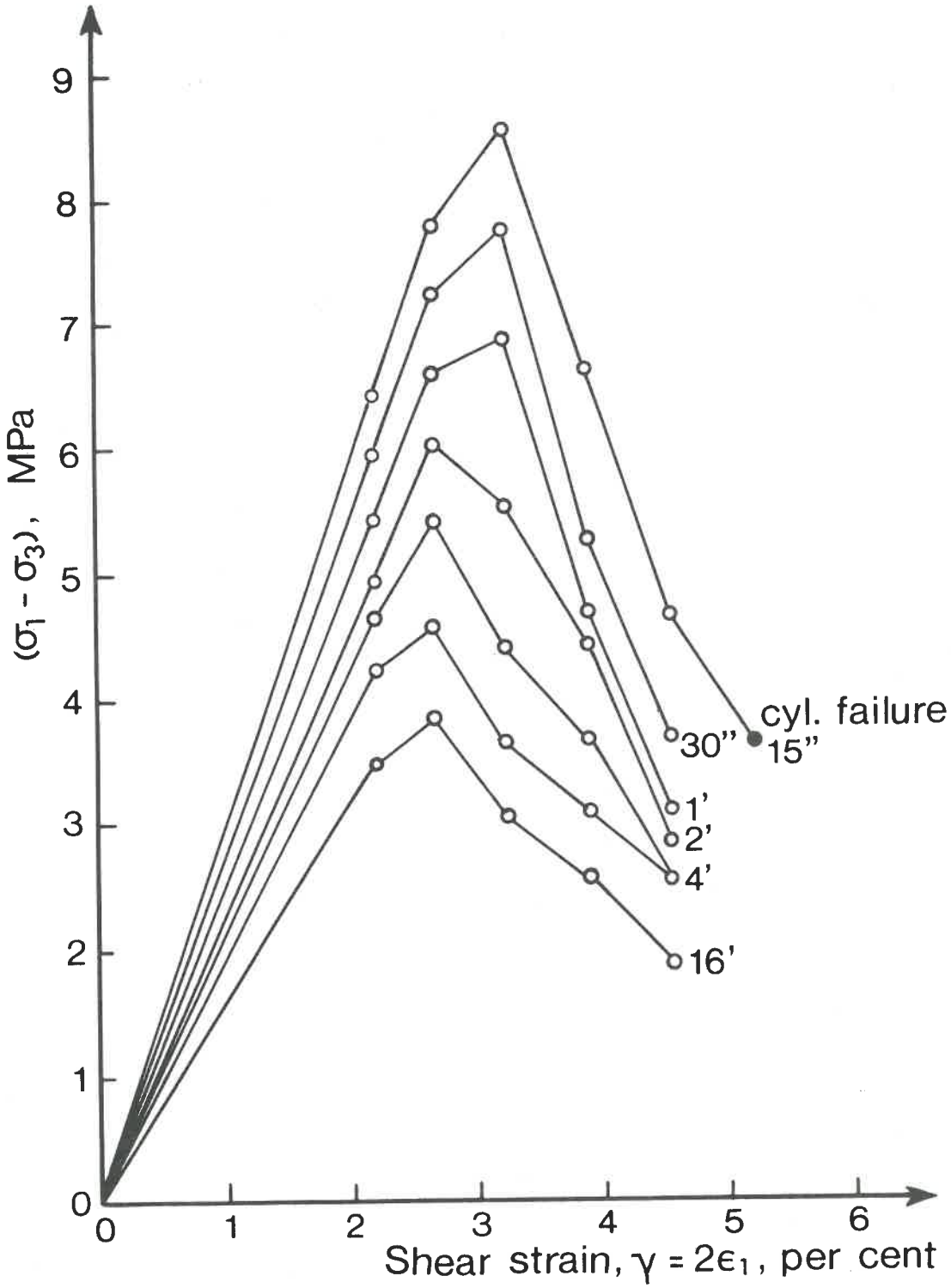

FIGURE 8. DILATOMETER RELAXATION TEST IN A FRESH WATER ICE CYLINDER: STRESS-STRAIN CURVES AT CONSTANT RELAXATION TIMES.

Discussion

S. Beltaos:

My experience with prototype load bearing capacity tests is that a small-scale test giving a measure of the time-dependent behaviour of the ice sheet, would be very useful. Your method seems to be one possible way of doing this. Could you comment on

(1) how easy is your test to set up and carry out in the field?

(2) how variable would the test results be from, say, ten tests carried out simultaneously on the same ice sheet?

B. Ladanyi:

(1) Both the pressuremeter and the CSM-Cell test require essentially a carefully drilled smooth borehole with the diameter a little larger than the probe. For that purpose, in ice, a light hand-held gasoline ice-core drill is usually sufficient. All the equipment is easily transportable, but the CSM-Cell system is much lighter and easier to use than the pressuremeter, mainly because it does not require the compressed gas bottle. We have carried the equipment to the site on a snowmobile-driven sled. All the work can be done by two persons but, once the probe is in place, one person can easily handle all the loadings and readings. In good conditions, one can make up to five short-term tests per working day, but for long-term tests the equipment may be held in place for several days.

(2) If all the ten tests are made in a relatively small area, say, 3 m from one another, and at the same level, the variation of certain properties, such as the modulus E, the short-term compression strength q_f, and the creep parameters is not very large. However, there is usually a large variation of the tensile strength, which sometimes falls to zero, because of the presence of previous vertical cracks in ice around certain boreholes.

B. Michel:

Although the borehole dilatometer seems very simple to operate and gives very interesting results, I wonder about its applicability to ice engineering. If it is used to understand creep behaviour of ice, then I submit it must be hard

to interpret, as step load increases will not give the same results in ice as a constant strain rate test. Furthermore the area of interest for ice engineers is the area of ice yielding when primary creep equations can not be used any more for interpretation. Finally, the dilatometer operates over a certain length where the ice properties vary very much in function of ice temperature, crystal sizes and brine volume. Could you answer these various questions?

B. Ladanyi:

(1) It is true that a step-loaded test gives a different stress-strain behaviour of ice than a constant-strain-rate test. The stress-strain curves deduced from a short-term pressuremeter test and a CSM-Cell test, respectively, will not be the same, because the former is a step-loaded test, and the latter an approximately constant-strain-rate test. They are, nevertheless, expected to give comparable peak strengths for the same times to failure. In addition, as shown in the paper, the creep data deduced from a long-term pressuremeter test enable the constant-strain-rate curves to be calculated for any given rate within the time span covered by the tests.

(2) The purpose of the tests we have made in ice up to now was to describe its behaviour under load under reasonably short-term to long-term conditions. Since the ice fails usually at very low strains, the equipment, as it is now, can fail the ice within one or two minutes, but this can be made even shorter if the loading and recording system is mechanized. For example, if the piston of the CSM-Cell is made to move at a steady rate, it will produce the kind of constant-strain-rate test you are talking about.

(3) The length of the measuring portion of both the pressuremeter and the CSM-Cell is about 20 cm. However, the total length of the latter is smaller and there is no difficulty in making the tests at different levels in a thick ice cover or in testing ice covers that are not much thicker than the total length of the cell, i.e., 25 or 30 cm. In addition, if needed, one can have even a shorter cell made, provided the same length to diameter ratio of about 4 to 5 is retained.

GRAIN-SIZE INFLUENCE ON EFFECTIVE MODULUS OF ICE

N.K. Sinha
Division of Building Research
National Research Council of Canada

Introduction

Floating ice sheets are often used for landing aircraft and other transportation related purposes in cold environments. Ice platforms are also increasingly being used as working spaces for construction purposes as well as for offshore exploratory drilling. These are just a few of many examples which indicate that ice covers are subjected to loading for times ranging from a few fractions of one second to a few months.

Several analytical, as well as finite element techniques, have been used with varying degrees of success to solve bearing capacity problems (Nevel, 1976; 1978; Vaudrey and Katona, 1975). Each analysis must assume an appropriate constitutive creep equation for ice. The constitutive equations must be sufficiently general to account for all the observed creep properties, preferably under both biaxial and triaxial stress conditions. These equations must include not only the effects of all the external variables, such as stress, temperature, time and strain rate, but should also take into account the influences of internal variables such as distribution and size of grains, isotropy and anisotropy in the grain structure and in crystallographic orientation, and impurities and inclusions such as air bubbles, brine, etc.

A simple viscoelastic model was proposed by Sinha (1978a), which explained satisfactorily the various aspects of creep in ice (Sinha, 1977; 1978b), particularly the effects of external variables mentioned previously for a given grain size. This model was developed to have a suitable and realistic framework into which the influences of internal variables could be introduced, as they became better known. One such variable, grain size, has now been introduced in this model. The purpose of this report is to present briefly the physical basis of this modified model and discuss its applicability. An effort has been made to provide continuity with earlier reports by emphasizing those aspects of creep in ice that could not be dealt with previously.

Viscoelasticity of Polycrystalline Materials

When subjected to creep under constant load, polycrystalline ice exhibits an initial elastic deformation followed by a delayed elastic effect, a steady state and, finally, an accelerating flow. The flow properties were observed to be extremely sensitive to stress, temperature and type of ice.

Creep of polycrystalline ice is part of a larger field of study - creep of materials at elevated temperatures. A better appreciation of the deformation behaviour of ice can be obtained by comparing its properties with those of other materials with similar grain structures, at similar homologous temperatures and under comparable stresses.

When a single crystal is stressed, it responds immediately because of the distortion of crystal lattices. Elastic response of a single crystal is described by a number of elastic moduli corresponding to the different lattice planes. Polycrystalline materials, on the other hand, exhibit a mixed single crystal elastic response. Thus the elastic response of an isotropic polycrystalline material (usually represented as Young's modulus, shear modulus, etc.) represents an average of the corresponding elastic moduli of a single crystal.

Creep in single crystals is governed by the stress induced and the thermally activated mobility of point or line defects. Shear or sliding at or near the grain-boundary regions introduces additional complexities to the creep of polycrystalline materials at high temperatures, particularly in the range important to ice engineering problems.

Several attempts have been made in the last quarter century to devise methods of determining grain-boundary displacements in materials during creep, and thereby predict the contribution of grain-boundary sliding to the total strain. These experiments have provided a wealth of information on sliding aspects of creep in metals, alloys and metallic oxides at high temperatures. No constitutive equation has been formulated, however, to describe the dependence of sliding on grain size and external variables.

The present author hypothesized that a degree of reversibility in the sliding processes, including its accommodation, might be associated with the delayed elasticity. This elastic effect in ice of known grain size was experimentally investigated and formulated by this author, (Sinha, 1978a), but no information is yet available on the intergranular displacements in polycrystalline ice. An indirect approach was then taken to correlate the delayed elastic

strain to the strain due to the grain-boundary sliding. The result was the development of a mathematical model capable of explaining satisfactorily all the observed dependence of sliding on stress, time, strain, temperature and grain size in other materials. This analysis also assisted in introducing the influence of grain size on the creep of polycrystalline materials at elevated temperatures including that of ice (Sinha, 1978c). For the purpose of this article, it is thought sufficient to describe the creep equation directly without detailing its development any further.

Viscoelastic Equation

The total strain, ε_t, at time, t, in pure randomly oriented, polycrystalline ice of average grain size, d, subjected to an uniaxial stress, σ, at a temperature, T, is given by

$$\varepsilon_t = \frac{\sigma}{E} + c_1 \left(\frac{d_1}{d}\right) \left(\frac{\sigma}{E}\right)^s [1 - \exp\{-(a_T t)^b\}] + \dot{\varepsilon}_{v_1} t \left(\frac{\sigma}{\sigma_1}\right)^n \quad (1)$$

where E is Young's modulus, nearly equal to 10 $GN \cdot m^{-2}$; $\dot{\varepsilon}_{v_1}$ is the viscous strain rate for unit stress, σ_1; c_1 is a constant corresponding to the unit grain size, d_1; b, n and s are constants; a_T is a constant at a given temperature. The constant n represents the usual stress exponent for viscous flow; s is implied as the stress exponent for delayed elasticity or grain-boundary sliding.

Both $\dot{\varepsilon}_{v_1}$ and a_T are dependent on temperature, such that

$$\dot{\varepsilon}_{v_1}(T_1) = \frac{\dot{\varepsilon}_{v_1}(T_2)}{S_{1,2}} \quad (2)$$

and

$$a_T(T_1) = \frac{a_T(T_2)}{S_{1,2}} \quad (3)$$

where $S_{1,2}$ is a shift function, given by

$$S_{1,2} = \exp\left\{\frac{Q}{R}\left(\frac{1}{T_1} - \frac{1}{T_2}\right)\right\} \quad (4)$$

where Q and R are the activation energy and gas constant respectively; T_1 and T_2 are temperatures in the Kelvin scale.

Preliminary studies indicate that s is close to unity and this value will be maintained here. The constant c_1 in equation (1) replaces the coefficient c used in the previous reports (Sinha, 1977; 1978b) and its numerical value has been changed (Sinha, 1978c) in order to accommodate the introduction of grain size in a demensionless form in the delayed elastic term. The magnitudes of the other constants have been kept the same as before. Thus equation (1) maintains a continuity with the formula proposed earlier.

Effective Modulus

The mechanical response of a non-linear viscoelastic material, as pointed out earlier (Sinha, 1977), can be analyzed for engineering applications, in terms of a creep compliance function, D_t^σ, or an effective modulus, E_t^σ, defined as

$$E_t^\sigma = \frac{1}{D_t^\sigma} = \frac{\sigma}{\varepsilon_t} \qquad (5)$$

where ε_t is given by the equation (1).

Equation (5), in conjunction with equation (1), shows that E_t^σ and hence D_t^σ are strongly dependent on stress, time, temperature and grain size.

It is advantageous, as discussed in the earlier report, to use the normalized quantities of E_t^σ and D_t^σ for graphical presentation:

$$\frac{E_t^\sigma}{E_o^\sigma} = \frac{D_o^\sigma}{D_t^\sigma} = \frac{\varepsilon_o}{\varepsilon_t} = f\ (\sigma,\ t,\ T,\ d) \qquad (6)$$

where the subscript o indicates the response at zero time after loading, implying $E = E_o^\sigma = 1/D_o^\sigma$; ε_o is the pure elastic strain, given by the first term of equation (1).

Therefore, equation (6) can be rewritten as

$$\frac{E_t^\sigma}{E} = \frac{1}{ED_t^\sigma} = \frac{\varepsilon_o}{\varepsilon_t} = f\ (\sigma,\ t,\ T,\ d) \qquad (7)$$

The average strain rate to time t is given by

$$\dot{\varepsilon}_{t(ave)} = \frac{\varepsilon_t}{t} \qquad (8)$$

Equations (5) and (8) provide a simple method of predicting the initial tangent modulus (strictly speaking it is the secant modulus) as a function of strain rate, provided σ is kept small. This has been verified for coarse-grained ice (Sinha, 1977).

For dynamic problems, time is usually expressed in terms of frequency, f. Frequency is related to t, for engineering purposes, by

$$f = \frac{1}{2t} \qquad (9)$$

Discussion

Equation (1) to (9) can be used to examine the dependence of the effective modulus on stress, time, temperature, grain size, strain rate and frequency.

A set of computations, as examples, are illustrated in Fig. 1 for an arbitrarily chosen stress of 0.3 $MN \cdot m^{-2}$ at -10°C for a few representative grain sizes. The value of $E = 9.5\ GN \cdot m^{-2}$ was used in all these calculations. The effects of stress on ice of two different grain sizes at -10°C are shown in Fig. 2. The use of a linear scale for the effective modulus, however, gives poor resolution at longer times. A logarithmic scale would be more useful in these ranges but that would remove the details at higher values of the modulus (Fig. 3).

The influence of temperature on the effective modulus can be seen by shifting the curves in Figs. 1 to 3 along the time scale by the corresponding shift function obtained from equation (4). Temperatures higher than -10°C will translate the curves toward the left, i.e., shorter times, whereas lower temperatures will move them in the reverse direction. For example, at -5°C, the curves will be shifted to about half the times and at -25°C, the shift will be by a factor of six. A difference in temperature between -5°C and -25°C will therefore translate the curves along the time scale in Figs. 1 to 3 by about one order of magnitude. A set of examples of computed values are given in Fig. 4 to show the variations expected in the effective modulus with different temperatures and grain size, for measuring times of 5 s and 30 s.

Natural ice is rarely isotropic and certainly never consists of grains of uniform size. It is equally improbable

to have ice in nature free from inclusions. In spite of these additional inherent differences in various types of ice, the previous examples indicate the large variations to be expected in the mechanical properties of ice. These examples also reveal that the scatter and the apparent contradiction in the reported results come about not only from structural differences in the ice but also from test methods and conditions of measurements under which the experiments were conducted. The author has already shown that there was agreement in many of the earlier apparently conflicting results on creep of ice (1977; 1978b). Some of the discrepancies, which could not be explained before without bringing in the effect of grain size, will be discussed here briefly.

Response at Very High Frequencies

If the measurements are carried out in the MHz range, equation (1) shows and Fig. 1 indicates that the effective modulus may not be detectably different from Young's modulus E, and will be independent of grain size. The variation with temperature, in the usual temperature range, will be small and similar to the response of a single crystal. Thus there will be little scatter and hence more reproducibility.

Response at Intermediate and Low Frequencies

As the frequency of measurements decreases or as the time increases, the contribution of the delayed elastic strain to the total strain will increase depending on grain size and temperature. The effective modulus will be increasingly different from Young's modulus and will also show a marked dependence on grain size (Fig. 1 to 4). The scatter in the measurements will therefore tend to increase. Experimental examples of frequency dependence together with some calculated results, are shown in Fig. 5; the temperature dependence can be seen in the experiments of Gold (1958) and Sinha (1978b). The dependence of the effective modulus on strain rate, as depicted in Fig. 1, has already been discussed (Sinha, 1977) for a coarse-grained ice.

Figure 1 indicates that the effective modulus of fine-grained ice could be measurably lower than E and would show a temperature sensitivity even in the seismic frequency range of 1 to 10 kHz. Observations on fresh water ice (Fig. 5) and the large number of field as well as some laboratory investigations of sea ice at these frequencies (Weeks and Assur, 1967), support this observation. With the minimum dimension of the sub-grains varying from 0.3 to 0.5 mm, sea ice could be considered as fine-grained ice. The presense of brine at the sub-grain boundaries will, of course, add complexities to the flow properties of sea ice.

Static Response

The contribution of viscous flow to the total strain will increasingly be more significant compared to that of the total elastic and delayed elastic strain as time is increased to the range of static problems. Moreover, since the stress exponent for viscous flow is nearly three times larger than that of delayed elasticity, the total strain will exhibit increasingly more non-linearity in its dependence on stress. This will introduce a non-linear stress dependence in the effective modulus as shown by the divergence of the curves in Figs. 2 and 3. The degree of non-linearity depends on grain size, temperature and time for a given stress range.

Linearity Limit

Nevel (1976) pointed out that if it could be assumed that ice was a linear viscoelastic material, solution to problems would be easier and furthermore the superposition principle could be used for multiple loads. It is appropriate, therefore, to use the proposed model to examine the conditions under which ice can be considered to be a linear viscoelastic material, i.e., thermorheologically simple.

Let us consider $t = 4 \times 10^4$ s (11.1 h) at -10°C for 0.5 mm ice. As shown in Fig. 3, E^{σ}_t/E values are 0.056 and 0.051 respectively for 0.1 and 0.2 $MN \cdot m^{-2}$. The effective modulus for the lower stress is 10% higher than that for the higher stress. Suppose ±5% is the error in measurements of the effective modulus in a hypothetical experiment, then the above 10% difference is within the allowable maximum error. One could approximate this ice as linear viscoelastic for the range of stresses mentioned, up to this time at -10°C or up to 2.24×10^4 s (6.2 h) at -5°C. If this criteria of judgment is applied to 3 mm ice, then the corresponding times, as can be seen in Fig. 3, are reduced to 1.8 hrs and 1 hr at -10°C and -5°C respectively. The limit of linearity, therefore, reduces significantly as the grain size increases.

These examples showed the use of the normalized effective modulus for a comparative study of the limits of linearity of different types of ice under similar externally applied conditions. This method is questionable, however, if the practical limits of linearity are to be established on the same type of ice but in different ranges of stress. Under these conditions, linearity is better assessed from equation (1) by the usual method of examining the stress-strain relationship at various creep times. This can also be accomplished by a slightly different treatment of the effective modulus, as illustrated below.

Consider again the first example on fine-grained ice. The normalized effective moduli are 0.056 and 0.051 for 0.1 and 0.2 $MN \cdot m^{-2}$ respectively at $t = 4 \times 10^4$ s (11.1 h) and a temperature of -10°C (Fig. 3). Since $E_t^\sigma/E = \varepsilon_o/\varepsilon_t$ from equation (7), the strains, ε_t, are known. The total strains are 1.86×10^{-4} and 4.14×10^{-4} for the two stresses. The difference between the strain for 0.2 $MN \cdot m^{-2}$ and twice the strain for 0.1 $MN \cdot m^{-2}$ is 0.4×10^{-4}. Suppose the error of strain measurement is $\pm 2 \times 10^{-5}$ in the hypothetical experiment considered earlier, then the above difference in the two strains is within the acceptable scatter; this ice could again be considered as linear viscoelastic. Now suppose this experiment is extended to cover the stresses to 0.6 $MN \cdot m^{-2}$ keeping the same accuracy of strain measurement. Examination of Fig. 3 and the subsequent computations revealed that the total strains for 0.1 and 0.6 $MN \cdot m^{-2}$ at 1×10^3 s (16.6 min) were 9.8×10^{-5} ($E_t^\sigma/E = 0.107$) and 6.3×10^{-4} ($E_t^\sigma/E = 0.100$) respectively. These strains are linearly related with the stresses within the maximum allowable scatter of strain measurement. Consequently the ice could be considered as linear viscoelastic for this stress range up to 16.6 min or an equivalent of 9.3 min at -5°C. The drastic reduction in the time would make the non-linearity for the larger stress range almost immediately noticeable after loading. Note the present difference (7%) in the effective moduli compared to that (10%) for the lower stresses.

Experimental Evidence of the Limit of Linearity

Jellinek and Brill (1956) conducted creep experiments on snow-ice at -5°C and observed the behaviour to be linear viscoelastic up to a duration of five hours for stresses below 0.2 $MN \cdot m^{-2}$. Similar observations were also made by Brill and Camp (1961) on snow-ice in direct-tension. These observations bear a close resemblance to the example of fine-grained ice discussed previously in the stress range of 0.1 to 0.2 $MN \cdot m^{-2}$. Kuo (1972) performed compressive creep tests on snow-ice at -4.5°C in the stress range of 0.16 to 2.74 $MN \cdot m^{-2}$, but did not discuss the primary creep. Nevel (1976) concluded from Kuo's data that the ice behaved non-linearly (presumably meaning - within very short time after loading) for stresses greater than 0.7 $MN \cdot m^{-2}$, which again agreed with the discussion presented previously on fine-grained ice in the range 0.1 to 0.6 $MN \cdot m^{-2}$.

It was shown earlier that the practical limit of linearity decreases rapidly, for the same stress range, as the grain size increases. Coarse-grained ice will therefore readily appear to be non-linear. The literature supports this by the absence of a linear-viscoelastic model for coarse-grained ice (Gold, 1965). There is a great deal of evidence

in the glaciological literature, however, of the variation of the stress dependency of the viscous flow rate from nearly linear at low stresses to highly non-linear at higher stresses. This aspect of ice creep can also be explained by the proposed model and has been discussed in detail elsewhere (Sinha, 1978b). It was shown that the reported variation in the stress-exponent of creep rate could be the result of either inaccurate measurement or terminating the tests too early.

Summary

A rheological model of polycrystalline ice, incorporating the grain size effect, has been presented and discussed to explain the mechanical properties of various types of ice. The delayed elasticity was shown to be the primary factor controlling the deformation properties of ice during the transient creep period. Since the delayed elastic effect is affected by grain size, the transient creep will exhibit significant dependence on the size of the constituent grains.

The proposed rheological model and the subsequent analysis suggest that the applicability of a linear viscoelastic model to ice is limited. It appears that the non-linear response may not be avoidable in the static bearing capacity problems involving ice. There are, however, a number of quasi-static and certainly several dynamic problems where assumption of a linear response would not be unrealistic. As shown here, the limits of linearity are governed by the time for which the contribution of the viscous flow to the total strain becomes significant. In other words, the first two terms in equation (1) are sufficient to describe the behaviour in the linear range. Since these are also the terms that describe the effective elasticity, ice behaves essentially as an elastic material within the linear limits. Since there is no name in the rheological literature to describe exclusively this aspect of ice creep, the term "Elasto-delayed elastic" is suggested. Thus the limit of linearity reduces to the limit of elasto-delayed elasticity.

References

Brill, R. and Camp. P.R. (1961). Properties of ice. Research Report 68, U.S. Army Snow, Ice and Permafrost Research Establishment (CRREL), Hanover, N.H., U.S.A.

Gold, L.W., (1958). Some observations on the dependence of strain on stress for ice. Canadian Journal of Physics, Vol. 36, No. 10, pp. 1265-75.

Gold, L.W. (1965). The initial creep of columnar-grained ice, Part I: Observed behaviour, Part II: Analysis. Canadian Journal of Physics, Vol. 43, No. 8, pp. 1414-1434.

Gold, L.W. (1977). Engineering properties of fresh-water ice, Journal of Glaciology, Vol. 19, No. 81, pp. 197-212.

Jellinek, H.H.G., and Brill, R. (1956). Viscoelastic properties of ice. Journal of Applied Physics, Vol. 27, No. 10, pp. 1198-1209.

Kuo, S. (1972). Stress and time effect on the creep rate of polycrystalline ice. Ph.D. Thesis, Michigan State University, Dept. of Civil Engineering.

Nevel, D.E. (1976). Creep theory for a floating ice sheet. Special Report 76-4, Cold Regions Research and Engineering Laboratory, Hanover, N.H., U.S.A.

Nevel, D.E. (1978). Bearing capacity of river ice for vehicles. Report 78-3, Cold Regions Research and Engineering Laboratory, Hanover, N.H., U.S.A.

Sinha, N.K. (1977). Effective elasticity of ice. Proceedings of Workshop on the Mechanical Properties of Ice, 24-25 January, Calgary, Alberta. National Research Council of Canada, ACGR Tech. Memo. No. 121, pp. 112-123.

Sinha, N.K. (1978a). Rheology of columnar-grained ice. Experimental Mechanics, Vol. 18, No. 12, pp. 464-70.

Sinha, N.K. (1978b). Short-term rheology of polycrystalline ice. Journal of Glaciology, Vol. 21, No. 85, pp. 457-73.

Sinha, N.K. (1978c). Grain-boundary sliding in polycrystalline materials. (To be published).

Vaudrey, K.D., and Katona, M.G. (1975). Viscoelastic finite element analysis of sea ice sheets. Proceedings, 3rd International Symposium on Ice Problems, International Association of Hydraulic Research, CRREL, Hanover, N.H., U.S.A., pp. 515-525.

Weeks, W., and Assur, A. (1967). The mechanical properties of sea ice. Monograph 11-C3, Cold Regions Research and Engineering Laboratory, Hanover, N.H., U.S.A.

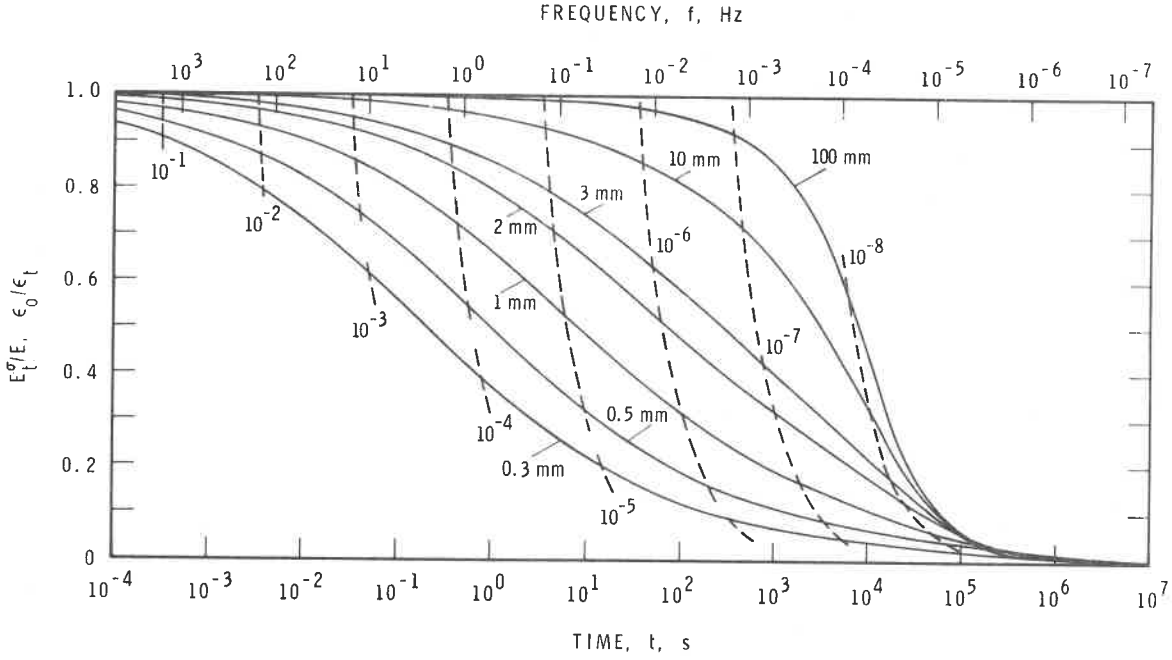

FIGURE 1

TIME OR FREQUENCY DEPENDENCE OF NORMALIZED EFFECTIVE MODULUS FOR VARIOUS GRAIN SIZES AT -10°C; σ = 0.3 MN·m^{-2}, E = 9.5 GN·m^{-2}. BROKEN LINES INDICATE THE SCALE OF AVERAGE STRAIN RATE IN s^{-1}

BR 5805-1

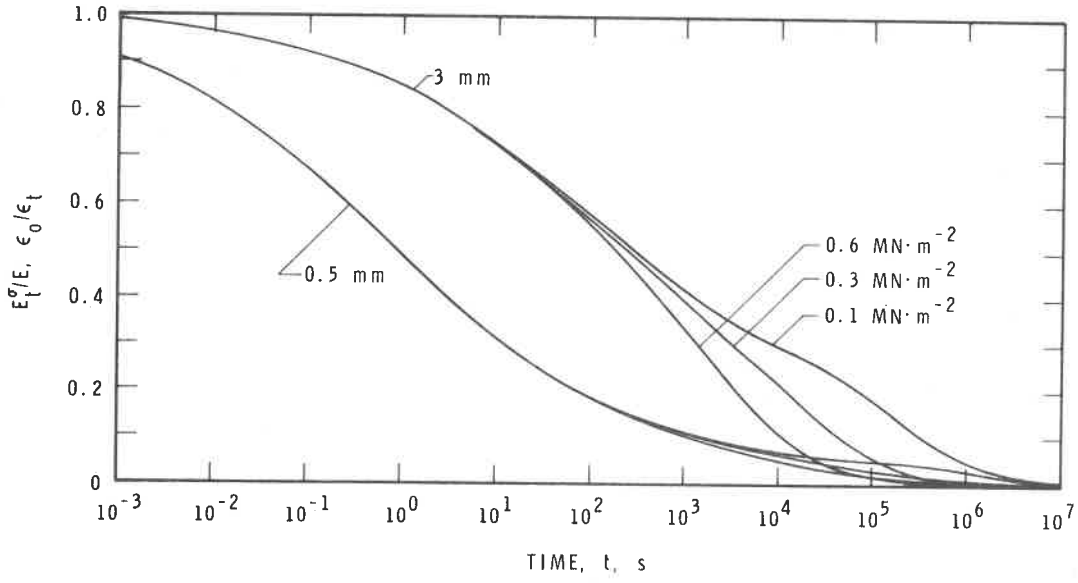

FIGURE 2

DEPENDENCE OF EFFECTIVE MODULUS ON STRESS AND TIME AT -10°C FOR ICE OF AVERAGE GRAIN SIZES OF 0.5 mm AND 3 mm; E = 9.5 GN·m^{-2}

BR 5805-2

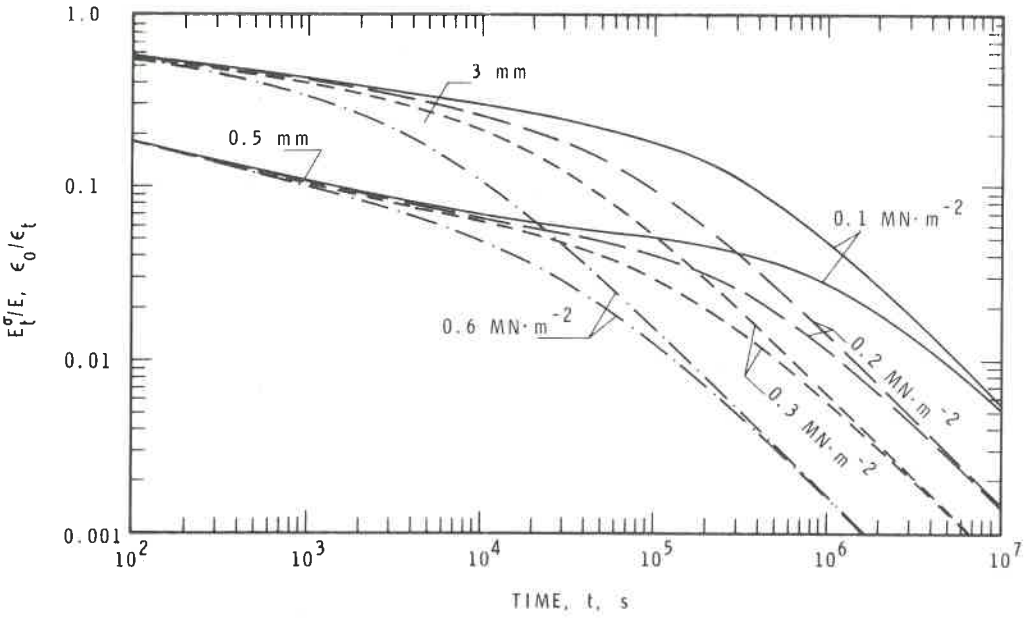

FIGURE 3

TIME AND STRESS DEPENDENCE OF EFFECTIVE MODULUS AT -10°C FOR ICE OF AVERAGE GRAIN SIZES OF 0.5 mm AND 3 mm; E = 9.5 GN·m^{-2}

BR 5805-3

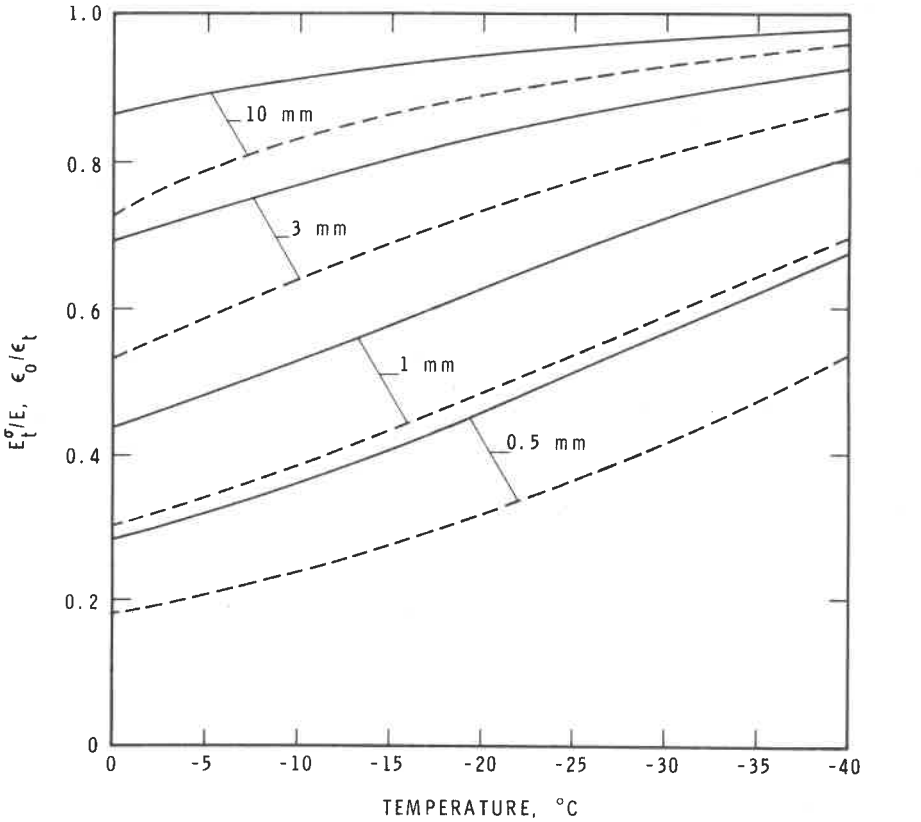

FIGURE 4

TEMPERATURE DEPENDENCE OF NORMALIZED MODULUS AT 5 s (SOLID LINES) AND 30 s (BROKEN LINES) FOR A FEW REPRESENTATIVE GRAIN SIZES; σ = 1 MN·m^{-2}, E = 9.5 GN·m^{-2}

BR 5805-4

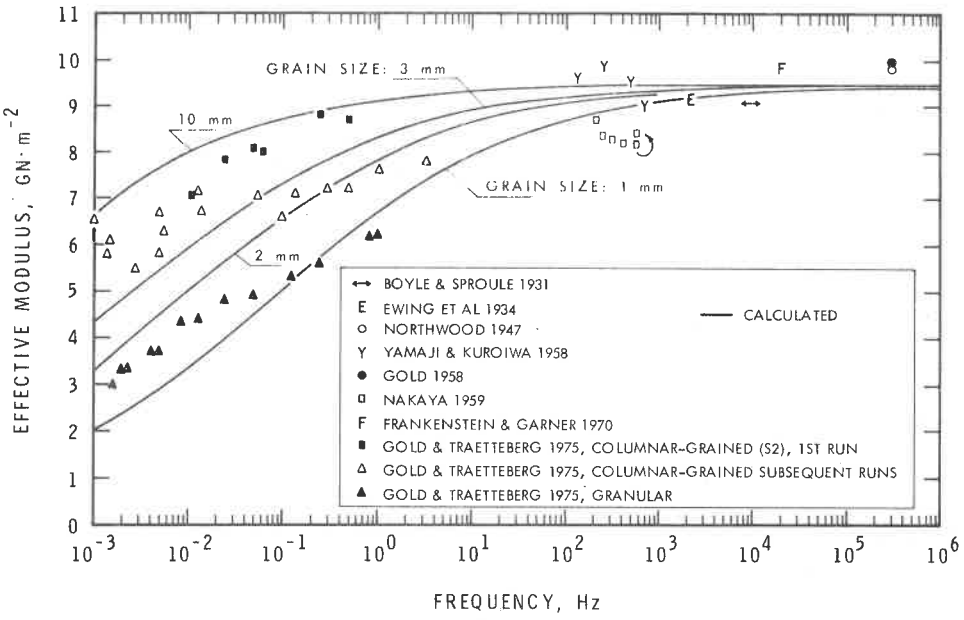

FIGURE 5

FREQUENCY DEPENDENCE OF EFFECTIVE MODULUS FOR POLYCRYSTALLINE ICE AT -10°C. EXPERIMENTAL DATA ARE TAKEN FROM GOLD (1977) WHICH INCLUDES THE OTHER REFERENCES CITED IN THIS FIGURE. CALCULATED RESULTS ARE SHOWN BY THE SOLID LINES FOR STRESS AMPLITUDE OF 0.3 $MN \cdot m^{-2}$, E = 9.5 $GN \cdot m^{-2}$

BR 5620-1

Discussion

D.M. Masterson:

What E values do you get for 30 to 60 second field tests?

N.K. Sinha:

As you will see in the text, the value will depend on temperature, stress and grain size conditions. For an example, 60 second-modulus will have values of about 5.8 $GN \cdot m^{-2}$ and 2.0 $GN \cdot m^{-2}$ for average grain sizes of 3 mm and 0.5 mm respectively for an average temperature of -10°C and for stresses less than about 0.5 $MN \cdot m^{-2}$. So far, the proposed rheological model has not taken into account the effect of impurities, anisotropy or internal cracks in the ice. The presence of brine in the ice will reduce the effective modulus further than predicted here and the reduction will depend on brine volume.

R. Gerard:

What is delayed elasticity? Is the strain associated with it of the nature of 'elastic' (i.e. associated with deformation of lattice) or of 'plastic' strain (i.e. associated with movement of dislocations, grain-boundary rotation, etc.)? If the latter, what 'drives' this strain?

N.K. Sinha:

Elastic strain is usually referred to the strain that can be recovered. Pure elastic strain describes the strain that is recovered immediately after the load removal and is associated with the lattice deformation. As the name suggests, delayed elastic strain is synonymous to the time-dependent (i.e. delayed) recoverable strain. Hence it is not the plastic strain because plastic strain is used to describe the non-recoverable or permanent strain.

Delayed elasticity does not seem to be associated with the deformation of the lattice or the movement of lattice dislocations because single crystals of ice show negligible recoverable creep. The present author has hypothesized (reference 1978c) that the delayed elasticity could be associated to the recoverable part of the grain-boundary sliding mechanisms and associated complex interactions with the intragranular and intergranular substructures. This concept was used to develop the model presented here.

B. Michel:

Did you subtract the permanent computed strains in the given values of delayed elasticity?

N.K. Sinha:

Delayed elastic strain is referred to here as the time-dependent recoverable strain. Experimental methods of determining this strain have been described in reference (Sinha, 1978a).

Summary of Panel Discussion on Performance Measurements

The discussion began around the question of what type of creep was being observed in the ice platforms: primary or secondary. If primary creep is occurring, it was suggested that stresses might not be relaxing as significantly as calculated assuming secondary creep. It was pointed out that the observed time dependence for strains of $t^{0.47}$ was consistent with linear viscoelastic theory for a floating plate which would represent more closely secondary creep. The importance of the changing load on a floating platform was emphasized by noting that a true steady state could never be reached in the creep.

Discussion shifted to the use of the borehole dilatometer as an in-situ measurement device. Concerns were raised that formulations based on primary creep would not provide answers required for ice failures at higher stress and strain rate levels. Although cracking activity does nullify assumptions used in the interpretation, it was suggested that alternate analyses could be developed to account for ice cracking. The use of results as index values for ice strength was suggested as an alternative to detailed theoretical analysis. However concern was voiced that care was required in applying index values in situations in which they might be inappropriate. The application of the instrument to the problem of indentation forces on piles was noted as especially pertinent and the fact that theoretical developments had been made was mentioned.

The discussion returned to strain and its measurement with two major points. One was to emphasize the importance of tieing strain measurements to deflection measurements for moving load problems. It was also noted that machinery had been seen to have both electrical and mechanical low frequency influence of in-situ instrumentation. In particular on ice platforms, some of the drilling operations were thought to have influenced strain meter readings in a way which could not be fully understood. Instances of 40 - 80 microstrain fluctuations over 50S and ±10,000 microstrain fluctuations over a period of days were reported.

TIME-DEPENDENT DEFLECTION OF AN ICE PLATE

B. Michel, and L. Gagnon
Université Laval

Introduction

The time-dependent behaviour of ice plates is a very important problem for the development of cold and arctic regions. Ice covers and ice plates are often used as foundation for semi-permanent and static loads.

The following article deals with the time-dependent behaviour of simply supported ice plates without elastic foundation, concentrically loaded on a circular area of variable diameter.

Experiment

The experiment was realized with real fresh water ice of S2 type. The circular ice plates were simply supported by an invar circular ring equipped with a calibrated heating wire to prevent adherence of ice to the metal and permit free rotation of the plate around the support. The deflection was measured and recorded at seven positions along the plate diameter with linear variable differential transformers as illustrated on Fig. 1.

The sampling interval of time could vary (1 sec - 1 hr) from an experiment to another. The static loads that were applied on the ice plate were supported by an aluminum disk of variable diameter (Fig. 1). The influence of the following parameters was studied: load, temperature, radius of area of loading and thickness of the ice plate. The deflection of the plates was studied for loads between 25% and 100% of the breakthrough load in brittle behaviour of the ice plate as measured in a typical test.

Viscoelastic Model

A linear viscoelastic model of Maxwell type was used for interpretation of experimental results. The Maxwell type model neglects the part of primary creep in the creep curve representing the uniaxial behaviour of ice, by assuming both instantaneous and retarded elastic strain of ice as a total instantaneous strain. We chose the model because it represented, simply, the secondary creep of ice (Fig. 2).

The basic relations of the model are for any state of stress in the triaxial Cartesian system:

$$s_{ij} + \frac{G}{\eta} s_{ij} = 2G \dot{e}_{ij} \qquad (1)$$

$$\sigma_{ii} = 3K \varepsilon_{ii} \qquad (2)$$

with s_{ij} - stress deviator

e_{ij} - strain deviator

σ_{ii} - hydrostatic stress

ε_{ii} - mean normal strain

K - bulk modulus

G - rigidity modulus

η - viscosity

i,j - can take the values 1, 2, 3 corresponding to a three-dimensional Cartesian coordinate system.

The solution for the case of the plate studied in the experiment can be obtained by solving two differential equations. Because the model is linear, the solution can be obtained as a function of the solution for an elastic plate similar to the case studied. The first differential equation to solve is then the classical elastic plate equation in cylindrical coordinates, with the limit conditions of the experimental case:

$$\nabla^4 \omega\ (r,\theta) = \frac{F(r,\theta)}{D} \qquad (3)$$

with D - rigidity of the plate

F - load function.

The second differential equation to solve is the time-dependent function. The equation is:

$$B_1\ [h\ (t)] = D\ g\ (t) \qquad (4)$$

where B_1 - operational form of D, for Maxwell type relations

h - time-dependent deflection function

g - load function.

Solution of this equation can be obtained with the Laplace transform in operational calculus. As already mentioned, the solution for time-dependent deflection becomes a time-dependent function associated with the solution for an analogue elastic plate. The time-dependent deflection of the ice plate can be written:

$$\omega = \omega_e \left(\frac{3K+G}{3K+4G}\right)\left[\frac{K+G}{K}\left(\frac{t}{T}\right) - \frac{G^2}{(3K+G)K^{exp}}\left\{\left(\frac{-3K}{3k+G}\right)\frac{t}{T}\right\}\right] \quad (5)$$

with ω_e - elastic deflection, function of space

T - relaxation time, η/G

t - time.

The relation is illustrated on Fig. 3.

The model was calibrated with a measured value of the deflection at the centre at a definite time during secondary creep. The measures are compared with the model on Fig. 4 for a typical test. Note that X is the ratio of the radius at which deflections were measured to the radius of the plate, and β is the ratio of the diameter of the loaded area to the diameter of the plate. The curves coincide, rather well, but this depends on the high dependence of the model to the adjusted value at centre, and the edge conditions.

In fact, the behaviour of ice is essentially non-linear as we know by Glen's type relation between strain rate and stress. Linear models may sometimes be used to represent behaviour of ice when it is submitted to a uniform stress, as in the case of uniaxial traction. In the case of the bending of plates, the experimental results showed that time-dependent behaviour of ice cannot be easily interpreted with a calibrated linear viscoelastic model, and more so in the case of infinite ice covers, when the influence of edge conditions would be negligible.

We have found, by also using thinner plates, where the edge conditions have less influence than in the thicker ones, that the model curves get farther away from experimental

curves. This can be seen on Fig. 5 where the measured deflection at a certain time during secondary creep is compared to the adjusted model.

Secondary Creep

The secondary creep rate was related to the stress by a Glen's type relation assuming an elastic behaviour, as Frederking and Gold (1975) did in their study of time-dependent deflection of floating ice plates. The best fit relation was found to be:

$$\dot{\varepsilon} = B \times \sigma^{2.5} \qquad (6)$$

The relation is shown with the experimental measures on Fig. 6. This relation between the strain rate and the stress assuming an elastic behaviour of the ice has not been shown as clearly for floating plates. The value of n is probably low because the state of secondary creep is never really attained in the tests.

Semi-empirical Solution

Kingery et al., (1962), Frederking and Gold (1975) showed that the time-dependent deflection of a floating ice plate could be computed with the classic relations for elastic plates taking into account the characteristic length of the plate as a function of time.

In the case of simply supported plates, we may instead compute the deflection of the plate with the classic equation for elastic plates, but taking the rigidity of the plate, D, as a function of time. Figure 7 shows the variation that D should have in function of time for the elastic relations to correspond to experimental measures.

The best relation was found to be of the type

$$D = A_1 \, t^{-g} \qquad (7)$$

with g - $0.62 \pm 5\%$

A_1 - adjustable constant.

We then get a relation of the type:

$$\omega = \frac{\omega_e \times D \times t^{(0.62 \pm 5\%)}}{A_1} \qquad (8)$$

Then adjusting A_1 for each experiment, we get a very good estimate of the deflection of the plate at any time, as shown in Fig. 8 for one particular experiment.

Influence of Temperature

The behaviour of the ice was found to obey to Arrhenius' law as already made clear by many authors in simpler types of testing during ice creep. We have related the strain rate in secondary creep to the temperature with the Arrhenius equation:

$$\dot{\varepsilon} = A\, e^{\frac{-Q_c}{R_1 \theta^*}} \qquad (9)$$

where θ^* - temperature in Kelvin scale

A - constant depending on stress

R_1 - universal gas constant

Q_c - creep activation energy.

Figure 9 shows the relation obtained between the strain rate and the reciprocal of the temperature. The two curves represent two different states of stress. We thus found two different values for the creep activation energy of ice (slope of the curves shown in Fig. 9).

Table 1 shows that our values for creep activation energy of ice (S2 type) are smaller than those found by other authors. Only three points are used in each case, and this may explain this discrepancy.

Primary Creep

When the initial load is applied on the ice, or when supplementary loads are added, the ice plate is in the phase of primary creep characterized by retarded elasticity. A while after the additional load is applied, the ice goes in the secondary or permanent creep at a higher constant strain rate.

A linear relation was found between the total (instantaneous and retarded) strain, ε^*, and the stress at that point. The equation is shown on Fig. 10 and can be expressed:

$$\sigma = E^* \varepsilon^* \qquad (10)$$

where E* is the apparent Young modulus. In other words, it is the minimum value the elastic modulus can take for this type of ice. From Fig. 10 we find:

$$E^* = 3.8 \times 10^8 \ N/m^2$$

Collapse

In each experiment the ice plate collapsed; it happened during the primary creep phase a short while after an increase in load.

The cracks appeared from the centre towards the sides when the load broke through. The cracks cut the plate in sectors as shown in a typical collapse crack pattern (Fig. 11).

The maximum stresses causing fracture are given in Table 2. They were computed on the assumption that the section can resist a plastic moment, 30% higher than the moment the section could resist if the ice was considered purely elastic (Drouin et al., 1972; Meyerhof, 1960; Nadreau, 1976). Those maximum stresses involve a diameter of the grains corresponding to the value we have measured. The fracture then really occurs at stresses corresponding to the maximum bending stresses related in the literature (Michel, 1978).

Behaviour at Unloading

When the plates were unloaded, we observed that the deflection diminished in an almost instantaneous manner to a certain value of permanent deflection (Fig. 12).

The linear viscoelastic model gave better reliability in the behaviour after unloading, because the non-linear part of the material is inactive when the stress is absent. If the unloading occurs at $t = t_1$, the deflection becomes for $t = t_1$:

$$\frac{\omega}{\omega_e} = \frac{3K+G}{3K+4G}\left[\bar{t}_1 + \frac{G^2(e^{A'\bar{t}_1} - 1)e^{-A'\bar{t}}}{(3K+G)K}\right] \qquad (11)$$

with

$$A' = \frac{3K}{3K+G}$$

$$\bar{t}_1 = \frac{t_1}{T}$$

$$\bar{t} = \frac{t}{T}$$

Conclusion

This study showed that the creep bending of ice plates cannot be easily interpreted if the ice is considered as a linear viscoelastic material.

The experiment also proved that we could use quite accurately, and very simply, a semi-empirical relation based on the classical relations for elastic plates in which we use a time-dependent rigidity for estimating the deflection through time all over the plate.

We also found a linear relationship between stress and the total elastic strain, and this giving a value for the apparent elastic modulus of ice.

Finally we verified that the stresses causing fracture correspond to the maximum bending stresses found previously for ice of S2 type which was used for the testing.

References

Drouin, M. and B. Michel (1972). "La résistance en flexion de la glace du St-Laurent déterminée en nature". Rapport GCT-72-09-26, Laboratoire de Mécanique des Glaces, Université Laval.

Frederking, R. and L.W. Gold (1975). "The bearing capacity of ice covers under static loads". Second Canadian Hydraulics Conference, Burlington.

Kingery, Cutcliffe and Coble (1963). "Elastic and time-dependent deformation of ice sheets". From Ice and Snow, Ed Kingery, M.I.T. Press, Cambridge, Mass.

Mase, G.E. (1960). "Behaviour of viscoelastic plates in bending". Journal of the Engineering Mechanics Division, ASCE, Vol. 86, EM 3, pp. 25-39.

Meyerhof, G.G. (1960). "Bearing capacity of floating ice sheets". ASCE, Vol. 86, EM 5, pp. 113-145.

Michel, B. (1978). "The strength of polycrystalline ice". Can. Jour. Civil Engineering, Vol. 5, No. 3, pp. 285-301.

Nadreau, J.P. (1976). "Etude de fluage de poutres de glace columnaire". Rapport GCS-76-04, Laboratoire de Mécanique des Glaces, Université Laval.

AUTHORS	CREEP ACTIVATION ENERGY [cal/mole]	DETAILS
Mugurama, 1969	16,143	constant stress
Gold, 1972	20,986	constant stress $-5^{o}C < \theta < 15^{o}C$
Michel et Paradis, 1976	21,662	constant strain rate
This study	12,400	constant stress

Table 1: Creep activation energy of S_2 type of ice.

Test	h [mm]	β	P [N]	σmax [N/m^2]
2	25	0.1	765	1.81×10^6
4	25	0.2	981	1.83×10^6
9	15	0.3	441	1.86×10^6
				d* [mm]
				2

Table 2: Failure stresses and corresponding dimension of grains.

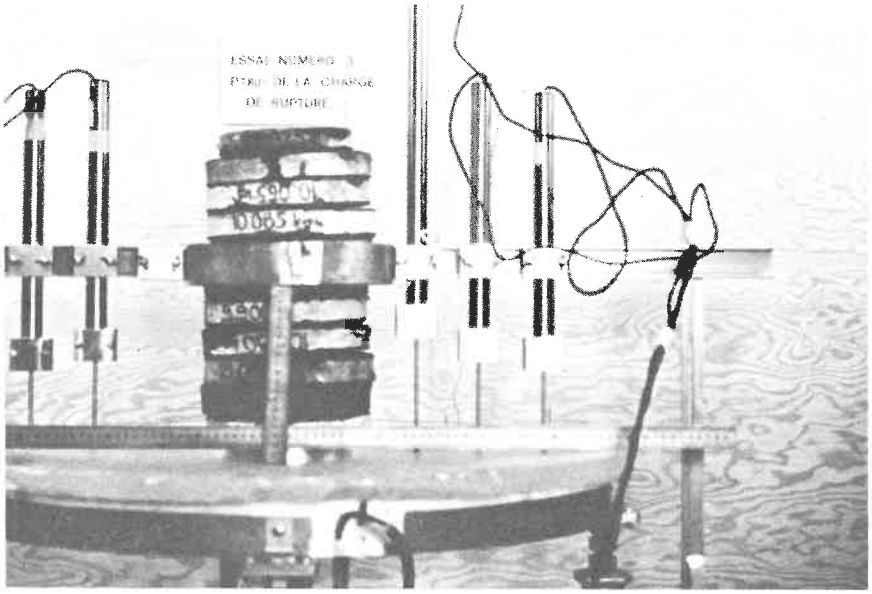

Figure 1

Loads on ice plate with LVDT's.

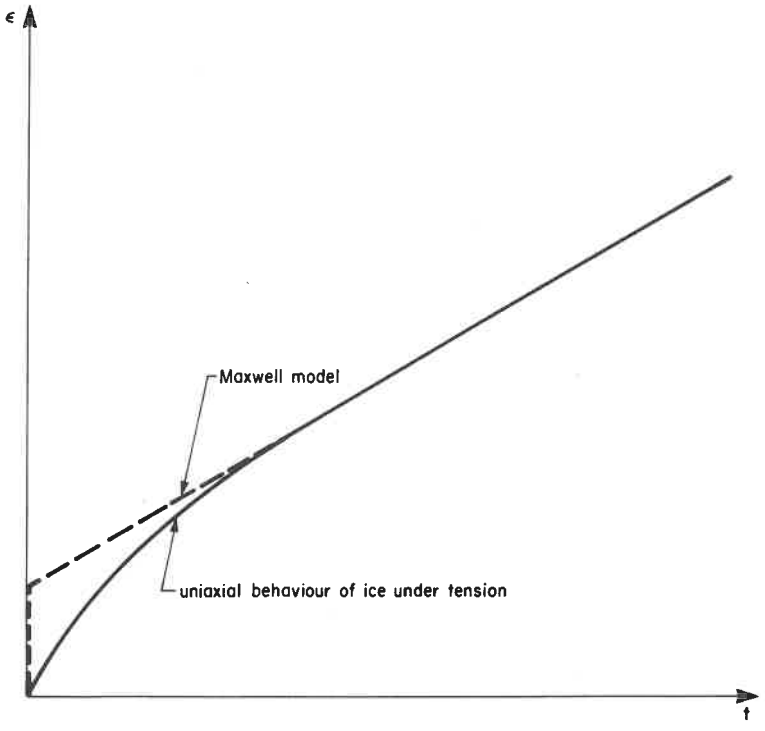

Fig. 2 — UNIAXIAL BEHAVIOUR OF ICE.

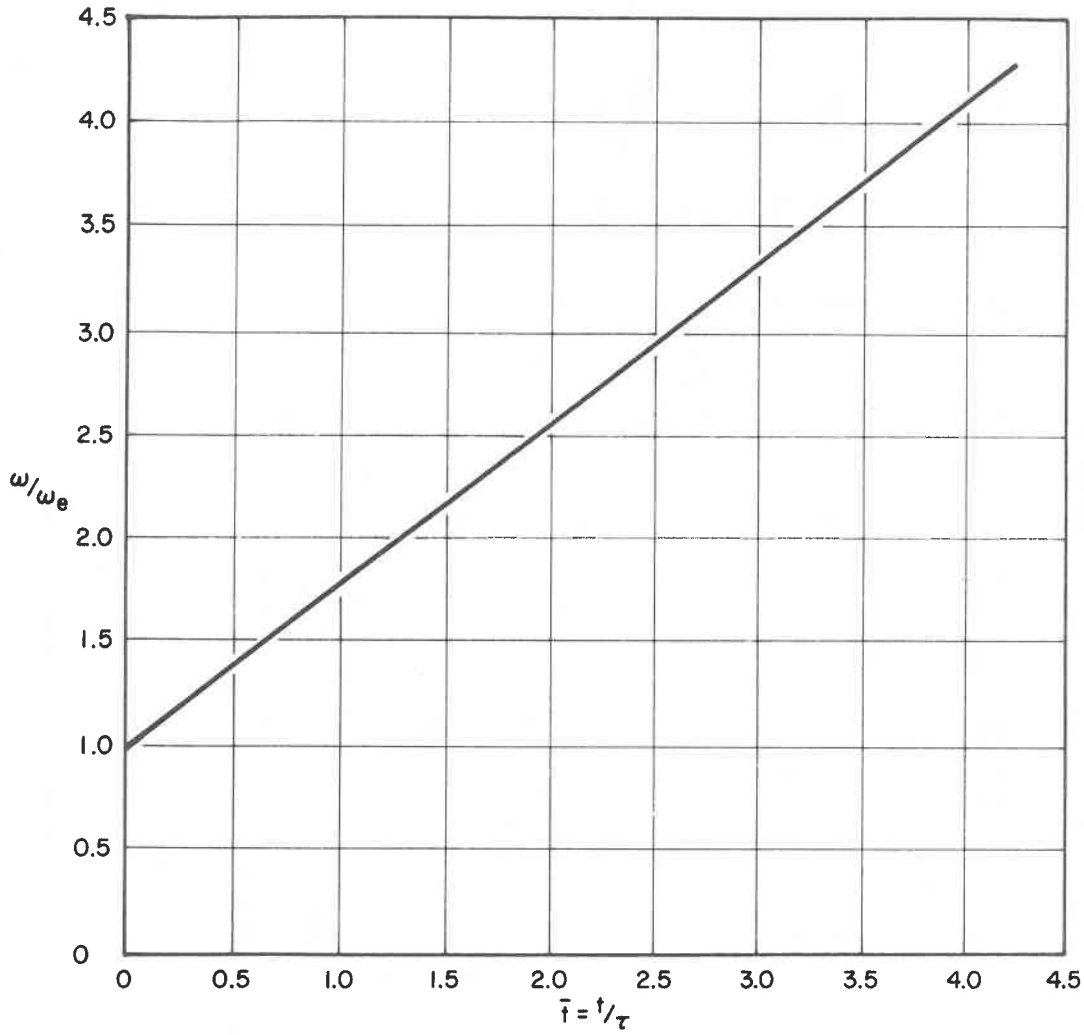

Fig. 3 — TIME-DEPENDENT DEFLECTION OF A VISCOELASTIC PLATE OF A MAXWELL MATERIAL.

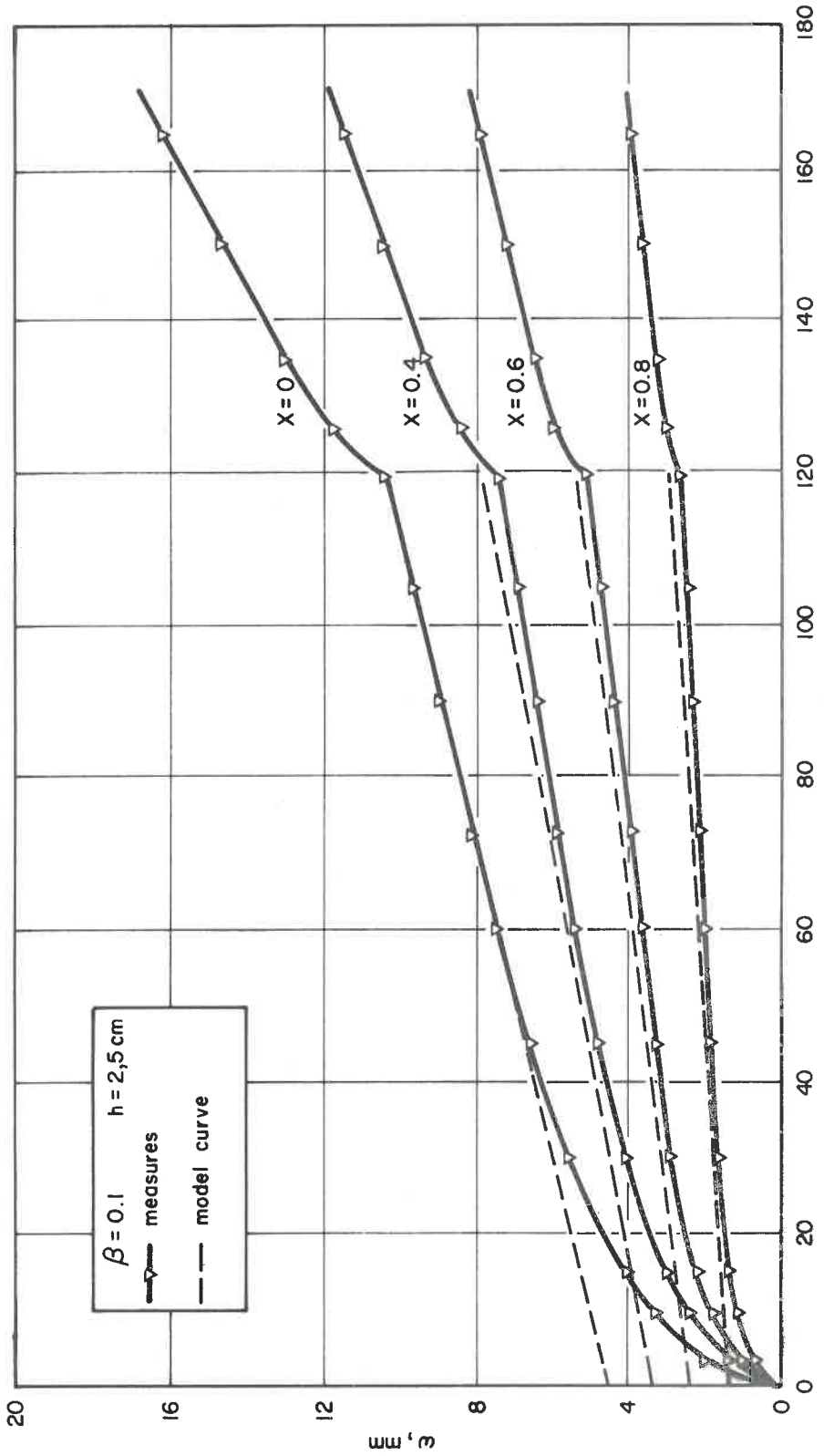

Fig. 4 — MEASURES AND THEORETICAL MODEL.

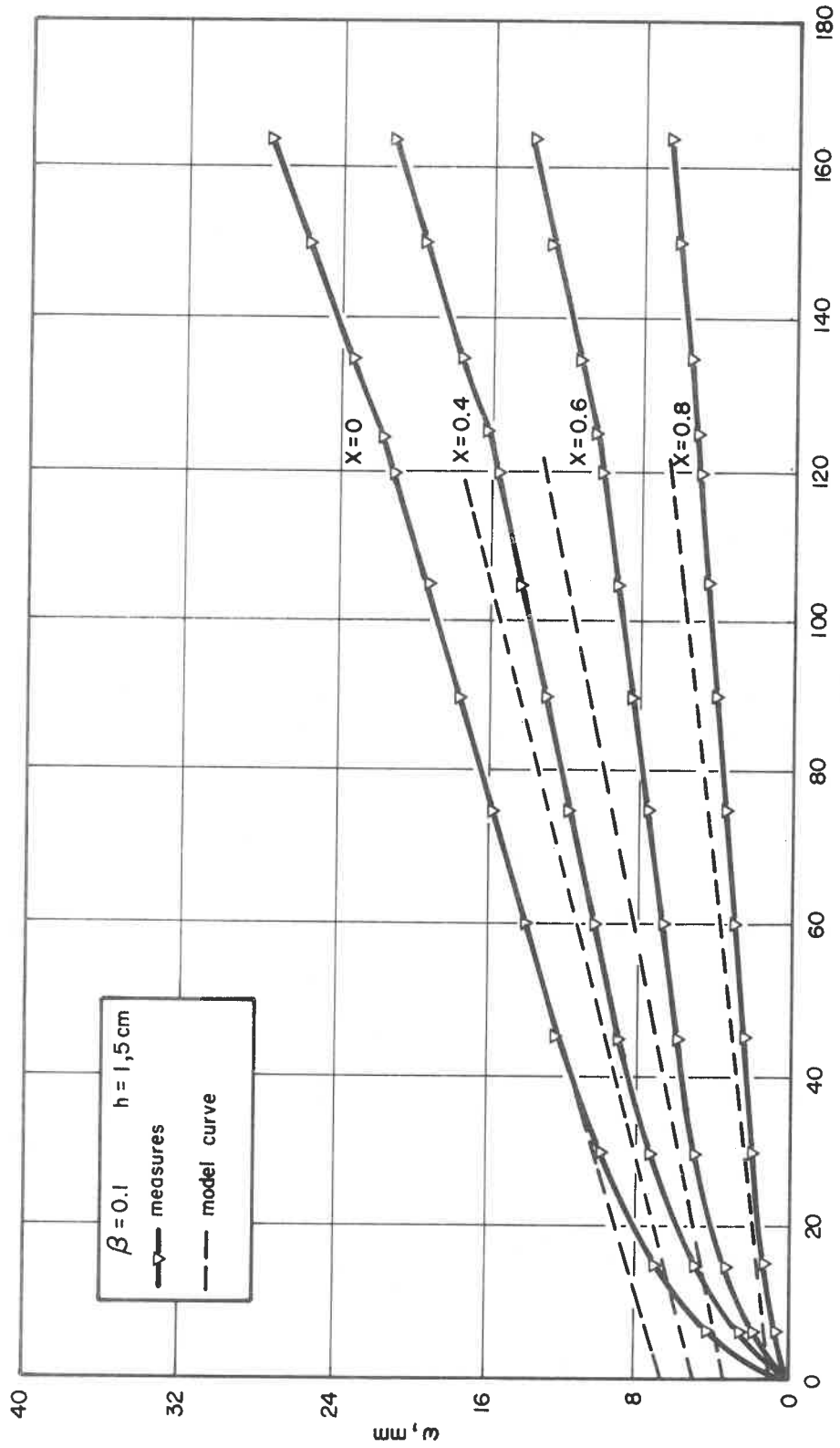

Fig.5 — MEASURES AND THEORETICAL MODEL, THIN PLATE.

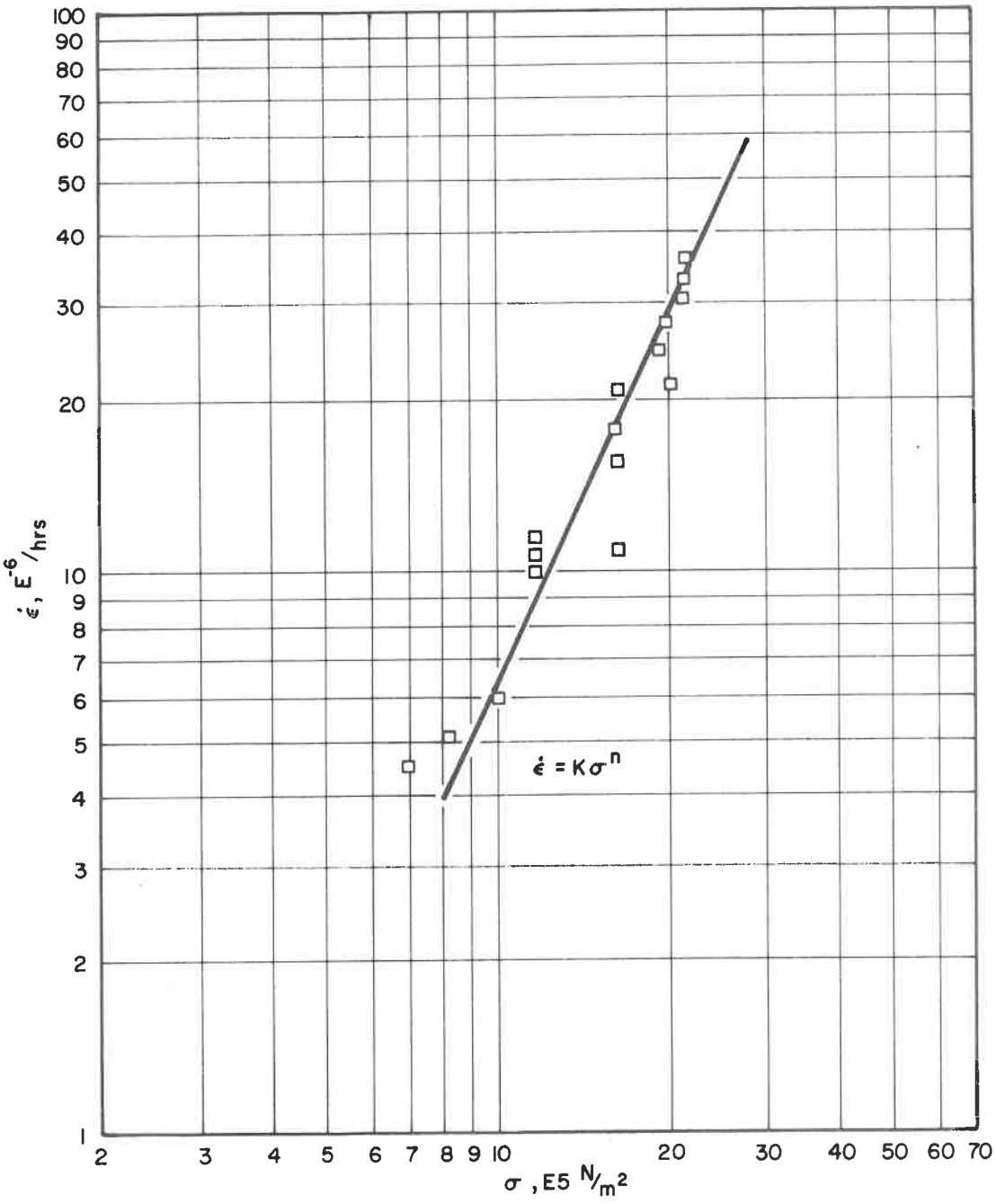

Fig. 6 — GLEN'S RELATION

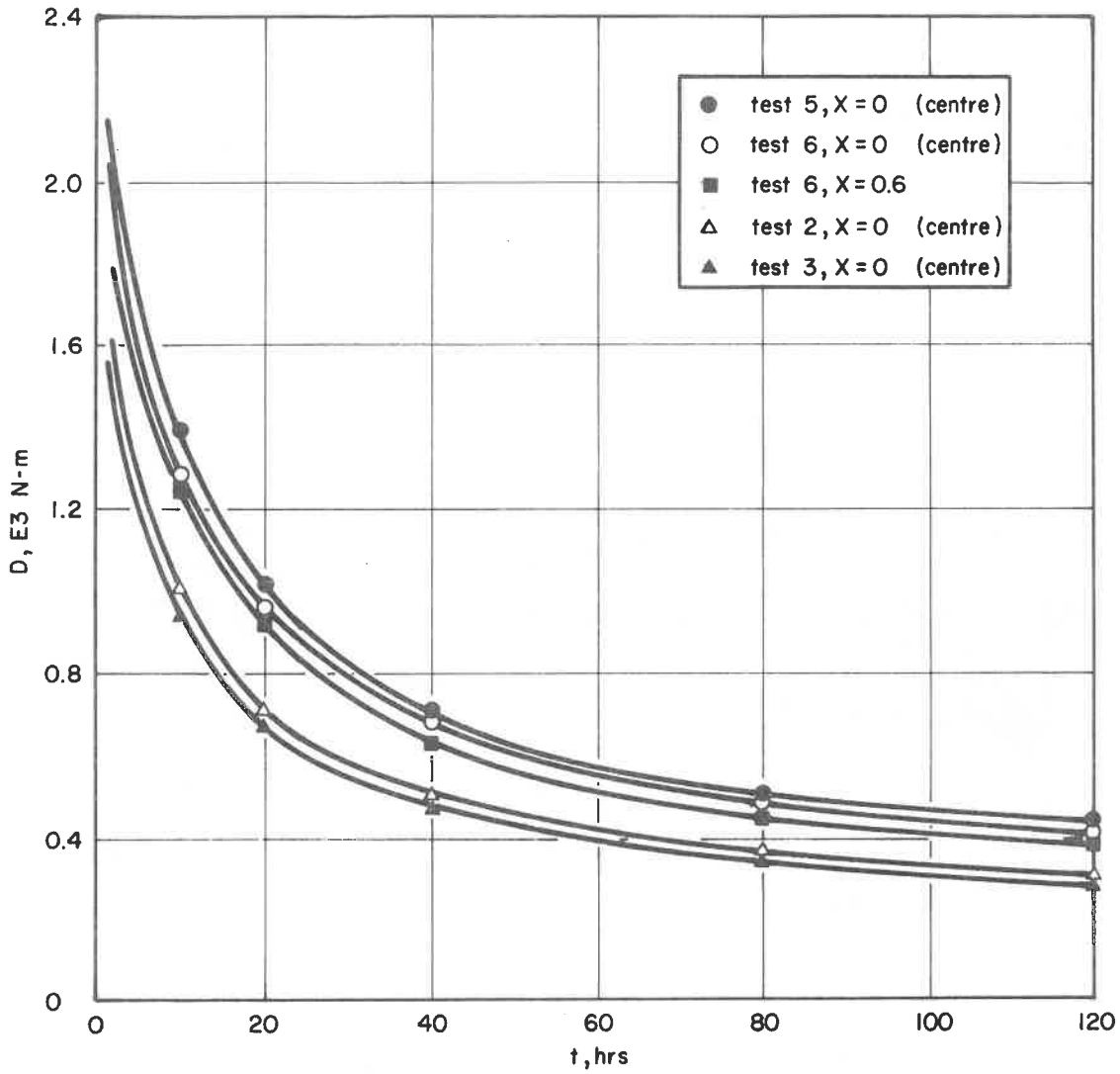

Fig. 7 — TIME-DEPENDENT RIGIDITY OF THE PLATE.

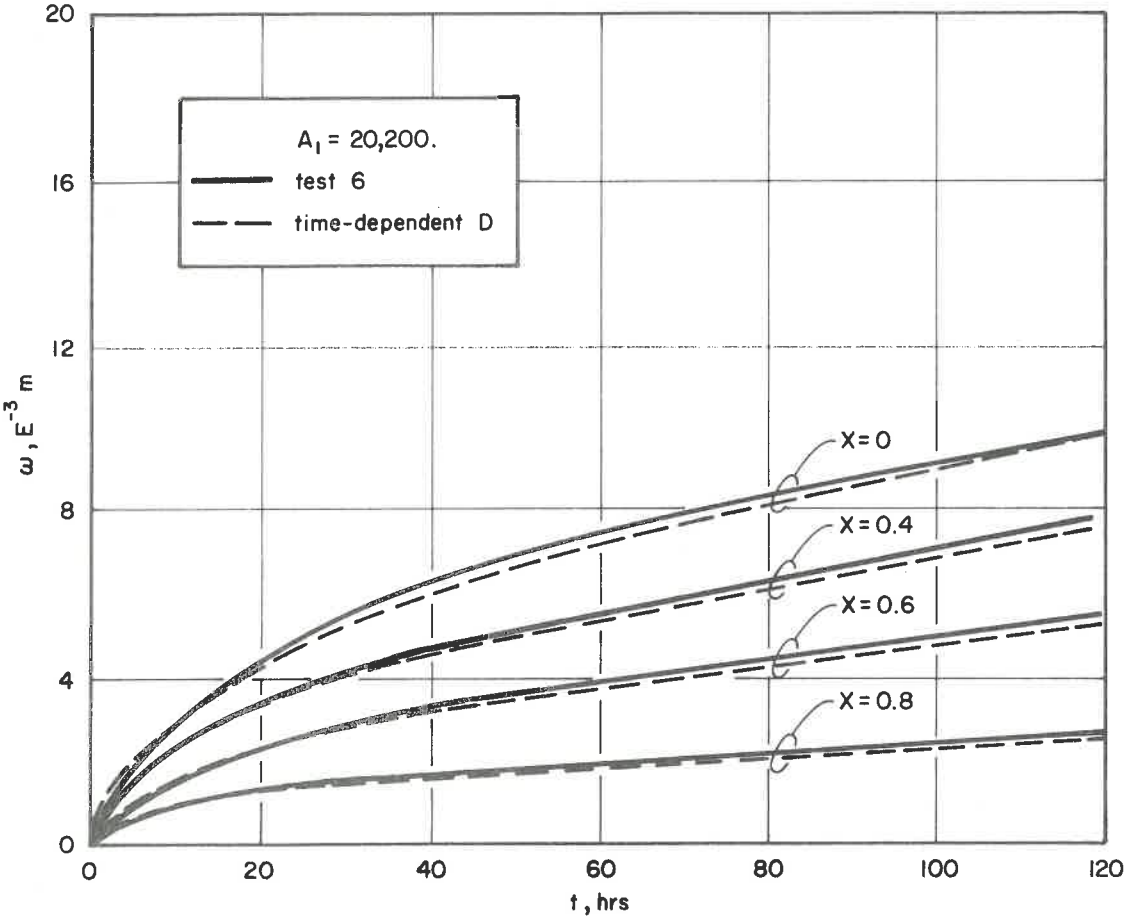

Fig. 8 — TIME-DEPENDENT DEFLECTION WITH EQUATION [8] COMPARED TO THE MEASURES.

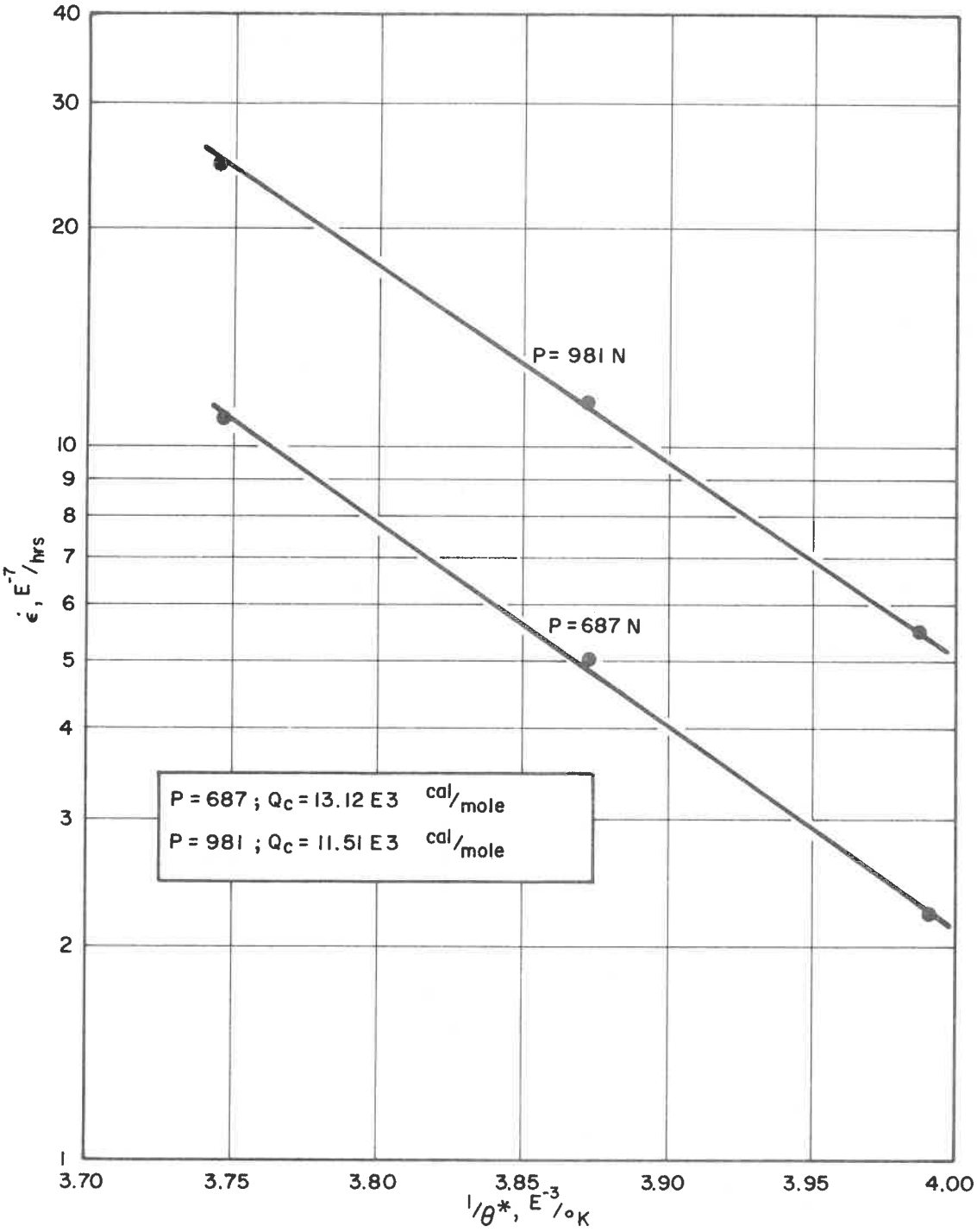

Fig. 9 — TEMPÉRATURE INFLUENCE.

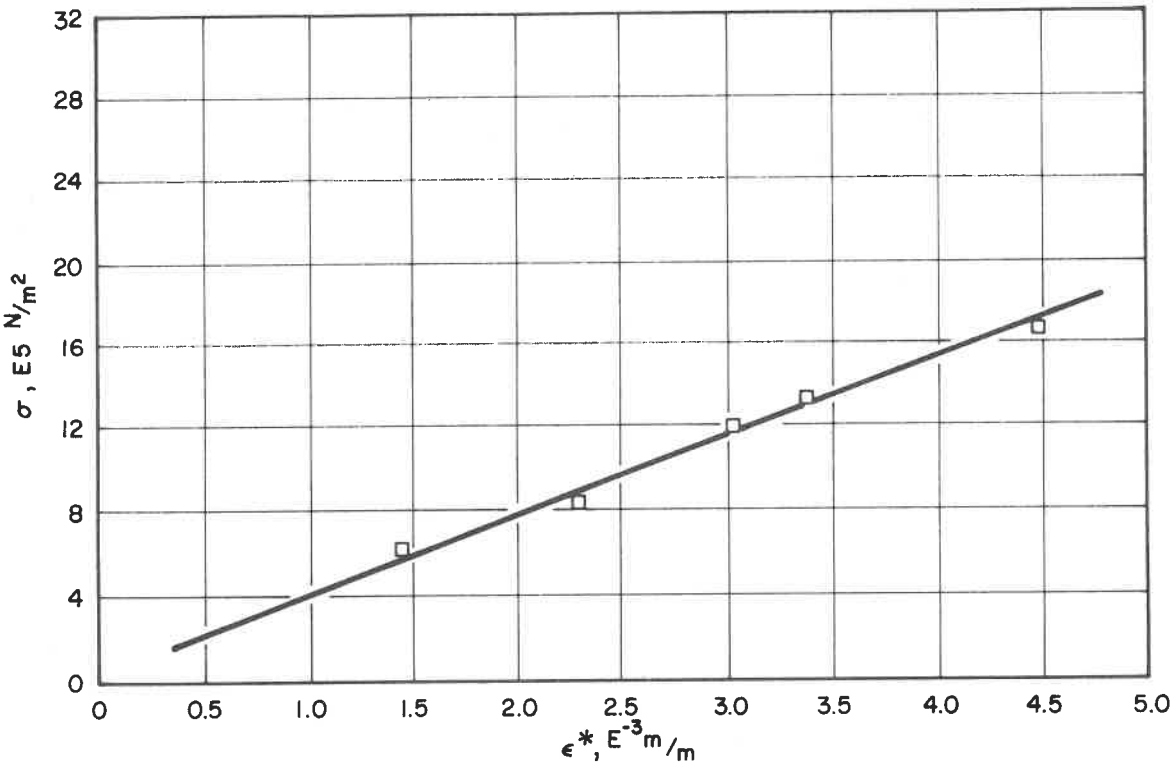

Fig. 10 — STRESS FUNCTION OF TOTAL ELASTIC STRAIN.

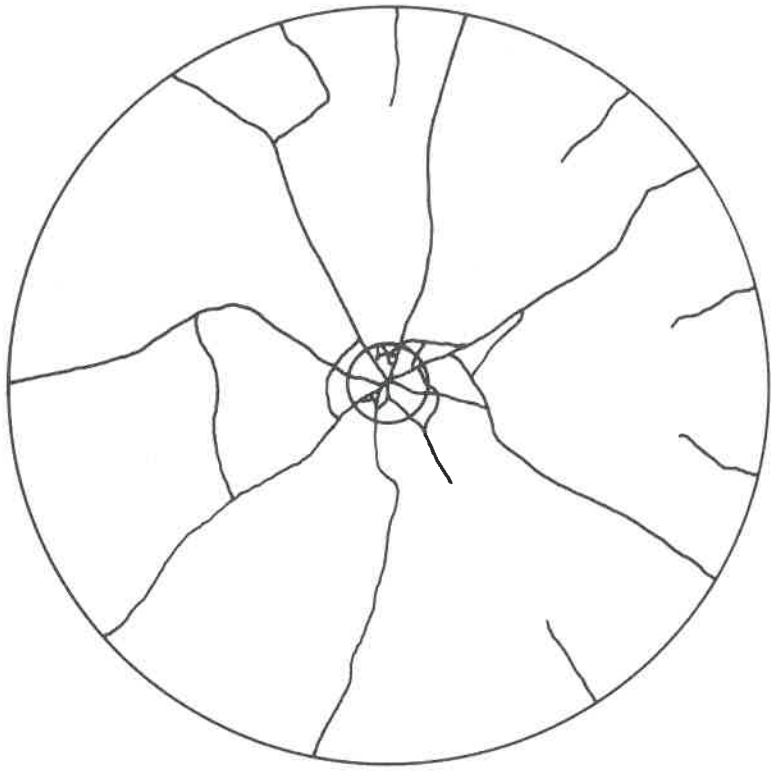

Fig. 11 — TYPICAL CRACK PATTERN.

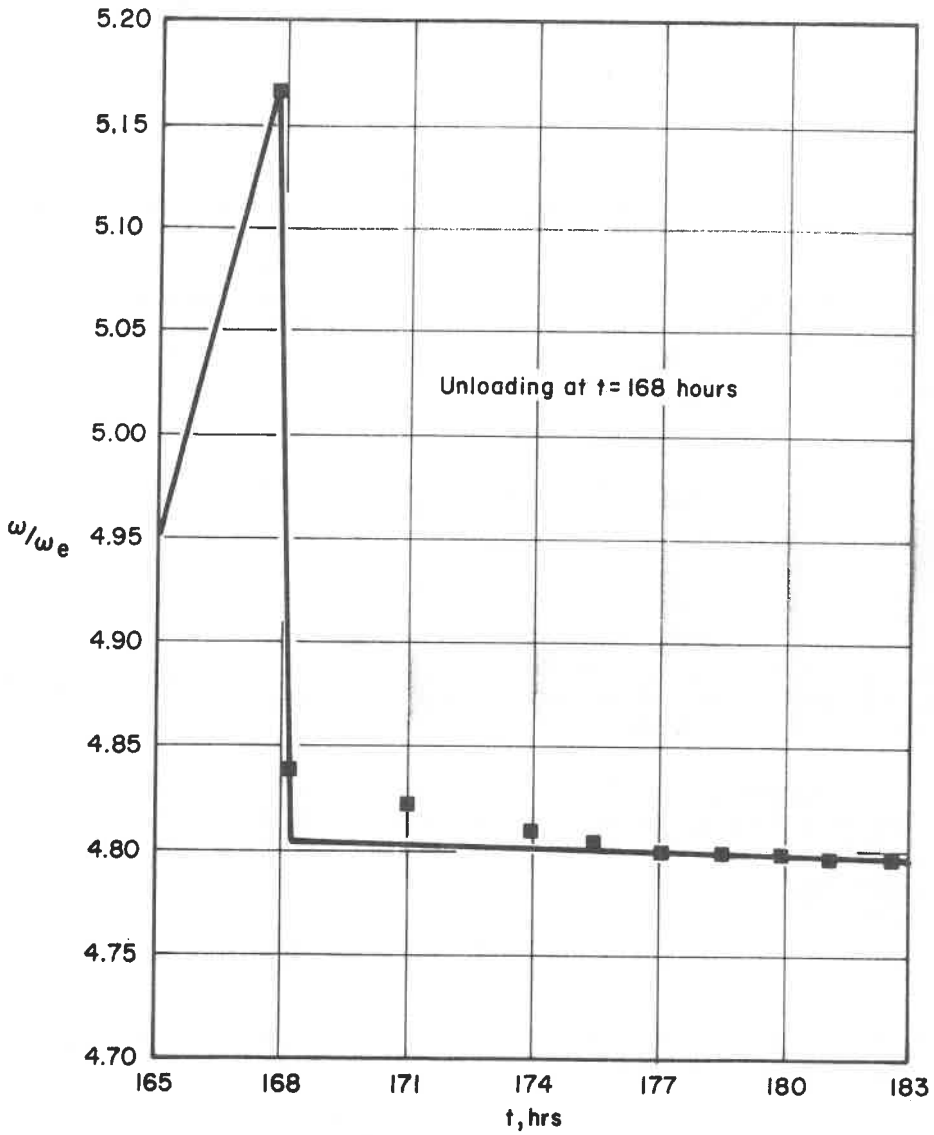

Fig. 12 — TYPICAL TEST-BEHAVIOUR AT UNLOADING.

STRENGTH OF ICE PLATES

B. Michel
Université Laval

I would like to broaden the question of failure of ice sheets that was partly discussed in the preceding paper.

As was observed, the ice failed in the primary phase of deformation, after the addition of incremental loads, on three occasions. This behaviour is very similar to what we have observed previously in extensive testing of ice beams, and the interpretation can be given in the following manner.

Let us start with the resisting moment M_r of an ice beam subject to loading. It is given in the elastic range by:

$$M_r = \frac{\sigma_b \, h^2 \, b}{6}$$

where σ_b is the tensile strength of the extreme layer of the beam, in the case of a brittle fracture, h and b are thickness and width of the beam.

However, if the rate of loading of ice is low, we will have ductile behaviour and the stress distribution will not be linear in the beam, so that the resisting moment will be given by:

$$M_r = b \int_o^h \sigma(z) \; z \; dz$$

where z is the distance counted from the top of the beam. This will give an expression of the form:

$$M_r = \lambda \frac{\sigma_o \, h^2 \, b}{6}$$

where λ is a coefficient of stress distribution always higher than one in the ductile range and σ_o the tensile strength of ice at the lower fiber.

Tests done in our laboratory have shown, conclusively, that the hypothesis of linear strain distribution in the cross-section of a beam is maintained during ductile deformation (Nadreau, 1978) so that we have a linear relation between strains and position within the beam:

$$\frac{\varepsilon}{\varepsilon_o} = \frac{z - z_o}{h - z_o}$$

where ε_o is the strain at the bottom fiber and z_o the position of the neutral axis. For ice the value of strain is related to that of stress, by Glen's law. During yield, we can assume steady creep, so that, for a uniform temperature distribution:

$$\frac{\sigma}{\sigma_o} = \left(\frac{z - z_o}{h - z_o}\right)^{1/n}$$

Integrating these values to obtain the resisting moment, we get:

$$\lambda = 3n/(2n+1)$$

in the case where $n = 3$, $\lambda = 1.3$.

If we include the temperature in the stress distribution, we have:

$$\frac{\sigma}{\sigma_o} = \left\{\left(\frac{z-z_o}{h-z_o}\right) \exp\ [q\ (1-z/h)]\right\}^{1/n}$$

where

$$q = \frac{Q_c\ |\theta_s|}{R(273)^2}$$

where Q_c is the energy of activation of the type of ice, θ_s its upper surface temperature in °C and R the universal gas constant.

The integration for the resisting moment with usual values of q from 1 to 4, gives:

q	λ
0	1.3
1	1.57
2	1.97
4	2.00

This shows a large increase in resisting moment in function of the ice temperature at the surface.

Thus if under any condition of loading the strength at failure of an ice beam or an ice plate is computed with a formula for elastic behaviour, we may speak of an apparent flexural strength σ_{fa} such that:

$$\sigma_{fa} = \sigma_o \lambda(\dot{\varepsilon})$$

where σ_o is the uniaxial strength for the given strain rate and λ the coefficient of plastification of the ice. For a completely brittle fracture $\sigma_o = \sigma_b$ and $\lambda = 1$.

Figure 1 shows the uniaxial strength of S2 ice at -10°C in function of strain rates. It increases in the ductile range with strain rates up to a maximum at the transition zone. It is then constant in the brittle range (Michel, 1978).

Figure 2 shows the maximum resisting moment for beams of snow ice with four points loading in function of strain rates (Lafleur, 1971). These are tests done at constant speed of deformation.

At lower rates of deformation, the resisting moment increases with the strain rate as does the value of σ_o and the value of λ is that given for a fully plastiziced ice section. In this range the beam does not fail but deforms continuously. This is usually valid for strain rates:

$$\dot{\varepsilon} < 10^{-5}\ s^{-1}$$

There is then a transition zone from $10^{-5}\ s^{-1} < \dot{\varepsilon} < 10^{-3}\ s^{-1}$, when the value of σ_o attains that of brittle fracture σ_b but the coefficient of plastification λ passes from full plastification to that given for brittle fracture, $\lambda = 1$.

Finally for $\dot{\varepsilon} > 10^{-3}\ s^{-1}$ brittle fracture occurs with the formation of the first brittle crack.

Figure 3 shows the same effects when the load is increased by steps on beams made of S2 ice. When the last incremental addition of load gives the stress needed for formation of a brittle crack, the beams fail (Nadreau, 1978).

In the present study on ice plates, fracture occurred for three cases of increased loading on the ice plates. The stresses were computed using the plastic resisting moment and the corresponding stress obtained corresponds exactly to the uniaxial strength of the ice which was tested (Table 2 of previous paper).

This proves that ice plates, without an elastic foundation, follow exactly the same law at failure as ice beams. This condition can be computed directly from the uniaxial strength of ice at the corresponding strain rate, the plastification coefficient and the unidirectional resisting moment within the ice.

References

Lafleur, P. (1971). "Propriétés mécaniques de la glace de neige en flexion". Thèse M.Sc., Université Laval, Québec.

Michel, B. (1978). "The strength of polycrystalline ice". Can. Journal of Civil Eng., Vol. 5, No. 3, pp. 285-301.

Nadreau, J.P. (1978). "Etude du fluage de poutres de glace columnaire". Thèse M.Sc., Université Laval, Québec.

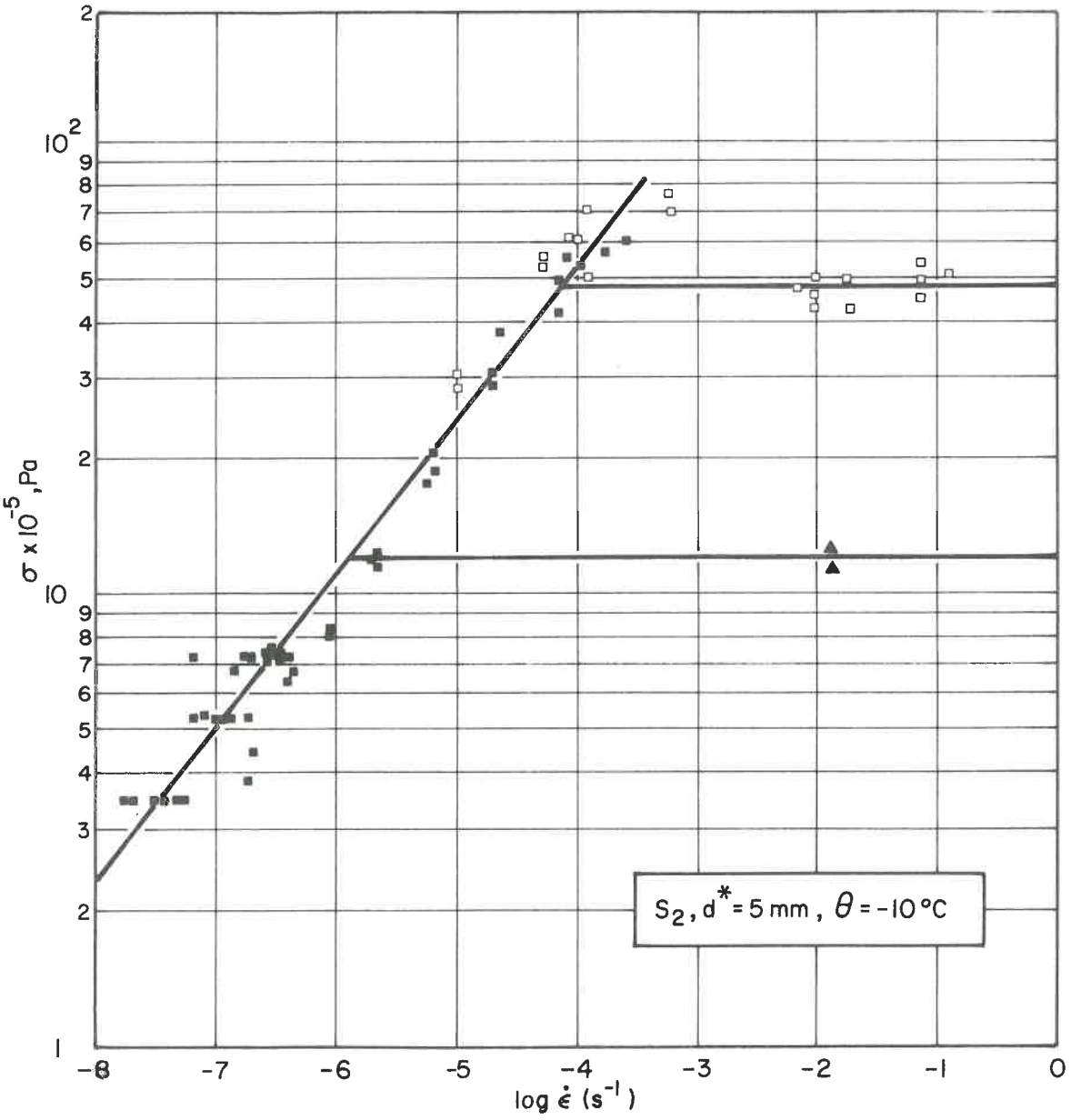

Fig. 1 - Universal diagram of strength of S2 ice at -10°C in function of strain rates $\dot{\epsilon}$.

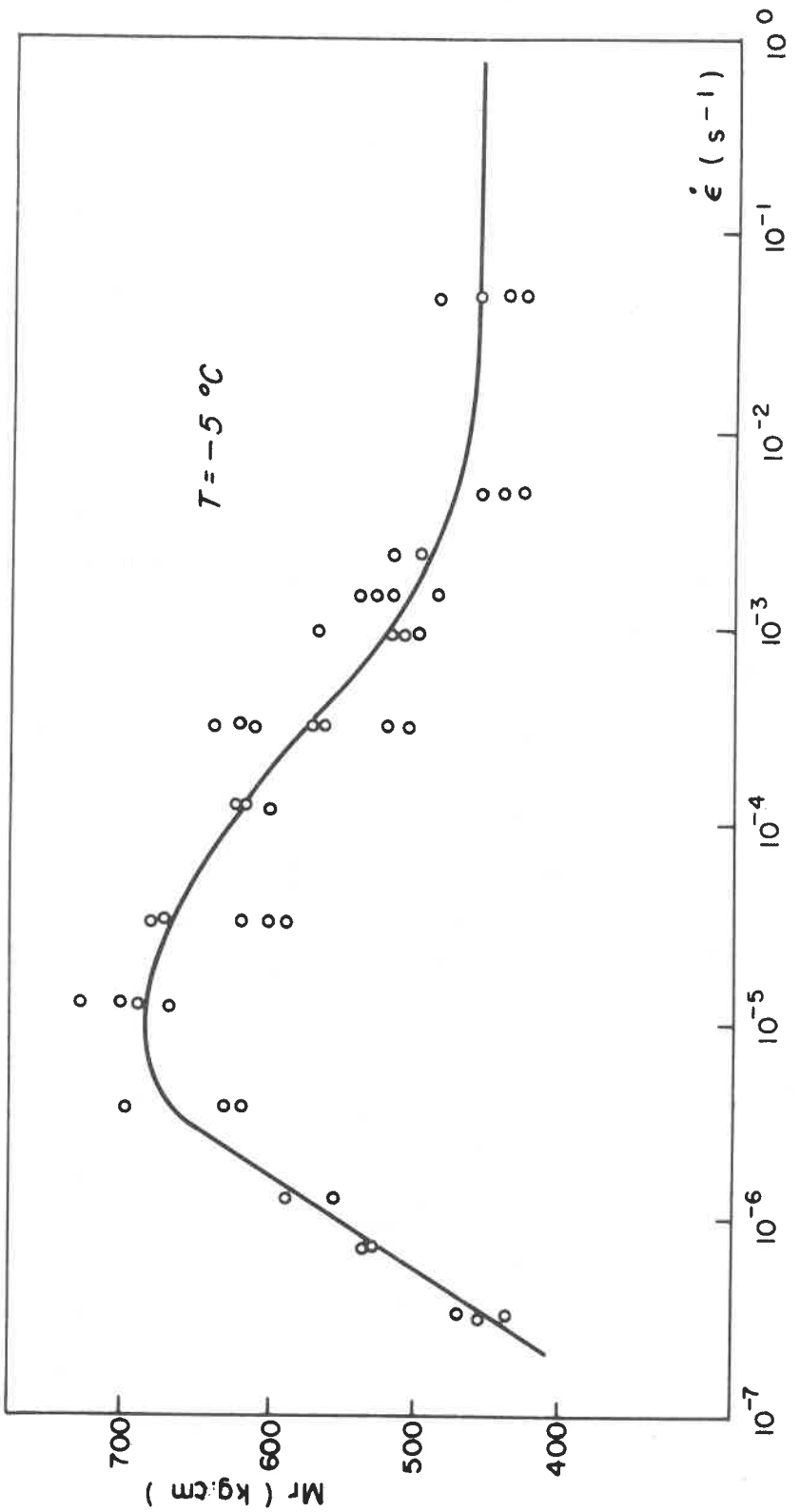

Fig. 2 - Resisting moment of beams of snow ice (T1) at various strain rates $\dot{\varepsilon}$.

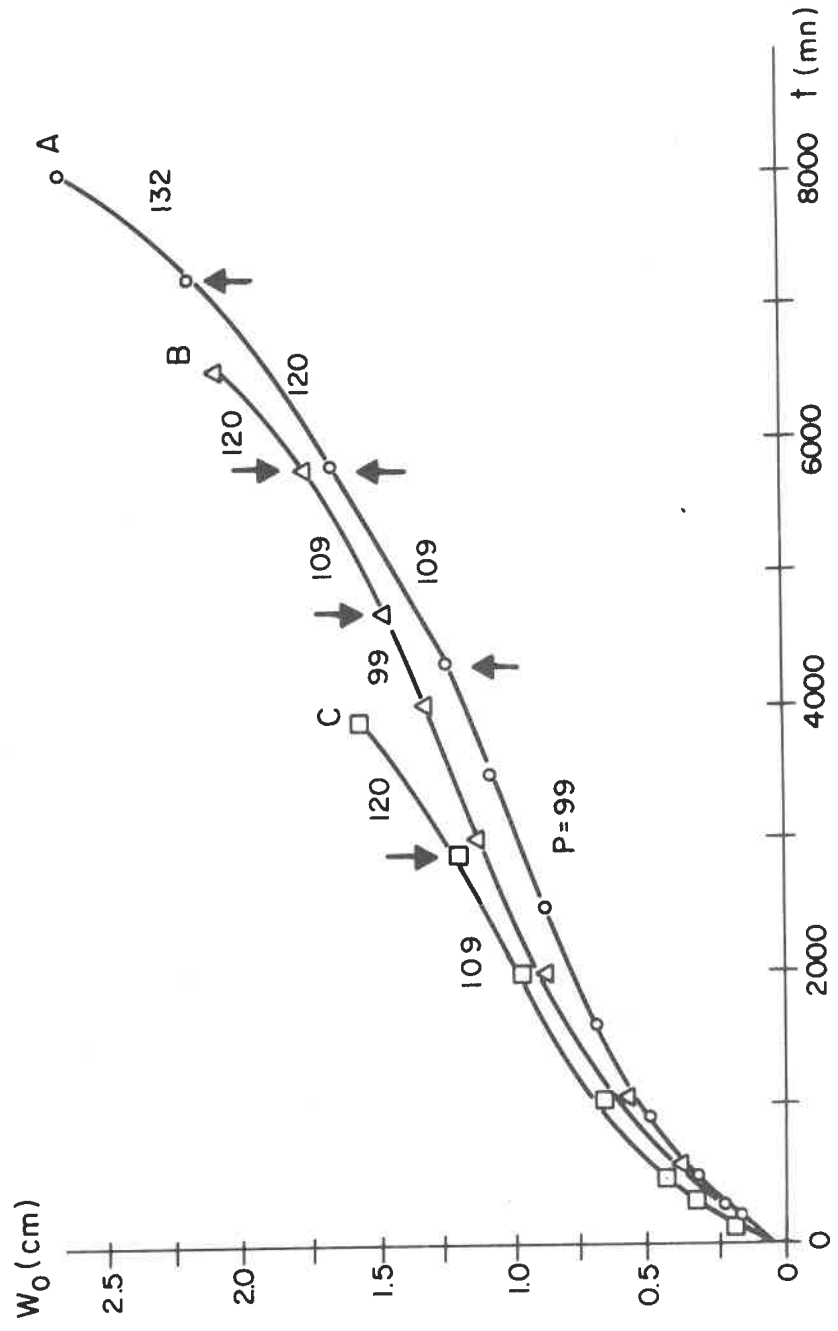

Fig. 3 - Deflection of beams of S2 ice with increasing loads in Kg.

Discussion

D. Masterson:

At strain rates of 10^{-10} to 10^{-9} s^{-1}, what flexural strength do you get? Also what is the order of deflection relative to ice thickness?

B. Michel:

We made no test at those very low values of strain rates which corresponds to creep of glaciers. We studied deflection of the ice plates for strain rates around 10^{-6} to 10^{-4} s^{-1} corresponding to loads from 25 to 80% of the brittle fracture load. The maximum stress values were between 0.5 and 5.0 MN/m^2.

For the cases of loading just mentioned, the deflection at the centre was of the order of ½ to 1 time the thickness of the plate after 100 hours of creep. For higher loads we even measured deflections up to 3½ times the thickness of the ice plate.

D.J. Goodman:

You present data on the strength of ice plates but you have not discussed the propagation of cracks that may exist in the ice and which probably control its strength.

B. Michel:

The data presented on the strength of ice was found to be compatible with theoretical values of ice strength. Those theoretical values were taken from Michel (1978) and were computed on the basis of crack formation in one crystal and propagation.

The critical condition for the formation of a crack in ice is the release of the elastic energy of a grain of measured diameter to form a crack along the basal plane of ice (Michel, 1978). There is considerable evidence that in polycrystalline ice, micro-cracks when formed, extend to the full size of each grain throughout the basal plane (Gold, 1960; Michel, 1978). These initial cracks propagate and cause collapse of the ice plate.

But you are more concerned with cracks that already exist in the ice and that could propagate to cause failure of the ice plate. You are right when you say cracks may initially exist in the ice. There is always some structural

stress risers present in natural ice that can start the nucleation of a crack. The usual one is the airbubble that will set up a concentrated stress field (Michel, 1978).

If a crack is already present in ice, there is a concentration of stress on the neighbouring crystals when the plate is loaded. In fact, there is a large increase in tensile stresses at the tips of the crack. Sadowsky and Steinberg (1949) have obtained the stress concentration at the tips of the crack, σ_d, in function of stress at infinity σ. For the ratio $a_o/d = 0.05$.

$$\sigma_d = 13.5\ \sigma$$

The crack will propagate following the basic principle related earlier, when the tensile energy is higher than the energy needed to form a surface. From this we have the minimum stress needed to propagate the crack:

$$\sigma^1 > \sqrt{\frac{2\ \sigma_{cv}\ E_{33}}{90.6\ H}}$$

with $\sigma_{cv} = 0.109\ J\ m^{-2}$, is the surface energy of ice in contact with its saturated vapour

H = height of the crystal
E_{33} = elastic modulus of ice along the c axis.

Then for an average height of the crystals of ice of one centimeter (1 cm), we have the maximum stress, σ^1, needed to propagate a crack already formed in a crystal of the ice plate at 0°C:

$$\sigma^1 \geq 5.8 \times 10^4\ N/m^2$$

this value is about 14 times smaller than the value of the tensile strength of S2 type of ice at the same temperature.

So it may be expected that existing cracks must heal very quickly and that the strength of ice is given by the formation and propagation of a new one.

A LABORATORY INVESTIGATION OF CIRCULAR SEA-ICE PLATES

J.-R. Murat and R. Tinawi
Ecole Polytechnique de Montréal

Introduction

A number of short and long-term flexural tests have been performed on sea-ice beams and plates at Ecole Polytechnique as part of the overall bearing capacity study.

Flexural tests have the advantage of involving relatively large samples of ice, thus avoiding part of the scale problem and simulating a realistic state of stress within the ice thickness. This is specially true for plate tests.

In a first phase (Murat and Tinawi, 1977), simply supported sea-ice beams have been tested in flexure, providing an index for the strength and the elastic modulus values.

This paper describes the results obtained from the instantaneous loading of simply supported circular sea-ice plates, 2.13 m in diameter and 9 to 14 cm in thickness. An analysis of the experimental deflections, by use of thin plate theory as well as the AXI program (a special purpose Finite Element program: Murat, 1976a and 1976b) has been reported elsewhere (Tinawi and Murat, 1978; Murat, 1978). This work will be confined to the study of the failure loads.

Two different approaches have been proposed for the estimation of the breakthrough load of floating ice sheets:

i) In the first one (Nevel, 1958; 1961) the ice is regarded as a brittle material and an elastic analysis is performed on the cracked plate (wedge analysis)

ii) On the other hand, Meyerhof (1962) has considered the ice as perfectly plastic, thus promoting the use of a yield line theory (limit analysis).

In fact, saline ice (Tabata, 1966) as well as fresh water ice (Carter and Michel, 1971) is known to exhibit both behaviours, depending on the applied stress rate. Analysis of the obtained failure loads indicates that, for some loading conditions, a mixed failure mode should be considered.

As for the calculation of the ultimate bending moment, different limit stress distributions are assumed at a plastic hinge and a comparison with the experimental results is reported.

Experimental Set-Up

Artificial sea-ice is grown in the freezing tank shown in Fig. 1 where the geometry and loading configuration common to all plate tests are illustrated. All the experimental details have been previously reported (Murat and Tinawi, 1977). The major part of the formed ice sheet is of the S2 columnar type (Michel and Ramseier, 1971) and typical salinity and temperature distribution across the ice thickness are illustrated in Fig. 2. If the salinity variation is assumed parabolic, it can be shown using the formula of Frankenstein and Garner (1967) that:

$$\nu_b \ (°/_{oo}) = (8Z^2-8Z+6) \left[\frac{49.185}{8Z+2} + 0.532\right] \qquad (1)$$

where ν_b is the ice brine volume and $0 \leq Z \leq 1$ is measured from the bottom of the plate.

From beam tests, the flexural strength corresponding to a brine volume $\nu_b = 26°/_{oo}$ was found to be 570 kPa and the value of the elastic modulus averaged 3.89×10^6 kPa.

Hence a parabolic approximation in E yields:

$$E = 4.32 \times 10^6 \ (0.572+0.931 \ Z-0.655 \ Z^2) \ kPa \qquad (2)$$

As for the tensile flexural strength:

$$\sigma_f = 957 \ (0.173+1.33 \ Z-0.917 \ Z^2) \ kPa \qquad (3)$$

Equations (2) and (3) are shown graphically in Fig. 3.

The experimental conditions for each test are summarized on Table I, along with the experimental failure load P_{fe}.

For isothermal tests (plates no. 6, 9 and 10), the water level was lowered after the formation of the required ice thickness. A 24-hour delay was allowed before testing in order to ensure a uniform temperature within the ice. The other plates were tested with the water in contact with the lower surface hence creating a temperature differential across the thickness. This temperature varied from the freezing temperature at the bottom surface in contact with the water, to -10°C at the upper surface in contact with the air.

The load was applied over an area 178 mm in diameter, with a rate of about 500 N/s. In order to minimize the influence of the water pressure (as an elastic foundation), the load has been applied in steps, allowing at each loading the water to evacuate through the overflow pipe.

Plate No. 6 was not tested to failure as it was used again for elastic tests at -13°C and -5°C. The maximum applied load in this case was 4.5 kN. Plate No. 7 is not reported due to technical difficulties encountered.

Analysis of Failure Loads

The bearing capacity of floating ice plates has been thoroughly reviewed by Kerr (1975). The analysis of short-term loadings can be divided into two parts:

1) the determination of the load at which the first crack occurs (P_{cr});

2) the determination of the breakthrough load (P_f) as the occurrence of the first crack does not necessarily cause the complete failure of the system, for most plate geometry.

A floating ice sheet under a vertical load can be represented by a plate on an elastic foundation (the water) of the Winkler type. This system is usually analyzed using classical elastic thin plate theory. Although this theory is quite adequate most of the time, the flexural rigidity is no longer given by $Et^3/12(1-\mu^2)$. The reason is that the elastic modulus varies across the plate thickness. However, as shown by Kerr and Palmer (1972), the solutions obtained for homogeneous plates may be used provided a modified flexural rigidity is defined.

The alternative is to consider an elastic theory where the normal and shearing stresses as well as the variation in E are considered. The AXI program has been used to analyze such a stress distribution in ice plates.

The first cracking load P_{cr}, as reported in Table I was obtained by comparing the state of stress in the plate to the limit strength of the ice. Figure 3b gives the limit stress for the plates tested with water underneath. As for the other plates, a value of 570 kPa was used. It appears that the experimental breakthrough loads are 3 to 5 times higher than P_{cr}.

On the other hand, if the ice plate is assumed to be perfectly plastic (Meyerhof, 1962) and capable of resisting a full plastic moment M_p without cracking, the ultimate load of a simply supported circular plate (Fig. 4) can be easily estimated. Hopkins and Prager (1953) obtained, for a material obeying the yield condition of Tresca (Fig. 5b).

$$P_{f_1} = 6\pi M_p \frac{1}{3-2a/R} \tag{4}$$

Now, for the geometry and loading under consideration, the plate cannot reach the flow limit without becoming plastic at the centre thus $M_R = M_T = M_p$ (a state of stress represented by point A in Fig. 5). Furthermore, the radial bending moment M_R will decrease along a radius, to vanish at the support (a condition represented by point B). The overall plate is thus in the same plastic region shown by segment AB in Fig. 5. It follows that the ultimate failure load P_{f_1} applies also for the Rankine and the Mohr-Coulomb criteria; the last one being the more likely to apply for ice (Hawkes and Mellor, 1972; Haynes, 1973; Nevel and Haynes, 1976).

In his analysis, Meyerhof (1962) used the following expression for the limit moment:

$$M_p = \sigma_p \frac{h^2}{4} \tag{5}$$

where σ_p is the yield stress and h the height of the section. This formulation is based on the stress distribution of an homogeneous plate as shown in Fig. 6a. Taking for σ_p the flexural strength of the bottom ice layer (σ_f = 165 kPa) yields:

$$M_p = 41.2\ h^2 \tag{6}$$

for a plate resting on the water. The value of h is expressed in meter and M_p in kN.m/m.

As the material properties of the ice vary across the plate thickness, Kerr (1975) proposed a limit stress distribution in the form of Fig. 6b.

The position α of the plastic neutral axis is defined by:

$$\int_0^{\alpha} \sigma(Z)\ dZ = \int_{\alpha}^{1} \sigma(Z)\ dZ \tag{7}$$

and the corresponding limit moment will be given by:

$$M_p = -\int_0^{\alpha} Z\ \sigma(Z)\ dZ + \int_{\alpha}^{1} Z\ \sigma(Z)\ dZ \qquad (8)$$

Substituting (3) into (7) and (8) yields:

$$\alpha' = 0.574; \quad M'_p = 117.8\ h^2 \qquad (9)$$

This formulation implies that the yield stress is equal in tension and in compression and depends only on the brine volume. Taking into consideration the findings of Hawkes and Mellor (1972) and the conclusions of the beam tests, it seems reasonable to assume the compressive yield stress to be about three times larger than the tensile one. Therefore the stress configuration of Fig. 6c yields:

$$\alpha'' = 0.783; \quad M''_p = 172.4\ h^2 \qquad (10)$$

Substituting relations (6), (9) or (10) into equation (4) yields the values noted P_{f1}, P'_{f1} and P''_{f1} respectively in Table 2.

For plates 9 and 10, tested at a uniform -10°C temperature, the yield stress has been assumed to be constant (570 kPa) across the section (Fig. 6d and 6e).

The ratio P''_{f1}/P_{fe} as calculated in Table II appears strongly affected by the plate thickness (4.2 for h = 90 mm and 2 for h = 137 mm). As the three proposed stress distributions yield similar expressions for the ultimate moment (a dependence on h^2), it is expression (4) of the ultimate load which has to be reconsidered.

This expression was based on the assumption that the plate was perfectly plastic throughout. On the other hand, one of the conclusions drawn from the analysis of deflections (Tinawi and Murat, 1978) is that the central part of the plate exhibits a brittle behaviour which causes radial cracks to develop (Fig. 7). The deflection w of the plate during the plastic flow will be in the shape of an obtuse cone:

$$w = w_o\ (1 - \frac{r}{R}) \qquad (11)$$

where w_o is the central deflection and r the radius.

The rotation θ_T associated with bending moment M_T will be expressed as:

$$\theta_T = - \frac{1}{r} \frac{dw}{dr} = \frac{w_o}{rR} \tag{12}$$

The energy dissipated in a plastic hinge of unitary length is:

$$u_p = M_p \theta_T \tag{13}$$

Integrating over the plastic region yields a total internal energy:

$$U_p = \int_b^R M_p \theta_T 2\pi r dr = 2\pi M_p w_o (1 - \frac{b}{R}) \tag{14}$$

The work done by the external uniform load p acting over a circular area of radius a is:

$$U_e = \int_o^a 2\pi p w_o(1 - \frac{r}{R}) r dr = 2\pi p w_o(\frac{a^2}{2} - \frac{a^3}{3R}) \tag{15}$$

Equating (14) and (15) and substituting for the total load $P_{f2} = \pi a^2 p$ yields:

$$P_{f2} = 6\pi M_p \frac{1-b/R}{3-2a/R} \tag{16}$$

where M_p is the limit moment, R the radius of the simple support, a the radius of the uniform load and b the radius corresponding to the transition between brittle and ductile behaviour.

The failure mode of sea-ice, as related to the applied stress rate has been mainly studied by Tabata (1966). Figure 8 summarizes the conclusions obtained from simply supported beam tests in flexure (isothermal conditions). It appears that for a uniform temperature of -10°C within the ice (plates tested without water), a ductile behaviour will be obtained for stress rates lower than 11 kPa/s, which corresponds to an octaedral shear stress rate of about 5 kPa/s. As the transitional stress rate is strongly affected by the ice temperature, the choice of the corresponding value that would apply to plates subjected to a temperature differential is not straightforward. It should be noted, however that the transitional stress rate increases with temperature. The formation of a plastic hinge will thus be controlled by the

behaviour of the coldest ice layer which is the top one, at -10°C. Hence the same value (5 kPa/s) will be applied to both testing conditions.

For each plate tested, the distribution of the octaedral shear stress rate along a radius has been computed using the finite element program AXI. Typical results (for plates no. 4 and 8) are shown in Fig. 9 along with the corresponding values of b. Ratios b/R as obtained for each tested plate have been reported in Table III. The theoretical failure loads P_{f_2}, P'_{f_2} and P''_{f_2}, computed from equation (16) and corresponding to the three possible ultimate moments (equations (6), (9) and (10)) are also reported.

It is clear that the stress distribution corresponding to the Mohr-Coulomb criterion (Fig. 6c and 6e) gives the best approximation of the experimental failure load.

The ratios P''_{f_2}/P_{fe} indicate a much better correlation than the one previously obtained. A distinction should still be made between the results of the plates with and without a temperature differential across the thickness.

The predicted values corresponding to an isothermal condition (plates 9 and 10) are under-estimated as one could expect from a limit analysis.

On the other hand, the ultimate loads calculated for the plates tested with water in contact are always over-estimated. This disagreement may be imputed to the somewhat erratic tensile behaviour of the lower ice layer in contact with the water, which could decrease the effective depth of the ice sheet.

Conclusion

The ultimate failure loads as obtained from flexural tests performed on simply supported circular sea-ice plates were reported.

The experimental breakthrough loads were found to be 3 to 5 times higher than the first cracking load determined using elastic theory. As the classical ultimate analysis did not yield satisfactory predictions, a modification has been proposed which accounts for the brittle behaviour of sea-ice associated with higher stress rates.

As for the ultimate moment, a limit stress distribution in the form of the Mohr-Coulomb criterion was found to be satisfactory. In this distribution, the limit stress

varies through the plate thickness with the compressive stress three times the value of the tensile one.

Finally, use of the ultimate moment yields failure loads under-estimated for isothermal plates and over-estimated for plates in contact with water. This presence of the water seems to affect the overall behaviour of the ice sheet.

Acknowledgments

This research was sponsored by Polar Gas Project through Montreal Engineering Company Ltd., under Grant No. CR 366-75 as part of their overall sea-ice bearing capacity studies. Grants from the National Research Council of Canada No. A-8958 and CINEP Project 109 are also gratefully acknowledged.

References

Carter, D., Michel, B. (1971). "Lois et Mécanismes de l'Apparente Fracture Fragile de la Glace de Rivière et de lac". Université Laval, Québec, rapport S-22.

Frankenstein, G.E., Garner, R. (1967). "Equation for Determining the Brine Volume of Sea-Ice from -0.5°C to -22.9°C". Journal of Glaciology, Vol. 6, no. 48, pp. 943-944.

Hawkes, I., Mellor, M. (1972). "Deformation and Fracture of Ice under Uniaxial Stress". Journal of Glaciology, Vol. 11 no. 61, pp. 103-113.

Haynes, F.D. (1973). "Tensile Strength of Ice under Triaxial Stresses", CRREL Research Report 312.

Hopkins, H.G., Prager, W. (1953). "The Load Carrying Capacities of Circular Plates", Journal of the Mechanics and Physics of Solids, Vol. 2, pp. 1-13.

Kerr, A.D., Palmer, W.T. (1972). "The Deformation and Stresses in Floating Ice Plates", Acta Mechanica, Vol. 15, pp. 57-72.

Kerr, A.D. (1975). "The Bearing Capacity of Floating Ice Plates Subjected to Static or Quasi-Static Load - A Critical Survey", Research Report No. RR 333, CRREL.

Meyerhof, G.G. (1962). "Bearing Capacity of Floating Ice Sheets", with discussion by Messrs. H.G. Hopkins; L.W. Gold; R.H. Wood, N.C. Lind and D.T. Wright, A. Assur; G.Y. Sebastyan and F. Penner and G.G. Meyerhof - ASCE Transactions, Vol. 127, Part I, pp. 524-581.

Michel, B., Ramseier, R.O. (1971). "Classification of River and Lake Ice", Can. Geotech. J., Vol. 8, pp. 36-45.

Murat, J.R (1976a). "Axi-symmetric Finite Element Formulation of Non-Homogeneous Floating Ice Sheets - Part I: Linear Analysis", Ecole Polytechnique de Montréal, (Canada) EP-76-R-11.

Murat, J.R. (1976b). "Axi-symmetric Finite Element Formulation of Non-Homogenous Floating Ice Sheets - Part II: Creep analysis", Ecole Polytechnique de Montréal, (Canada) EP-76-R-37.

Murat, J.R., Tinawi, R.A. (1977). "Sea-Ice Testing in Flexure", Fourth International Conference on Port and Ocean Engineering under Arctic Conditions, St-John's, Newfoundland, Canada.

Murat, J.R. (1978). "Essais en Flexion de Plaques de Glace de Mer", Ecole Polytechnique de Montréal, publication EP-78-R-17.

Nevel, D.E. (1958). "The Theory of a Narrow Infinite Wedge on an Elastic Foundation". Trans. Eng. Inst. of Canada, Vol. 2, no. 3.

Nevel, D.E. (1961). "The Narrow Free Infinite Wedge on an Elastic Foundation", USA - SIPRE Research Report 79.

Nevel, D.E., Haynes, F.D. (1976). "Interpretation of the Tensile Strength of Ice under Triaxial Stresses", CRREL Report 76-5.

Tabata, T. (1966). "Studies of Mechanical Properties of Sea-Ice X - The Flexural Strength of Small Sea-Ice Beams", Int. Conf. on Low Temperature Science, Sapporo, Japan, Physics of Snow and Ice, Vol. 1, pp. 481-497.

Tinawi, R.A., Murat, J.R. (1978). "Sea-Ice - Flexural Creep", IAHR Symposium on Ice Problems, Lulea, Sweden, Aug. 1978.

Table I: Tests on circular simply supported plates: experimental conditions.
P_{fe} = Experimental failure load;
P_{cr} = First cracking load

PLATE NO	THICKNESS mm	SALINITY ‰	TEMPERATURE (°C)		P_{fe} kN	P_{cr} kN
			Top	Bottom		
1	90	4	-10	- 2	2.22	0.85
2	95	5	-10	- 2	2.36	0.94
3	95	5	-10	- 2	3.31	0.94
4	92	4.75	-10	- 2	2.65	0.88
5	99	4.25	-10	- 2	4.05	1.00
6	95	4	-10	-10	—	—
	95	4	-13	-13	—	—
	95	4	- 5	- 5	—	—
8	137	5	-10	- 2	10.94	1.90
9	102	4.75	-10	-10	8.30	3.66
10	108	4.5	-10	-10	8.50	4.10

Table II: Analysis of the breakthrough loads; perfectly plastic plate (figure 4)

PLATE NO	THICKNESS mm	P_{fe} kN	P_{f1} kN	$P_{f'1}$ kN	$P_{f''1}$ kN	$\frac{P_{f''1}}{P_{fe}}$
1	90	2.22	2.24	6.41	9.38	4.2
2	95	2.36	2.50	7.14	10.46	4.4
3	95	3.31	2.50	7.14	10.46	4.5
4	92	2.65	2.35	6.70	9.81	3.7
5	99	4.05	2.72	7.76	11.35	2.8
8	137	10.94	5.20	14.85	21.74	2.0
9*	102	8.30	9.96	9.96	14.94	1.8
10*	108	8.50	11.17	11.17	16.75	2.0

*Plates tested without water (isothermal, -10°C, condition)

Table III: Analysis of breakthrough loads: ductile-brittle plate (figure 7)

PLATE NO	THICKNESS mm	P_{fe} kN	$\frac{b}{R}$	P_{f2} kN	$P_{f'2}$ kN	$P_{f''2}$ kN	$\frac{P_{f''2}}{P_{fe}}$
1	90	2.22	0.75	0.56	1.60	2.35	1.1
2	95	2.36	0.68	0.80	2.29	3.35	1.4
3	95	3.31	0.68	0.80	2.29	3.35	1.0
4	92	2.65	0.72	0.66	1.88	2.75	1.0
5	99	4.05	0.64	0.98	2.79	4.09	1.0
8	137	10.94	0.36	3.33	9.51	13.91	1.3
9*	102	8.30	0.60	3.98	3.98	5.98	0.72
10*	108	8.50	0.64	5.14	5.14	7.80	0.92

*Plates tested without water (uniform -10°C temperature).

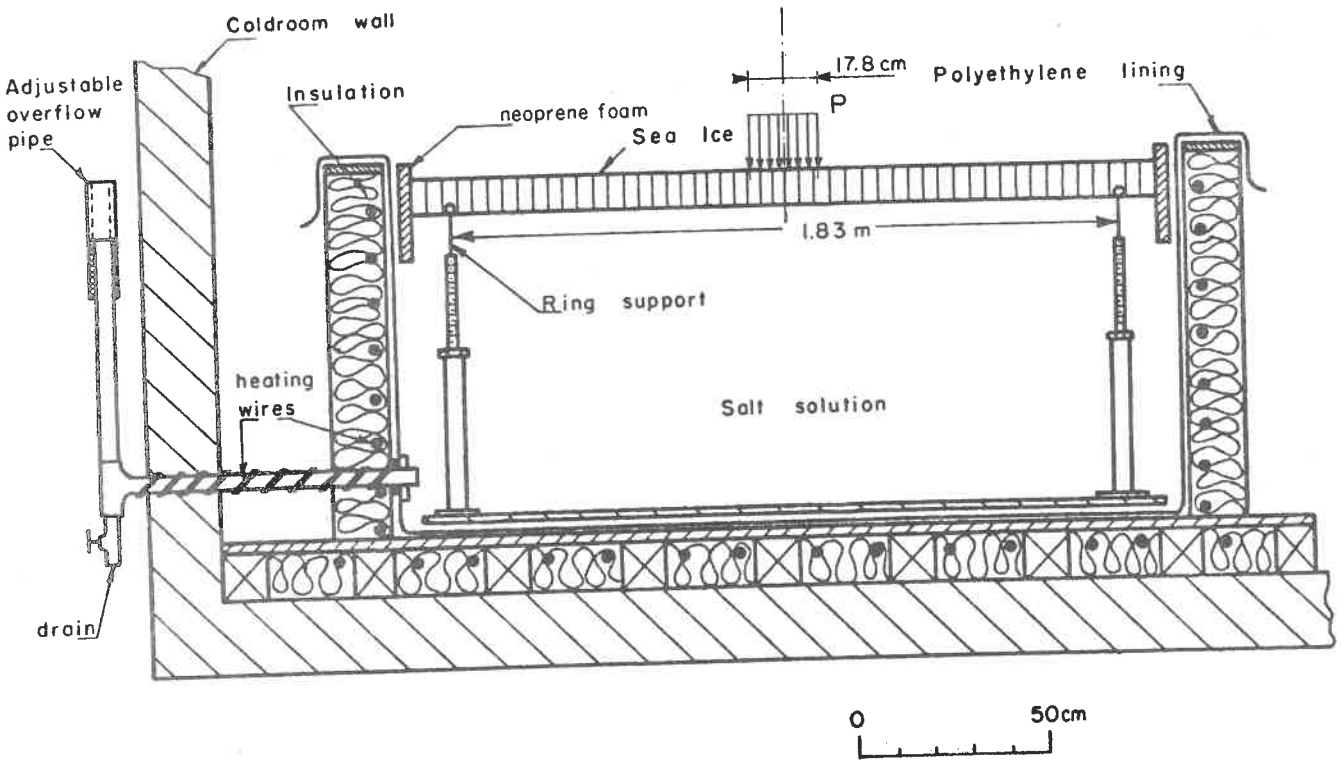

Figure 1: Freezing tank and experimental sea-ice plate

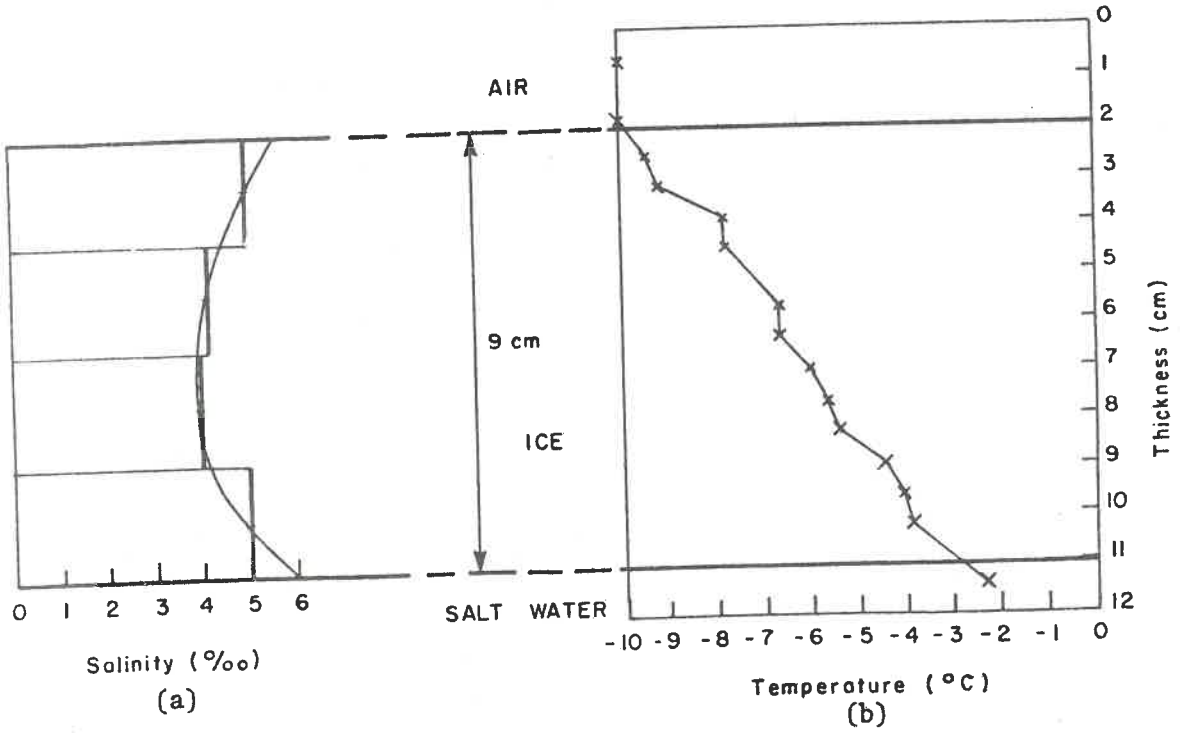

Figure 2: Salinity and temperature variation through ice thickness.

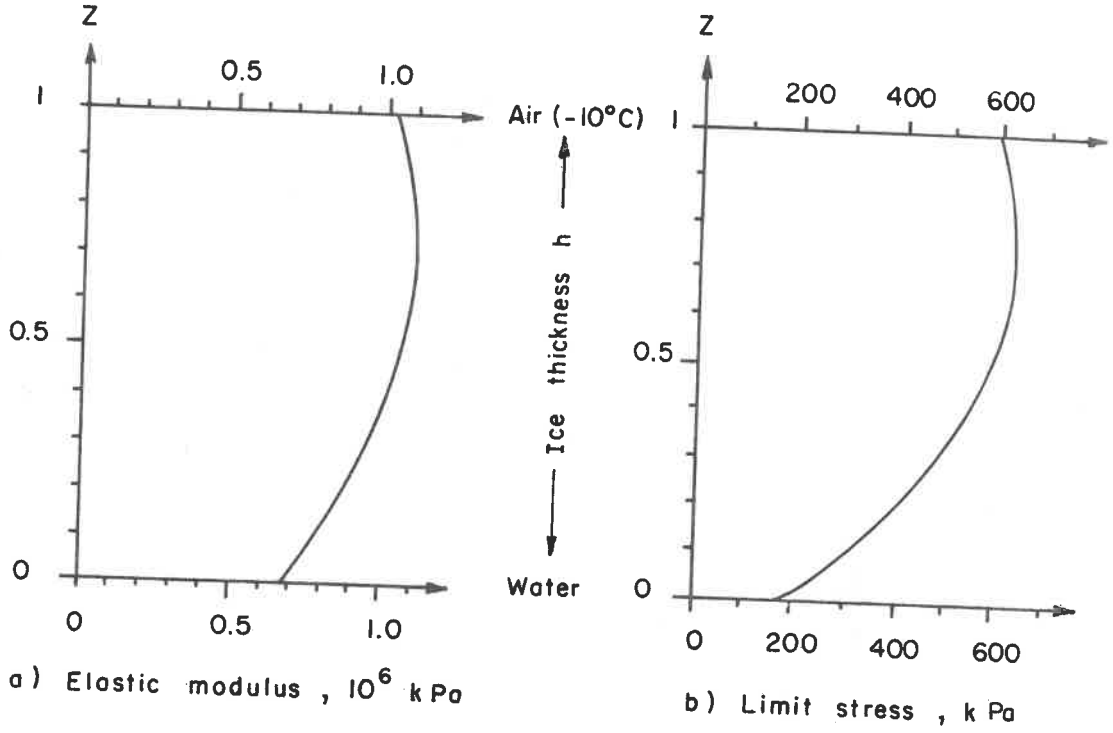

Figure 3: Variation of elastic modulus and limit stress through the plate thickness.

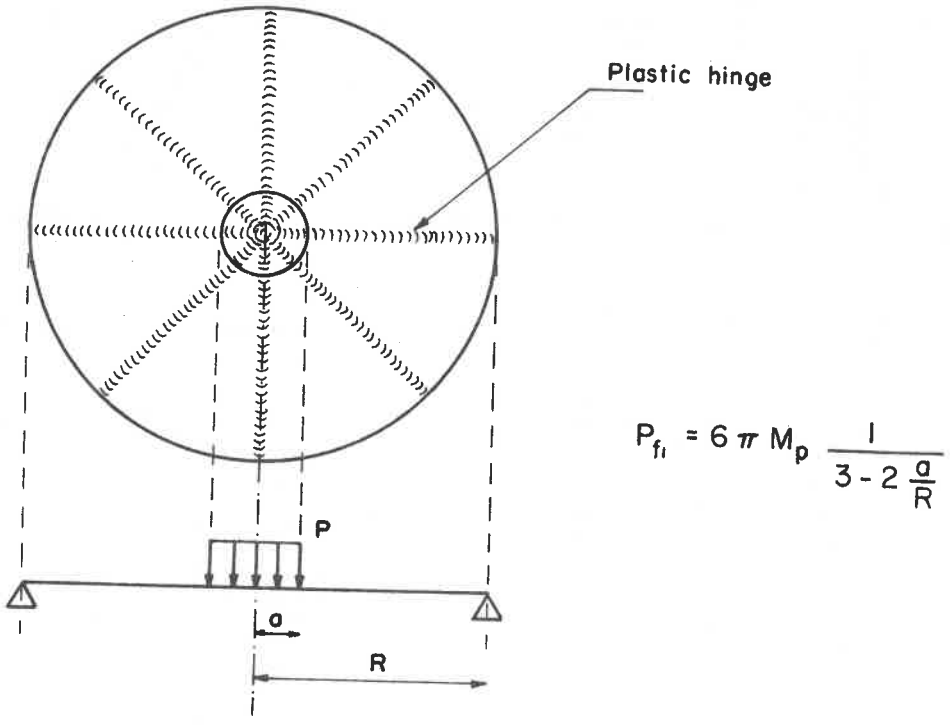

Figure 4: Ultimate failure of a perfectly plastic plate.

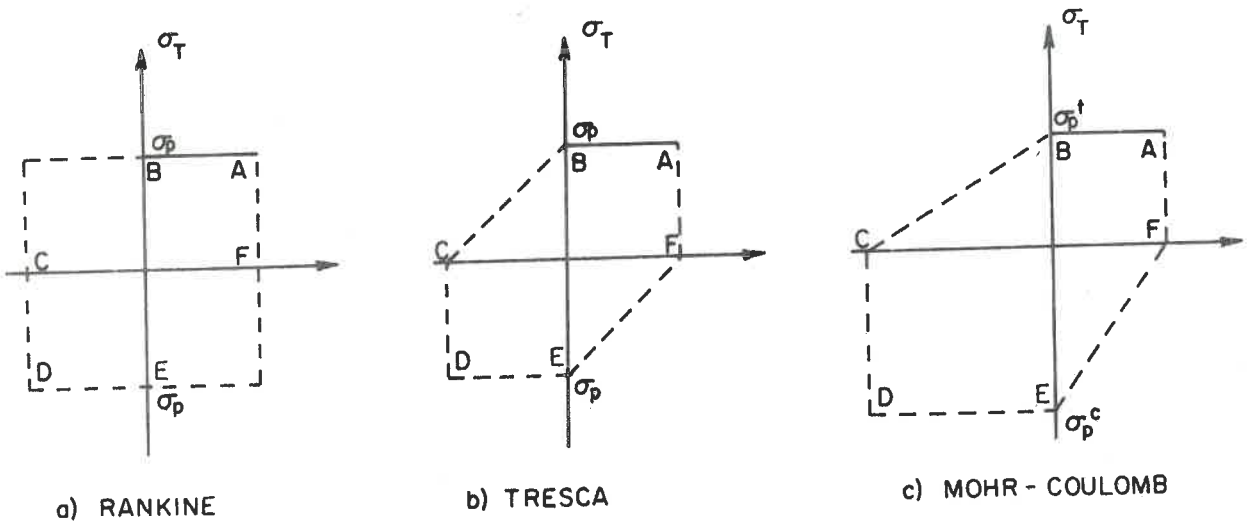

Figure 5: Stress criteria proposed for sea-ice

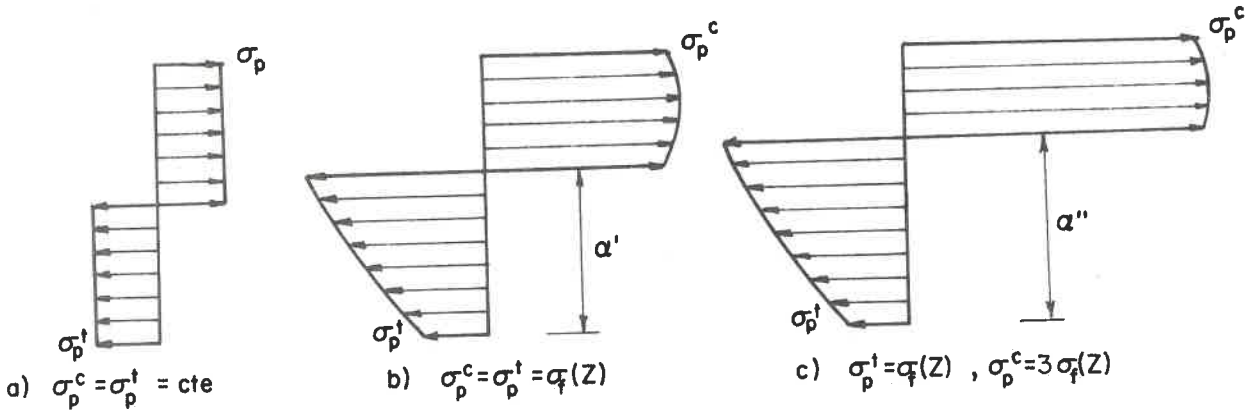

Plates tested on water: homogeneous (a), non-homogeneous with Tresca (b) and with Mohr-Coulomb (c) criterion

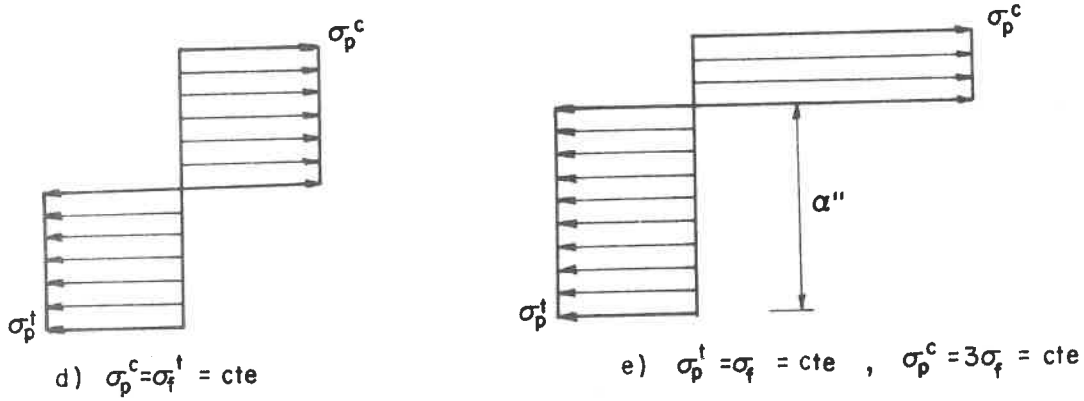

Isothermal plates with Tresca (d) and with Mohr-Coulomb (e) criterion

Figure 6: Limit stress distribution in a plastic hinge.

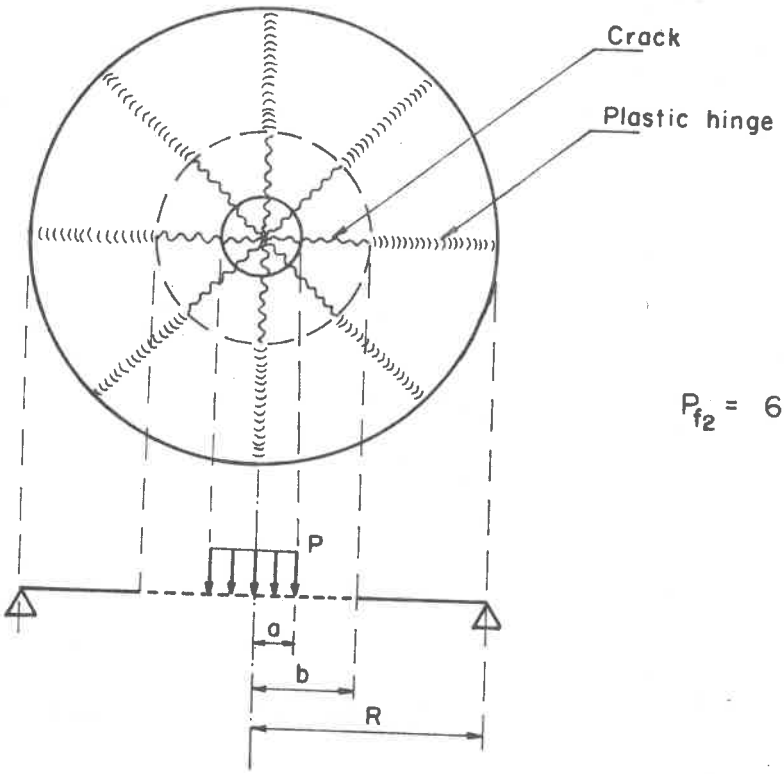

$$P_{f_2} = 6\pi M_p \frac{1 - \frac{b}{R}}{3 - 2\frac{a}{R}}$$

Figure 7: Ultimate failure of a brittle - ductile plate

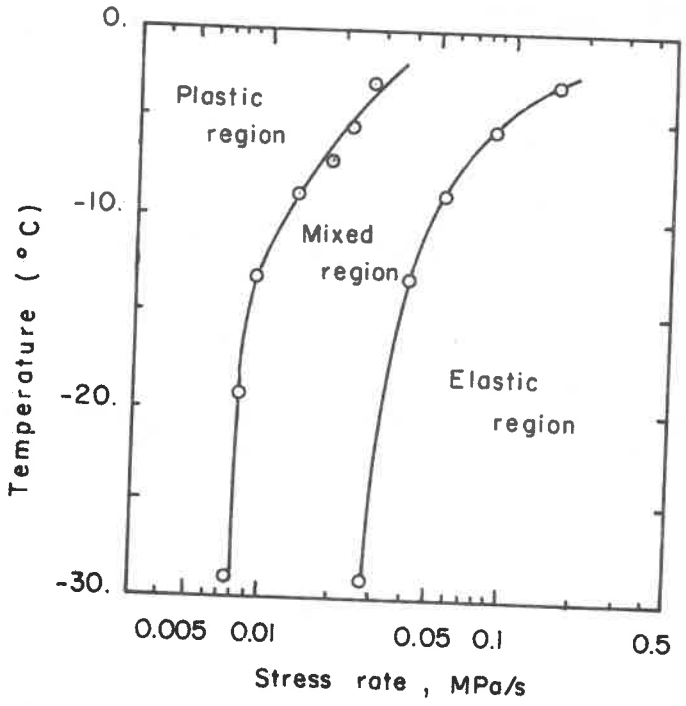

Figure 8: The border lines among elastic and plastic region in relation to the temperature and the rate of stress. (Tabata, 1966)

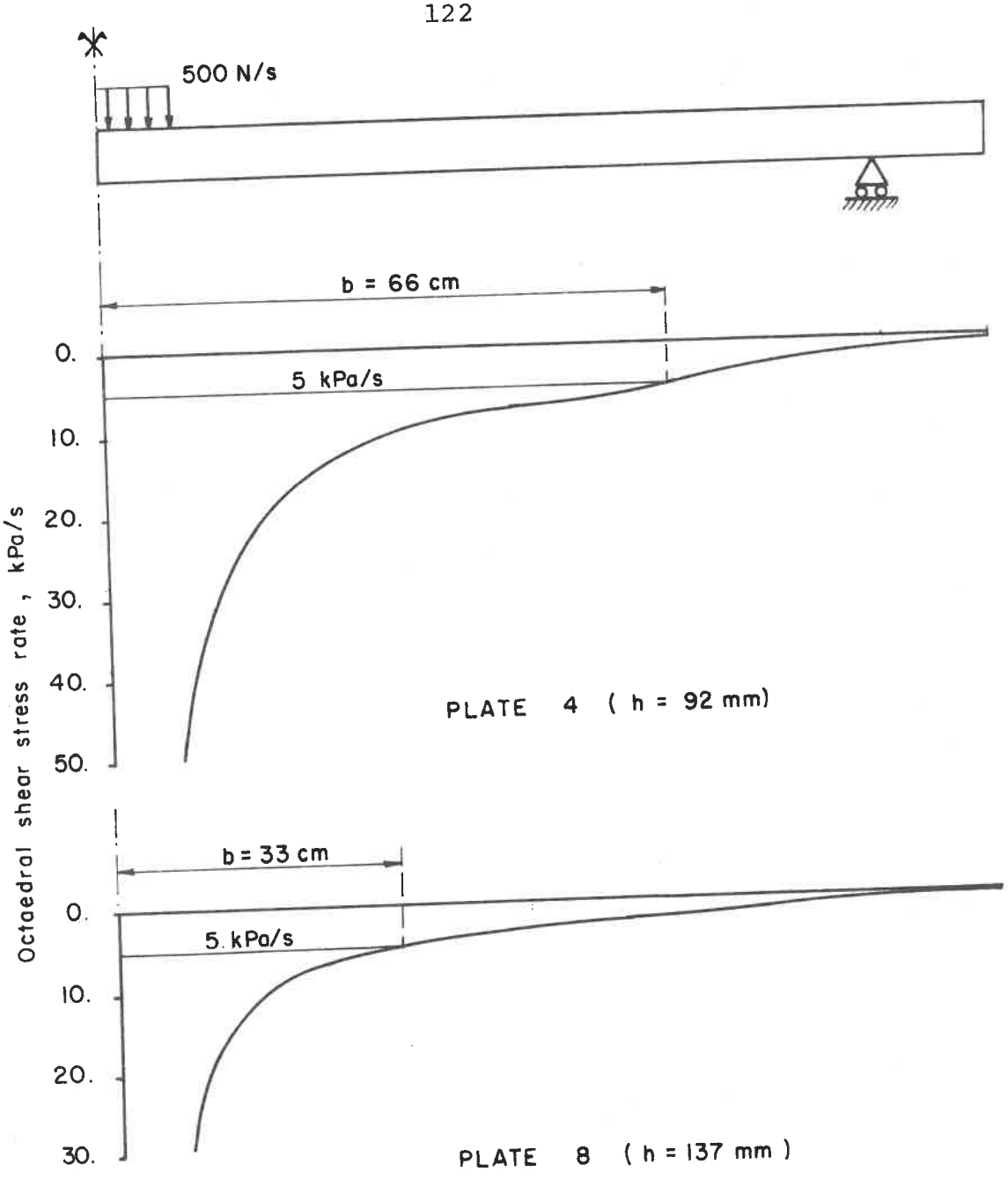

Figure 9: Octaedral stress rate variation along a radius of a simply supported plate loaded at 500 N/s.

Discussion

R. Frederking:

Does the water have an effect other than that which might be associated with the temperature gradient induced by it?

J.-R. Murat and R. Tinawi

It seems so. In the analysis of the floating plates, we took into account the effect of temperature and salinity distributions. The comparison between the results obtained from tests with and without water shows that there is still a difference.

R. Gerard:

In your 'cracked' plastic analysis, presumably you must assume the number of cracks - were your results sensitive to this? Also, with the stress-strain curves found for ice, is it reasonable to assume even approximate constant stresses will be developed across the tension or compression zones? (If I recall correctly this is an assumption associated with plastic hinges?)

J.-R. Murat and R. Tinawi

(1) From the experimental work, the number of radial cracks was found to be 5 to 7. We thus assumed that the central cracked part completely lost its global rigidity and behaves like a set of rigid wedges.

(2) The limit stress distribution in a plastic hinge does not have to be uniform. In fact we used a variable stress distribution as shown in Fig. 6c (for the plates tested with water underneath

S. Beltaos:

Could the authors comment on how the parameter b was determined and how large it was relative to the radius of the load and the characteristic length of the ice plate?

J.-R. Murat and R. Tinawi

I think that this question is answered in the paper itself. [The stress distribution in the plate is computed by a finite element program. The stress rate distribution is deduced (Fig. 9). Radius b is obtained by the interaction between this curve and the line $\dot{\delta}$ critical. The best value is obtained from the conclusions of Tabata (Fig. 8).]

AN EMPIRICAL ANALYSIS OF THE CREEP OF FLOATING ICE SHEETS*

S. Beltaos and A.W. Lipsett
Transportation and Surface Water Engineering Division
Alberta Research Council

Introduction

An increasing use of arctic areas of the world has focused attention on the engineering properties of floating ice sheets. Ice covers are being used as winter transportation routes and also as structural foundations for heavy machinery employed in northern resource exploration. To utilize these ice covers in a safe manner, the load bearing capacity of the ice sheet must be known or estimated. The main complicating factor is that the ice behaves as a visco-elastic material which creeps under the applied load. This renders the load bearing capacity problem time-dependent.

The load bearing capacity of an ice sheet could be predicted for any loading history if the following information were available:

1) a failure criteria, expressed in terms of an observable quantity, eg. critical deflection, critical load.

2) a method of predicting the temporal behaviour of the ice sheet, eg. deflection-time variation.

Beltaos (1977) presented a maximum strain energy criteria of failure which agreed well with available field data on the load bearing capacity of ice sheets. This criteria introduced the concept of the "onset of failure"[1] and can be stated as: The onset of failure occurs when the work done by the load reaches a critical value. This value is proportional to the ice thickness raised to the power 5/2.

This paper deals with the problem of predicting the temporal variation of the ice deflection, which, as pointed out above, is the second item needed for a complete prediction of the load bearing capacity.

---

[1]The onset of failure is defined as the instant at which the variation of the maximum ice deflection with time begins to depart from a previously established pattern and starts to increase at an accelerating rate until ultimate breakthrough of the load.

*Alberta Research Council Contribution Series 937

Nevel (1966, 1976) has developed theoretical equations for the time-dependent deflection of floating ice sheets based on the theory of linear viscoelasticity. Use of these equations requires knowledge of two or more spring and dashpot constants, depending on the complexity of the assumed model. Evaluation of these constants using prototype test results (Frankenstein, 1966) showed that they varied widely. This variation could not be explained satisfactorily by corresponding variations in ice properties. Further work by the authors, using results of loading tests conducted by Alberta Research Council during the period 1974-1977, seems to support the above findings. The discrepancy between theory and observation can, at least partially, be explained from the following consideration.

If Nevel's (1966) equations are applied to a segment of an experimental time-deflection curve, the associated constants can be selected so that the theory adequately describes the deflection data within the corresponding time interval. However, if these constants are used to extend the theoretical prediction of deflection to other time intervals of the same experimental curve, significant error occurs. The selection of the constants is therefore dependent on the particular time interval chosen for their evaluation. This could account for a part of the unexplained variation of these constants determined for a given series of tests.

The analysis presented in this paper retains the concept of linear viscoelasticity inasmuch as deflection is assumed to be proportional to the load, but is based on an empirical determination of the basic deflection-time curve which results from the simplest loading history (load = constant).

It is now known (see, for example, Sinha, 1977) that ice is not a linearly viscoelastic material, except when subjected to very low stresses. However, the assumption of linear viscoelasticity, though physically questionable, affords a great practical advantage; i.e., it permits efficient application of the principle of superposition, as will be shown later.

Analysis

Numerous prototype bearing capacity tests have been performed by the Transportation and Surface Water Engineering Division of Alberta Research Council during the period November 1974 - March 1977. Analysis of the results of these tests indicated that a similarity-type relationship exists for the deflection-time curve associated with tests which approximated the simplest loading history, i.e., a constant load applied instantaneously. This relationship is expressed by the simple empirical equation:

$$\frac{w}{w_{el}} = f\left(\frac{t}{\tau}\right) = 1 + \sqrt{\frac{t}{\tau}} \; ; \quad P = \text{Constant}, \; t \geq 0 \qquad (1)$$

where w is the maximum deflection under the load; w_{el} is the initial (t = 0), presumably elastic, component of the deflection; t is the time from commencement of loading; and τ is the time when the deflection reaches twice the elastic deflection[2]. Figure 1 shows the results of nine "instanteneous" loading tests plotted in the form suggested by (1). Equation 1 is seen to adequately describe the deflection history for these tests.

Also shown in Fig. 1 is the similarity curve that would be obtained from Nevel's theory[3], for comparison purposes. This theory $\tau = 2.57\ \eta_1/E_1$, where E_1 is a spring constant with dimensions of stress and η_1 is a dashpot constant with dimensions of viscosity. Evidently, for a truly linear viscoelastic material, τ can be considered a material property. Thus in the case of ice, it would be expected that in addition to a material property, τ also reflects the stress level in the ice sheet.

The elastic component, w_{el}, is given by the well known relation (Meyerhof, 1962):

$$w_{el} = \frac{P}{8\gamma\ell^2} \qquad (2)$$

where P is the load, γ is the subgrade modulus (in this application γ = unit weight of water), and ℓ is the characteristic length of the ice sheet, defined by:

$$\ell = \left\{\frac{Eh^3}{12(1-\mu^2)\gamma}\right\}^{\frac{1}{4}} \qquad (3)$$

Here, E is Young's modulus, h is the thickness of the ice and μ is Poisson's ratio for ice (usually taken as $\mu = 1/3$).

In order to evaluate the deflection response for any type of loading history, it is assumed that the deflection, as implied by (1) and (2), is directly proportional to the

---

[2]Note that (1) complies with this condition since f(1) = 2.

[3]For convenience, this curve was derived from a graphical representation of the theoretical prediction, Nevel (1968).

load and that the principle of linear superposition of loads (and deflections) is valid. To find the deflection w(t), due to a general loading history P(t), consider the loading situation shown in Fig. 2. Here, the elemental load dP commences at time T, and acts for a period t-T. By considering this elemental load as a constant load beginning at T, the incremental deflection response due to this load is obtained using (1) as follows:

$$dw = dw_{el}\left(1 + \sqrt{\frac{t-T}{\tau}}\right) \tag{4}$$

where the elemental elastic deflection dw_{el}, is given by (2) using the load dP.

In order to calculate the total deflection at time t, due to the entire loading history P(t), (4) is integrated from T = 0 to T = t. This sums all of the elemental deflection responses due to the elemental loads. Performing the required integrations results in:

$$w(t) = w(0) + \frac{1}{8\gamma\ell^2}\int_0^t \frac{dP}{dT}\left(1 + \sqrt{\frac{t-T}{\tau}}\right) dT \tag{5}$$

For a linearly increasing load (ramp load), $dP/dT = \dot{P}$ = constant and the integration results in:

$$w_{\dot{P}}(t) = \frac{\dot{P}\tau}{8\gamma\ell^2}\left\{\frac{t}{\tau} + \frac{2}{3}\left(\frac{t}{\tau}\right)^{3/2}\right\};\ P = \dot{P}t \tag{6}$$

assuming that the initial deflection is zero. The subscript $\dot{P}$ indicates that the deflection is associated with a ramp load.

The ramp loading was chosen for analysis because most practical loading histories can be generated using a linear combination of ramp loads. For example, consider the loading histories shown in Fig. 3. A simple creep type test is shown in Fig. 3a while the multiple load and the cyclic load are two other common types of loading configurations.

As the loading history is constructed by the linear combination of ramp loads, the resulting deflection response is generated by the sum of the individual responses due to each ramp load. For example, the deflection response for the case of the simple creep test (Fig. 3a) is given by:

$$w(t) = w_{\dot{P}}(t) = \frac{\dot{P}\tau}{8\gamma\ell^2}\left\{\frac{t}{\tau} + \frac{2}{3}\left(\frac{t}{\tau}\right)^{3/2}\right\};\ 0 \leq t \leq t_1$$

$$w(t) = w_{\dot{P}}(t) - w_{\dot{P}}(t-t_1) = \frac{\dot{P}\tau}{8\gamma\ell^2}\left\{\frac{t_1}{\tau} + \frac{2}{3}\left(\frac{t}{\tau}\right)^{3/2} - \frac{2}{3}\left(\frac{t-t_1}{\tau}\right)^{3/2}\right\};$$

$$t_1 \leq t \qquad (7)$$

using (6). The loading time t_1, is the time required to achieve the desired load. For loading at a constant rate, such as is usually the case when the load is applied by pumping water in large tanks, $\dot{P} = P/t_1$.

To apply (6), two parameters must be known or estimated. These are the time parameter τ and Young's modulus E. The present analysis allows for the computation of these two parameters in the initial stages of the bearing capacity tests. Subsequent deflection predictions can be made using the appropriate linear combinations of (6) and the values of τ and E found in the initial stage.

Dividing (6) by t yields:

$$\frac{w_{\dot{P}}(t)}{t} = \frac{\dot{P}}{8\gamma\ell^2} + \frac{\dot{P}}{12\gamma\ell^2}\left(\frac{t}{\tau}\right)^{\frac{1}{2}} \qquad (8)$$

which indicates that a plot of $w_{\dot{P}}(t)/t$ versus $\sqrt{t}$ will yield a straight line of slope $\dot{P}/12\gamma\ell^2\sqrt{\tau}$ and intercept $\dot{P}/8\gamma\ell^2$. From the intercept, the value of the characteristic length can be determined and the corresponding value of Young's modulus can be found using (3). The value of the time parameter τ may then be found using the slope of the line. It should be noted that the value of Young's modulus so calculated represents an initial elastic value.

Application

To illustrate the application of the present analysis, the bearing capacity test carried out at Joseph Lake on November 19, 1976 will be considered. A load of 13.35 kN was achieved by pumping water into six barrels until the barrels were full. The loading time was 5.5 min and the ice thickness was measured at 0.12 m. Figure 4 shows the loading history and resulting measured deflection response. Note that a distinct onset of failure is clearly evident at 100 minutes after commencement of loading. Breakthrough occurred at 113 minutes after commencement of loading.

The procedure to calculate τ and E is as follows. First $w_{\dot{P}}(t)/t$ is plotted versus $\sqrt{t}$. To find $w_{\dot{P}}(t)$ for any time, two time regions must be investigated. These are the time up to the loading time and the time after the loading time. As is shown by (7), $w_{\dot{P}}(t) = w(t)$ for the interval $0 \leq t \leq t_1$, where t_1 is the loading time. However, for the time interval $t_1 \leq t$, rearrangement of (7) results in $w_{\dot{P}}(t) = w(t) + w_{\dot{P}}(t-t_1)$. To calculate $w_{\dot{P}}(t)$[4] in this range a graphical solution can be used. The graphical determination of $w_{\dot{P}}(t)$ is shown in Fig. 5. By this method a graph of $w_{\dot{P}}(t)/t$ versus $\sqrt{t}$ can be generated and is shown in Fig. 6. The resulting points define a straight line of slope equal to 3.23×10^{-4} $m/min^{3/2}$ and intercept equal to 5.5×10^{-3} m/min. Using these values and the relationships described previously results in $\ell = 2.37$ m, $E = 1.92 \times 10^6$ kPa, and $\tau = 129$ min. These parameters were evaluated based on the first 40 min of the test and can be used for the subsequent prediction of the deflection response. As shown in Fig. 4, the deflection predicted by (7) agrees well with the measured deflection up to the onset of failure.

To further illustrate the capabilities of the present analysis, two examples of prototype bearing capacity tests are presented. The first is the test that was conducted at Joseph Lake between November 18-26, 1976. Figure 7 shows the loading history and measured deflection response for this test. The test proceeded for several days and at various time intervals the load was increased. This type of loading is similar to the multiple loading shown in Fig. 3b. Deflection measurements were taken for a few hours on most days, resulting in a scarcity of measured deflections. The two parameters τ and E, calculated by the method described above were found to be: $\tau = 207$ min and $E = 1.0 \times 10^6$ kPa. These parameters were evaluated based on the first 70 min of the test and the subsequent predicted deflection is shown in Fig. 7. Reasonable agreement with the measured deflection is shown for a significant portion of the remainder of the test.

The ice thickness on November 18 was 0.112 m and by November 20 the ice had thickened to 0.17 m. An adjustment of the predicted deflection must be made in order to account for the increased ice thickness. It can be shown using (2) and (3) that the deflection is inversely proportional to the ice thickness raised to the power 3/2, that is, $w \alpha h^{-3/2}$. The deflection was predicted based on a constant value of ice thickness (h = 0.112 m) and then was corrected using the above proportionally relationship and assuming that the ice thickened at a constant rate during the test. This enables the use of a single value for each of τ, ℓ and E to describe the bearing capacity test.

---

[4]Note that $w_{\dot{P}}(t)$ is the deflection that would occur if the load had continued to increase at a rate $\dot{P}$ beyond the time t_1.

The second test is that reported by Eyre and Hesterman (1976) at the Riverhurst ice crossing in Saskatchewan on March 11, 1975. The ice thickness for this test was 0.723 m and the loads were two trucks, one 177.8 kN and the other 231.2 kN. The loading history consisted of first driving one truck and then the other to a location over a deflection transducer and allowing creep to occur. Then the trucks were removed and the ice rebound recorded. The complete observed time deflection curve is shown in Fig. 8[5]. The loading history for this test is similar to that shown in Fig. 3c for the first cycle of a cyclic load. However, these loads approximate a load applied instantaneously and (1) now becomes the relevant equation for deflection prediction.

As can be seen from Fig. 8 the initial elastic deflection is w_{e1} = 0.022 m. Using (2) and a load of 177.8 kN yields a characteristic length ℓ = 10.15 m, and from (3) Young's modulus is $E = 2.96 \times 10^6$ kPa. To calculate τ, consider the deflection at the time just before application of the second load. From Fig. 8, the deflection is w (7 min) = 0.0265 m. The time response parameter is now found from (1) as τ = 167.3 min.

The predicted deflection using τ = 167.3 min and $E = 2.96 \times 10^6$ kPa is also shown in Fig. 8. Agreement with the observed deflection is shown for the entire deflection response. The predicted deflection is based on the results of the first seven minutes of the test and the subsequent deflection prediction is seen to be satisfactory through a period about 14 times this interval.

Discussion

The analysis described herein has been applied to the results of some 25 prototype ice loading tests. The time response parameter was found to vary in the range of 40 to 210 min, and Young's modulus E varied between 1.0 and 4.8 million kPa. It is believed that these variations are caused principally by:

1) Variations in ice properties, such as those related to ice temperature.

2) The fact that the ice is likely to behave as a non-linear viscoelastic material. If this is so, then τ and E would be expected to vary with some measure of the loading intensity, such as P/h^2 for constant load tests. This aspect is now under consideration.

---

[5]This graph was generated from the graphical representation of the test presented in Eyre and Hesterman (1976).

Despite the shortcomings noted above, the present method is at least capable of predicting the entire deflection curve without having to change the assumed values of the experimental constants τ and E for different time intervals of this curve. In practice, the present method could be utilized in conjunction with long term loads as follows: Monitor the deflection for the first hour or so of loading. Use this information to deduce τ and E and apply the method to predict the subsequent development of deflection.

Summary and Conclusions

The prediction of the temporal deflection of a floating ice sheet subject to a load is formulated based on an empirical similarity relationship derived from numerous prototype bearing capacity tests. The empirical analysis requires the calculation of a time parameter τ and a modulus of elasticity E. These parameters may be evaluated during the initial stages of a bearing capacity test and then used for subsequent deflection prediction. This can then be used in conjunction with a failure criterion (see also Beltaos, 1977) to predict the time to failure.

The values of the parameters τ and E were found to vary considerably for the twenty-five tests analyzed. Work is continuing to identify possible correlations of τ and E with ice properties and loading intensity.

Acknowledgments

The work reported herein is a part of a continuing research program to study the load bearing capacity of floating ice sheets. This program is carried out by the Transportation and Surface Water Engineering Division of Alberta Research Council in cooperation with Alberta Transportation under the auspices of the Alberta Cooperative Research Program in Transportation and Surface Water Engineering.

The tests quoted herein could not have been carried out without the assistance of M. Anderson, G. Childs, G. Putz, T. Ridgway and J. Thompson of the Division. R. Gerard and B.P. Shields reviewed a draft of the manuscript.

References

Beltaos, S. (1977). "A Strain Energy Criterion for Failure of Floating Ice Sheets", NRC Workshop on the Mechanical Properties of Ice, Calgary, Alberta. NRC Tech. Memo. No. 121, pp. 82-106.

Eyre, D. and Hesterman, L. (1976). "Report on an Ice Crossing at Riverhurst During the Winter of 1974-75", Saskatchewan Research Council Report No. E76-9.

Frankenstein, G.E. (1966). "Strength of Ice Sheets", Proceedings, Conference on Ice Pressures Against Structures, Laval University, Quebec. NRC Technical Memorandum No. 92, pp. 79-87.

Meyerhof, G.G. (1962). "Bearing Capacity of Floating Ice Sheets", Transactions ASCE, Vol. 127, Part I, pp. 524-577.

Nevel, D.E. (1966). "Time Dependent Deflection of a Floating Ice Sheet", U.S. Army Cold Regions Research and Engineering Laboratory, Research Report 196.

Nevel, D.E. (1968). "Bearing Capacity of Floating Ice Sheets", U.S. Army Cold Regions Research and Engineering Laboratory, Terrestrial Sciences Centre, Hanover, N.H.

Nevel, D.E. (1976). "Creep Theory for a Floating Ice Sheet", U.S. Army Cold Regions Research and Engineering Laboratory, Special Report 76-4.

Sinha, N.K. (1977). "Short Term Rheology of Polycrystalline Ice", Symposium on Physics and Chemistry of Ice, Cambridge, Sept. 1977.

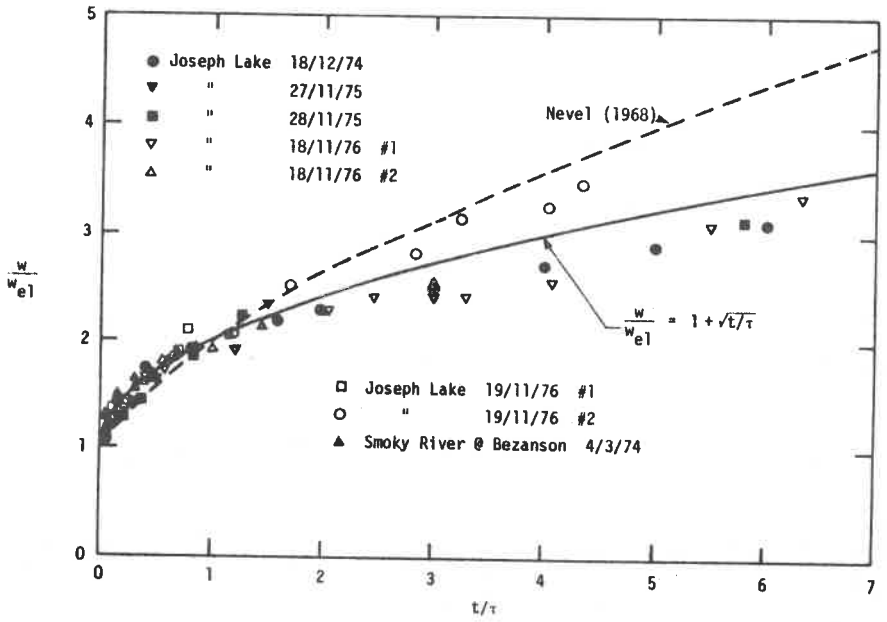

FIGURE 1. Similarity relationship for bearing capacity tests

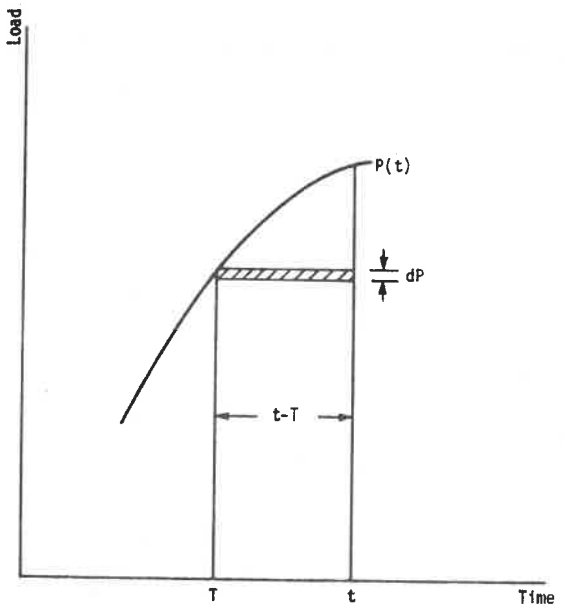

FIGURE 2. General loading history

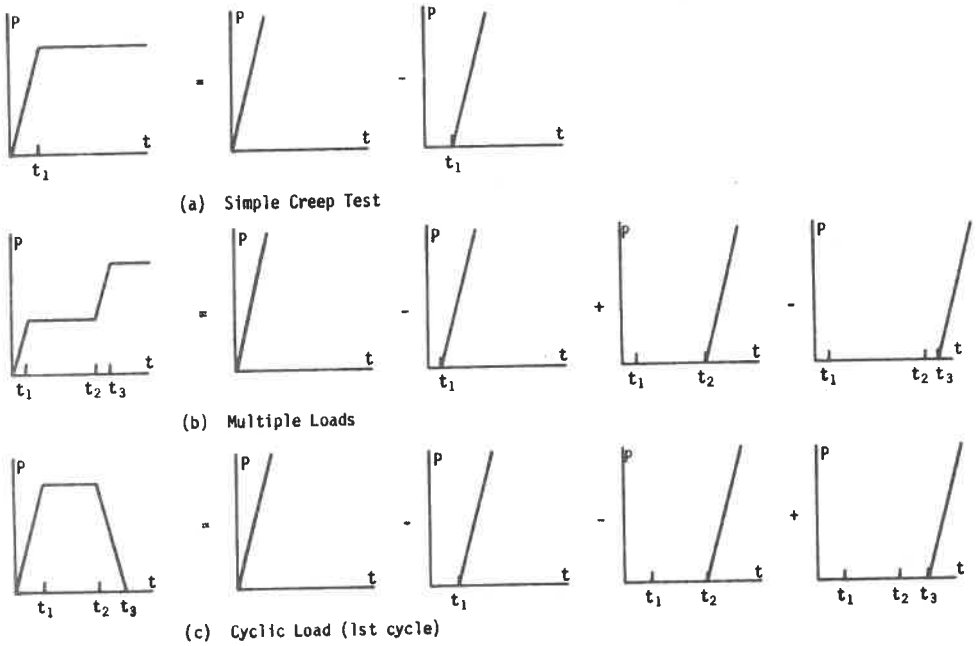

FIGURE 3. Linear combinations of ramp loads

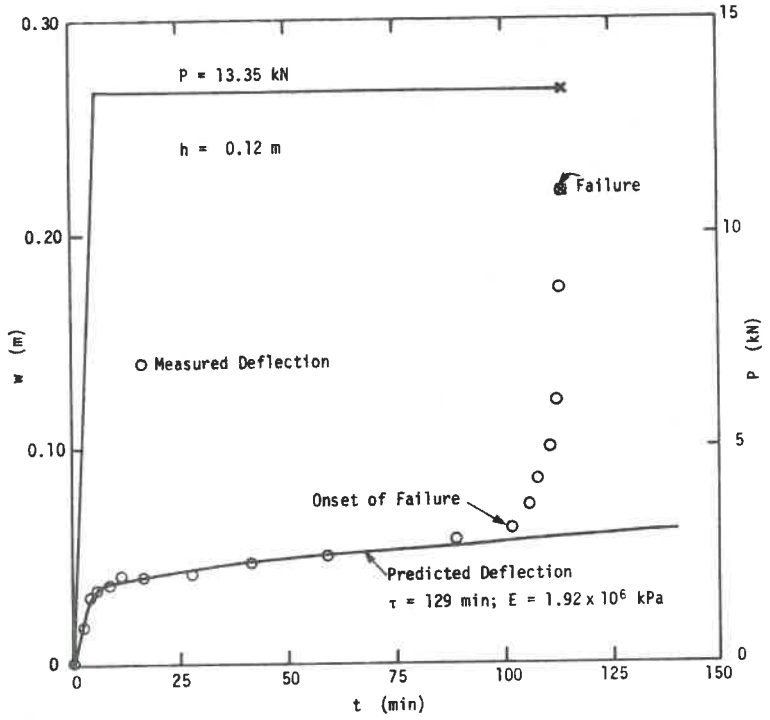

FIGURE 4. Creep test, Joseph Lake, November 19, 1976

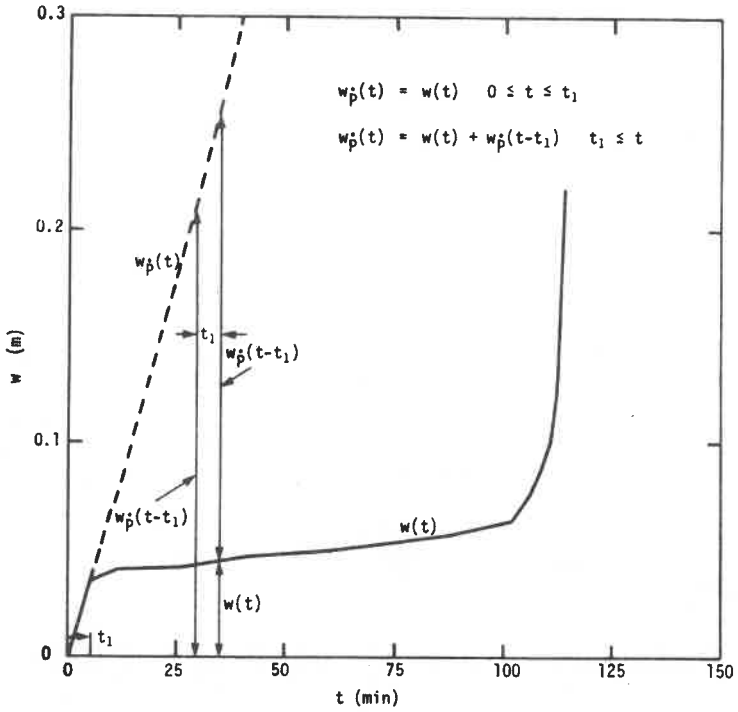

FIGURE 5. Calculation of $w_p^*(t)$, Joseph Lake November 19, 1976

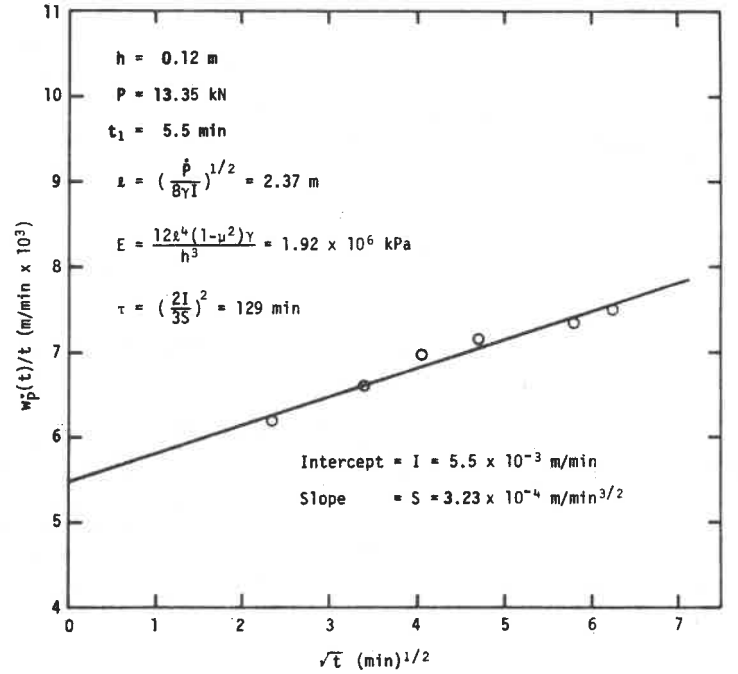

FIGURE 6. Calculation of τ and E for creep test, Joseph Lake, November 19, 1976

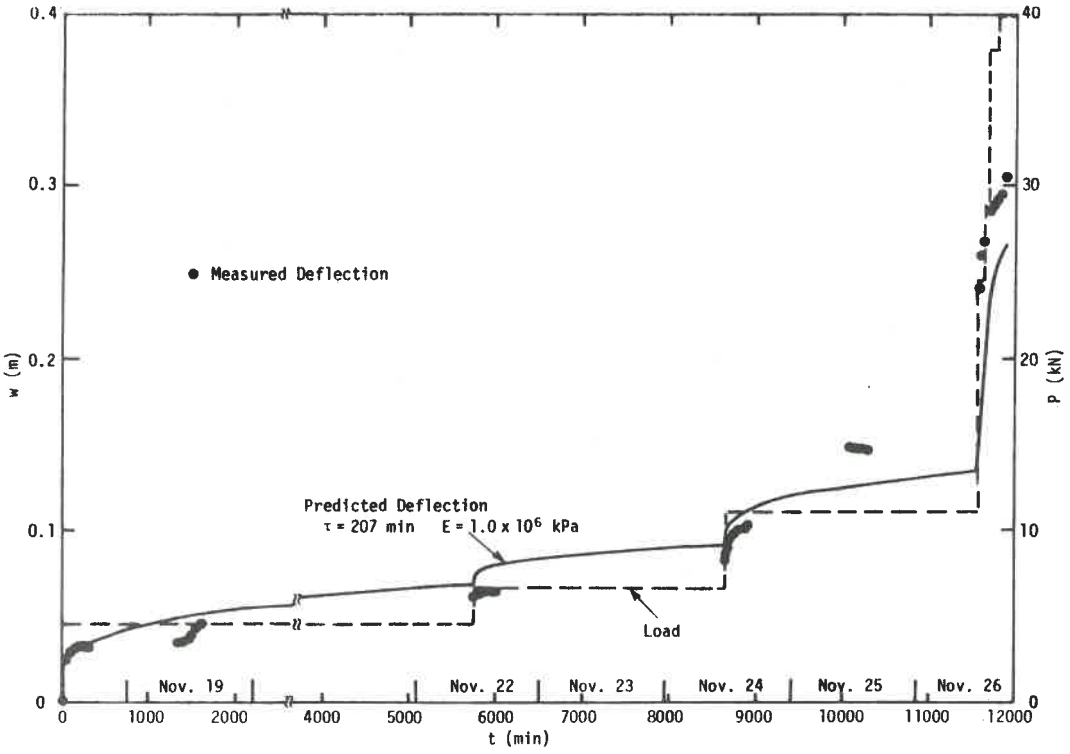

FIGURE 7. Multiple load creep test, Joseph Lake, November 18-26, 1976

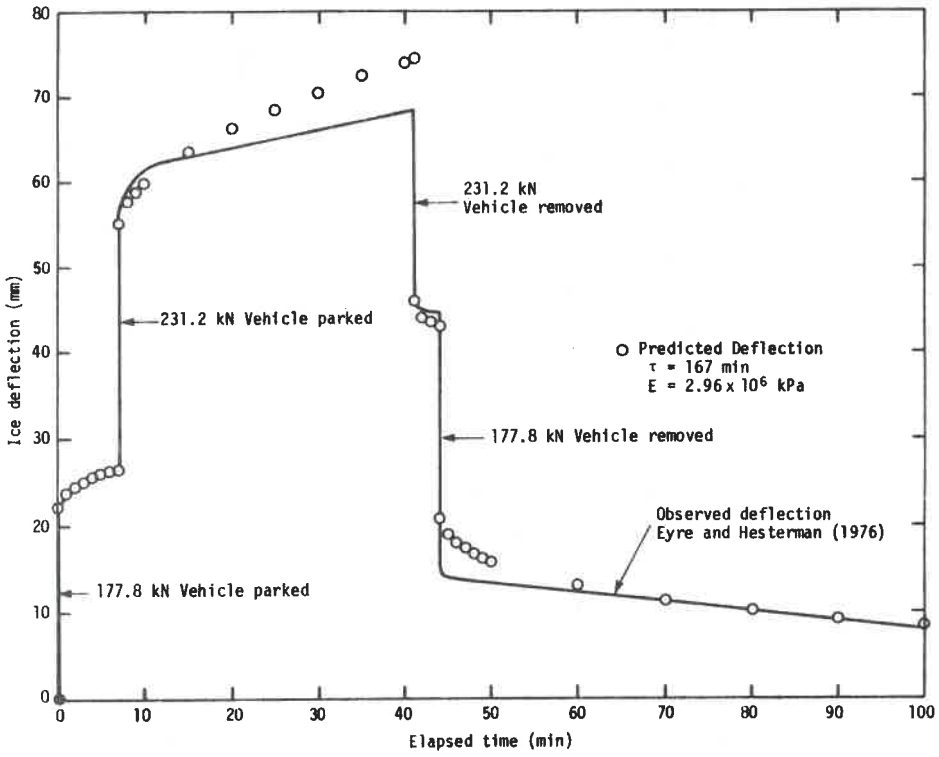

FIGURE 8. Bearing capacity test at Riverhurst ice crossing, March 11, 1975

Discussion

J.-R. Murat:

Does your analysis give a reasonable approximation of the actual deformed shape of the plate. This is important if one wants to deduce from this formulation a value of the strains and a failure criteria.

S. Beltaos and A.W. Lipsett:

Our present analysis deals exclusively with the temporal development of the maximum deflection. To determine the shape of the entire deflection bowl and thence estimate the strain, one could utilize an empirically established property of similarity; this similarity seems to be valid at any time (see Beltaos, 1977; Rose, Masterson and Friesen, 1975) and can be stated quantitatively as:

$$\frac{w}{w_m} = f(\eta);\ \eta = \frac{r}{\ell(t)};\ t = \text{time} \qquad (9)$$

where w is the deflection of the ice at a distance r from the centre of the load; w_m is the value of w at r = 0, $\ell(t)$ is an "effective characteristic length of the ice sheet" and $f(\eta)$ is a function that can be determined from an elastic solution of the problem (i.e., for t = 0). The value of ℓ can be calculated at any time from

$$8\gamma\ell^2 w_m = P \qquad (10)$$

If $\varepsilon(r, t)$ is the strain, then

$$\varepsilon(r, t) \simeq \frac{h}{2}\ \frac{\partial^2 w}{\partial r^2} \qquad (11)$$

Using (9) and (10), (11) becomes:

$$\varepsilon(r, t) = \frac{4\gamma h w_m^2}{P}\left(\frac{d^2 f}{d\eta^2}\right)_{r\,=\,\eta\ell(t)} \qquad (12)$$

which can be used for estimating the strain ε.

Additional Reference: Rose, G.D., Masterson, D.M., and Friesen, C.E. (1975). Some Measurements of Laterally Loaded Ice Sheets, Proceedings, IAHR Third International Symposium on Ice Problems, Hanover, N.H., pp. 555-566.

Comment (R. Tinawi):

I am glad to hear Dr. Frederking say that the concept of a characteristic length is also dependent on the stress rate and not on a single value of E.

PROBLEMS RELATED TO THE STRUCTURAL MODELLING OF ICE COVERS

R. Tinawi
Department of Civil Engineering
Ecole Polytechnique de Montréal

Introduction

The Polar Gas Project (McGovern 1977) has stimulated an intensive research program at Ecole Polytechnique for the theoretical as well as the experimental investigation of sea-ice. The work relates primarily to the bearing capacity under short-term as well as long-term loading.

Although a few classical solutions exist for the elastic solutions of infinite or semi-infinite floating ice sheets, the long-term loading problem is an order of magnitude more complicated. This complexity arises not only because of the mathematical difficulties but they are also compounded by the lack of an accurate description of the mechanical properties of sea-ice.

However, the more experimental and field tests are performed, the more knowledge will be obtained for the mechanical properties of the material, specially for the creep problem. Once these properties are defined with the deserved degree of confidence a tool is readily available for the solution of the analytical problem. This tool is the Finite Element Method.

The technique is more than twenty years old (Turner et al 1956) and has been thoroughly used in the air by the Aerospace industry; on the ground by the construction industry; below ground in geotechnical work and on the water by ship-builders. At the same time as research and development on the method itself is ending or slowing down, it seems appropriate to ask if finite elements can float so that ice covers could be simulated.

The purpose of this paper is to show that the Finite Element Technique is an extremely versatile tool for analysis of ice covers for both the linear as well as the creep problems. Emphasis is placed on the type of elements used and their performance for practical problems.

Thin Plate Theory

The physical dimensions of an ice cover that varies from 0.5 to 2 m in thickness is such that the problem can be considered within the realm of the classical thin plate theory (Timoshenko 1959). Such a plate resting on an elastic foundation (the water) and commonly known as a Winkler type foundation obeys a differential equation of the form:

$$\frac{\partial^4 w}{\partial x^4} + \frac{2\partial^4 w}{\partial x^2 \partial y^2} + \frac{\partial^4 w}{\partial y^4} = \frac{q}{D} - \frac{fw}{D} \qquad (1)$$

where:

w is the vertical deflection
q is the loading on the plate
f is the foundation modulus such that the pressure on the foundation itself is simply fw.

The flexural rigidity D is defined as:

$$D = \frac{Et^3}{12(1-\nu^2)} \qquad (2)$$

where:

E is the elastic modulus of the plate
t is the plate thickness
ν is Poisson's ratio.

In the case of ice covers, f is equivalent to the water density. A limited number of approximate or series solutions are reported by Timoshenko (1959) and Nevel (1965) for relatively "simple" loading and boundary conditions.

The Finite Element Method

Over the past twenty years, the number of papers, conferences as well as books (Zienkiewicz, 1967, 1972, 1977; Przieminiecki, 1968; Gallagher, 1975; Cook, 1974; Huebner, 1975; and many others) has been overwhelming. Two major factors contributed to such a fast development rate of the method:

a) the advent of faster and cheaper computers. It is obvious that without computers the Finite Element Method could be classified as an elegant but useless academic exercise.

b) it is the only technique that has offered hope for the possible solution of complex non-linear problems in structural mechanics.

The plate-bending problem, which is of interest here, has been "solved" satisfactorily with Finite Elements when Civil Engineering contributions to the method started in the mid-sixties.

Plate-Bending Elements

A number of elements of various types (Clough et al. 1965, 1968, Gallagher, 1969) have been proposed in the literature. However, they can be classified into two major types:

- ordinary or elementary elements;
- high-precision elements.

Normal elements are usually based on a cubic polynomial for the displacement w and can have different shapes as shown in Fig. 1a. Continuity between the displacements and rotations of an assemblage of elements requires that for each model the following degrees of freedom be defined:

$$\{w_i \; w_{xi} \; w_{yi}\}$$

These degrees of freedom are normally encountered when cubic polynomials or shape functions are used.

On the other hand, high-precision elements are usually based on quintic polynomials. Because of the higher order polynomial expansion or shape functions, more degrees of freedom are required at each node, namely,

$$\{w_i \; w_{xi} \; w_{yi} \; w_{xxi} \; w_{xyi} \; w_{yyi}\}$$

Figure 1b shows a triangle (Cowper et al, 1968) or a rectangle (Lindberg et al, 1972) based on a quintic polynomial. A quadrilateral could be formulated, if desired, by a sub-assemblage of triangles.

One of the major advantages offered by the use of high-precision elements is the fact that continuity of the curvatures, at the nodes, is achieved. This, in turn, yields continuity in the bending moments and stresses. This is not the case for elements based on cubic expansions. Furthermore, a higher order element enjoys a cubic variation of the bending moments as compared to a linear variation within the element for the others. Hence fewer elements would be required and

a higher accuracy is achieved specially in the regions of high stress gradients.

The development of a single element is based on thin plate theory where the following relations hold:

$$\{M\} = [E]\ \{\chi\} \tag{3}$$

or

$$\begin{bmatrix} M_x \\ M_y \\ M_{xy} \end{bmatrix} = D \begin{bmatrix} 1 & \nu & 0 \\ \nu & 1 & 0 \\ 0 & 0 & \frac{1-\nu}{2} \end{bmatrix} \begin{bmatrix} w_{xx} \\ w_{yy} \\ w_{xy} \end{bmatrix} \tag{4}$$

where the left-hand-side represents the internal moments in the plate and the vector on the right is the corresponding curvature vector. Now if the curvatures are related to the degrees of freedom $\{r\}$ of the element such that

$$\{\chi\} = [B]\ \{r\} \tag{5}$$

it can be shown that the stiffness matrix $[k]$ of an element is simply given by:

$$[k] = \int_A [B]^t\ [E]\ [B]\ dA \tag{6}$$

where A is the element area.

Having obtained the stiffness matrix of all elements in the structure, these are assembled in a global matrix relating the degrees of freedom at all the nodes to the corresponding forces at these nodes. This produces a set of simultaneous equations which can then be solved for the generalized displacements.

Figure 2 shows the convergence of cubic and quintic elements for a simply supported square plate. Although the high precision elements present a definite advantage, care must be exercised in their utilization under special conditions.

Elastic Foundation

In the problem of floating ice covers, the contribution of the elastic foundation must be added to equation (6). Although lumped vertical springs can be used to simulate the foundation, it is more desirable to use a consistent formulation (Carpenter 1973). In such cases the stiffness due to the elastic foundation is simply:

$$[k_f] = \int_A [N]^t f [N] \, dA \qquad (7)$$

where f is the water density and [N] is a vector of shape functions for the degrees of freedom of the element. The addition of the foundation matrix to the element stiffness matrix changes the whole problem in certain situations. This is illustrated in Fig. 3 where a systematic increase of the foundation modulus has produced a serious deterioration in the bending moments. It appears, therefore, that in order to maintain a certain accuracy in the results for a given mesh size, the element size should be of the same order as the characteristic length. The characteristic length L_c is given as:

$$L_c = \sqrt[4]{\frac{D}{f}} \qquad (8)$$

Fortunately in ice covers such a value varies between 18 and 25 m in which case the elastic foundation does not present a serious problem for a finite element modelling.

Mesh Size

A reasonable grid for plates on elastic foundation might be obtained using a combination of triangular or rectangular elements. It is preferable to have a finer mesh around the load application as well as rectangular elements since the simulation of partial pressures can then be handled easily (Tinawi 1975). A typical element side might be 2-3 m in length in the critical areas. However, in the case where the ice covers extend indefinitely, the total model need not be greater than four times the characteristic length. Experience has shown that such dimensions will ensure that deflections and stresses are nearly zero at such a distance from the load.

Concentrated Loads

A much more serious problem in the modelling of thin plates using Finite Elements is the simulation of concentrated loads. Many analysts or engineers tend to simulate a tank or a vehicle as a concentrated load at the nodes. Although such a procedure is advantageous from the modelling point of view, it gives rise to a totally unreliable value of the bending moments, in the plates, at the concentrated load. In fact classical thin plate theory predicts an infinite value of the moments. However, the finite element models will produce a finite value depending on the accuracy of the mesh around the central load. Two methods are suggested for overcoming this problem: the first is to choose an element size

coincident with the pressure area applied to the whole element. If the element size is too large, a partial pressure could be applied as shown in Fig. 4. The second alternative is to simulate for a given total load P a variation in the pressure by varying the applied area. A plot on a log-linear scale is then performed as shown in Fig. 5. The linearity is always obtained. Hence by simulating two load vectors on a constant mesh by simply varying the contact areas, a line can always be drawn. From this line, the correct value of the bending moment is obtained for the given contact area. Experience has shown that this linearity is also applicable to plates with other boundary conditions or shape.

Temperature Variation

The variation of the temperature and salinity through the ice cover can lead to a variation in brine volume and therefore in the elastic modulus E through the thickness (Frankenstein and Garner 1967). If the variation of E is expressed as a polynomial of the form

$$E(Z) = \sum_{i=1}^{m+1} \beta_i \, Z^{i-1} \tag{9}$$

where m is the polynomial order and Z is the vertical distance from the neutral axis, it can be shown that the flexural rigidity is simply given by:

$$D = \frac{1}{1-\nu^2} \sum_{i=1}^{m+1} \frac{\beta_i}{i+2} \left[C_1^{\,i+2} - C_2^{\,i+2}\right] \tag{10}$$

where C_1 and C_2 are shown in Fig. 6. However, in order to get E(Z), the position of the plate neutral axis must be known. Hence if

$$E(Z') = \sum_{i=1}^{m+1} \alpha_i \, Z'^{\,i-1} \tag{11}$$

where Z' is measured from the bottom of the plate, the value of C_2 must be given by:

$$C_2 = \frac{\sum_{i=1}^{m+1} \frac{\alpha_i}{i+1}}{\sum_{i=1}^{m+1} \frac{\alpha_i}{i}} \, t \tag{12}$$

As a consequence of the variation of E(Z) the bending stresses across the plate vary as shown in Fig. 6. This variation is of the order m + 1 where m is the polynomial order for E(Z). As a consequence, the maximum tensile stress may not necessarily be at the bottom of the surface (Kerr, 1975). In any case, the finite element formulation does not change since the values of D obtained from equation (2) are incorporated into the evaluation of [k]. However, for the creep problem this presents a serious difficulty as will be discussed later.

Dependence of the E on the Loading Rate

The variation of the elastic modulus through the thickness does not seem difficult to incorporate. However since E is strongly dependent on the loading rate (Tabata, 1966) it appears that for a given loading rate on an ice cover the elastic modulus should not be constant in the horizontal direction. In other words, the elastic modulus should vary from element to element. This has been confirmed by experimental evidence coupled with a theoretical investigation (Tinawi and Murat, 1978; Murat,1978). Such a variation in the elastic modulus is very easily incorporated in a Finite Element model. However, if high precision elements are used, care must be exercised in order to ensure continuity in the elastic modulus at the nodes. In this case a variation of elastic modulus within the element can be incorporated (Tinawi 1972).

Creep Problem

Sea-ice creeps under a constant load. During this process deflections increase and stresses relax. In the case of beams or plates not resting on an elastic foundation, the integrals of the bending stresses, i.e., the bending moments are the same before and during creep. However, in the case of plates on elastic foundations, the problem is different. First, the increase in deflections lead to an increase in water pressure under the load and therefore the bending moment arising from the stress integral is lowered. Secondly the variation in the elastic modulus through the thickness can cause a shift of the neutral axis with time. Therefore it is important to realize that thin plate theory is no longer applicable for the creep problem unless the neutral axis is assumed fixed at the centre of the plate.

On the other hand, a more refined theory would lead to the development of a three-dimensional solid formulation which in terms of finite elements represents at least an order of magnitude increase in cost and labor. However, before attempting to apply thin plate or any other theory with or without variation in the elastic modulus, knowledge of a creep law must be known.

Creep Analysis of an Infinite Ice Sheet

A Finite Element program "AXI" has been developed by Murat (1976a, b) for the special case of axi-symmetric solids on elastic foundations. Elastic or creep analysis can be performed based on the initial strain technique (Zienkiewicz 1977). Furthermore, a variation of elastic modulus through the element has been incorporated without difficulty. Three elements with increasing sophistication have been fully reported. For the high-precision rectangular, non-homogeneous axi-symmetric solid, the element accuracy or performance in the elastic range is identical to the high-precision quintic element derived from thin plate theory (Tinawi 1975). Therefore the "AXI" program can be used to study the effect of non-homogeneity during creep. This can be done since the theory is based on a three dimensional continuum but under axi-symmetric conditions in order to reduce computer and development costs. Therefore the "AXI" program is not based on the concept of a neutral axis. Should the non-homogeneity through the thickness prove to be unimportant for creep, then thin plate theory could be used without problem providing the neutral axis is fixed in the middle and the uniform equivalent flexural rigidity is found for the plate.

Figure 7 shows a floating ice sheet loaded at its centre by a load of 4.45 MN and distributed over a radius of 3.05 m. The ice thickness is 1.83 m and is assumed to be uniform. The finite element model used in AXI is as shown in Fig. 7 at the top. Each element is rectangular and represents a section of a body of revolution. Six degrees of freedom are allocated at each node namely:

$$\{U \; U_r \; U_z \; V \; V_r \; V_z\}$$

where r and z are the radial and axial (vertical) directions respectively. The variation of the elastic modulus is given by:

$$E(Z') = 1928 + 12177\, Z' - 15982\, Z'^2 + 12642\, Z'^3 - 5263\, Z'^4 + 877.6\, Z'^5 \qquad (13)$$

This expression is obtained by fitting a polynomial through data points obtained by measurements of salinity and temperature through the thickness. The plot of equation (13) is shown in Fig. 7 and the neutral axis was found to be 1.02 m from the bottom.

Assuming a secondary creep law of the form

$$\dot{\varepsilon}_c = 3.19 \times 10^{-14} \sigma^{3.5} \qquad (14)$$

where σ is in kPa and the time is measured in hours. This law can be considered quite typical. However in some cases the exponents could have a lower value (Murat et al, 1977, Murat, 1978).

A plot of deflections versus time is shown in Fig. 8 for a variable as well as a constant elastic modulus. Both curves are extremely close and therefore any sophistication in the analysis is not warranted. However, the correct flexural rigidity must be known, taking into account the variability of E through the depth. Once the correct value of D is established, thin plate theory is quite adequate for prediction of long-term deflections. As for the stresses, these tend to relax and are of no direct interest in the creep process.

The other observation worth commenting on is the fact that deflections never reach a steady state or constant rate of increase as expected from a secondary creep law. The reason for this is simply the presence of the elastic foundation. This also explains the choice of the initial strain technique for the Finite Element formulation.

Conclusion

A review of the structural modelling of floating ice sheets has been presented by use of the Finite Element technique. For the linear analysis thin plate theory can be used. Inclusion of the elastic foundation and the non-homogeneity of the material properties presents no difficulties. Partial or full pressure loads on an element is always recommended in place of concentrated point loads.

Thin plate theory is applicable for creep problems by assuming the neutral axis is fixed in the middle and that an equivalent uniform modulus for the plate is used.

Acknowledgments

This work was carried out under grants from the National Research Council (NRC A-8958) and Montreal Engineering Co. Ltd. (Grant CR366-75).

References

Carpenter, W.C. (1973). "Analysis of Plates on Elastic Foundations". Int. J. Num. Methods in Eng., Vol. 8, No. 3, pp. 408-410.

Clough, R., Fellippa (1968). "A Refined Quadrilateral Element for Analysis of Plate Bending". Proc. 2nd Conf. Matrix Methods in Struct. Mech. Air Force Inst. of Tech. Wright Patterson A.F. Base, Ohio.

Clough, R.W., Tocher, J. (1965). "Finite Element Stiffness Matrices for the Analysis of Plate-Bending", Proc. of First Conf. on Matrix Methods in Struct. Mech. Wright Patterson A.F. Base, Ohio.

Cook, R.D. (1974). "Concepts and Applications of the Finite Element Analysis", John Wiley & Sons Inc.

Cowper, G.R., Kosko, E., Lindberg, G.M., Olson, M.D. (1968). "A High-Precision Triangular Plate Bending Element". NRC, NAE Aero. Report LR-514 National Research Council of Canada.

Frankenstein, G.E., Garner, R. (1967). "Equation for determining Brine Volume of Sea-Ice from -0.5°C to -22.9°C." J. of Glaciology, Vol 6 No. 48, pp. 943-944.

Gallagher, R. (1975). "Finite Element Analysis - Fundamentals", Prentice Hall Inc.

Gallagher, R. (1969). "Analysis of Plate and Shell Structures", Proceeding of the Symposium on Application of Finite Element Methods in Civil Engineering, Nashville, Tennessee.

Huebner (1975). "The Finite Element Method for Engineers", John Wiley & Sons Inc.

Kerr, A.D. (1975). "The Bearing Capacity of Floating Ice Plates to Static or Quasi-Static Loads. A Critical Survey". Research Report No. RR333. CRREL.

Lindberg, G. Hrudey, T.M., Cowper, G.R. (1972). "Refined Finite Elements for Folded Plate Structures". Proc. of the Conference on Finite Elements in Civil Engineering, Montreal.

McGovern, R.. Bruce, D., Humphries, A.D. (1977). "Sea-Ice Bearing Capacity Investigation for Polar Gas Project". POAC 77, St-John's, Nfld.

Murat, J.-R. (1976a). "Axi-symmetric Finite Element Formulation of Non-Homogeneous Floating Ice Sheets". Part I-Linear Analysis, Ecole Polytechnique Report EP 76-R-11.

Murat, J.-R. (1976b). "Axi-symmetric Finite Element Formulation of Non-Homogeneous Floating Ice Sheets". Part II-Creep Analysis Ecole Polytechnique Report EP 76-R-37.

Murat, J.-R., Tinawi, R. (1977). "Sea-ice Testing in Flexure", POAC 77, St-John's, Nfld.

Murat, J.-R. (1978). "Essais en Flexion de Plaques de Glace de Mer". Ecole Polytechnique Report EP 78-R-17.

Murat, J.-R. (1978). "La Capacité Portante de la Glace de Mer", Ph.D. Thesis, Ecole Polytechnique. (To be published).

Nevel, D. (1965). "A Semi-Infinite Sheet on Elastic Foundation", Research Report No. 136 CRREL.

Przeminiecki, J.S. (1968). "Theory of Matrix Structural Analysis", McGraw Hill Book Co. Ltd.

Tabata, T. (1966). "Studies of Mechanical Properties of Sea-Ice X. The Flexural Strength of Small Sea-Ice Beams". Int. conf. on low temperature Science, Sapporo, Japan, Physics of Snow and Ice, Vol. 1, pp. 481-497.

Timoshenko, S., Woinowsky-Kreiger, S. (1959). "Theory of Plates and Shells", McGraw Hill Book Co. Ltd.

Tinawi, R. (1972). "Anisotropic Tapered Elements Using Displacement Models", Int. J. Num. Methods Eng., Vol. 4, No. 4, pp. 475-489.

Tinawi, R. (1975). "PLATE - Program for Analysis of Plates on Elastic Foundations", Report submitted to Montreal Engineering Co. Ltd. Montreal.

Tinawi, R., Murat, J.-R. (1978). "Sea-Ice: Flexural Creep". IAHR Symposium on ice problems, Lulea, Sweden.

Turner, M., Clough, R.W., Martin, H., Topp, L. (1956). "Stiffness and Deflection Analysis of Complex Structures", J. Aero. Sci., Vol. 23, No. 9, pp. 805-823.

Zienkiewicz, O.C. (1967). "The Finite Element Method in Structural and Continuum Mechanics", McGraw Hill Publishing Co.

Zienkiewicz, O.C. (1972). "The Finite Element Method in Engineering Science", McGraw Hill Book Co.

Zienkiewicz, O.C. (1977). "The Finite Element Method", Third Edition, McGraw Hill Book Co. Ltd.

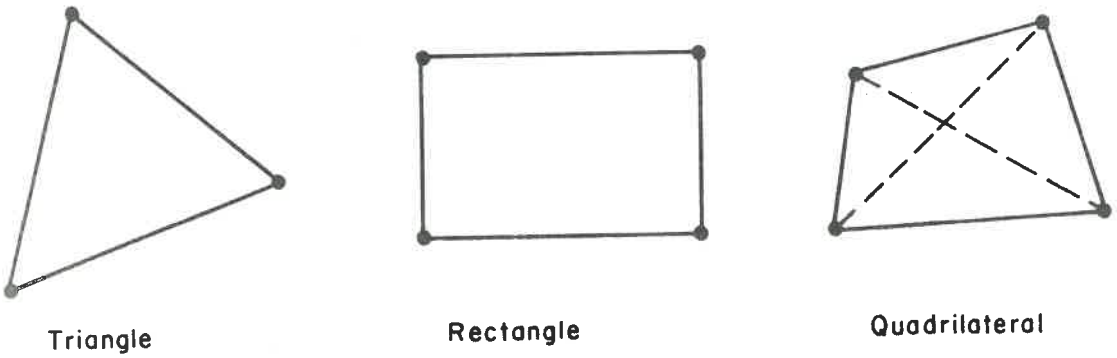

(a) Cubic interpolations

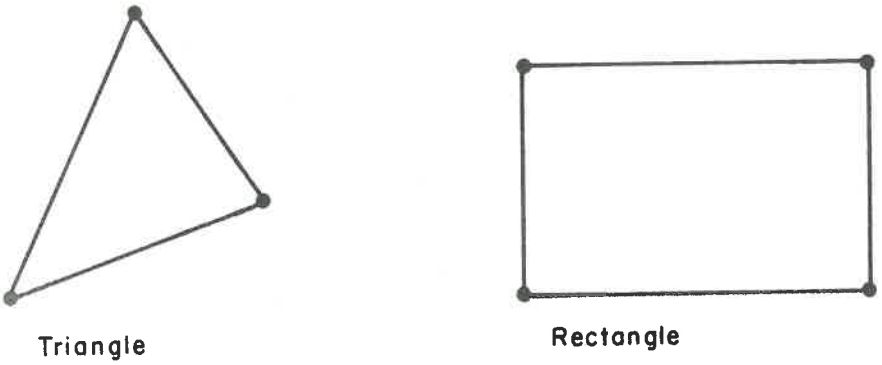

(b) Quintic interpolations

Figure 1: Plate bending finite elements

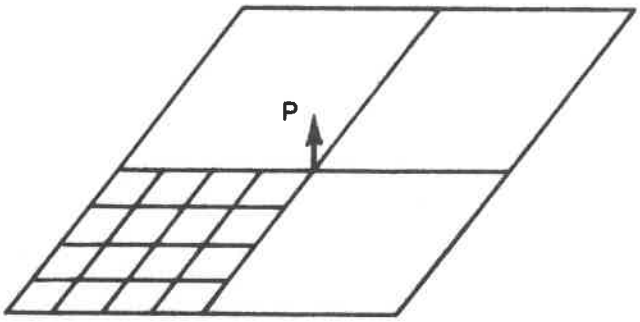

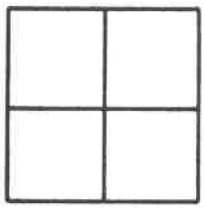

N = 2 for quarter plate (rectangles)

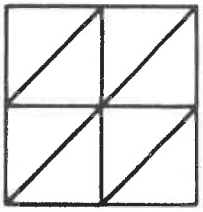

N = 2 for quarter plate (triangles)

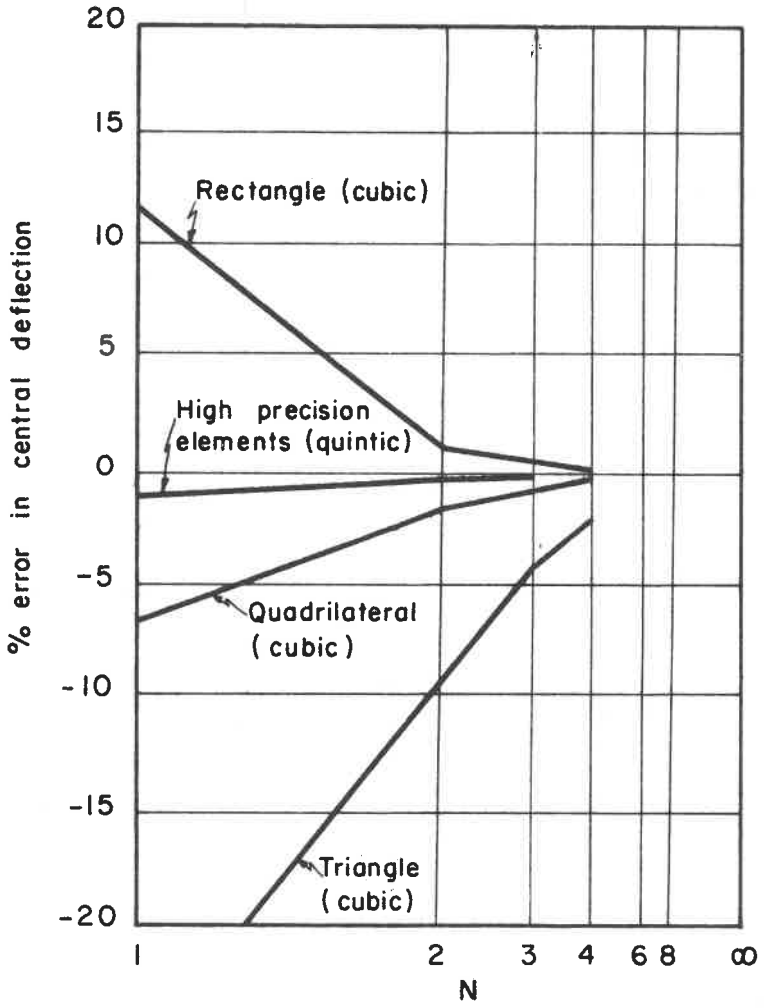

Figure 2: Convergence of central deflection for a simply supported square plate.

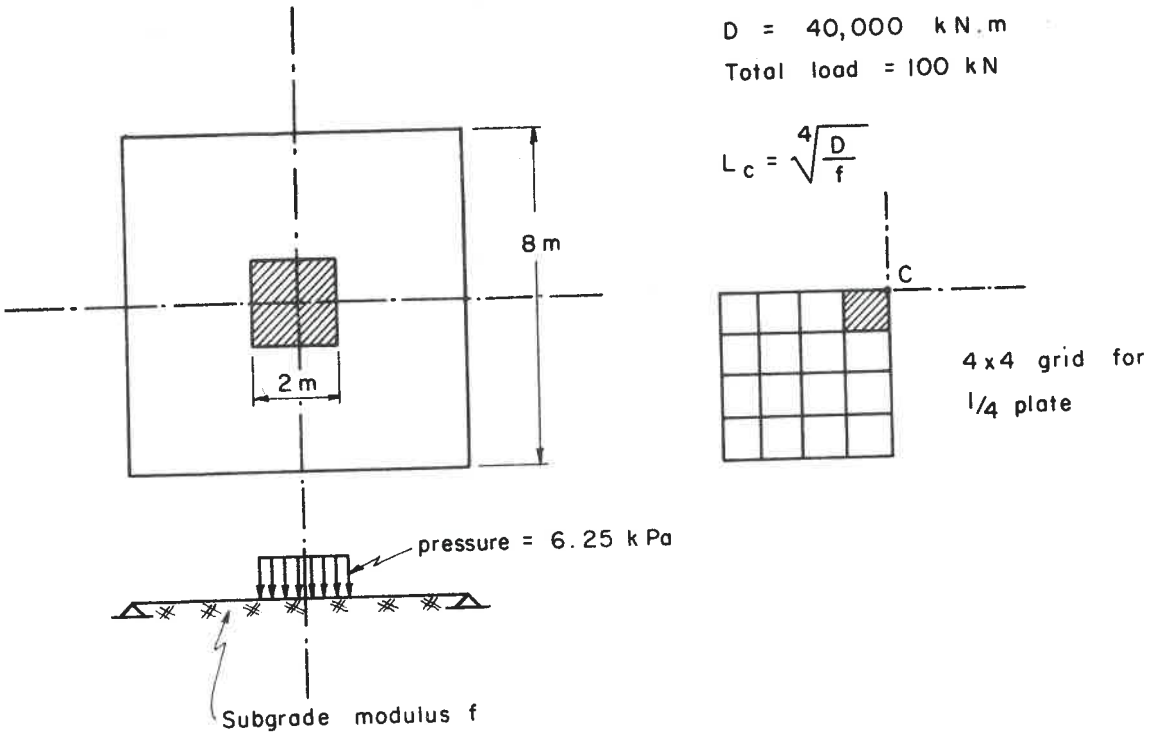

f	L_c	W_c	Exact	M_c	Exact
100	4.47	$.48931 \times 10^{-2}$	$.48932 \times 10^{-2}$	14.50	14.574
10,000	1.41	$.37415 \times 10^{-3}$	$.37420 \times 10^{-3}$	3.45	3.473
1,000,000	0.45	$.67880 \times 10^{-5}$	$.67799 \times 10^{-5}$	.048	.0041

Figure 3: Simply supported square plate on elastic foundation. Comparison of central deflection and bending moments with exact solutions.

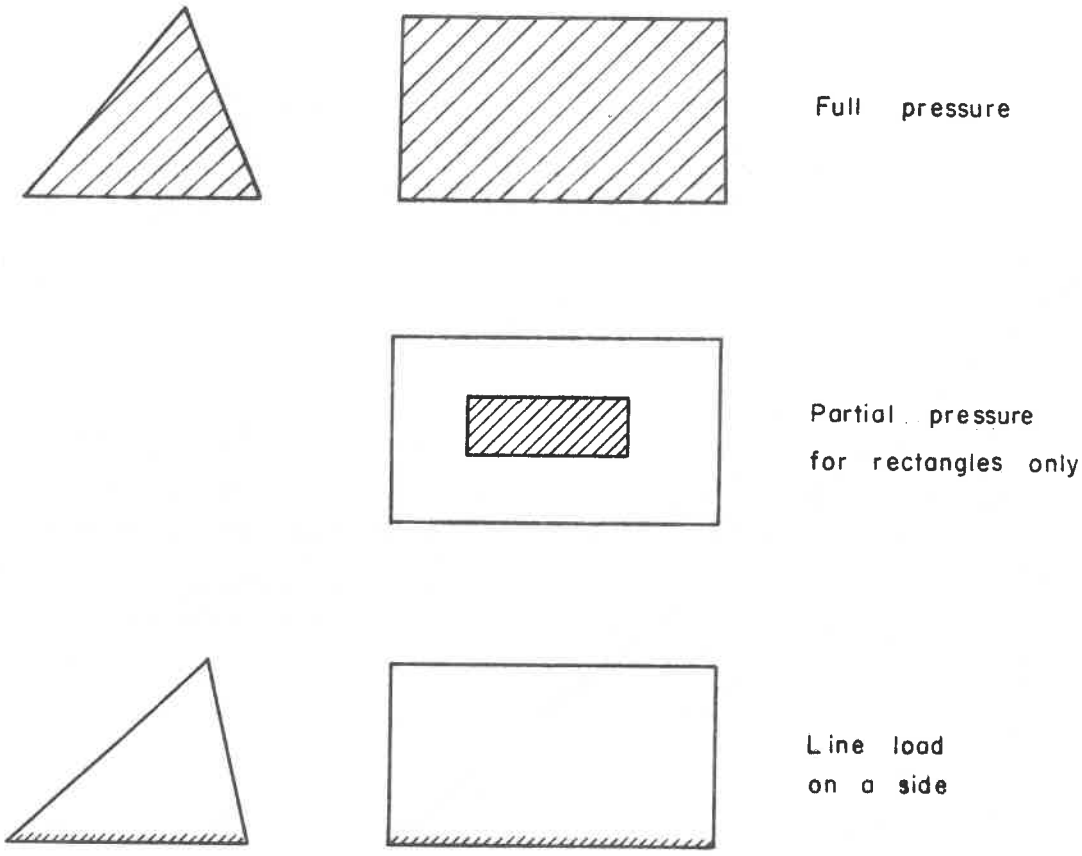

Figure 4: Techniques for avoiding a concentrated load at a node.

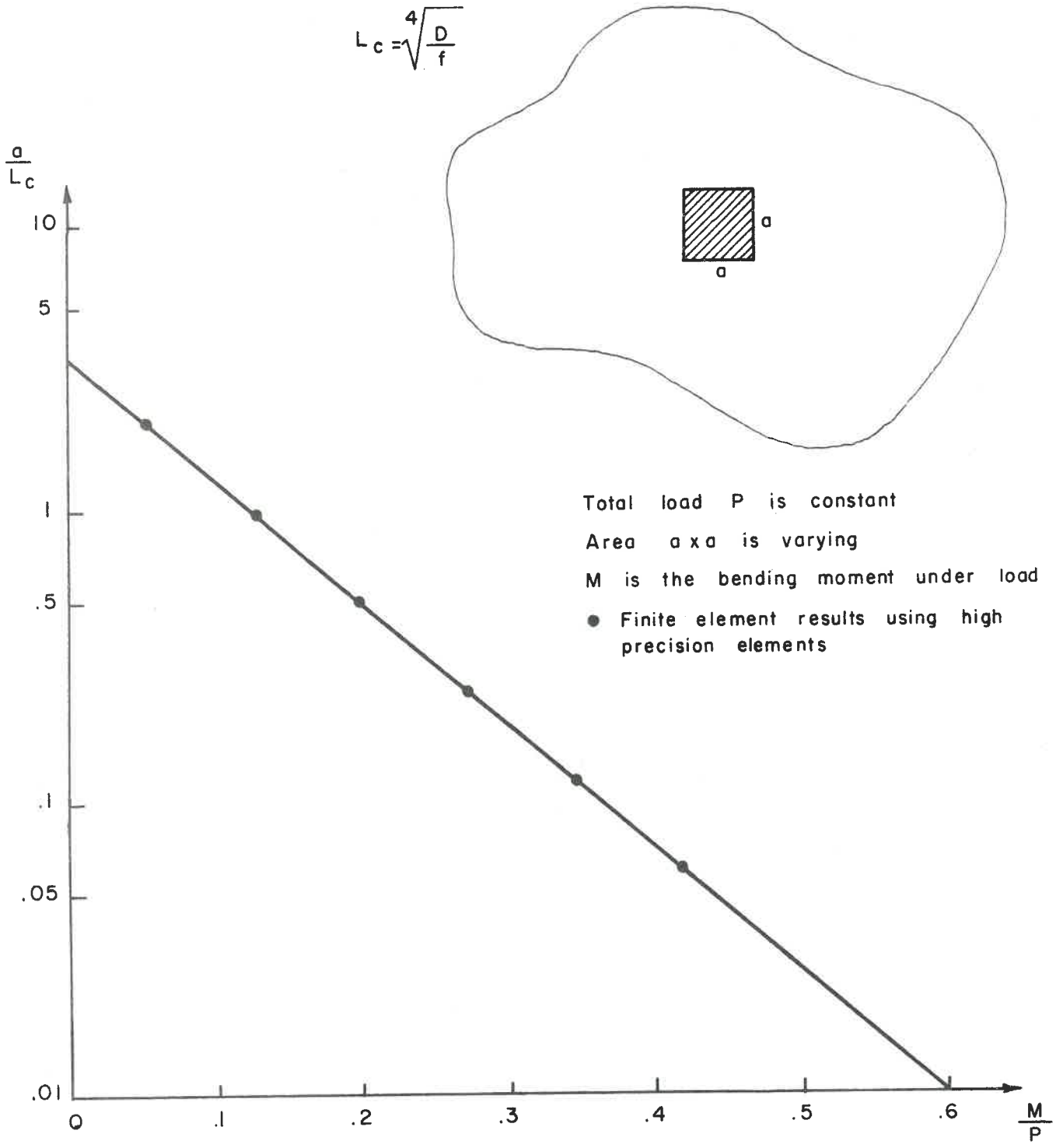

Figure 5: Infinite sheet on elastic foundation f.

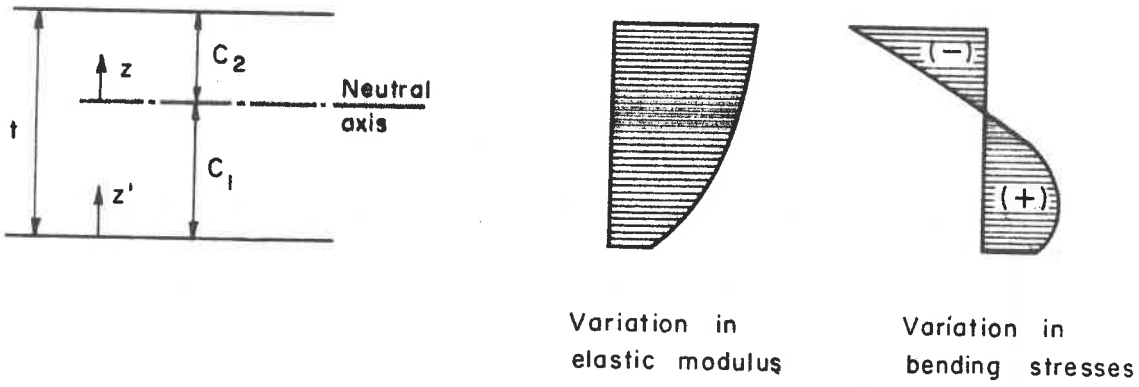

Figure 6: Ice plate with variable elastic modulus.

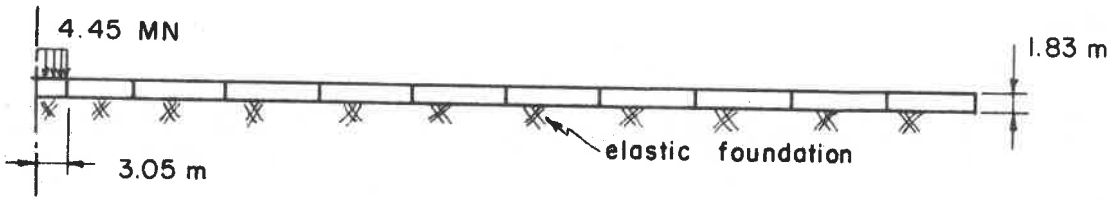

(a) Finite element model using axi-symmetric high precision elements

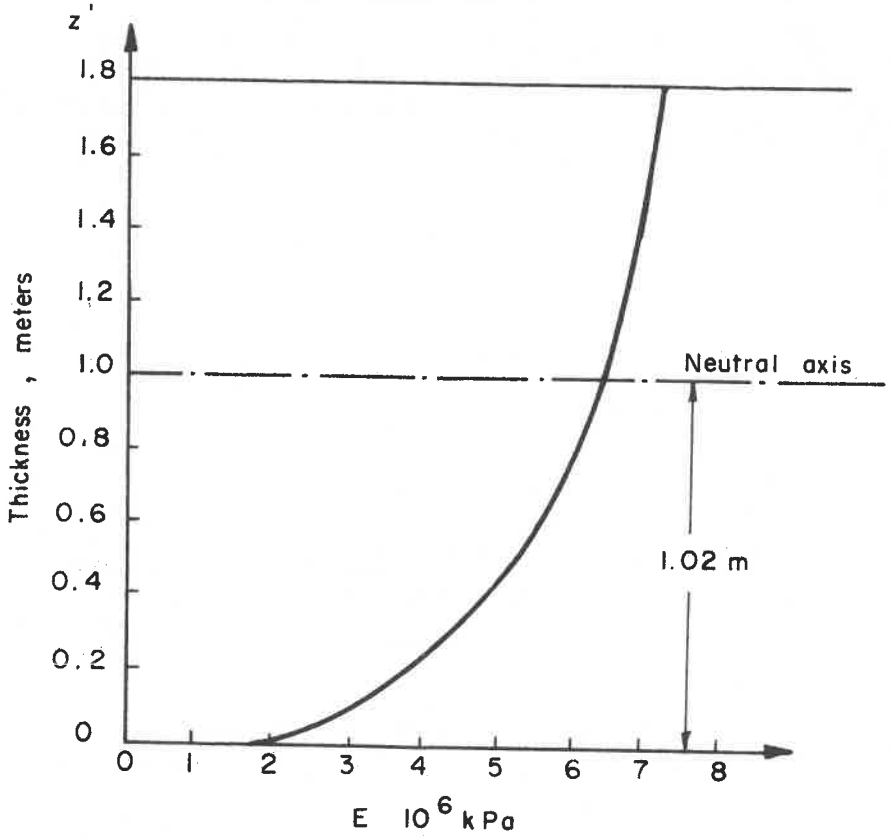

(b) Variation of elastic modulus through depth

Figure 7: Infinite ice sheet idealisation using AXI program

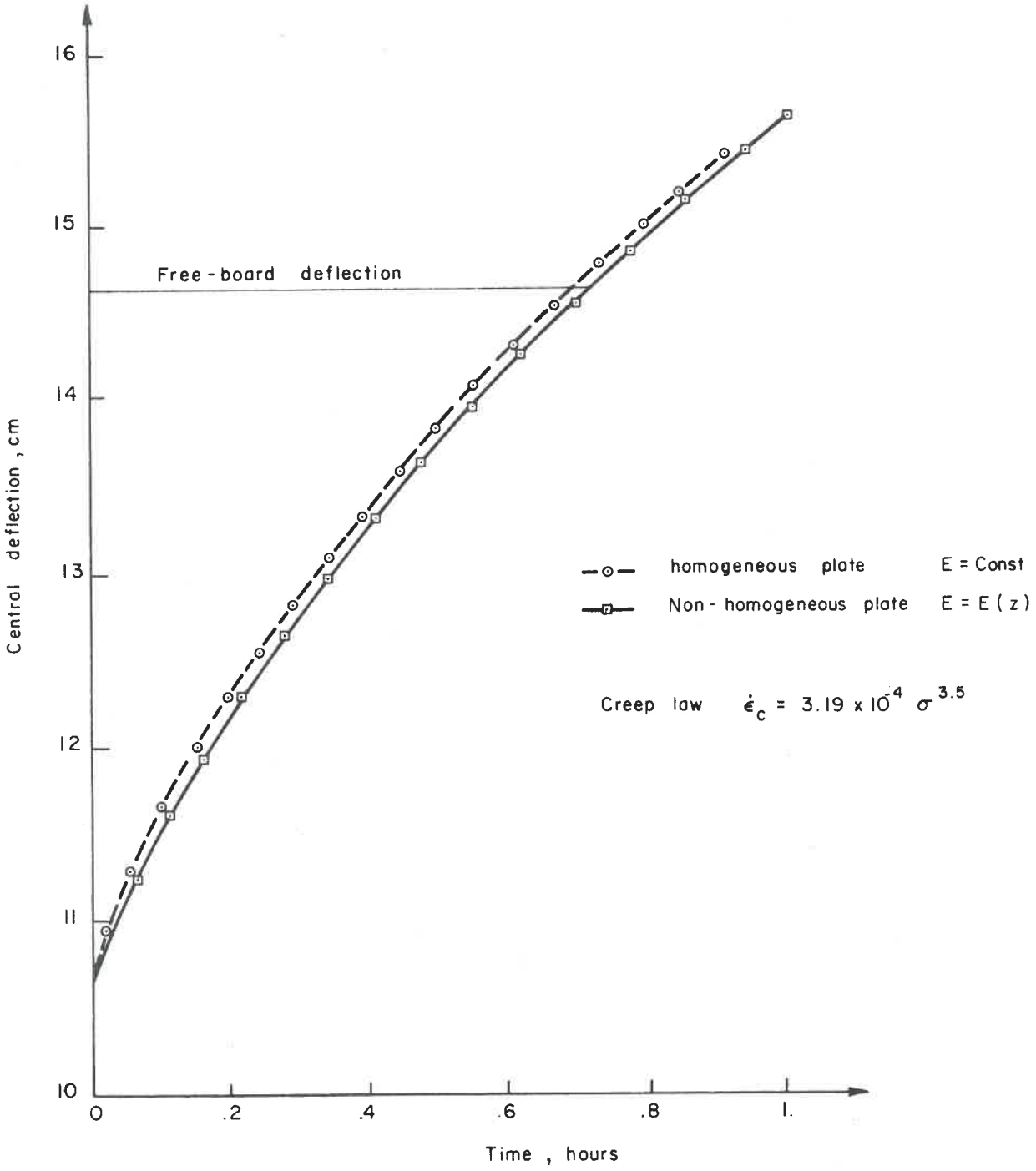

Figure 8: Central deflection due to creep for infinite sheet of figure 7. (Murat 1978).

Discussion

R. Gerard:

Given the power of the finite element method, is it not fair to say the problem of predicting ice behaviour in practice comes down to defining -

(i) constitutive relations (as applied to ice in the field),

(ii) failure criteria (about which little seems to be known, particularly for long-term loads),

and that therefore the question of the load bearing capacity of ice sheets comes down to a problem of material science rather than engineering? Perhaps some of the vast sums being spent on this subject should be used to support more work by such people in ice.

R. Tinawi:

There is no point investing any effort in the analytical solution of ice problems. Whether static or creep problems, a tool is readily available, namely, the F.E. method. What we really badly lack is the knowledge of good creep laws and failure criteria.

D.V. Reddy:

Can you compare your finite element formulation with that for the software developed by Katona and Vaudrey - Fever, Visice, etc? I would appreciate your comments on the validity of the creep law used in your analysis?

R. Tinawi:

Katona and Vaudrey used a simpler element and had to have 6 or 7 layers through the depth in order to get the desired accuracy. We used a more sophisticated element and were able to maintain only 1 element through the depth for a comparable accuracy. As for the creep law, we used a power law where the exponent n was set arbitrarily equal to 3.5. This value is somewhat higher than the experimental findings we had later after running the program.

S. Beltaos:

Could the author comment on the time required for a typical application of a finite element program for obtaining the deflection-time curve through a time of, say, 2-3 hours? Also what would the associated computer usage cost be?

R. Tinawi:

For 2D axi-symmetric models, the time involved in preparing a F.E. model is relatively short. However, it all depends on the experience of the user in handling programs and poring through users' manuals.

For 2D plate models this might be more time-consuming than axi-symmetric models. In any case, computer costs are becoming negligible and man-hour costs account for a major part of the expenses in any analysis.

Typical computer runs for creep problems vary between $50 - $100 depending on grid size.

R. Gerard:

You suggested that the use of an equivalent elastic modulus, constant across the section, can be used to replace an elastic modulus that varies across the section. How did you say you find this equivalent constant elastic modulus?

R. Tinawi:

If we know the temperature and salinity through depth, we can get the brine volume from which we can get the elastic modulus. This value could be variable through the depth. To obtain an equivalent constant elastic modulus, we equate the actual rigidity of the plate to one obtained from use of an equivalent modulus.

LONG-TERM LOADING ANALYSIS OF FLOATING ICE PLATFORMS USING FINITE ELEMENT TECHNIQUES

D.M. Masterson and A.G. Strandberg
FENCO Consultants Ltd.

Introduction

The use of the natural ice cover in the Arctic Islands, thickened to required dimensions by flooding and freezing in thin layers, has made it possible for Panarctic Oils Ltd. to drill 9 offshore exploratory wells and one completion well (Baudais et al., 1976). Since the first platform was designed by FENCO Consultants Ltd. and the first well was drilled in 1974, the trend has been to increase the drilling rig loads and drilling time. There is, at the same time, a desire to minimize required platform thicknesses, decreasing construction time and increasing available drilling time.

Initial designs made use of formulas developed for plates of constant thickness with circular, uniform loads. Thus a method was sought which would model more accurately such things as section taper, non-uniform load distribution, holes in the plate such as the moonpool for drilling and, finally, the creep properties of the material. A finite element method was required and the Marc CDC collection of programs were chosen as those most suited to the task.

Description of the Finite Element Program

The Marc CDC finite element program has several elements available. The one chosen for the ice platform analysis is called element Type 22. It is a rectangular shell element with 8 nodes, 4 nodes at the corners of the element and 4 at the middles of the sides. Each node has 5 degrees of freedom, allowing displacements along the x, y and z axes (z axis is normal to the shell in local coordinates) and rotations about the x and y axes. Stress data is outputed at 4 "integration" points located at the outer quarter points of the element diagonals.

Viscoelasticity of the material can be modelled using a supplied subroutine which contains expressions for thermal strain, plastic strain, creep strain and Kelvin model strains. The creep law provided is the well known exponential formula

$$\frac{d\varepsilon}{dt} = \dot{\varepsilon} = K\,\sigma^{n} \qquad (1)$$

However, user supplied creep laws, either analytic or in the form of curve data, can be inputed. The authors chose to use the exponential creep law.

Accuracy of the Model

Once the program and element type were chosen, tests were done to determine the comparative accuracy of the method with well established analytical procedures (Westergaard, 1926, Wyman, 1950). Also ice sheets are relatively infinite in extent and it would not be possible to cover the entire sheet with elements in a computer model. The model must be terminated at some distance from the load. Curves published by Westergaard (1926) indicated this could be done at 3 to 4 stiffness lengths from the load centre. The stiffness length of a 5 m ice sheet is approximately 30 m so the model could be terminated at 90 to 120 m from load centre.

Finally, the size of elements chosen to make up the element grid has a bearing on the accuracy of the answers. This as well had to be checked.

The first grid used is shown in Fig. 1. Complete axi-symmetry allowed the use of a quarter grid. Three point loads of 141 tonnes were applied at nodes 20, 1 and 17. Deflections and tangential and radial stresses are plotted in Figs. 3, 4 and 5.

Next, a finer grid, shown in 2, was used. The loads were applied to this grid in different ways, as three point loads around element 1 and as a distributed load over element 1. Deflections and stresses are plotted in Figs. 3, 4 and 5. The conclusions are as follows:

1. To a distance of 1.5 to 2 stiffness radii the Marc program gave deflections for both grids very closely approximating those obtained from analytical solutions (Fig. 3). Towards the edges of the grid the finite element and analytical solutions differ by wider margins (as much as 100 percent). However, at these locations (2.5 to 4 stiffness radii) the deflections are at most 15 percent of those beneath the load. The distributed or three-point load makes little difference to the calculations.

2. Tangential stresses for both grids and the three load cases are very close (Fig. 4). An exception is the tangential stress very close to the loads for the 3 point load or the finer mesh. The stress nearest the load is 81 percent of that for the other load type and mesh type. The stress

rises sharply to 86 percent and then drops, following the other curves closely.

3. Radial stresses (Fig. 5) agree very closely except again for the 3 point loads were stresses near the loads are about 80 percent of those for the other cases.

In general, the finite element and analytical solutions gave close answers. However, the magnitude of the calculated stress very near the load is seen to depend both on assumed load distribution and mesh fineness. Discontinuing the plate at 3.8 stiffness radii ensured that stresses and deflections were modelled correctly in the critical zone.

Effects of a Hole in the Ice (Moonpool)

The hole in the ice platform through which drilling takes place affects the stress distribution in this area. This is also the area where the heaviest loads are applied (rig substructure load). The drilling operation necessitates the opening of quite a large hole with the heavily loaded subbeams being supported on the ice adjacent (Baudais et al., 1976). Since long-term deflections are stress dependent (equation 1), it was desired to analyze precisely the effect of the hole on them.

The results of the analysis are presented in Fig. 6, where the moonpool area was left full of ice, and Fig. 7, where the moonpool was empty. It can be seen that, at the stress output points very close to the moonpool (a distance from the edge about $\frac{1}{2}$ the moonpool side dimension) removing the ice caused increases of stress from 0 to 1.43 times. At 1.7 times the side dimension away (9.4 m), the maximum stress increase is about 5 percent. Thus, the effects of the hole are very local, possibly resulting in some local yielding of the ice but having little overall effect on the platform behaviour.

Effects of Section Taper

A 7 m thick ice platform with constant thickness over a radius of 23 m and then tapering to a natural ice thickness of 1.5 m was analyzed. The grid used is shown in Fig. 8. 1047 tonnes load total was applied, 1/3 at each of the points shown on element 1. 15:1 and 10:1 horizontal to vertical tapers were tried. It can be seen from Fig. 8 that effect on the large stresses nearer the load is nil. Even towards the edge the effect is comparatively small. Deflections at the load centre increased by 10 percent when the taper went from 15:1 to 10:1. 15:1 tapers are normally used in design.

Effects of Fixing the Grid Edges Against Rotation

The same grid as for the previous section was used to ascertain the effects of fixing the mesh edges against rotation about a parallel axis. The results are presented in Fig. 9. Near the load, the effect is nil and toward the edges it is comparatively small.

Effects of Natural Ice Thickness

The natural ice thickness used for Fig. 8 was 1.5 m and that used for Fig. 9 was 2.4 m. The effect of this value is seen to have no effect on stress in critical areas.

Long-Term or Creep Deflection

As stated previously, the Marc CDC program has provisions for viscoelastic analysis. Elastic, thermal, plastic, creep and Kelvin model strain components can be calculated. The process of calculating time dependent creep strains and stresses are iterative. After initial parameters are specified, a time interval ΔT is chosen and stresses and strains are calculated at each "integration point" in each element with increasing time. Tolerance limits can be set on the maximum allowable change in strain and stress per time increment. For the analysis described a change in total stress for any time interval at the highest stress point was limited to 10 and 12.5 percent. Strain changes during any time increment were limited to 50 percent of the elastic strain. These controls are important and prevent instability during the solution.

The creep law used in Marc is the exponential law given in equation 1. Thus the total strain at time t is

$$\varepsilon(t) = \varepsilon_e + K \sigma^n t \qquad (2)$$

A value of n = 3.1 (Glen, 1955, Gold, 1965, Gold, 1973) was used. K is much harder to define that n and the determination of a proper value will now be described.

Data obtained during the drilling of a well for Panarctic Oils Ltd. with West-Hi Rig. No. 2 was used. This rig and its load distribution have been described previously (Baudais et al., 1976). Total weight of the rig is 455 tonnes. The maximum ice thickness in the central portion of the platform in question was 4.9 m. The natural ice thickness was 2.3 m. Cross sections used for analysis are given in Fig. 10. The grid used is shown in Fig. 11. A general plan view of these platforms is given in Baudais et al., 1976. Material properties were

E = 690 MPa,
Poisson's Ratio = 0.20 and
subgrade modulus = 9.8 KN/m^3 (1T/m^3).

The results of the analysis and comparisons with measured values are presented in the deflection - time curves of Fig. 12. The measured deflections were obtained using standard surveying methods and a float-gauge or freeboard recorder installed next to the rig. Two initial runs were made with K values of:

6.18×10^{-12} ε/day/kPa^n and

56.16×10^{-12} ε/day/kPa^n.

In both runs it was assumed the load was applied instantaneously. The results are plotted in Fig. 12.

Since deflections at the rig are measured continuously from the time the first rig mat is laid (time of zero load) and since rig-up normally requires about 10 days before the platform is fully loaded, it can be seen that the assumption of instantaneous load application is in error and will never allow the theoretical derivation of the curve of measured values.

To correct this, the calculated elastic deflection of 74 mm was considered to occur over the first 10 days from start of rig-up. Admittedly, the deflection during this period would be caused by a combination of elastic and creep strain but load increases gradually over this period as first the rig structure and then drilling supplies are brought in and thus creep deflection would be considerably smaller than had the load been applied suddenly. This can be seen by examining equations 1 and 2. Stress is linearly dependent on load and strain rate and deflection rate are dependent on stress to the 3.1 power. Field measurements and theory (Frederking and Gold, 1976, Masterson and Kivisild, 1978) show that the ratio of strain rate to deflection rate is constant. Thus, further analysis was conducted assuming creep strain to start at day 10.

Admittedly, a more proper method of analysis would have been to increment the load from zero to full value over the 10 days. However, funds and time did not permit this and the above procedure was adopted as being reasonable.

Neither of the K values initially chosen resulted in large enough deflections at 37 days. To obtain the proper K value the following procedure was adopted. The measured creep deflection at 37 days was 204 mm total - 74 mm elastic

or 130 mm. The calculated creep deflection was 48 mm. Comparison of deflection and stress values from the first two runs revealed that the K value chosen only affected the time to reach certain values. That is, if a stress and deflection using a certain K were calculated to occur at time t, that same stress and deflection would occur at 1/10 t if a value 10K were used in the program. This meant that additional creep curves for other K values could be derived by simple proportioning of the times associated with a particular stress and/or deflection.

To obtain quickly the K value needed to predict measured deflections, a curve of best fit was derived for the points from run 2. A relation between creep deflection was derived for run 2 in the form of an exponential curve. It was found that, had the program been allowed to continue running, the measured creep deflection of 130 mm would have occurred after an interval of 79 days. The actual measured interval was 27 days. Thus K had to be increased by

$$\frac{79}{27} = 2.93.$$

This was done and the final curve of Fig. 12 was derived. An exponential curve of best fit is also shown. The agreement between the curves derived from finite element analysis and field data is good and the finite element method, particularly using this element and the exponential creep equation, is capable of a very accurately analyzing time dependent behaviour of laterally loaded ice plates.

Long-term deflections for this platform had also been calculated using an effective or reduced modulus and equally good results had been obtained, although they were less detailed. Also, stress relaxation near the heavy loads is quite rapid and pronounced. The finite element analysis shows this, while calculations using elastic plate formulas and the reduced modulus do not (Masterson et al., 1978). Thus, if detailed information over time of deflections and stress is required, viscoelastic analysis with finite elements is preferable. If only final deflections are required, then the effective or reduced modulus method is adequate, quicker, and much cheaper.

For any one rig, platform dimensions do not vary considerably and it would be feasible to produce families of curves which could be used for prediction of time dependent events. This has been done using the effective modulus method for specific load durations. The finite element analysis would produce more continuous and complete design curves.

Summary and Conclusions

The analysis of thickened sea ice floating platforms used as a support for offshore drilling in the Arctic Islands has been refined through the use of finite element techniques. Marc CDC programs were chosen for the calculations described in this paper. Both elastic and viscoelastic or creep stresses and strains were computed and deflections over time compared with an available case history.

Elastic analysis was done to determine the effects of element size, grid size, outer boundaries fixed or free to rotate, section taper, natural ice thickness and holes in the plate. An exponential creep law, available within the program was used for the creep analysis. A value of 3.1 was used for the exponent and the creep constant was determined by comparison to case histories.

The following conclusions are drawn: -

1. Discontinuing the finite element grid at 3.8 stiffness radii from the load centre resulted in a model which gave stresses and deflections for simple loading cases very close to those derived from established analytical formuals. For distributed loads the agreement is nearly exact near the load centre where stresses and deflections are 5 to 10 times those near the edges.

2. Element size and load distribution was found to affect stress at the load centre. Three point loads produced a maximum stress 14 percent less than a distributed load.

3. The fixing or freeing of grid outer boundaries against rotation about their own axes had no effect on critical stress areas near the load centre and relatively small effects elsewhere.

4. A large hole (moonpool for drilling, 5.5. × 5.5 m) caused stresses at 2.7 m from the moonpool edge to increase from 0 to 1.43 times. At 9.4 m the maximum stress increase was 5 percent. Plate thickness at the load centre was 7 m.

5. Changing the outer section taper from 15:1 horizontal to vertical to 10:1 increased deflections by 10 percent but had no effect on the large stresses near load centre. Natural ice thickness had no effect on stress in critical areas.

6. By allowing for initial gradual loading of the platform where deflections were considered to be elastic, the deflection - time curve of a platform used for drilling was very closely approximated using time dependent finite element analysis. n = 3.1 was used and K was found to be

   164.55×10^{-12} ε/day/kPa^n.

7. Total long-term deflections calculated using a reduced modulus and elastic plate formulas agreed well with the finite element creep solution. However, much more detail over time is provided by the finite element method.

Recommendations

The results of applying finite element analysis to floating ice platform analysis are very encouraging and it is recommended that all case histories should be analyzed this way. Since, for any rig, platform geometry does not vary considerably, it would be possible to present sets of design curves relatively cheaply giving detailed information on elastic and time dependent stresses, strains and deflections.

Acknowledgment

The authors would like to thank Panarctic Oils Ltd. for granting permission to present the data contained in this publication. Thanks is also expressed to Control Data Canada Ltd. for their assistance with programming.

References

Baudais, D.J., Watts, J.S., and Masterson, D.M. (1976). "A System for Offshore Drilling in the Arctic Islands", Offshore Technology Conference, Paper No. OTC 2622, Houston, Texas, May, 1976.

Frederking, R.M.W. and Gold, L.W. (1976). "The Bearing Capacity of Ice Covers Under Static Load", Can. J. Civ. Eng., Vol. 3, No. 2, pp. 288-293.

Glen, J.W. (1955). "The Creep of Polycrystalline Ice", Proceedings of The Royal Society, A228, 1955, pp. 519-538.

Gold, L.W. (1973). "Activation Energy for Creep of Columnar-Grained Ice", Physics and Chemistry of Ice, Royal Society of Canada, 1973, pp. 362-364.

Gold, L.W. (1965). "The Initial Creep of Columnar-Grained Ice", Parts I and II, Canadian Journal of Physics, Vol. 43, pp. 1414-1434.

Marc CDC User Information Manual, Control Data Corporation, Minneapolis, 1976.

Masterson, D.M. and Kivisild, H.R. (1978). "Floating Ice Platforms: Offshore Oil Exploration", Annual ASCE Conference, Chicago Oil 16-20, 1978.

Masterson, D.M., Anderson, K.G. and Strandberg, A.G. (1979). "Results of Strain Measurements in Floating Ice Platform Using 3 m Long Resistance Win Gauges", Workshop on the Bearing Capacity of Ice Covers, Winnipeg, October 16-17, 1978, N.R.C.C. A.C.G.R.Technical Memorandum No. 123, May 1979.

Westergaard, H.M. (1926). "Stresses in Concrete Pavements Computed by Theoretical Analysis", Public Road, Vol. 7.

Wyman, M. (1950). "Deflections of an Infinite Plate", Canadian Journal of Research, Vol. A28.

Symbols

E elastic modulus (MPa)

h ice thickness (m)

K creep constant (strain/time/stress^n)

kPa $\times 10^{-3} = N/m^2$, $\times .145 =$ psi

k subgrade modulus = 9.8 KN/m^3 (1T/m^3) for floating ice

MPa $\times 10^{-6} = N/m^2$, $\times 144.98 =$ psi

n creep exponent

t time

ε strain

ε_e elastic strain

μ Poisson's Ratio

σ stress (kPa)

$$\text{stiffness length} = \left[\frac{Eh^3}{12(1-\mu^2)\,k}\right]^{\frac{1}{4}}$$

FIG. 1 9 ELEMENT GRID USED FOR LOAD CASE 1, 3 POINT LOADS AT NODES 20, 1 AND 17

1. NODES 1,17,2,18,3,19 & 9 FIXED FOR ROTATION AND BENDING ABOUT X AXIS.
2. NODES 1,20,5,27,9,34 & 13 FIXED FOR ROTATION AND BENDING ABOUT Y AXIS.

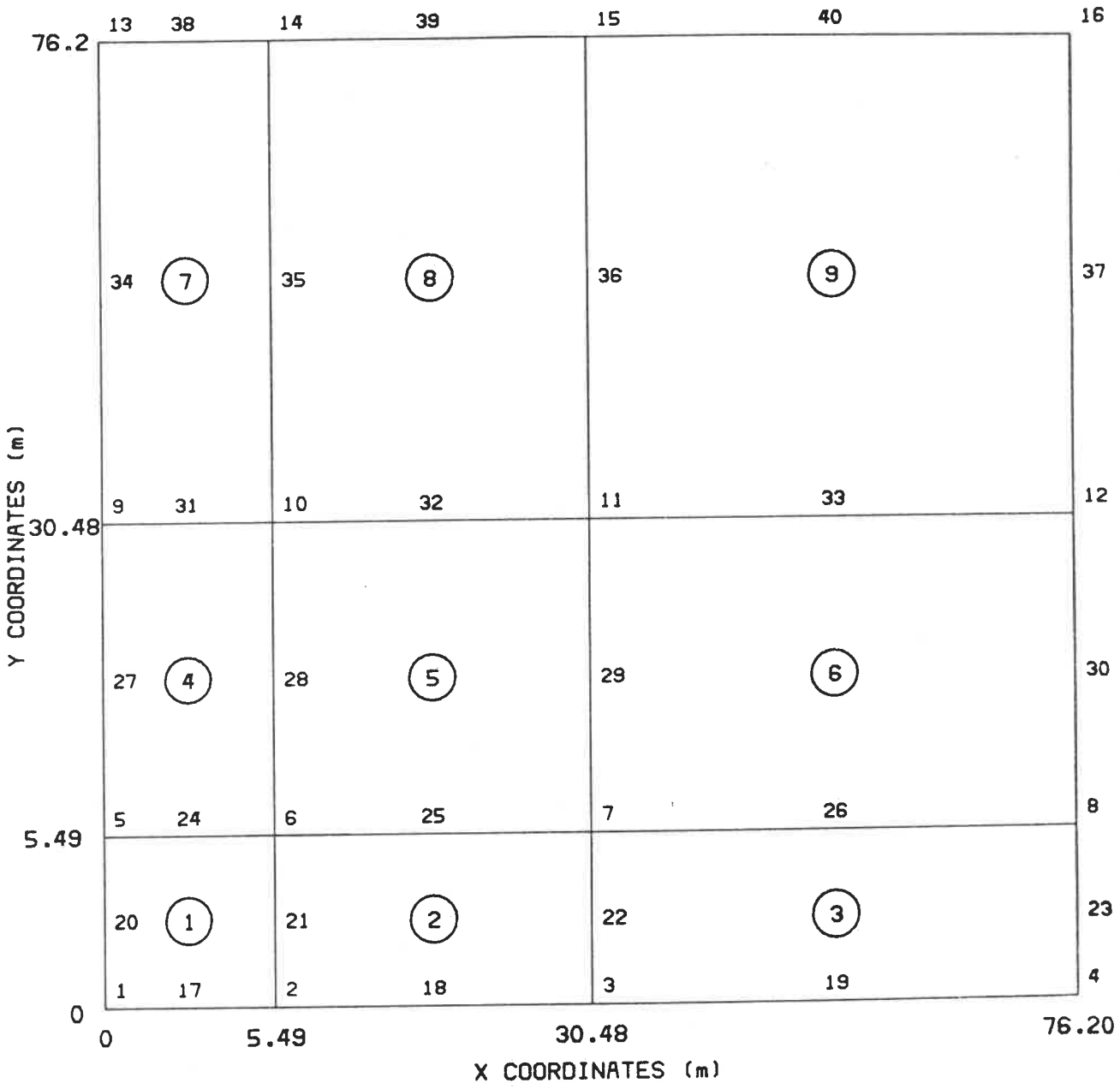

FIG.2 16 ELEMENT GRID USED FOR LOAD CASES 2 AND 3

1. NODES 1,26,2,27,3,28,4,29 & 5 FIXED FOR ROTATION AND BENDING ABOUT THE X AXIS.
2. NODES 1,30,6,39,11,48,16,57 & 21 FIXED FOR ROTATION AND BENDING ABOUT THE Y AXIS.

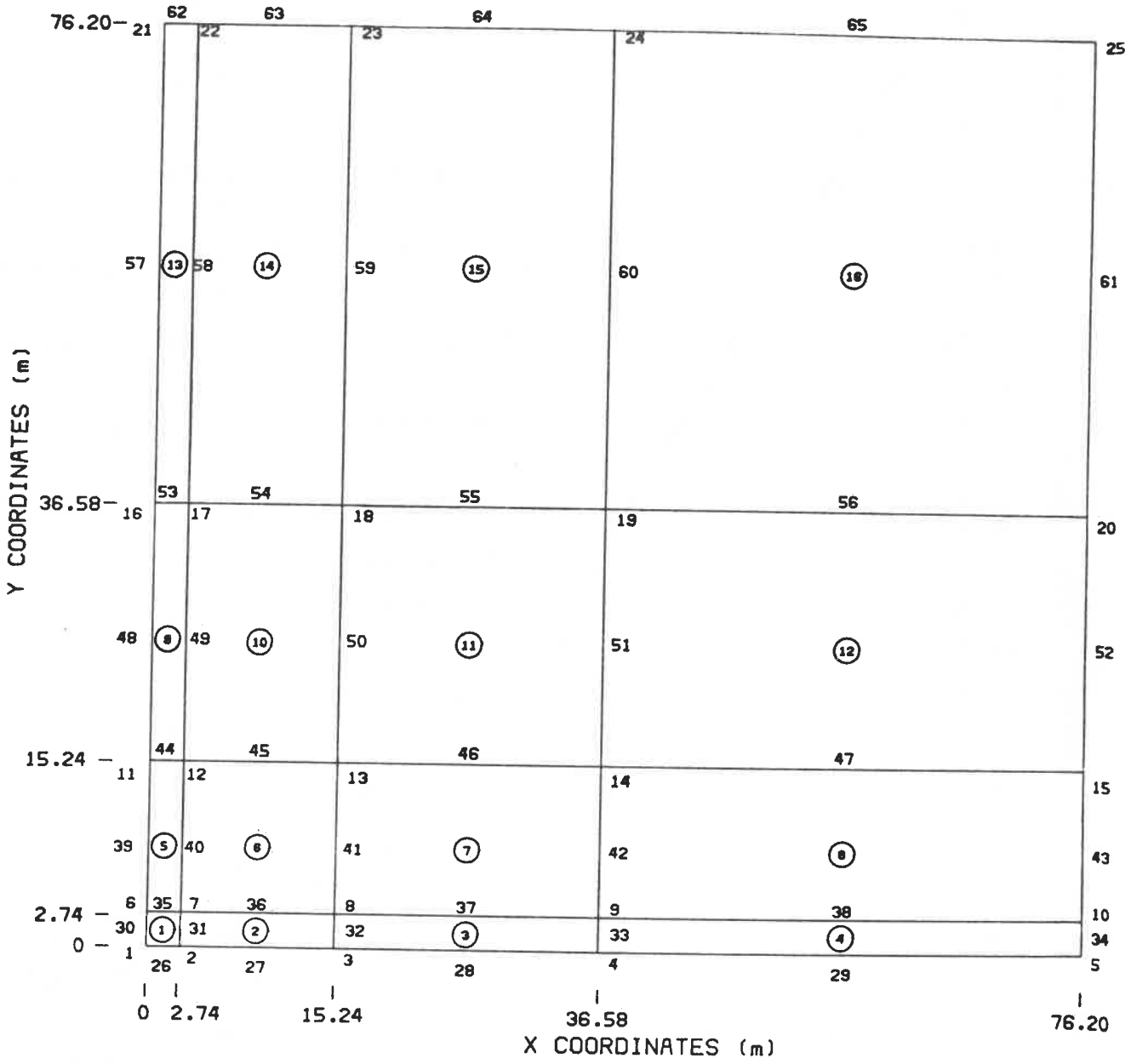

FIG.3 DEFLECTION VERSUS RADIAL DISTANCE FROM NODE 1

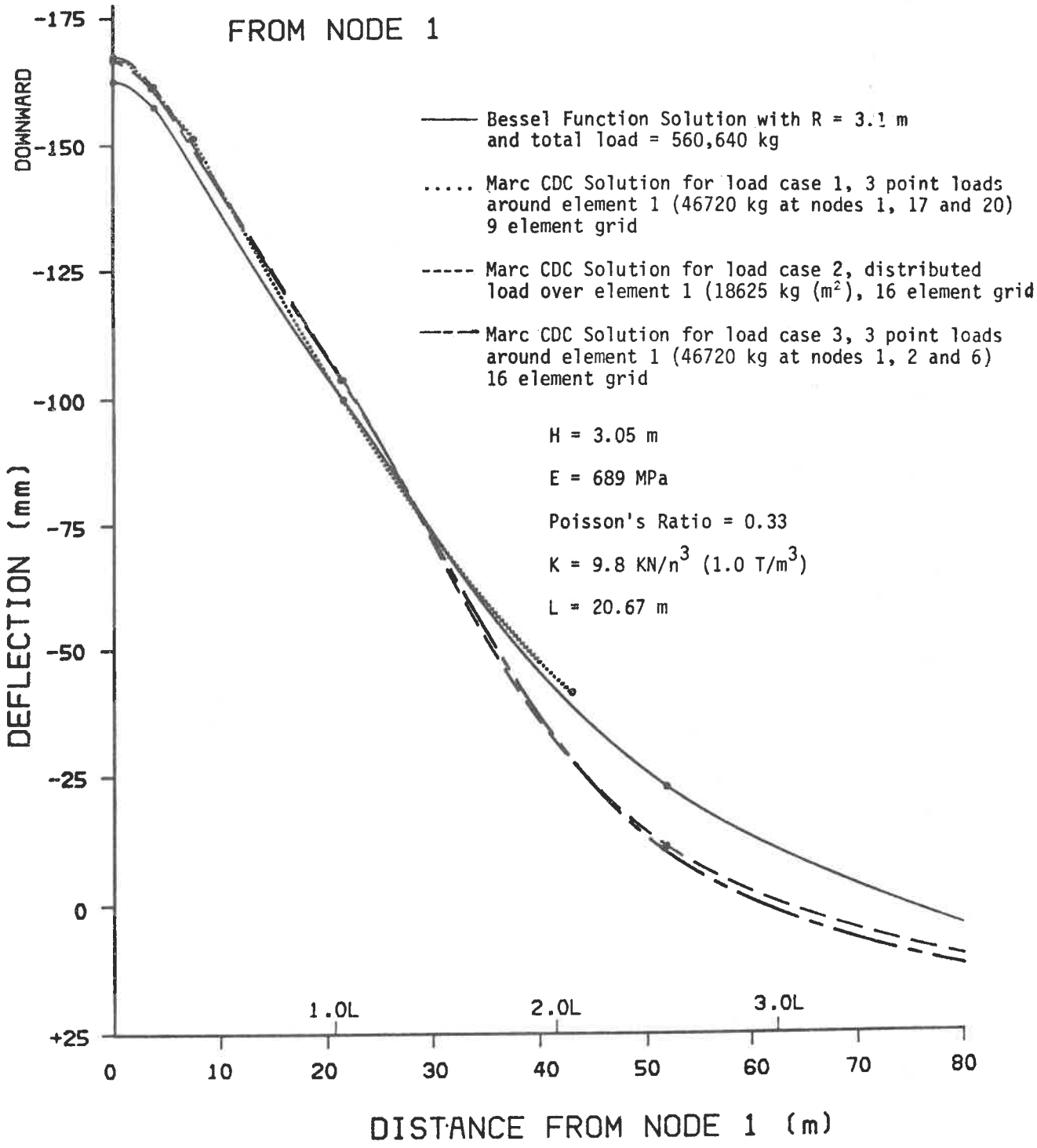

FIG. 4 TANGENTIAL STRESS VERSUS RADIAL DISTANCE FROM NODE 1

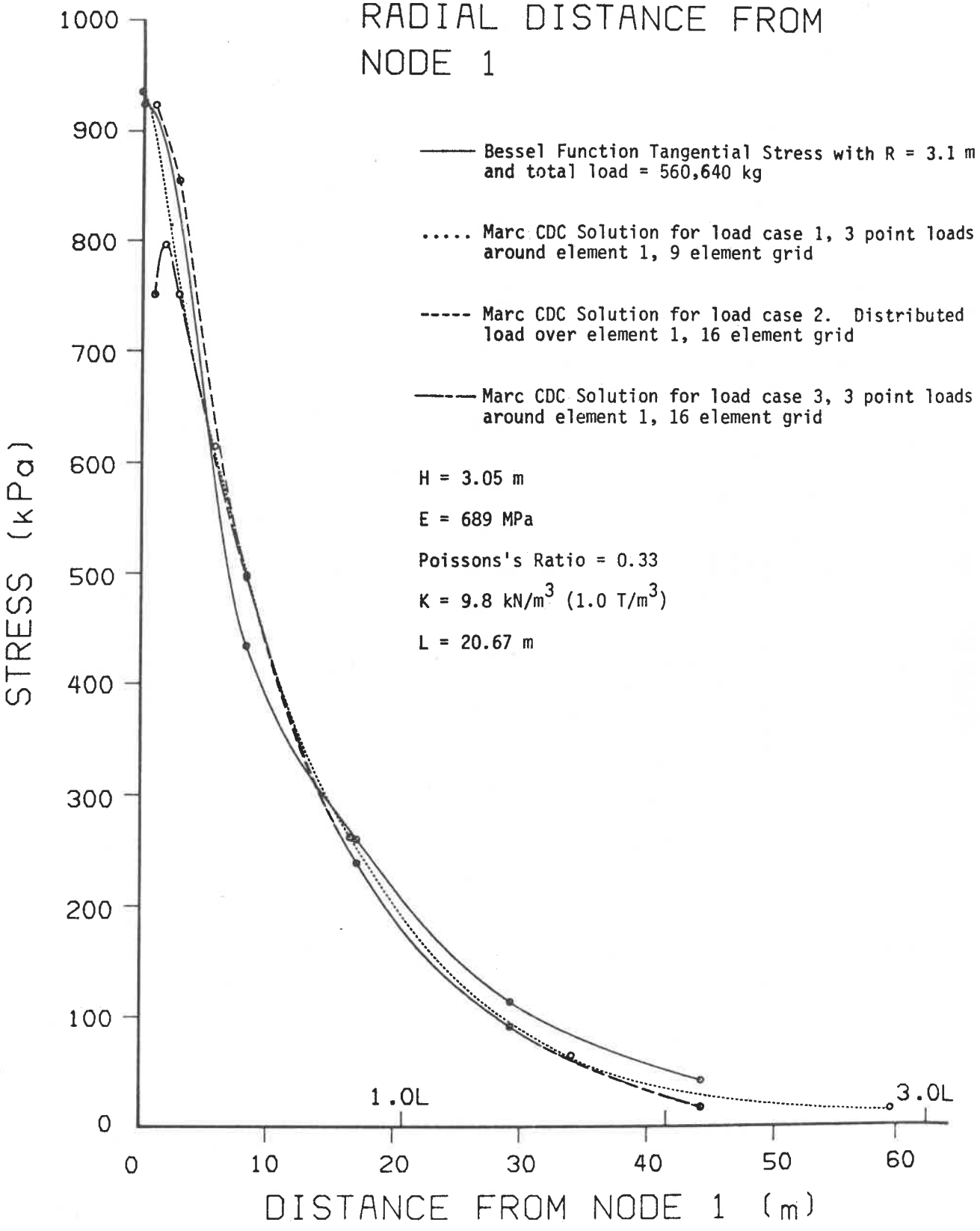

FIG. 5 RADIAL STRESS VERSUS RADIAL DISTANCE FROM NODE 1

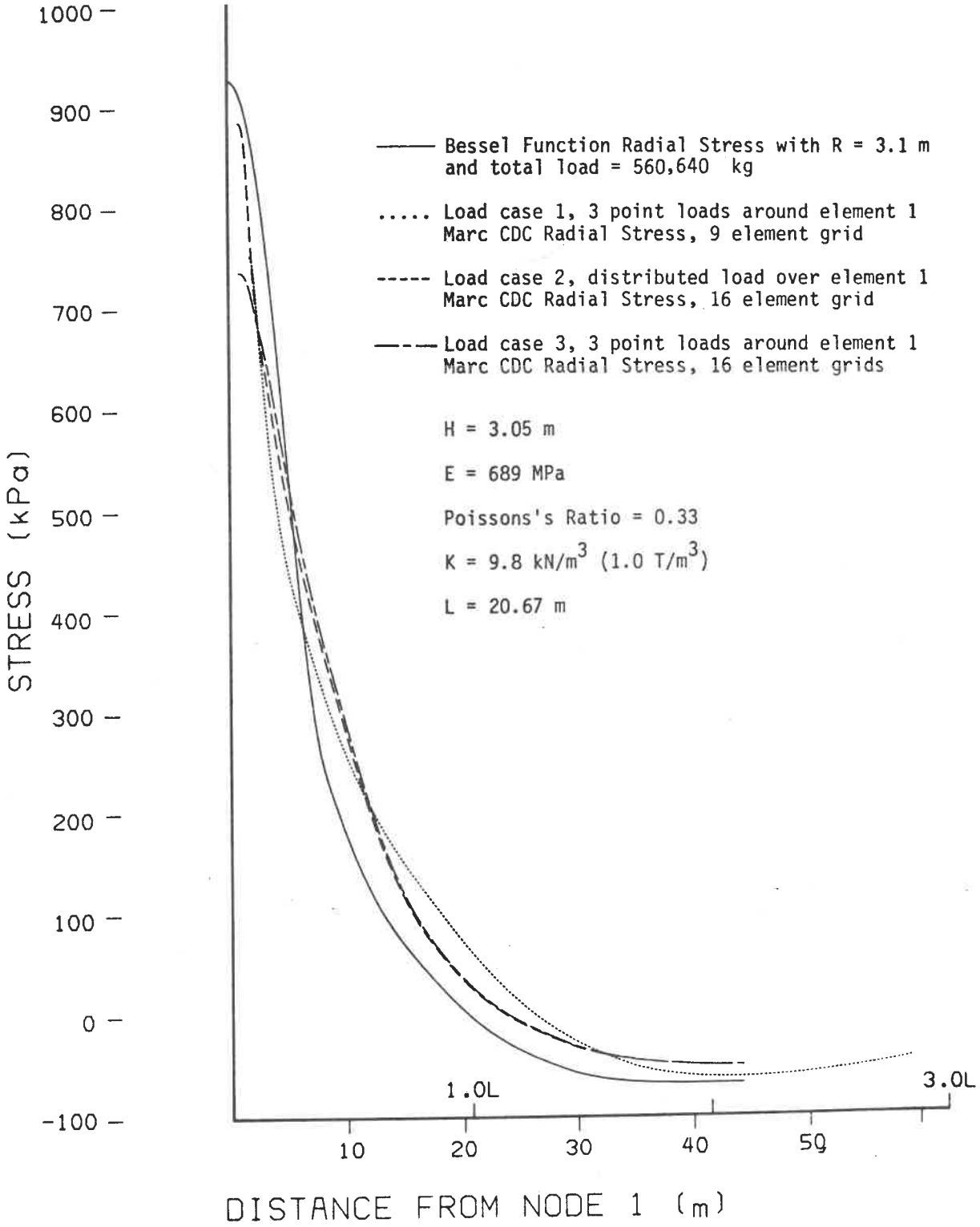

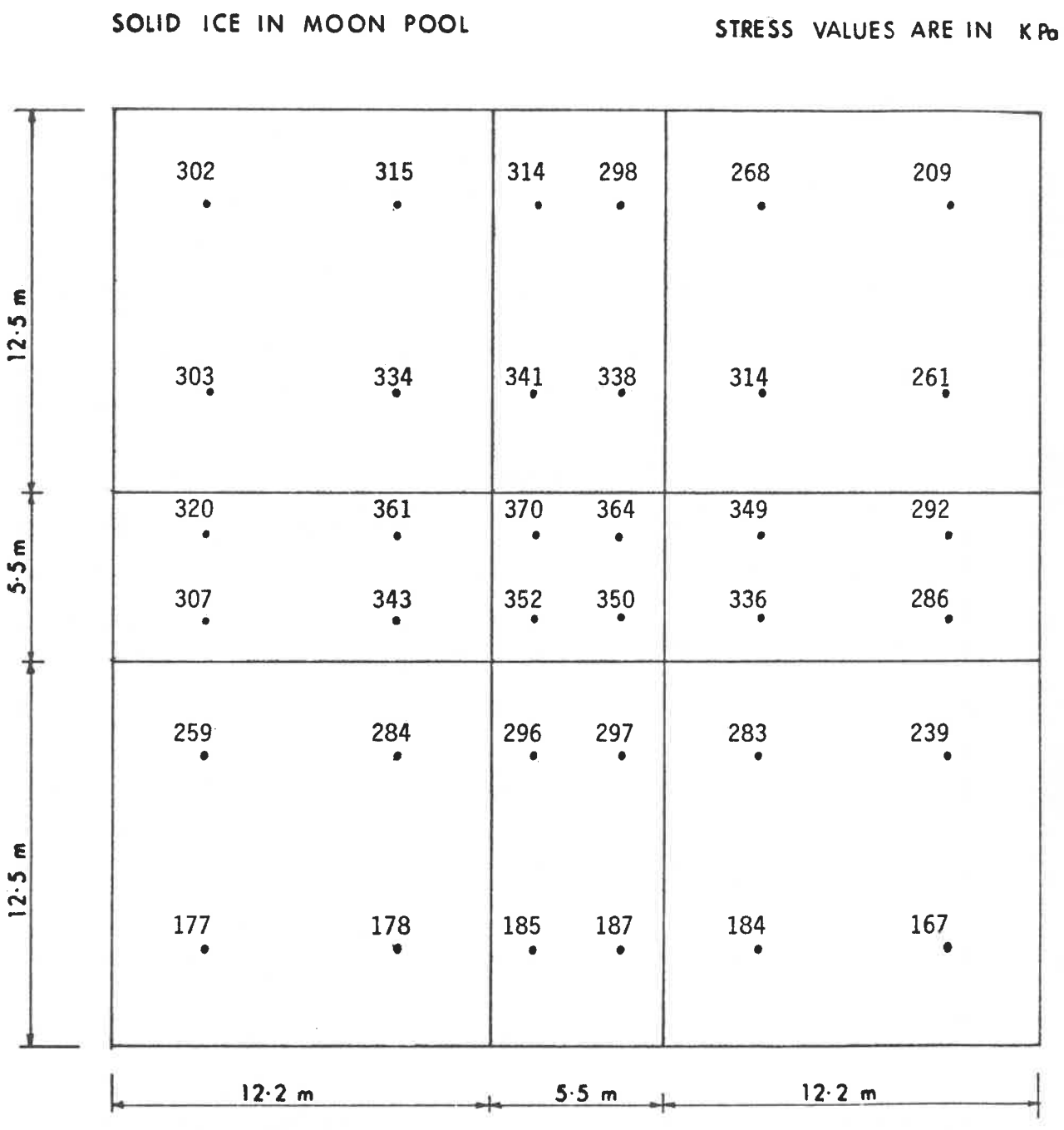

FIGURE 6 STRESS ANALYSIS NEAR MOON POOL USING MARC CDC

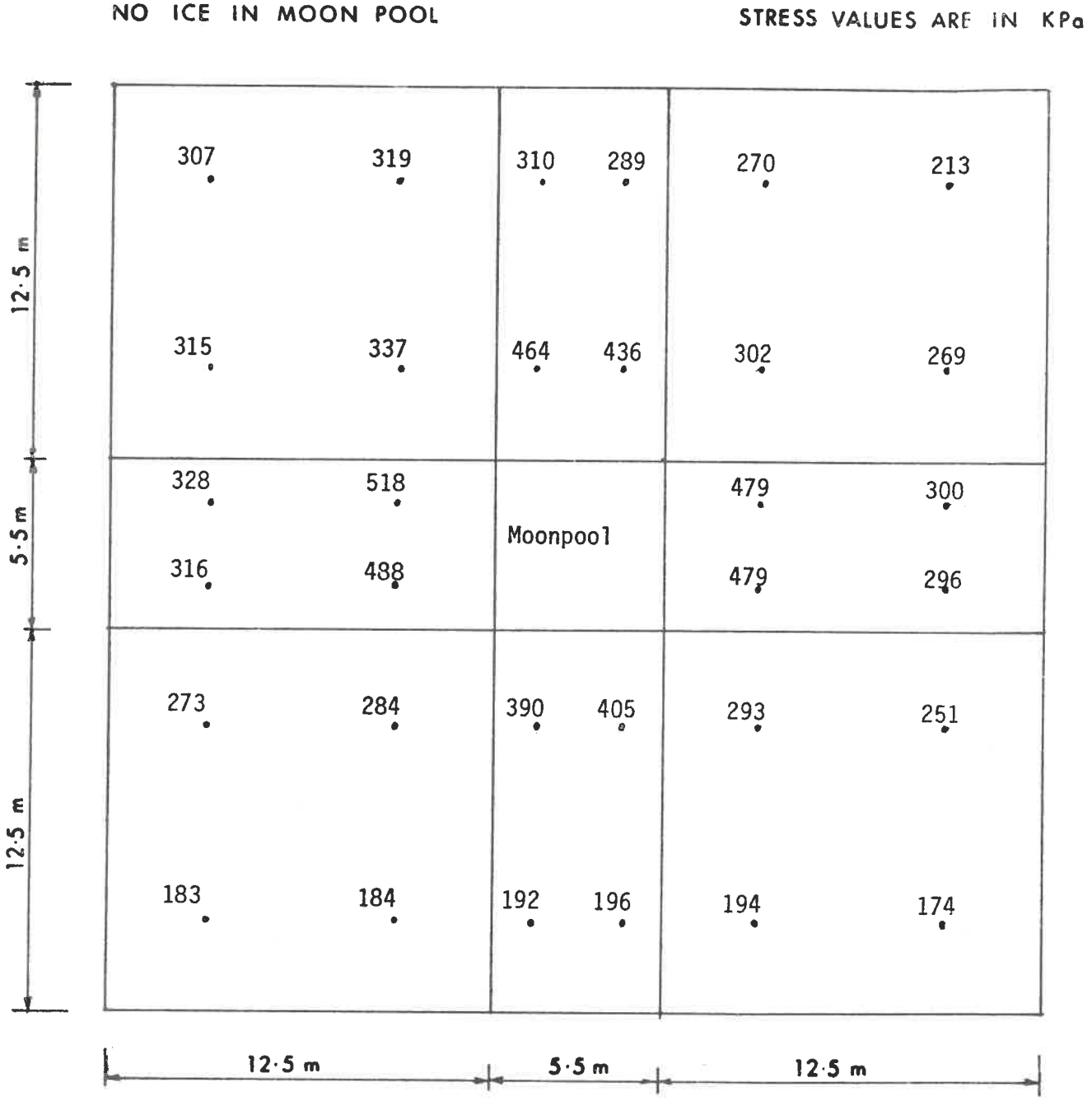

FIGURE 7 STRESS ANALYSIS NEAR MOON POOL USING MARC CDC

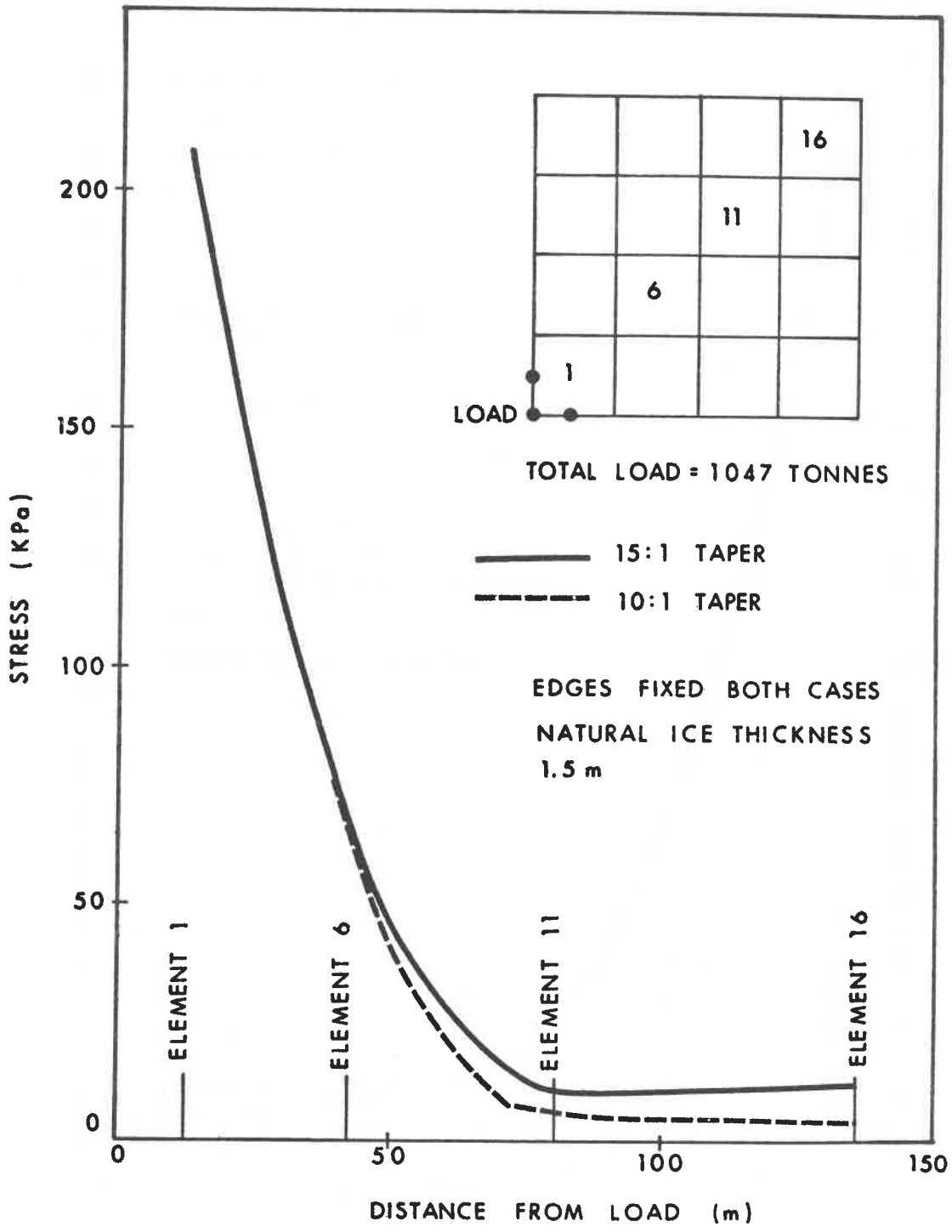

FIGURE 8 PLOT OF STRESSES ON DIAGONAL ELEMENTS 1, 6, 11, 16

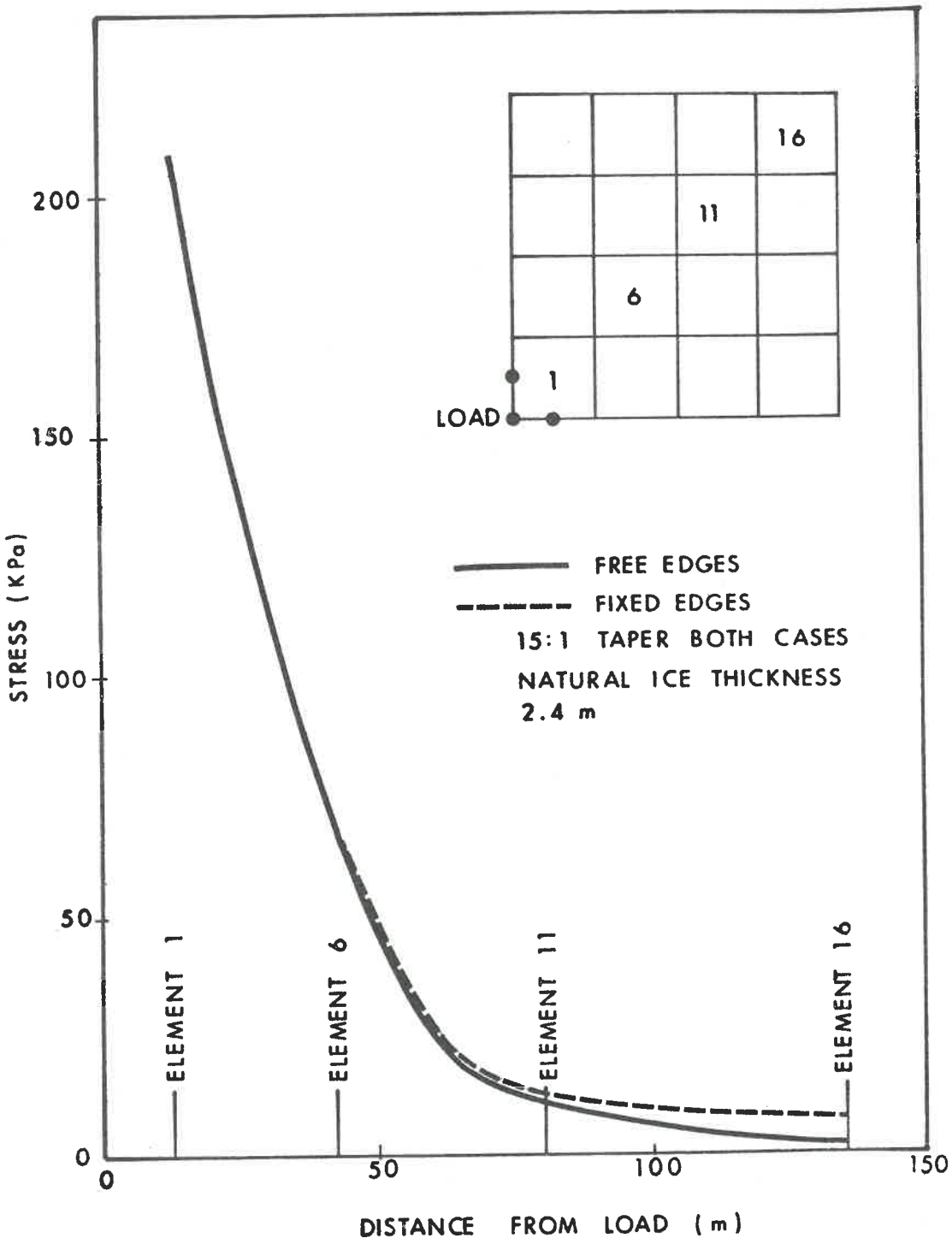

FIGURE 9 PLOT OF STRESSES ON DIAGONAL ELEMENTS 1, 6, 11, 16

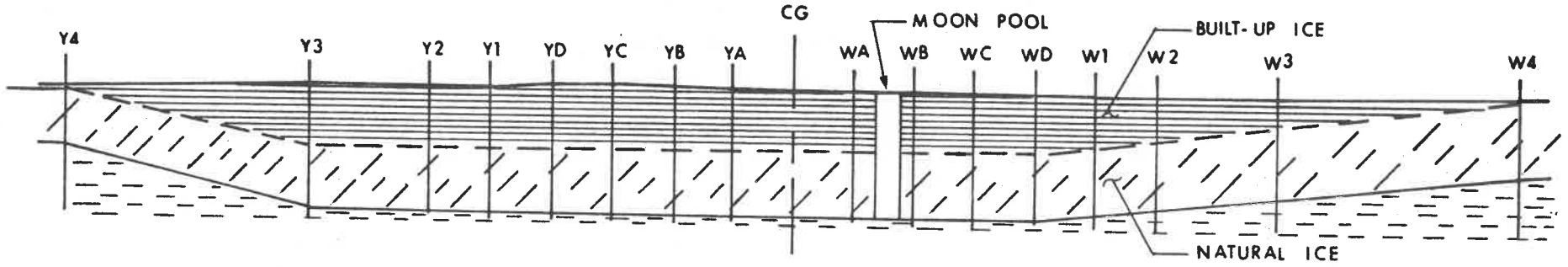

SECTION ALONG RIG AXIS

SCALES:

HORIZONTAL 0 5 10 15 20 m

VERTICAL 0 1 2 3 4 5 m

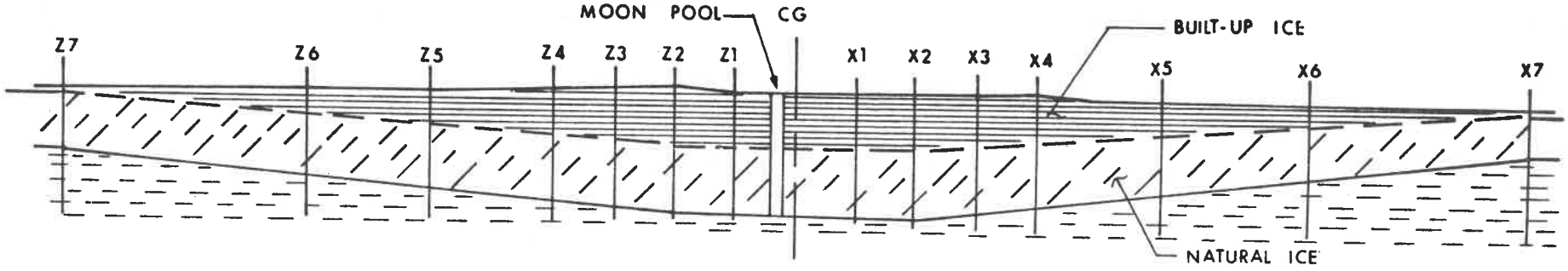

SECTION ACROSS RIG AXIS

FIGURE 10 SECTIONS OF ICE PLATFORM USED FOR MARC CDC CREEP ANALYSIS

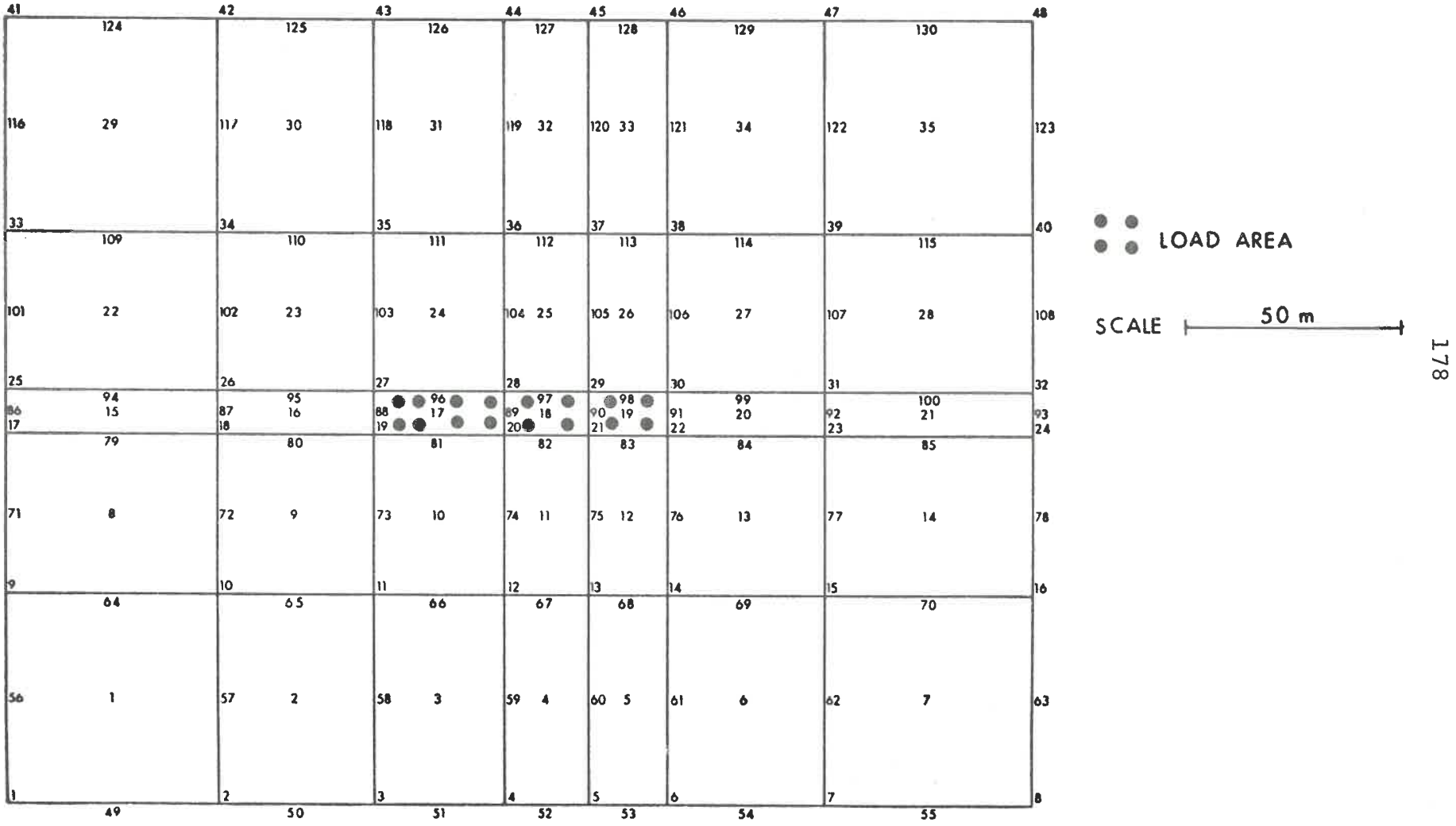

FIGURE 11 GRID USED FOR MARC CDC CREEP ANALYSIS

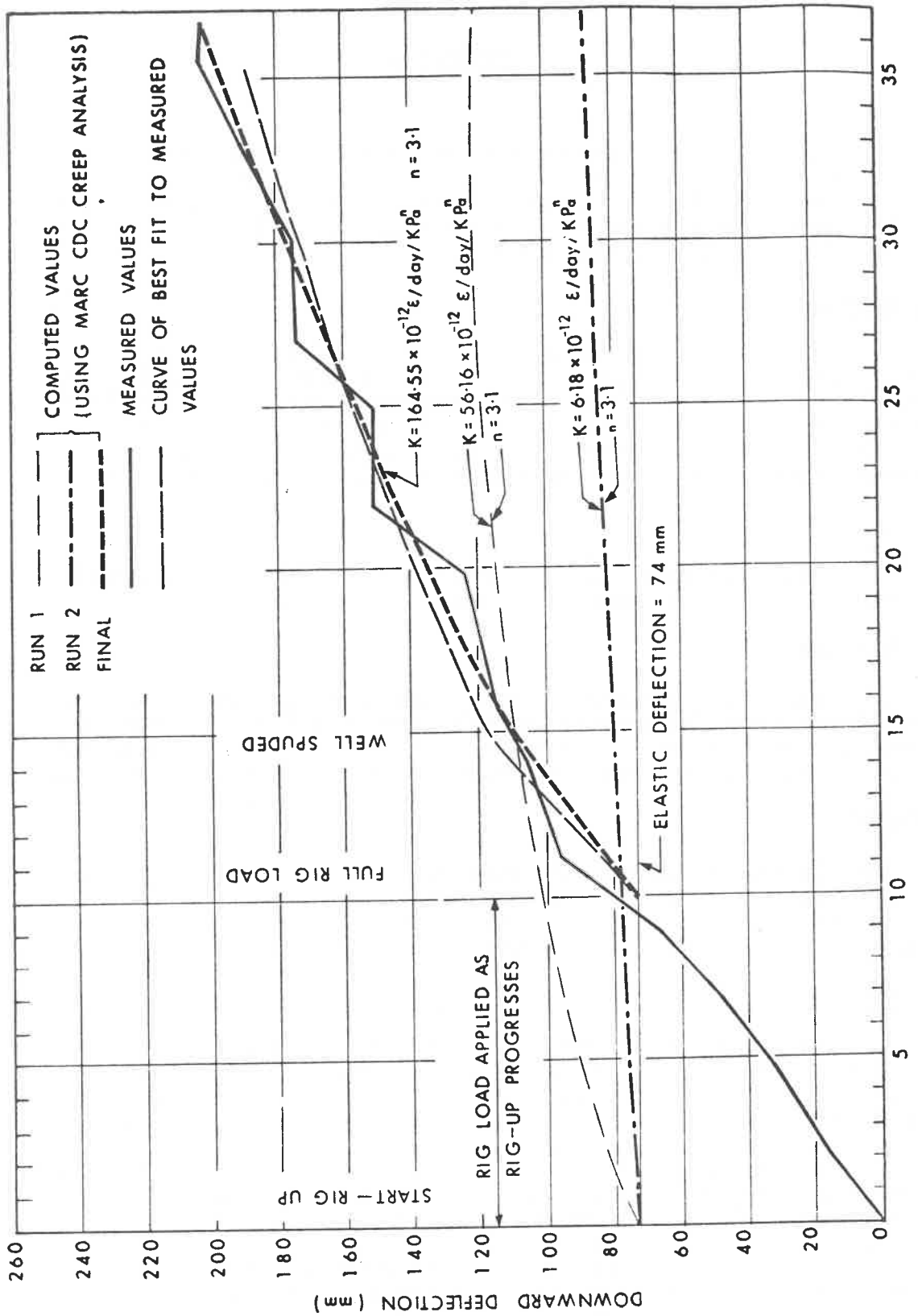

FIGURE 12 MEASURED AND COMPUTED CREEP DEFLECTION FOR C-58

Discussion

P.R. Kry:

Since stress concentrations due to a hole increase towards the hole, the magnitude of increased stress due to moonpool presence requires evaluation of stresses at the moonpool boundary. How close to the moonpool does the finite element program compute the stress?

D.M. Masterson:

The stress output points for the finite element program are shown in Figs. 6 and 7 of the paper. Stress profiles with and without ice in the moonpool are presented here (see figure following discussion) and show that the stress at the edge of the moonpool with ice removed is finite, although greater than for the other case.

R. Tinawi:

Did your model show a stress value for a concentrated load smaller than the case of a distributed load?

D.M. Masterson:

The model showed a lower stress value for 3 concentrated loads than for a distributed load equal to the sum of the concentrated loads. A single concentrated load placed at the grid corner gave higher stresses than the distributed load.

B. Michel:

Do the stresses decrease with time, to explain the strain hardening type of deformation using Glen's law for computation? Don't you find the value of 500 kPa high for the design of a platform at the lower layer of a sea ice sheet?

D.M. Masterson:

Decrease of stress with time is a result of relaxation within the ice. If high local stresses do not cause initial failure or fracture, then yielding and creep allow their dissipation.

The value of 500 kPa is normally used as the maximum, extreme fibre tensile stress due to lateral loading of ice sheets. This has been found to give safe results for short-term loading of sea ice sheets in the winter time. Creep and deflection under long-term loads often make it necessary to reduce this initial stress since long-term deflections have been found to be proportional to the initial stress to a power of 2.2.

D. Bruce:

On the figure which demonstrated the changes in stresses for an ice sheet with and without the moonpool, the stresses were not symmetrical. Was this due to a non-symmetric load?

D.M. Masterson:

Yes, the load was non-symmetric.

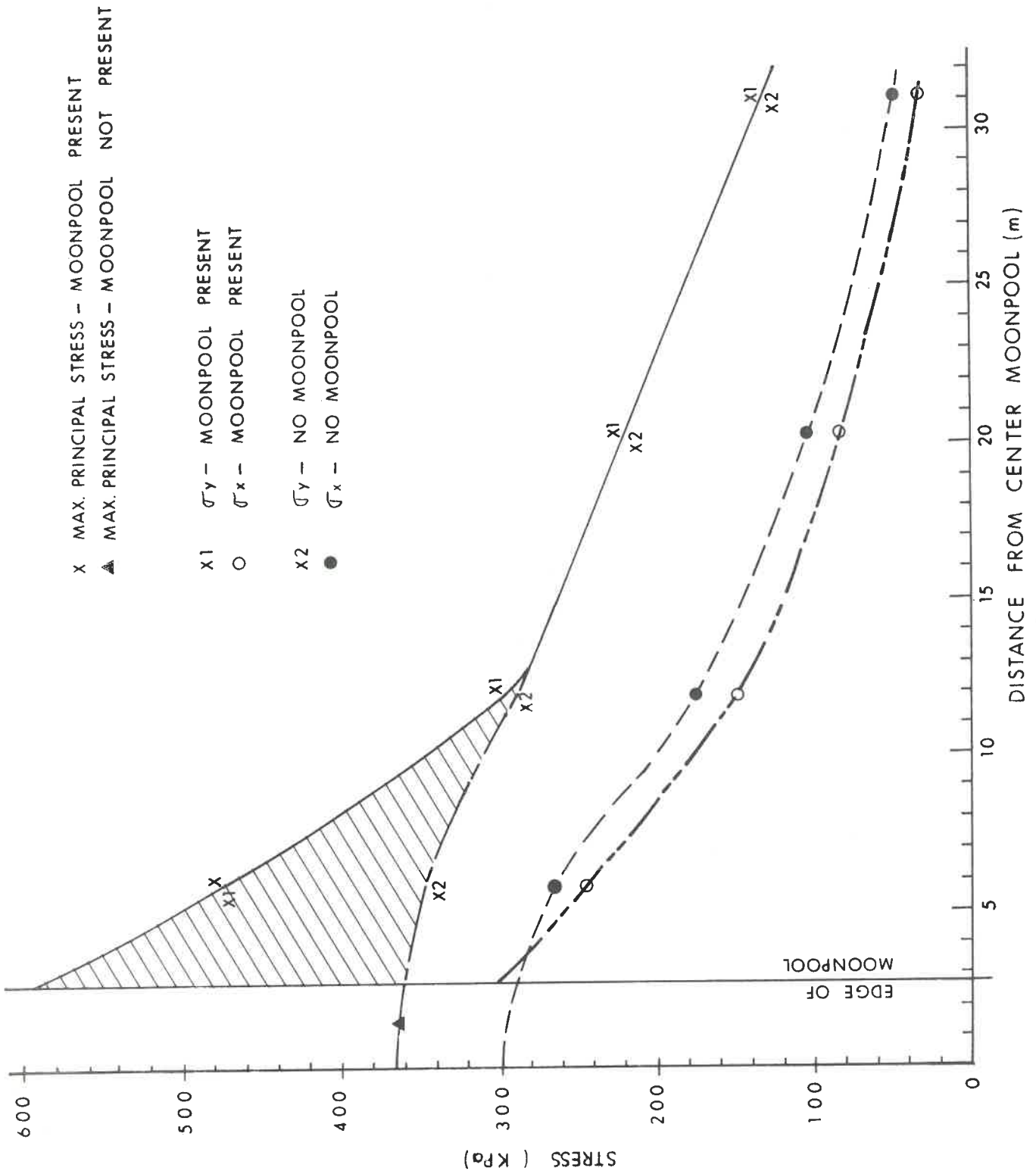
X MAX. PRINCIPAL STRESS – MOONPOOL PRESENT
▲ MAX. PRINCIPAL STRESS – MOONPOOL NOT PRESENT
X1 σy – MOONPOOL PRESENT
O σx – MOONPOOL PRESENT
X2 σy – NO MOONPOOL
● σx – NO MOONPOOL
STRESS (KPa)
600
500
400
300
200
100
0
EDGE OF MOONPOOL
5
10
15
20
25
30
DISTANCE FROM CENTER MOONPOOL (m)

VISCOELASTIC FINITE-ELEMENT ANALYSIS OF FLOATING ICE ISLANDS

A.S.J. Swamidas, H. El-Tahan, and D.V. Reddy
Faculty of Engineering and Applied Science
Memorial University of Newfoundland

Introduction

a) State-of-the-Art:

The emergence of the Arctic and Subarctic offshore areas as potential reserves of hydrocarbons has led to the development of innovatory methods for offshore drilling using the naturally existing ice-sheets. Also, the increased use of the polar regions for military and naval operations - airfields, roads and ports - has necessitated the use of the frozen ice surface for sustaining long or short-term loads. In addition to drilling operations, naval operations continue to depend on sea-ice airfields and roads to provide cargo and logistic support. As the average thickness of the natural ice cover is 1.5 to 2.0 m, the ice has to be thickened artificially to support the heavy loads placed on it due to drilling, air, naval or transport operations. To ensure safe operations under these conditions, a better understanding of the behaviour of artificially-thickened sea-ice sheets under various conditions is required.

Three fundamental catagories that influence ice strength are: material characterization, loading and geometry, and the failure criterion (Katona and Vaudrey, 1973). The material characterization category or stress-strain relationship, contains the parameters: temperature, salinity, density, age, crystal orientation, elastic or inelastic moduli and strength parameters such as tensile, compressive, flexural, confined or unconfined shear stresses. For the loading and geometry category, parameters can be standardized and simplified to adequately characterize the boundary value problem. The failure criterion can be divided into two parts: failure mechanism and failure law.

Analyses of the deformation of floating ice covers have been reported by many authors: a recent report describes a critical survey assessing the relative merits (Kerr, 1975) of the various analytical methods based on elastic (Wyman, 1950); elasto-plastic (Kheisin, 1964; Nevel, 1972); yield line (Meyerhof, 1960); and linear and non-linear viscoelastic (Panfilov, 1970; Hutter, 1973) theories. Computer codes have been

developed to determine the linear and non-linear elastic or viscoelastic deformations of floating ice covers (Katona, 1974a; Katona, 1974b).

Construction techniques for artificial ice platforms have been developed over the last two decades. First pioneered by the U.S. Navy for aircraft landing platforms (Dykins, 1962; Dykins, 1967); the liquid-filling can be carried out in three ways, viz., free flooding, confined flooding and spray sprinkling (Hood et al., 1975; Masterson et al., 1975; Baudais et al., 1974). Studies indicate that (i) thin-flooded layers, 3 to 4 in. depth, produce better ice than thick-flooded layers, (ii) circular-shaped built-up ice areas are better than square or rectangular-shaped built-up areas because of less severe distortion, (iii) quality control is very important for a better platform, and (iv) free-flooding is better than confined flooding.

W. Hecla N-52 and East Drake I-55 platforms have been constructed in the Melville Island offshore areas in water depths of 470 ft. (Kerr, 1975; Strain, 1975). More exploratory drilling ice islands are expected to be constructed in the Sverdrup basin gas field areas, between Bathurst and Ellef Ringnes Islands. Reinforcing of ice with asbestos, wood, paper mash, and fibre glass reinforcement (Coble and Kingery, 1962) may be resorted to provide greater strengths and stabilities to these platforms.

At both W. Hecla N-52 and East Drake I-55, the ice platforms were instrumented extensively to measure ice temperatures throughout the thickness of the ice sheet and vertical deflection due to the loading (Oil Week, 1974). The most critical measurement is the vertical deflection due to the weight of the drilling rig. Temperatures were monitored continuously during drilling to determine incidental temperature increases inside the ice sheet due to mechanical or thermal operations on the ice.

b) Viscoelastic Analysis:

The behaviour of a floating ice sheet under a long-term load could be characterized by two types of deflection-versus-time curves, as shown in Fig. 1. For an analytical determination of a 'safe' load $P<P_f$ and a "time to failure" t_f, it is desirable to have a viscoelastic theory for floating ice plates which for time $t=0$ yields the elastic response, and for $t>0$ yields responses according to Curves I and II, depending upon the load and the material parameters of ice (which in turn depend upon the temperature distribution, salinity, etc.); the recent work of Nevel (1976) proves to be a step in this direction. This theory should be supplemented by a crack

or failure criterion valid for the elastic and viscoelastic range. The elastic theory, in conjunction with crack criterion $\sigma_{max} = \sigma_f$, could if proven correct, be a special case of such a general theory.

Another failure criterion was proposed by Zubov (1942) and by Kobeko et al., (1946) based on data, for loads of short or long duration, a floating ice plate fails when a certain deflection w_f is reached;

$$w_{max} = w_f \qquad (1)$$

Nevel (1976) presented a unified theory for the primary, secondary and tertiary creep effects observed in transversely loaded ice sheets, shown in Curve II of Fig. 1 and in Fig. 2. He assumed the ice to behave like a six-parameter model with two Kelvin bodies and one Maxwell body in series; the stress-strain relations were assumed to follow linear viscoelasticity. The time-dependent strain (Fig. 2), under an applied stress σ, was expressed as

$$\varepsilon = \sigma\left(\frac{1}{E_1} + \frac{t}{\eta_1} + (1-e^{-E_2 t/\eta_2})/E_2 + (e^{E_3 t/\eta_3}-1)/E_3\right) \qquad (2)$$

The ice behaviour during the three regions of interest, primary, secondary and tertiary creep, is shown in Figs. 3, 4 and 5.

Katona (1974), Katona and Vaudrey (1973), and Vaudrey and Katona (1975a and 1975b) developed finite element computer programmes for a floating ice sheet. Assuming a linear viscoelastic stress-strain behaviour, and an axisymmetric load distribution, the long-term behaviour of a floating ice sheet was determined (Fig. 6). The material constants were allowed to vary along the depth.

Problem Formulation

The purpose of this investigation is to study the behaviour of an artificially thickened ice cover under the static load of the drilling rig, considering time and temperature-dependent ice properties.

The structure investigated is the W. Hecla N-52 offshore platform shown in Fig. 7, used by Panarctic Oils Ltd. for exploratory drilling off the coasts of the Sabine Peninsula of Melville Island, during the winter seasons of 1974 and 1975.

a) Computer Programmes Used in the Analysis:

The viscoelastic computer programme (VISICE) was developed by Katona (1974) for constant plate thickness. VISICE was modified by the first author (MODVIS) to account for variable thickness plates and temperature-dependent properties considering non-linear temperature profile. Again MODVIS was modified to account for reinforcement elements (RINVIS).

b) Ice Properties:

Ice properties are time as well as temperature-dependent. To account for the dependency of ice properties on time, the ice was considered as viscoelastic material following the behaviour of the "standard linear solid model" according to which the bulk and shear relaxation functions Bk(t) and Gk(t) are given by Katona (1974).

$$Bk(t) = Bk_o + Bk_1 \, e^{-t/a}, \qquad (3)$$

$$Gk(t) = Gk_o + Gk_1 \, e^{-t/a}, \qquad (4)$$

where

Gk_o and Gk_1, Bk_o and Bk_1, are Bulk and Shear Relaxation Moduli respectively.

a is the relaxation time,

and

t is the time,

Linear temperature-dependent relationships for the bulk and shear relaxation functions were assumed as follows

$$Kk(t,\theta) = Bk(t) \; (1 - 0.012\theta), \qquad (5)$$

and

$$Gk(t,\theta) = Gk(t) \; (1 - 0.012\theta), \qquad (6)$$

where

θ is the ice temperature.

c) Temperature Profile:

Based on field measurements the non-linear temperature distribution was assumed to follow the following equation given by Drouin and Michel (1974):

$$\theta = \frac{1}{b} \{-1 + \sqrt{1 + 2b(1 - (1 - z/d)(\theta_1 + \theta_1^2\, b/2))}\} \quad (7)$$

θ_1 top surface temperature,
θ ice temperature at distant z from the bottom, and
b empirical constant.

d) The Finite Element Model:

The platform is idealized as an axi-symmetric, elastically supported (Winkler-type fluid foundation), varying thickness ice plate, subjected to distributed loads of the rig and its accessories. The rig loads are replaced by two distributed loads of 610 Kips and 400 Kips separated by a distance of 75 ft. c/c, as shown in Fig. 8. Also in-plane loads of 40 psi are applied over the outer periphery to account for the stress transmitted from the adjacent ice areas. Figure 9 presents the finite element discretization of the platform with 441 elements and 508 nodal points.

e) Cases studied:

i) Behaviour of the platform under the actual load and environmental conditions,

ii) Effect of surface temperature on the platform behaviour. Three values are considered -30, -20 and -10°C with temperature profiles shown in Fig. 10, and

iii) Effect of reinforcing the platform on its stresses and deformations.

Reinforcing of ice with asbestos, wood, paper mash and fibre glass has been suggested to provide greater strength and stabilities of artificial ice platforms (Coble and Kingery, 1962) and Stanley and Glockner (1975). Asbestos is used in this investigation as reinforcement in tension zones with a parabolic configuration. Detailing of the reinforcement is shown in Fig. 11.

Results and Discussion

a) Platform Behaviour:

Figures 12 and 13 present radial stress and strain distribution at the platform centre vs. time. Figure 14 presents the deflection profile vs. time. The results indicate that i) distribution of stresses and strains is not linear, ii) deflections and strains increase, while stresses decrease

with time, and iii) the rates of change of stresses, strains and deflections are higher in the first hours. Comparison of field measurements reported by Baudais et al., (1974), and the calculated deflection showed satisfactory agreement.

b) Effect of Surface Temperature:

Figures 15 to 17 present the effect of surface temperature on the deflection profile. The results indicate that short-term stresses, strains and deflections are lower for low surface temperatures. The effect of surface temperature is higher on deflections than on stresses or strains. Long-term stresses, strains and deflections seems to be independent of surface temperature.

c) Effect of Reinforcement:

Figures 18 to 21 present the effect of reinforcement on fibre stress, fibre strain and deflection profiles, and deflection time history. The results indicate that reinforcing the platform reduces stresses, strains and deflections. The effect is larger on deflection. The long-term deflection is greatly affected by reinforcement due to the fact that ice loses its rigidity with time because of its viscoelastic behaviour while the properties of asbestos are time-independent.

Summary and Conclusions

Viscoelastic analysis has been carried out to study the behaviour of floating ice platform under service and wind loading. The effect of surface temperature and reinforcement of ice on platform behaviour have been studied. The conclusions are:

1. Stresses decrease while deformations increase with time.

2. Short-term stresses and deformations are affected by change in surface temperature, while long-term stresses and deformations are independent of surface temperature.

3. Stresses and deformations are lower for low surface temperatures.

4. Reinforcing the platform reduces its stresses and deformations. The effect of reinforcement on deflection is more significant, especially on long-term values.

5. Variation of ice properties with time should be taken into account in the analysis of ice structures (viscoelastic or viscoplastic analysis).

Acknowledgment

The authors would like to thank Dr. R.T. Dempster, Dean of the Faculty of Engineering and Applied Science, and Dr. A.A. Bruneau, Vice President of Professional Schools and Community Services, Memorial University of Newfoundland, St. John's, Newfoundland, for their continued support and encouragement. The support of the project under National Research Council of Canada Grant No. A 8119 is gratefully acknowledged.

References

Katona, M.G. and Vaudrey, K.D. (1973). Ice Engineering: Summary of elastic properties research and introduction to viscoelastic and non-linear properties of ice. Naval Civil Engineering Laboratory Technical Report R-797, Port Hueneme, California, 71 pp.

Kerr, A.D. (1975). The bearing capacity of floating ice plates subjected to static or quasi-static loads: A critical survey. Research Report 333, CRREL, Hanover, New Hampshire, 43 pp.

Wyman, M. (1950). Deflections of an infinite plate. Canadian Journal of Research, Vol. A 28; pp. 293-302.

Kheisin, D.E. (1964). On the problem of elastic-plastic bending of an ice cover (text in Russian): Trudy, Leningrad. Arkticheskii i Antarkticheskii.

Nevel, D.E. (1972). The ultimate failure of a floating ice sheet. II IAHR/AIRH Ice Symposium, Leningrad, U.S.S.R. 5 pp.

Meyerhof, G.G. (1960). Bearing capacity of floating ice sheets. Proc. ASCE-EMD, 86(5); pp. 113-145.

Panfilov, D.F. (1970). The change of the bearing capacity of an ice cover due to loads of long duration (text in Russian). Izvestia Vuzov, Stroitel stvo i Arkhitektura, No. 3.

Hutter, K. (1973). On the fundamental equations of floating ice. Mitteilungen der Vershuchsanstalt für Wasserbau, Hydrologie and Glaziologie, Nr. 8, Zurich, 150 pp.

Katona, M.G. (1974a). Viscoelastic finite element formulation, Naval Civil Engineering Laboratory, Port Hueneme, California.

Katona, M.G. (1974b). Ice Engineering: Viscoelastic finite element formulation. Technical Report R803, Naval Civil Engineering Laboratory, Port Hueneme, California, 59 pp.

Dykins, J.E. (1962). Construction of sea-ice platforms. 'Ice and Snow: Properties, Processes and Applications'. Proceedings of a Conf. at M.I.T., Cambridge, pp. 289-301.

Dykins, J.E. (1967). Interim aircraft load curves for sea-ice runways at McMurdo, Antarctica. Technical Note N-888, U.S. Naval Engg. Lab., Port Hueneme, California, 37 pp.

Hood, G.L., Strain, H.J., and Baudais, D.J. (1975). Offshore drilling from ice platforms. Proc. 50th annual fall meeting of the Society of Petroleum Engineers of AIME, Dallas, Texas, 12 pp.

Masterson, D.M., Baudais, D.J., and Wasilewski, B.R. (1975). Experience in ice platform construction for Arctic drilling, Annual Western Meeting, The Petroleum Society of C.I.M., Edmonton, Alberta, 26 pp.

Baudais, D.J., Masterson, D.M., and Watts, J.S. (1974). A system for offshore drilling in the Arctic Islands. The Journal of Canadian Petroleum Technology, 12 pp.

Strain, J.J. (1975). Drilling from ice raft in 467 ft. water. Ocean Industry, October, pp. 35-37.

Coble, R.L., and Kingery, W.D. (1962). Ice reinforcement. 'Ice and Snow'. Proc. of a Conf. at M.I.T., Cambridge, pp. 130-148.

Oil Week, (1974). First Islands offshore test a success, April 8, 3 pp.

Zubov, N.N. (1942). Osnovy ustroystva dorog na ledyanom pokrova (The basis of road construction of the ice cover), Moscow, Gidroemeteoizdat.

Kobeko, P.O., et al., (1946). Plasticheskaya deformatsiya i vyazkos' l'da (Plastic deformation and viscosity of ice), Adhurnal Tekhnicheskoy Fiziki, Tom 16(3), pp. 263-272.

Nevel, D.E. (1976). Creep theory for a floating ice sheet, Ph.D. Thesis, Thayer School of Engineering, Dartmouth College, Hanover, New Hampshire, 98 pp.

Katona, M.G., (1974). Ice engineering: Viscoelastic finite element formulation, U.S. Naval Civil Engineering Laboratory Technical Report R 803, Port Hueneme, California, 58 pp.

Katona, M.G., and Vaudrey, K.D. (1973). Ice engineering - summary of elastic properties research and introduction to viscoelastic and non-linear analysis of saline ice, Technical Report R 797, U.S. Naval Civil Engineering Laboratory, Port Hueneme, California, U.S.A., 71 pp.

Vaudrey, K.D., and Katona, M.G. (1975a). An elastic structural analysis of floating ice sheets by the finite element method, Proceedings of III International Conference on Port and Ocean Engineering Under Arctic Conditions, University of Alaska, Fairbanks, Alaska, pp. 439-453.

Vaudrey, K.D., and Katona, M.G. (1975b). Viscoelastic finite element analysis of sea ice sheets, Proceedings of IAHR/AIRH III International Symposium on Ice Problems, Hanover, New Hampshire, U.S.A. pp. 515-525.

Drouin, M., and Michel, B. (1974). Les Poussees d'origine thermique exercees par les couverts de glace sur les structures (Pressures of thermal origin exerted by ice sheets upon hydraulic structures), Laval, Quebec, Canada. Also Draft Translations 427, Cold Regions Research and Engineering Laboratory, Hanover, New Hampshire, U.S.A. 405 pp.

Stanley, R.G., and Glockner, P.G. (1975). Reinforced ice: Its properties and use in constructing temporary enclosures, Proceedings of the Third International Conference on Port and Ocean Engineering Under Arctic Conditions, University of Alaska, Alaska, U.S.A.

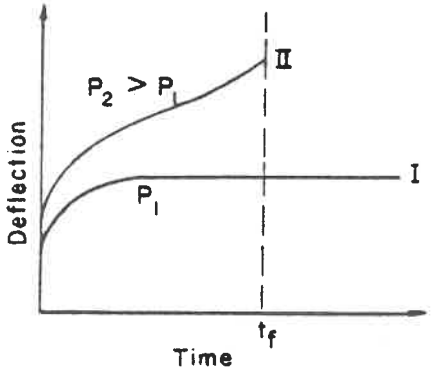

Fig. 1 Two characteristic curves of deflection versus time [Kerr, 1976]

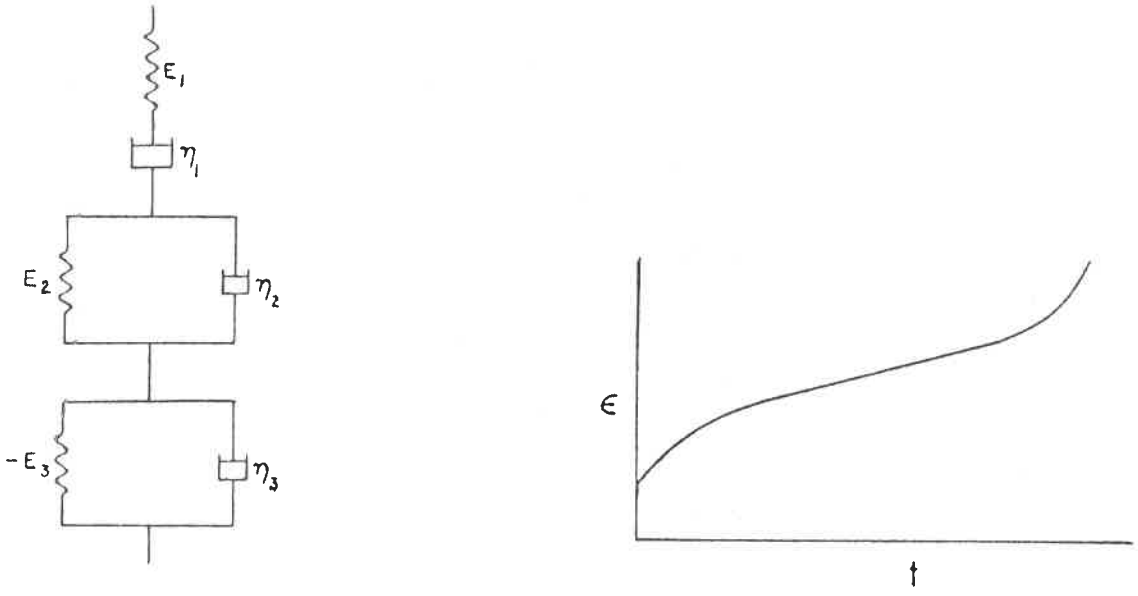

(a) Ice creep model (b) Ice creep curve

Fig. 2
[Nevel, 1976]

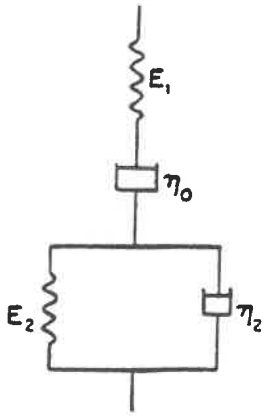

(a) Primary creep model

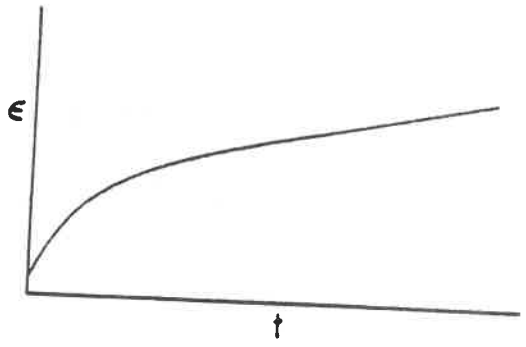

(b) Primary creep curve

Fig. 3
(Nevel, 1976)

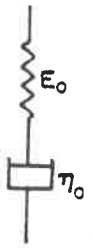

E_0 – Secondary creep elastic constant; $\frac{1}{E_0} = \frac{1}{E_1} + \frac{1}{E_2}$

η_0 – Viscous constant for secondary creep; $\frac{1}{\eta_0} = \frac{1}{\eta_1} + \frac{1}{\eta_2}$

(a) Secondary creep model

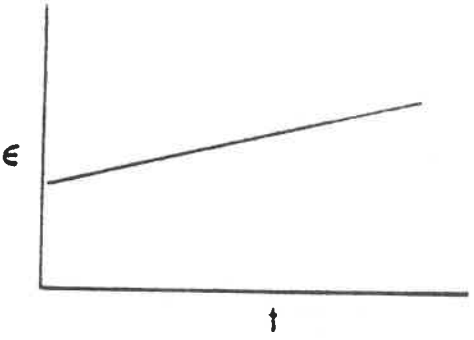

(b) Secondary creep curve

Fig. 4 [Nevel, 1976]

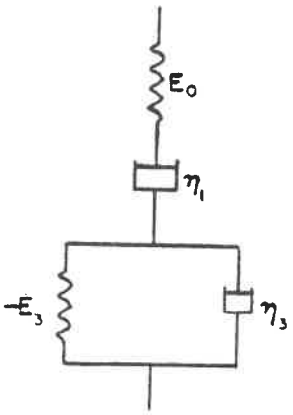

(a) Tertiary creep model

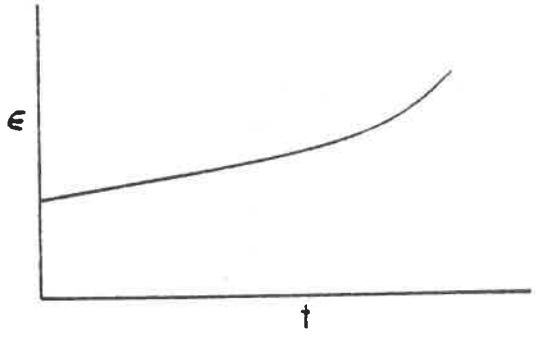

(b) Tertiary creep curve

Fig. 5
[Nevel, 1976]

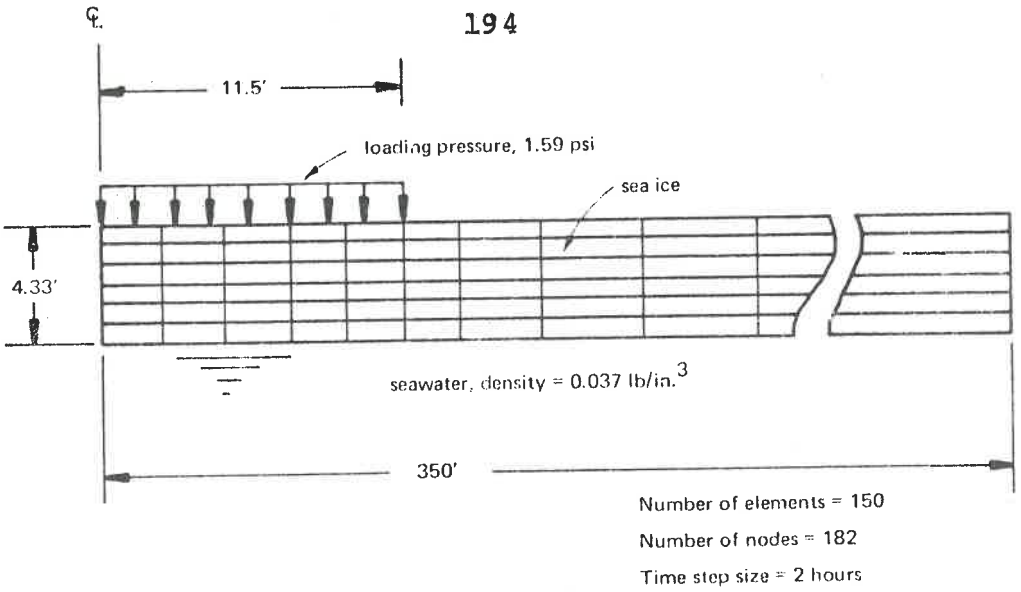

(a) Finite element idealization of ice sheet.

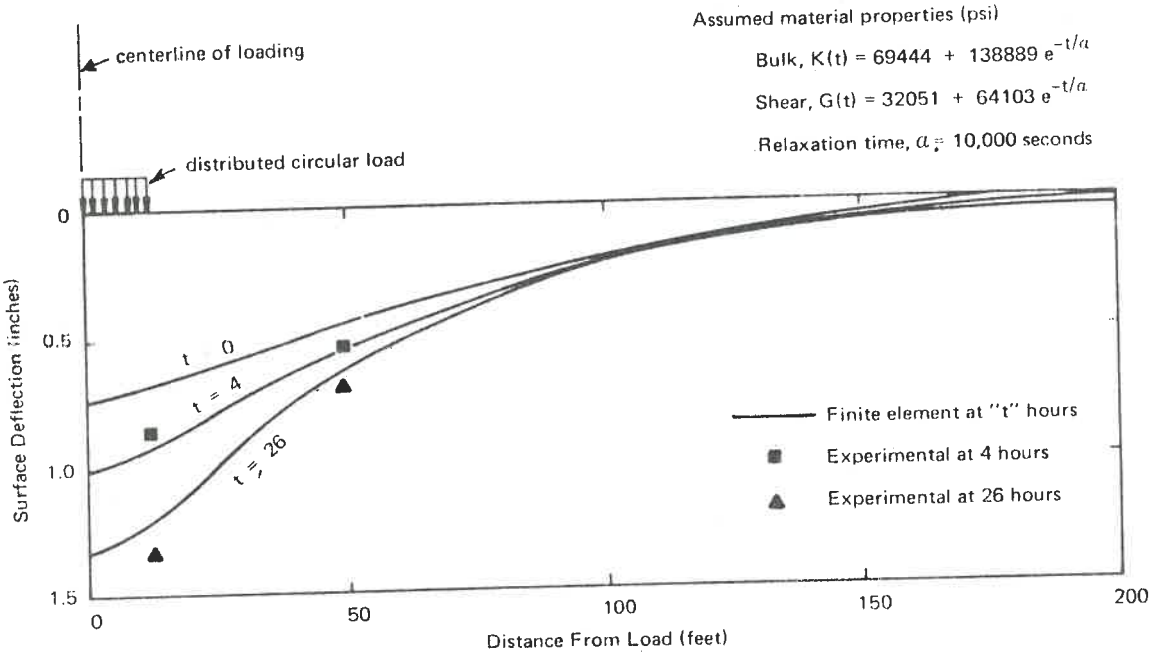

(b) Deflection profile versus time.

Fig. 6 Viscoelastic Analysis (Katona, 1974)

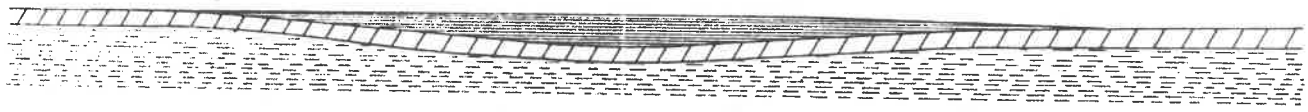

FIG. 7 · CROSS-SECTIONAL AREA OF THE W. HECLA N-52 PLATFORM

[Baudias, 1974]

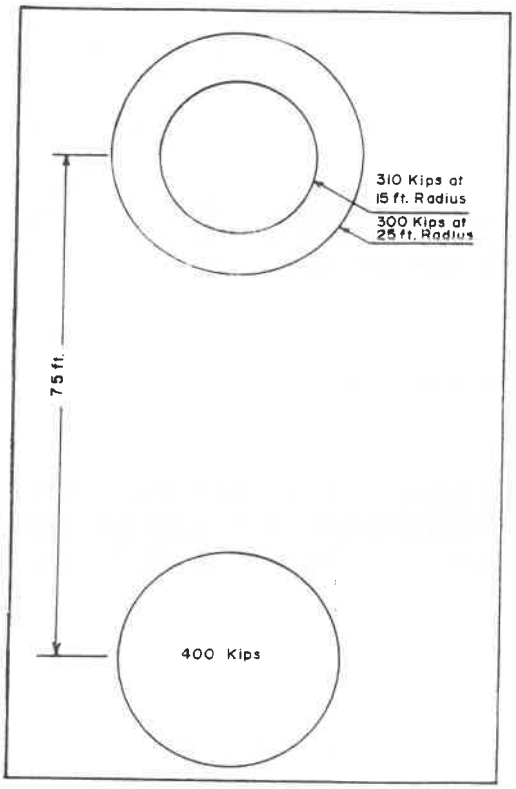

FIG. 8 - Stress analysis - load configuration
[Baudais and others, 1974]

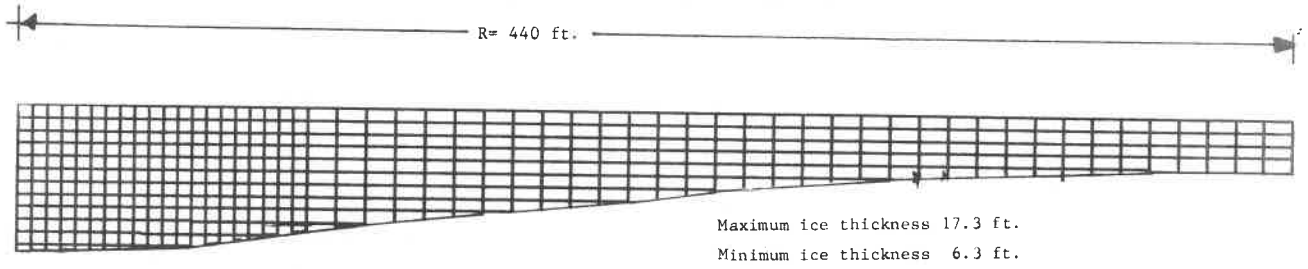

Fig. 9. Finite Element Idealization of the Platform.

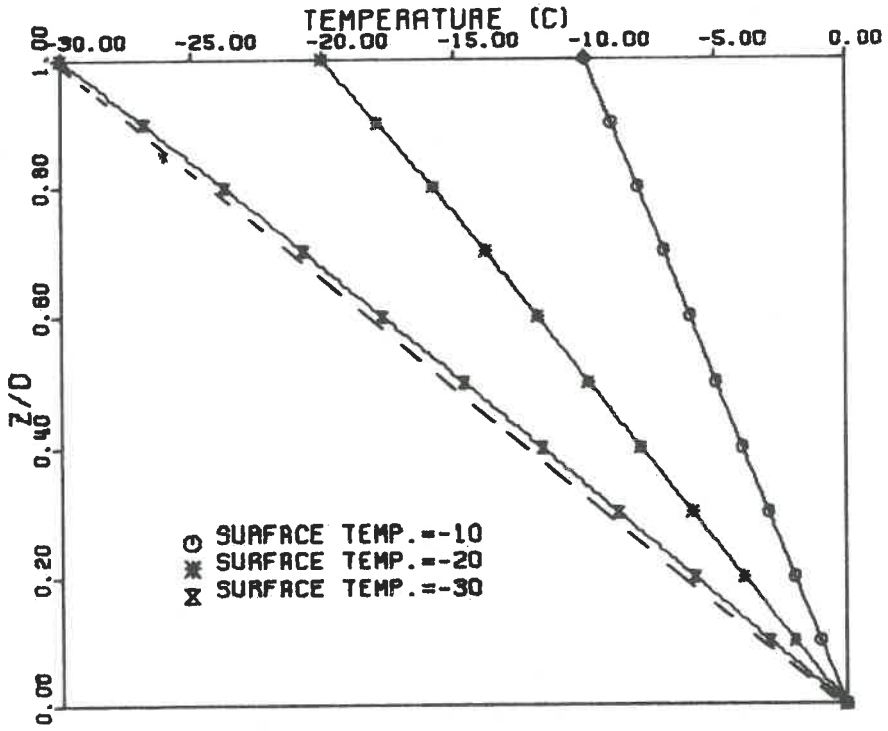

Fig. 10. NONLINEAR TEMPERATURE DISTRIBUTION ACROSS THE PLATFORM THICKNESS FOR THE THREE SURFACE TEMPERATURES USED IN THE ANALYSIS

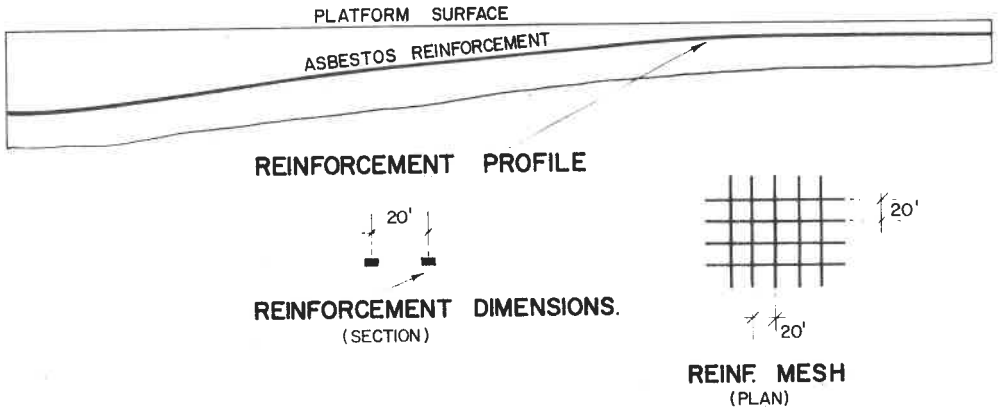

FIG. 11. DETAILING OF REINFORCEMENT

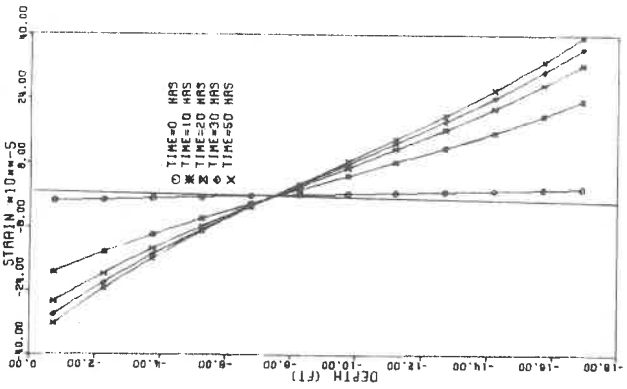

Fig. 13 NORMAL STRAIN DISTRIBUTION AT PLATFORM CENTRE FOR TIME = 0, 10, 20, 30 & 50 HRS - SURFACE TEMP. = -20

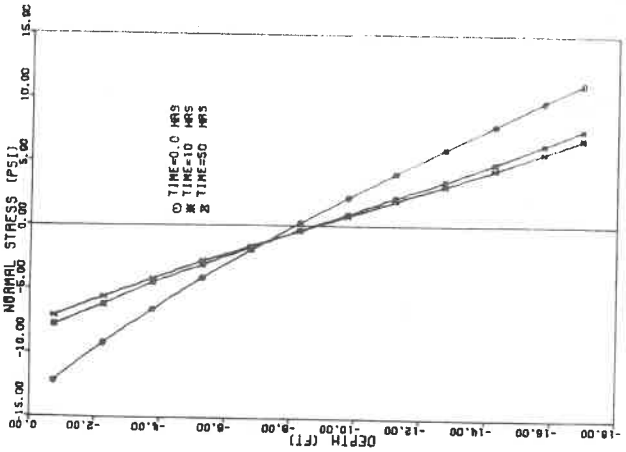

Fig. 12. NORMAL STRESS DISTRIBUTION AT PLATFORM CENTRE FOR TIME = 0, 10 & 50 HOURS - SURFACE TEMP. = -20

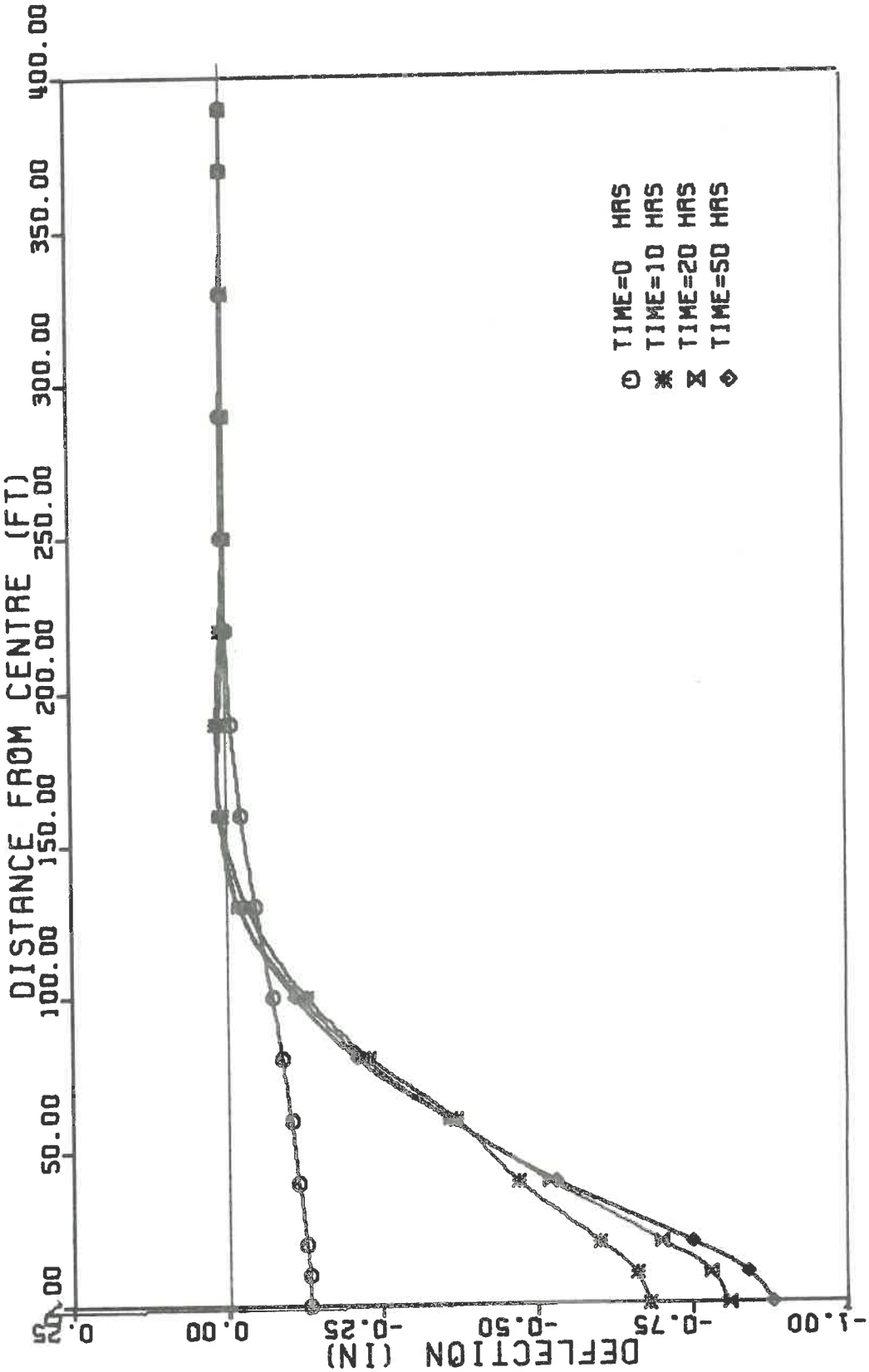

Fig. 14. DEFLECTION PROFILE VERSUS TIME
SURFACE TEMPERATURE = -20

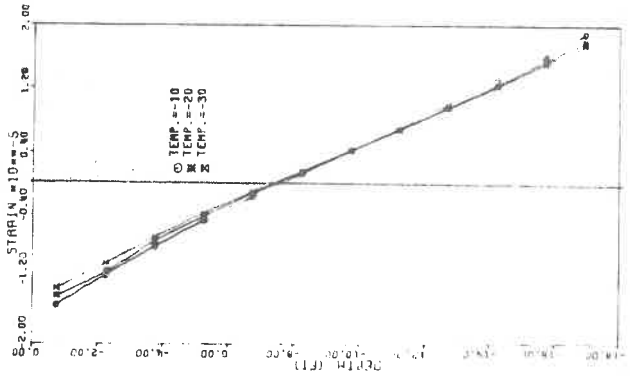

Fig. 16 STRAIN DISTRIBUTION AT PLATFORM CENTRE FOR DIFFERENT VALUES OF SURFACE TEMP. - TIME = 0

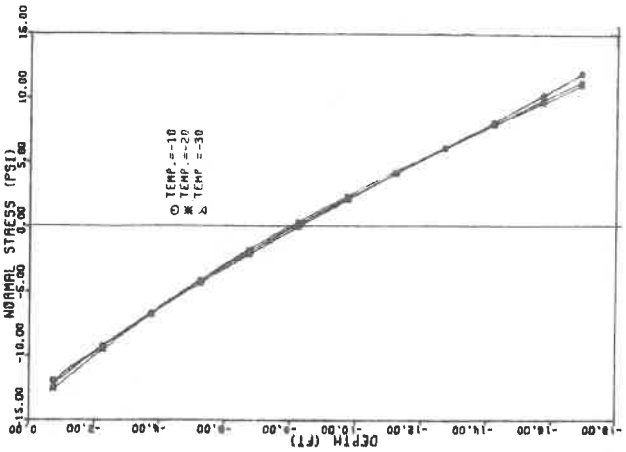

Fig. 15. NORMAL STRESS DISTRIBUTION AT PLATFORM CENTRE FOR DIFFERENT VALUES OF SURFACE TEMP. - TIME = 0

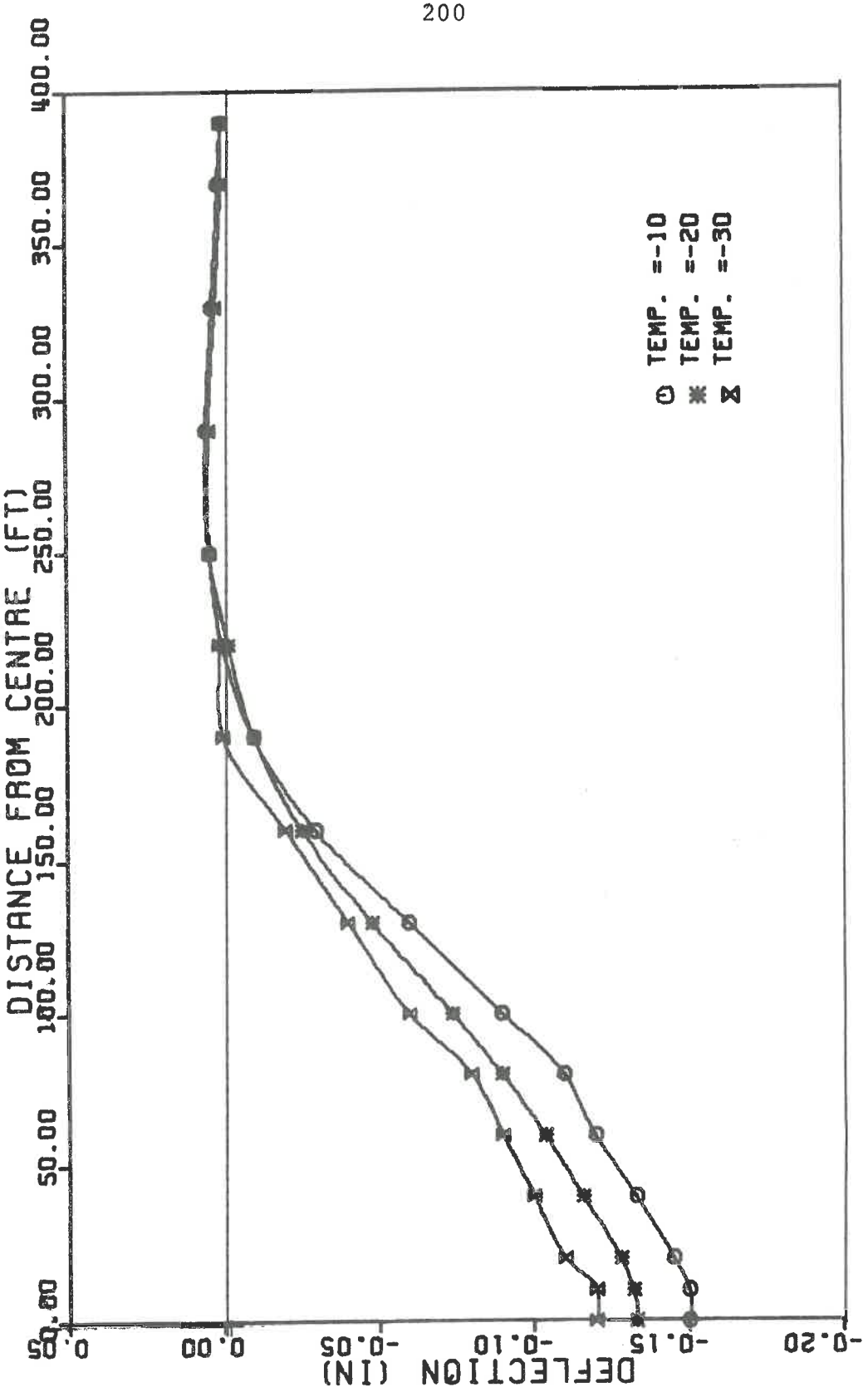

Fig. 17 DEFLECTION PROFILE AT TIME =0 FOR DIFFERENT SURFACE TEMPERATURES

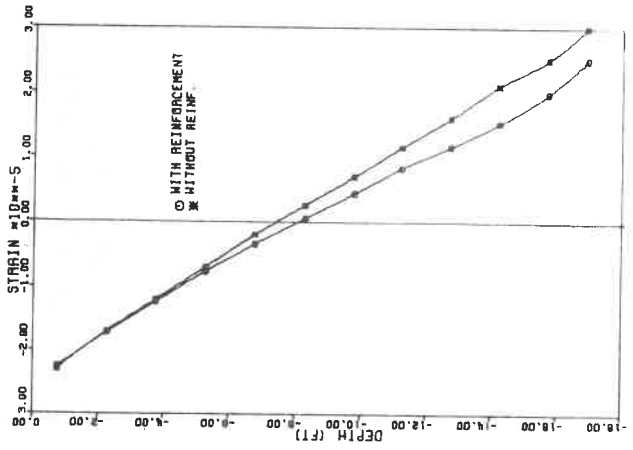

Fig. 19 EFFECT OF REINFORCEMENT ON THE STRAINS AT PLATFORM CENTRE - TIME = 0

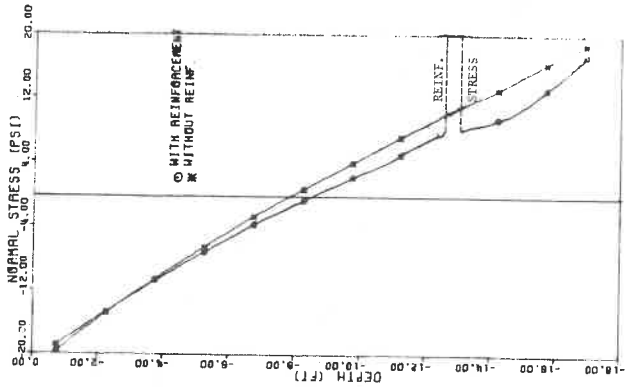

Fig. 18. EFFECT OF REINFORCEMENT ON THE STRESSES AT PLATFORM CENTRE - TIME = 0

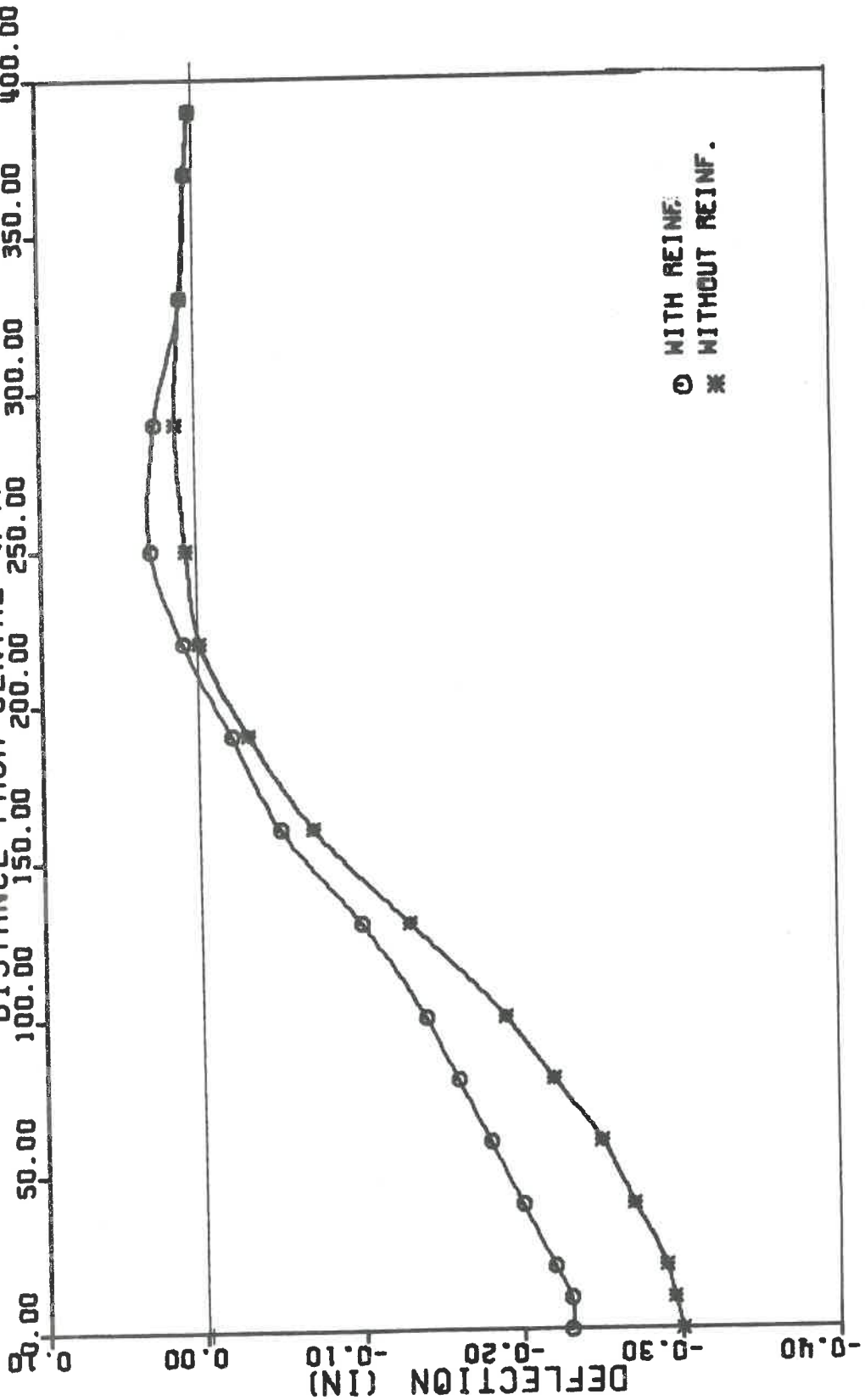

Fig. 20. EFFECT OF REINFORCEMENT ON DEFLECTION PROFILE AT TIME = 0

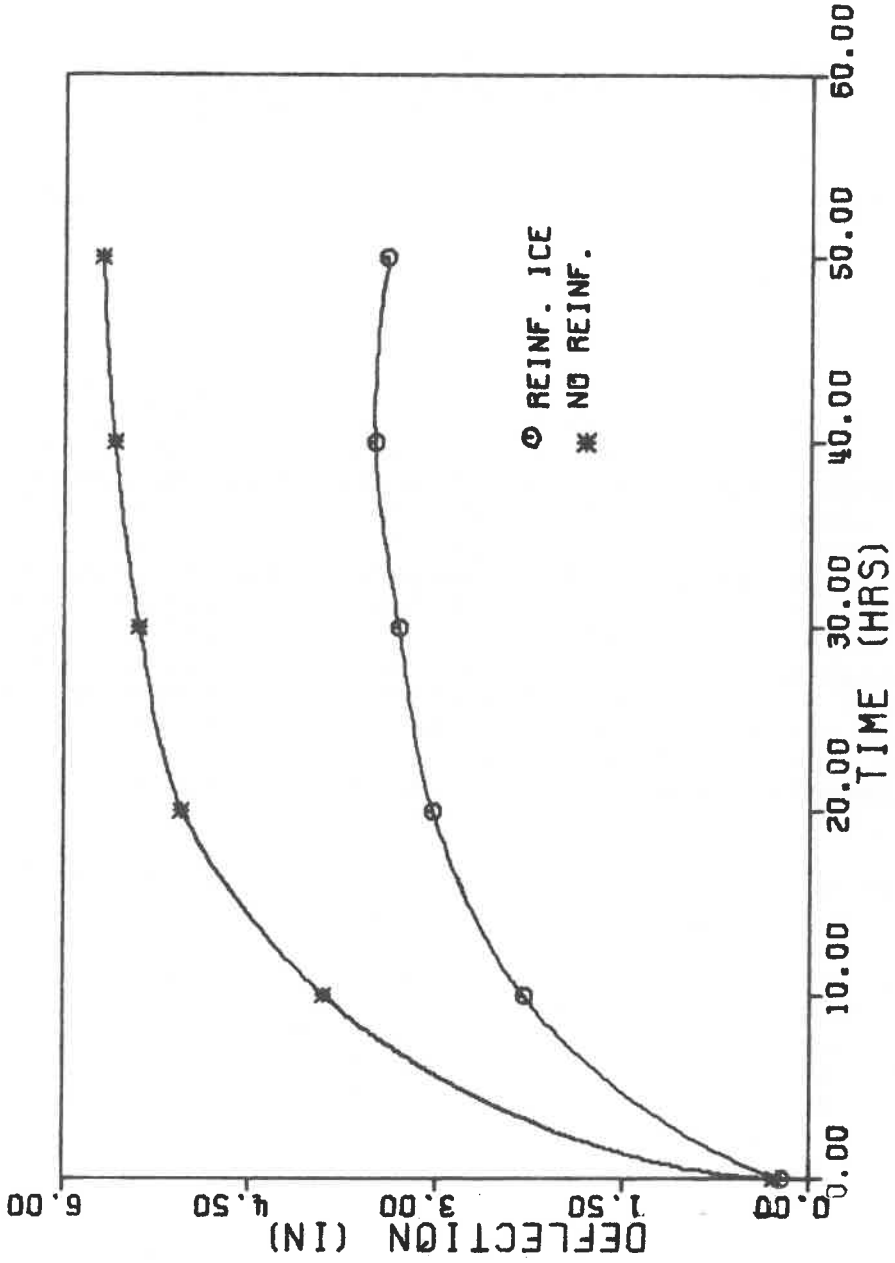

Fig. 21. EFFECT OF REINFORCEMENT ON THE DEFLECTION AT PLATFORM CENTRE -TEMP. = - 20°C

Summary of Panel Discussion on Time-Dependent Bearing Capacity

The Chairman suggested that the discussion should try to concentrate on:

(1) Assessment of the methodology to be used for predicting the long-term response of an ice sheet and examining the reliability of such predictions.

(2) Development of failure or constraining criteria and examination of the deficiencies and uncertainties of the existing criteria.

(3) Guidance for the direction of future research efforts.

The discussion mainly concentrated on examining the failure criteria. Various criteria were discussed and it became apparent that criteria of failure should be determined by the problem at hand. Different criteria are required to suit different problems. A freeboard criterion (i.e., limited deflection) might be good for long-term problems, whereas an instantaneous stress criterion (extreme fibre stress) might be useful for short-time loading conditions. It was emphasized that the long-term criterion is not to exceed the freeboard of the ice sheet. This is a useful practical criteria but it was also pointed out that this could lead to unsafe conditions because the initial stress could be sufficiently high to crack the ice before the freeboard is exceeded. Strain-energy criteria could be useful in many situations.

It was also pointed out during the discussion that the available analyses of bearing capacity problems, so far, did not make any effort to examine the influence of existing large as well as micro-cracks in ice. This limitation was recognized because crack-free ice is practically non-existent in nature. However, the discussions seemed to reveal that our present knowledge on this subject may be too limited to apply immediately, but efforts should be made in future to include the influence of existing cracks while solving bearing capacity problems.

SAFE ICE LOADS COMPUTED WITH A POCKET CALCULATOR

D.E. Nevel
U.S. Army Cold Regions Research and Engineering Laboratory

Introduction

When a load is placed on a floating ice sheet, the ice sheet is bent downward creating stresses within the ice. The downward deflection increases the water pressure on the bottom of the ice which in turn supports the load. If the maximum tensile stress within the ice exceeds the tensile strength of the ice, the ice will crack. Although the ice sheet can still carry more load before breakthrough occurs, the first crack is generally used to predict safe bearing capacity. In some cases, flooding of the ice sheet may create operational difficulties, and a limiting deflection is used rather than first crack.

Previously, the computations for the deflection and stresses of a floating ice sheet have been obtained by computers or programmable desktop calculators. Recently programmable pocket calculators have become powerful enough to perform these computations. Although they are slower, they do provide a means for computation in the field which has been non-existent before.

The purpose of this report is to provide a program to calculate the deflection and stresses for a floating ice sheet on the Hewlett-Packard model 67 pocket calculator. CRREL does not necessarily endorse the HP-67 since there are other programmable pocket calculators that may also perform the same computations.

The user of the program must select appropriate values for the mechanical properties of the ice in order to compute reliable deflection and stresses. Engineering judgment must be used in selecting the allowable ice strength and when dealing with non-ideal situations.

Required Information

A rectangular coordinate system must be defined on the ice sheet for locating the loads relative to each other. For each load, the coordinates of the centre of the load, the magnitude of the load, and the distribution of the load must be known. The load may be assumed to be uniformily distributed over a circular area or a rectangular area whose

dimensions and orientation are known. The load from a pneumatic tire can be assumed to be uniformly distributed over a circular area whose radius can be determined from the air pressure in the tire.

Young's modulus, Poisson's ratio, and the ice thickness must be specified for the ice sheet, as well as the density of supporting water.

The coordinates where the deflection and stresses are to be computed must be specified. For safe bearing capacity prediction, one should choose the coordinates that will give the largest stress within the ice sheet. When the loads are sufficiently far apart, the largest stress will occur directly under the centre of the heaviest load. When two loads of equal magnitude are extremely close together, the largest stress may occur between the loads. A few trial computations may be necessary to find where the stresses are the largest.

Theoretical Approximations and Limitations

The calculator program uses the elastic thin plate theory to represent a floating ice sheet of uniform thickness, and considers a load applied uniformly to a circular or rectangular area. Previously, the rectangular area solution has been expressed by a Fourier series which frequently is slowly convergent. This program uses a new solution expressed by a power series which is more rapidly convergent. In order to further reduce the space and time requirements, the deflection is calculated from four concentrated loads, one at each corner of the rectangular area. This is a good approximation because the deflection does not depend significantly upon the distribution of the load.

Even with these simplifications, the rectangular area solution requires much more time than the circular area solution. Further time-savings can be obtained by noting that the stresses becomes less dependent on the load's distribution as the calculation point moves farther away from the load. Hence, at a sufficiently large distance from the load, an equivalent circular area or concentrated load may be substituted for the rectangular area. For distances greater than five times the flexural rigidity length ℓ, the deflection and stresses are nearly zero for either the circular or rectangular area solution and the calculation may be omitted.

The elastic thin plate theory is adequate except for calculating the stresses in the vicinity of a relatively concentrated load. For this situation, the three-dimensional

theory of elasticity should be used. For this theory solutions exist for both rectangular and circular load distributions, but they are expressed inconveniently for numerical computation. In practice, loads distributed over a circular area (e.g. a pneumatic tire) tend to be more concentrated than loads distributed over a rectangular area (e.g. a crawler track). The program uses a method proposed by Westergaard (1926) when the stresses are evaluated directly under the centre of a circular area. The method replaces the radius a of the load distribution circle with $\sqrt{1.6\ a^2 + h^2} - 0.675\ h$, when the radius a is less than 1.742 times the ice thickness h. Using this new radius in the thin plate theory gives the same stress as the three-dimensional theory of elasticity.

Equations

The most convenient form of the solution for a load uniformly distributed over a circular area has been given by Wyman (1950). The symbols are defined as follows:

- E is Young's modulus of the ice,
- ν is Poisson's ratio of the ice,
- h is the thickness of the ice,
- k is the weight density of the water,
- ℓ is $[Eh^3/12k(1-\nu^2)]^{1/4}$, the flexural rigidity length,
- P is the total load,
- r and θ are polar coordinates from the centre of the load,
- R is r/ℓ, the non-dimensional radial coordinate,
- a is the radius of the load's distribution,
- A is a/ℓ, the non-dimensional load radius,
- w is the deflection of the ice sheet,
- σ_r is the radial stress at the bottom of the ice sheet,
- σ_θ is the tangential stress at the bottom of the ice sheet.

When R > A, the equations are:

$$\frac{(\sigma_r-\sigma_\theta)h^2\ \pi}{2P(1-\nu)\ 3} = \frac{2}{R}\ [-D\ \text{kei}'R + C\ \text{ker}'R] + \frac{(\sigma_r+\sigma_\theta)h^2\ \pi}{2P(1+\nu)\ 3},$$

$$\frac{(\sigma_r+\sigma_\theta)h^2\ \pi}{2P(1+\nu)3} = C\ \text{kei}\ R + D\ \text{ker}\ R,$$

$$\frac{wk\ell^2\ \pi}{P} = -\ D\ \text{kei}\ R + C\ \text{ker}\ R,$$

where $C = \frac{ber'A}{A}$ and $D = \frac{bei'A}{A}$. When A = O, C = O and D = 1/2.

When A > R, the equations are:

$$\frac{(\sigma_r-\sigma_\theta)h^2\ \pi}{2P(1-\nu)3} = \frac{2}{R}\ [-D\ bei'R + C\ ber'R] + \frac{(\sigma_r+\sigma_\theta)h^2\ \pi}{2P(1+\nu)3},$$

$$\frac{(\sigma_r+\sigma_\theta)h^2\ \pi}{2P(1+\nu)3} = C\ bei\ R + D\ ber\ R,$$

$$\frac{w\ k\ \ell^2\ \pi}{P} = -D\ bei\ R + C\ ber\ R + \frac{1}{A^2},$$

where $C = \frac{ker'A}{A}$ and $D = \frac{kei'A}{A}$. When R = O, $\sigma_r-\sigma_\theta$ = O.

The stresses must be determined relative to the x, y coordinate system in order to add to the stresses from other loads. The equations for this are

$$\frac{\sigma_x+\sigma_y}{2} = \frac{\sigma_r+\sigma_\theta}{2}$$

$$\frac{\sigma_x-\sigma_y}{2} = \frac{\sigma_r-\sigma_\theta}{2}\ \cos 2\theta$$

$$\sigma_{xy} = \frac{\sigma_r-\sigma_\theta}{2}\ \sin 2\theta$$

Consider a load uniformly distributed over a rectangular area as shown in Fig. 1. The symbols are defined by:

x and y are coordinates which define the centre of the load,

x_o and y_o are coordinates where the stresses are evaluated,

x_r and y_r are coordinates where the stresses are evaluated in a coordinate system whose origin is at the centre of the load and is parallel to the sides of the rectangle,

θ is the angle of the x_r axis measured from the x axis in a counterclockwise direction,

X is x_r/ℓ and Y is y_r/ℓ, non-dimensional coordinates,

a is one-half the length of the load in the x_r direction,
b is one-half the length of the load in the y_r direction,
A is a/ℓ and B is b/ℓ, non-dimensional length of the load, and
E, ν, h, k, ℓ, P and w are defined as before.

The equations to determine the x_r and y_r coordinates are:

$$x_r = (x_o - x) \cos\theta + (y_o - y) \sin\theta$$

$$y_r = -(x_o - x) \sin\theta + (y_o - y) \cos\theta$$

The equations to determine the stresses at the bottom of the ice sheet relative to the X, Y coordinate system are:

$$\frac{(\sigma_X \pm \sigma_Y)h^2}{2P(1\pm\nu)} = \frac{3}{4\pi AB}\,[I(X+A,Y+B) - I(X+A,Y-B) + I(X-A,Y-B) - I(X-A,Y+B)]$$

$$\pm \frac{3}{4\pi AB}\,[I(Y+B,X+A) - I(Y-B,X+A) + I(Y-B,X-A) - I(Y+B,X-A)]$$

$$\frac{\sigma_{XY}h2}{P(1-\nu)} = \frac{3}{4\pi AB}\,[\text{kei}\sqrt{(X+A)^2+(Y+B)^2} - \text{kei}\sqrt{(X+A)^2+(Y-B)^2} + \text{kei}\sqrt{(X-A)^2+(Y-B)^2} - \text{kei}\sqrt{(X-A)^2+(Y+B)^2}]$$

where

$$I(x,y) = \left(\frac{x}{2}\right)^2\left(\frac{y}{x}\right)\sum_{n=1,3}^{\infty}\frac{(-1)^{\frac{n+1}{2}}(x/2)^{2n}}{n!\,(n+1)!}\left[-\frac{\pi}{4}\right]\sum_{k=0,1}^{n}\frac{n!}{k!\,(n-k)!}\frac{(y/x)^{2k}}{2k+1}$$

$$+ \left(\frac{x}{2}\right)^2\left(\frac{y}{x}\right)\sum_{n=0,2}^{\infty}\frac{(-1)^{n/2}(x/2)^{2n}}{n!\,(n+1)!}\left[-\gamma - \text{Ln}\frac{\sqrt{x^2+y^2}}{2}\right.$$

$$+ \phi(n) + \frac{0.5}{n+1}] \sum_{x=0,1}^{n} \frac{n!(y/x)^{2k}}{k!(n-k)} \frac{1}{2k+1} + (\frac{x}{2})^{2} (\frac{y}{x}) \sum_{n=0,2}^{\infty}$$

$$\frac{(-1)^{n/2}(x/2)^{2n}}{n!\ (n+1)!} \sum_{k=0,1}^{n} \frac{n!(-1)^{k}}{k!(n-k)!} \frac{1}{2k+1} [- \frac{\arctan(y/x)}{(y/x)}$$

$$+ \sum_{r=0,1}^{k} \frac{(-1)^{r}(y/x)^{2r}}{2r+1}]$$

where γ is Euler's number and $\phi(n) = 1/1 \cdot 1/2 \cdot 1/3 \cdots 1/n$. The equations to determine the stresses relative to the x, y coordinate system are:

$$\frac{\sigma_x+\sigma_y}{2} = \frac{\sigma_X+\sigma_Y}{2}$$

$$\frac{\sigma_x-\sigma_y}{2} = (\frac{\sigma_X-\sigma_Y}{2}) \cos 2\theta - \sigma_{XY} \sin 2\theta$$

$$\sigma_{xy} = (\frac{\sigma_X-\sigma_Y}{2}) \sin 2\theta + \sigma_{XY} \cos 2\theta$$

General Procedure

Turn on the calculator and set the other switch to run. The program to compute the deflection and the stresses for a load uniformly distributed over a circular area is divided into two parts which are labelled 1 and 2. The program to compute the deflection and stresses for a load uniformly distributed over a rectangular area is divided into two parts which are labelled 3 and 4. Actual program listings appear in an appendix to this paper. The results of either program 2 or 4 are:

REG 0	Identification #
REG 6	Deflection w (inches)
REG 7	Stress sum $(\sigma_x+\sigma_y)/2$ (psi)
REG 8	Stress difference $(\sigma_x-\sigma_y)/2$ (psi)
REG 9	Shearing stress σ_{xy} (psi)

Program 5 adds the deflection and stresses from either program 2 or 4 to the respective sums which are in registers 1 through 4. From these new sums it determines and stores the maximum stress in register A and the angle from the x axis of the crack in register B. Between computation of each load, the sums are saved on a magnetic card referred to as the sum card. Side 2 of the program 5 magnetic card is not used, and can be used for the sum card.

Input Data

1. For a load uniformly distributed over a rectangular area (Fig. 1), the following data should be keyed into memory. Neither the length a or b of the rectangle may be equal to zero.

Register	Data (Units)	Definition
0	ID#	a load identification number
1	x (inches)	coordinate of the load's centre
2	y (inches)	coordinate of the load's centre
3	P (pounds)	magnitude of the load
4	a (inches)	rectangle half-length along x_r
5	b (inches)	rectangle half-length along y_r
6	θ (degrees)	the angle of x_r from x
7	E (psi)	Young's modulus of ice
8	ν	Poisson's ratio of ice
9	h (inches)	thickness of ice
A	k (lb/in^3)	weight density of water
B	x_o (inches)	coordinate of computations
C	y_o (inches)	coordinate of computations

2. For a load uniformly distributed over a circular area, the input is the same except for the distribution of the load in registers 4, 5 and 6. Registers 5 and 6 are not used, while register 4 contains the radius a (inches) of the circular area. This radius may be equal to zero.

3. To store data into a register, key the data into the display register, press STO followed by the register symbol. For example to store 1 for the ID#, press 1, STO, 0. To display data from a register in order to check the input, press RCL followed by the register symbol.

4. The operator may find it time-consuming to repeatedly key in all the data for each load. For each load the ice and water data as well as the place of computation do not change. The operator may find it convenient to record the input data for the first load on a magnetic card. Then for succeeding loads, this card may be read into memory and only data which are different need be keyed into memory.

When the computation is to be repeated for a different ice thickness or other parameter change, the operator may find it convenient to record the input for each load on a magnetic card. Then, for succeeding computations, each card can be read into memory, and only the appropriate parameter need be keyed.

If the input data is to be recorded on a magnetic card, the secondary registers should be clear since this allows memory to be recorded on one side of a magnetic card rather than on two sides. Consult the HP manual for ways to clear these registers.

To record the memory registers on a magnetic card, press f, W/DATA and insert the card. To read the registers from a magnetic card into memory, just insert the card.

5. The units of the input data are pounds, inches and degrees. A different force and length unit may be used for input which will give the deflection and stress expressed in these same units.

Programs 1 and 2

Program 1 is for a load uniformly distributed over a circular area. Program 2 is a continuation of program 1 and assumes that the results of program 1 are still in memory. The operating instructions are:

1. Read program 1 by inserting side 1 of the 1 magnetic card (side 2 is not used).

2. Store input data in memory.

3. Press A to start the program. After about 5 seconds, the calculator stops and displays 2, the next required program.

4. Read program 2 by inserting side 1 of the 2 magnetic card followed by side 2.

5. Press A to start the program. After about 30 seconds, the program stops and displays 5, the next required program.

6. Proceed to program 5.

Programs 3 and 4

Program 3 is for a load uniformly distributed over a rectangular area. Program 4 is a continuation of program 3 and assumes that the results of program 3 are still in memory. The operating instructions are:

1. Read program 3 by inserting side 1 of the 3 magnetic card followed by side 2.

2. Store input data in memory.

3. Press A to start the program. After about 60 seconds, the calculator stops and displays 4, the next required program.

4. Read program 4 by inserting side 1 of the 4 magnetic card followed by side 2.

5. Press A to start the program. After about 300 seconds, the calculator stops and displays 5, the next required program.

6. Proceed to program 5.

Program 5

Program 5 is a continuation of program 2 or 4. Program 5 assumes that the results of program 2 or 4 are still in memory. The operating instructions are:

1. Read program 5 into memory by inserting side 1 of the 5 magnetic card. Side 2 is not used by program 5.

2. For a succeeding load (any load except the beginning load of a computation), press A to start the program. The program pauses for about one second and displays the ID#. During this pause, insert the sum card, and the sums will be read. If the sum card is not inserted during the pause, the program will repeat until it is inserted.

   For the BEGINNING load of a computation ONLY, press B to start the program. This zeros the sum and eliminates the reading of the sum card.

3. When the program stops, CRD is displayed. Insert the sum card, and memory will be recorded.

4. The angle of the crack is stored in register B and the maximum stress is stored in register A as well as being displayed. If this was not the last load of a computation, process any additional load by either program 1 or 3.

Subroutines

The subroutines Kelvin (z) and I (x,y) may be of use in other programs. The following is a brief description of these subroutines that will allow their use for this purpose.

The Kelvin (z) subroutine is stored in steps 102 through 213 of program 2. This subroutine uses registers A, B, I, and 0 through 9. The subroutine also uses Euler's number $\gamma = 0.5772156649$ which is assumed to be in register E. Therefore, be sure that register E contains γ. To execute the subroutine, place the argument z in the x register and press E. The subroutine will compute ker (z), ber (z), ker' (z), ber' (z), kei (z), bei (z), kei' (z), bei' (z) in registers 1 through 8 respectively. The argument z will be in register A. The method of computation is by a series from Nevel (1959). The series is truncated when the last term becomes less than 10^{-6}. The exponent 6 is stored in step 159 and may be changed to obtain other accuracies.

The subroutine I (x,y) is stored in steps 61 through 220 of program 4. This subroutine uses registers A, B, I, and 10 through 19. The subroutine also uses Euler's number $\gamma = 0.5772156649$ which is assumed to be in register E. Therefore, be sure register E contains γ. To execute the subroutine, place the argument y in register y, the argument x in register x, and press E. The subroutine will give I (x,y) in register x. The series is truncated when the last term becomes less than 10^{-6}. The exponent 6 is stored in step 135 and may be changed to obtain other accuracies.

Examples

The following numerical examples are provided for the purpose of checking and debugging the programs. For the Kelvin (z) subroutine with the accuracy set at 10^{-6}, the results for z=1 are:

REG 1	2.867062088 -01	REG 5	-4.949946366 -01
REG 2	9.843817812 -01	REG 6	2.495660400 -01
REG 3	-6.946038910 -01	REG 7	3.523699135 -01
REG 4	-6.244575218 -02	REG 8	4.973965115 -01

For programs 1 and 2 there are various options which should be checked. For R>A, A may or may not be zero. For A>R, R may or may not be zero. For A>R and R=0, Westergaard's substitution may or may not be made. The following examples cover all cases.

The input data for program 1 are:

REG	R>A=0	A>R=0	Westergaard A>R=0
1	100	100	0
2	100	100	0
3	10000	10000	10000
4	0	20	5
7	10^6	10^6	10^6
8	1/3	1/3	1/3
9	10	10	10
A	62.4/1728	62.4/1728	62.4/1728
B	170	100	0
C	170	100	0

The output data from program 2 are:

REG	R>A=0	A>R=0	Westergaard A>R=0
6	5.982837411 -01	6.761493320 -01	6.790823603 -01
7	6.216841289 +01	1.935510530 +02	2.807218953 +02
8	0	0	0
9	-1.534340994 +01	0	0

The next two options can also be used to check program 5. The input data are:

REG	R>A≠0	A>R≠0	REG	R>R≠0	A>R≠0
0	1	2	8	1/3	1/3
1	0	63	9	10	10
2	0	63	A	62.4/1728	62.4/1728
3	10000	10000	B	70	70
4	20	20	C	70	70
7	10^6	10^6			

The output data from program 2 are:

REG	R>A≠0	A>R≠0
6	5.974546370 -01	6.748975099 -01
7	6.221160230 +01	1.857763777 +02
8	0	0
9	-1.501987756 +01	-1.943671630 +00

The results of program 5 are:

REG		
1	1.272352147 +00	ΣW
2	2.479879800 +02	$\Sigma(\sigma_x+\sigma_y)/2$
3	0	$\Sigma(\sigma_x-\sigma_y)/2$
4	-1.696354919 +01	$\Sigma\sigma_{xy}$
A	2.649515292 +02	maximum stress
B	4.500000000 +01	crack angle (degrees)

For the I (x,y) subroutine with the accuracy set at 10^{-6}, the result is I (1,.5) = 8.407935381 -02.

The example to check program 3 and 4 is:

REG	Input	Output	REG	Input	Output
1	0		7	10^6	6.566463388 +01
2	0		8	1/3	7.014794041 +00
3	10000		9	10	-1.337575308 +01
4	30		A	62.4/1728	
5	5		B	50	
6	30	6.566463388 -01	C	80	

Conclusion

The time has arrived when calculations for the bearing capacity of floating ice sheets can be made in the field by means of pocket calculators. The present limitations are the slow speed and small memory size. Therefore computors and desk-top calculators are still preferable for computations in the office. However, as the speed and memory size of the pocket calculator increases their use will increase in future years for these computations.

References

Nevel, Donald E. (1959). Tables of Kelvin functions and their derivatives, U.S. Army Snow Ice Permafrost Research Establishment (SIPRE), now Cold Regions Research Engineering Laboratory (CRREL), Technical Report 67.

Westergaard, H.M. (1926). Stresses in concrete pavements computed by theoretical analysis, Public Roads Vol.7, No. 2 pp. 25-35

Wyman, Max (1950). Deflections of an infinite plate, Canadian Journal of Research, A. 28, pp. 293-302.

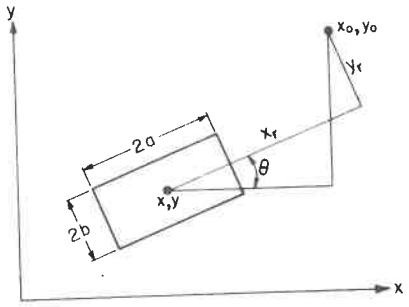

Fig. 1 Rectangular load distribution.

PROGRAM 1

1	LBL A
2	RCL 7
3	RCL 9
4	STO X 9
5	RCL 9
6	X
7	X
8	RCL A
9	1/X
10	STO 6
11	X
12	1
13	RCL 8
14	X^2
15	-
16	÷
17	1
18	2
19	÷
20	$\sqrt{\ }$
21	STO ÷ 6
22	$\sqrt{\ }$
23	STI
24	RCL C
25	RCL 2
26	-
27	RCL B
28	RCL 1
29	-
30	→ P
31	RCI
32	÷
33	STO 1
34	R ↓
35	2
36	X
37	STO 2
38	RCL 3
39	π
40	÷
41	STO X 6
42	RCL 9
43	÷
44	3
45	X
46	STO 7
47	STO X 8
48	RCL 8
49	STO + 7
50	-
51	STO 8
52	RCL 1
53	X ≠ 0
54	GTO 1
55	1
56	•
57	7
58	4
59	RCL 4
60	X^2
61	1
62	•
63	6
64	X
65	RCL 9
66	÷
67	1
68	+
69	$\sqrt{\ }$
70	•
71	6
72	7
73	5
74	-
75	X > Y
76	GTO 1
77	RCL 9
78	$\sqrt{\ }$
79	X
80	STO 4
81	LBL 1
82	RCL 4
83	RCI
84	÷
85	STO 4
86	•
87	5
88	7
89	7
90	2
91	1
92	5
93	6
94	6
95	4
96	9
97	STO E
98	2
99	RTN

PROGRAM 5

1	LBL A
2	4
3	STI
4	CF 3
5	RCL 0
6	MERGE
7	PAUSE
8	F? 3
9	GTO 1
10	GTO A
11	LBL 1
12	STO 0
13	RCL 6
14	STO + 1
15	RCL 7
16	STO + 2
17	RCL 8
18	STO + 3
19	RCL 9
20	STO + 4
21	P ≠ S
22	CL REG
23	P ≠ S
24	3
25	6
26	0
27	RCL 4
28	RCL 3
29	→ P
30	RCL 2
31	+
32	STO A
33	R ↓
34	X < 0
35	+
36	2
37	÷
38	9
39	0
40	-
41	STO B
42	RCL A
43	W/DATA
44	RTN
45	LBL B
46	CLX
47	STO 1
48	STO 2
49	STO 3
50	STO 4
51	STO 5
52	RCL 0
53	GTO 1

PROGRAM 2

```
 1  LBL A
 2  RCL 1
 3  RCL 4
 4  CF 0
 5  X ≤ Y
 6  SF 0
 7  X = 0
 8  GTO 9
 9  P ≷ S
10  GSB E
11  RCL 3
12  F? 0
13  RCL 4
14  RCL A
15  ÷
16  STO C
17  RCL 7
18  F? 0
19  RCL 8
20  RCL A
21  ÷
22  STO D
23  P ≷ S
24  LBL 7
25  RCL 1
26  P ≷ S
27  GSB E
28  8
29  F? 0
30  7
31  STI
32  RCL (i)
33  RCL D
34  X
35  STO 9
36  DSZ
37  DSZ
38  RCL (i)
39  RCL C
40  X
41  STO B
42  RCL (i)
43  RCL D
44  X
45  STO 0
46  DSZ
47  DSZ
48  RCL (i)
49  RCL C
50  X
51  RCL 9
52  -
53  2
54  X
55  DSZ
56  DSZ
57  RCL (i)
58  RCL D
59  X
60  RCL B
61  +
62  STO B
63  RCL A
64  X
65  +
66  RCL A
67  X ≠ 0
68  ÷
69  STO A
70  RCL (i)
71  RCL C
72  X
73  RCL 0
74  -
75  P ≷ S
76  F? 0
77  GTO 8
78  RCL 4
79  X²
80  1/X
81  +
82  LBL 8
83  STO X 6
84  RCL 2
85  RCL A
86  RCL 8
87  X
88  R ←
89  STO 8
90  R ↓
91  STO 9
92  RCL B
93  STO X 7
94  5
95  RTN
96  LBL 9
97  STO C
98  .
99  5
100  STO D
101  GTO 7
102  LBL E
103  2
104  ÷
105  STO A
106  CLX
107  STO 0
108  STO 1
109  STO 3
110  STO 4
111  STO 5
112  STO 6
113  STO 7
114  STO 8
115  STO 9
116  1
117  STO B
118  STO 2
119  RCL A
120  X ≠ 0
121  GTO 2
122  π
123  4
124  ÷
125  STO - 5
126  RTN
127  LBL 2
128  8
129  STI
130  GSB 3
131  GSB 4
132  RCL B
133  CHS
134  STO B
135  GSB 3
136  GTO 4
137  LBL 3
138  1
139  STO + 0
140  RCL 0
141  ÷
142  STO + 9
143  LBL 4
144  RCL A
145  RCL 0
146  ÷
147  RCL B
148  X
149  STO B
150  STO + (i)
151  DSZ
152  RCL 9
153  X
154  STO + (i)
155  DSZ
156  RTN
157  ABS
158  EEX
159  6
160  CHS
161  X ≤ Y
162  GTO 2
163  RCL A
164  LN
165  RCL E
166  +
167  STO B
168  RCL 8
169  X
170  STO - 7
171  RCL B
172  RCL 6
173  X
174  STO - 5
175  RCL B
176  RCL 4
177  X
178  STO - 3
179  RCL B
180  RCL 2
181  X
182  STO - 1
183  π
184  4
185  ÷
186  STO B
187  RCL 4
188  X
189  STO - 7
190  RCL B
191  RCL 2
192  X
193  STO - 5
194  RCL B
195  RCL 8
196  X
197  STO + 3
198  RCL B
199  RCL 6
200  X
201  STO + 1
202  RCL 6
203  RCL A
204  2
205  X
206  STO A
207  ÷
208  STO - 7
209  RCL 2
210  RCL A
211  ÷
212  STO -3
213  RTN
```

PROGRAM 3

```
 1  LBL A
 2  RCL 7
 3  RCL 9
 4  STO X 9
 5  RCL 9
 6  X
 7  X
 8  RCL A
 9  STO 7
10  ÷
11  1
12  RCL 8
13  X²
14  -
15  ÷
16  1
17  2
18  ÷
19  √‾‾
20  STO X 7
21  √‾
22  STI
23  RCL B
24  STO - 1
25  RCL C
26  STO - 2
27  RCL 6
28  RCL 2
29  RCL 6
30  RCL 1
31  R ↓
32  CHS
33  STO 1
34  R ↓
35  STO 2
36  R ↓
37  R ↓
38  STO -2
39  R ↓
40  STO -1
41  RCL 6
42  2
43  X
44  STO C
45  RCI
46  STO ÷ 1
47  STO ÷ 2
48  STO ÷ 4
49  STO ÷ 5
50  RCL 3
51  π
52  ÷
53  STO ÷ 7
54  RCL 4
55  RCL 5
56  X
57  RCL 9
58  X
59  ÷
60  •
61  7
62  5
63  X
64  STO 3
65  STO X 8
66  RCL 8
67  STO + 3
68  -
69  STO D
70  •
71  5
72  7
73  7
74  2
75  1
76  5
77  6
78  6
79  4
80  9
81  STO E
82  CLX
83  STO 6
84  RCL 1
85  RCL 4
86  STO + 1
87  -
88  STO 4
89  RCL 2
90  RCL 5
91  STO + 2
92  -
93  STO 5
94  RCL 4
95  GSB E
96  STO 9
97  RCL 2
98  RCL 4
99  GSB E
100 STO - 9
101 RCL 5
102 RCL 1
103 GSB E
104 STO - 9
105 RCL 2
106 RCL 1
107 GSB E
108 STO + 9
109 RCL D
110 STO X 9
111 RCL 7
112 8
113 X
114 STO ÷ 6
115 4
116 RTN
117 LBL E
118 → P
119 P ⇄ S
120 2
121 ÷
122 STO A
123 CLX
124 STO 0
125 STO 1
126 STO 3
127 STO 4
128 STO 5
129 STO 6
130 STO 7
131 STO 8
132 STO 9
133 1
134 STO B
135 STO 2
136 RCL A
137 X ≠ 0
138 GTO 2
139 π
140 4
141 ÷
142 CHS
143 GTO 5
144 LBL 2
145 8
146 STI
147 GSB 3
148 GSB 4
149 RCL B
150 CHS
151 STO B
152 GSB 3
153 GTO 4
154 LBL 3
155 1
156 STO + 0
157 RCL 0
158 ÷
159 STO + 9
160 LBL 4
161 RCL A
162 RCL 0
163 ÷
164 RCL B
165 X
166 STO B
167 STO + (i)
168 DSZ
169 RCL 9
170 X
171 STO + (i)
172 DSZ
173 RTN
174 ABS
175 EEX
176 6
177 CHS
178 X ≷ Y
179 GTO 2
180 RCL A
181 LN
182 RCL E
183 +
184 RCL 6
185 X
186 STO - 5
187 π
188 4
189 ÷
190 RCL 2
191 X
192 STO - 5
193 RCL 5
194 LBL 5
195 P ⇄ S
196 STO - 6
197 RTN
```

```
1   LBL A
2   RCL 5
3   RCL 4
4   GSB E
5   STO 7
6   STO 8
7   RCL 2
8   RCL 4
9   GSB E
10  STO - 7
11  STO - 8
12  RCL 4
13  RCL 5
14  GSB E
15  STO + 7
16  STO - 8
17  RCL 4
18  RCL 2
19  GSB E
20  STO - 7
21  STO + 8
22  RCL 2
23  RCL 1
24  GSB E
25  STO + 7
26  STO + 8
27  RCL 5
28  RCL 1
29  GSB E
30  STO - 7
31  STO - 8
32  RCL 1
33  RCL 5
34  GSB E
35  STO - 7
36  STO + 8
37  RCL 1
38  RCL 2
39  GSB E
40  STO + 7
41  STO - 8
42  RCL 3
43  STO X 7
44  RCL D
45  STO X 8
46  RCL C
47  RCL 9
48  RCL C
49  RCL 8
50  R ←
51  STO 8
52  R ↓
53  STO 9
54  R ↓
55  R ←
56  STO + 9
57  R ↓
58  STO - 8
59  5
60  RTN
61  LBL E
62  X = 0
63  RTN
64  ÷
65  X = 0
66  RTN
67  P ⇄ S
68  STO B
69  LST X
70  2
71  ÷
72  X^2
73  STO A
74  X
75  STO 2
76  1
77  RCL B
78  TAN^-1
79  → R
80  RCL B
81  ÷
82  -
83  STO 3
84  RCL B
85  X^2
86  STO B
87  1
88  +
89  RCL A
90  X
91  √
92  LN
93  RCL E
94  +
95  STO 9
96  -
97  •
98  5
99  +
100 X
101 STO 1
102 CLX
103 STO 0
104 GTO 1
105 LBL 2
106 GSB 3
107 •
108 5
109 RCL 0
110 1
111 +
112 ÷
113 RCL 9
114 -
115 X
116 STO + 1
117 SF 0
118 GSB 4
119 STO + 1
120 LBL 1
121 RCL 2
122 CHS
123 STO 2
124 CF 0
125 GSB 3
126 π
127 X
128 4
129 ÷
130 STO - 1
131 RCL 1
132 ÷
133 ABS
134 EEX
135 6
136 CHS
137 X ≤ Y
138 GTO 2
139 RCL 1
140 P ⇄ S
141 RTN
142 LBL 3
143 RCL A
144 1
145 STO + 0
146 RCL 0
147 +
148 ÷
149 RCL 0
150 1/X
151 STO - 9
152 X
153 STO x 2
154 LBL 4
155 CLX
156 STI
157 1
158 STO 5
159 F? 0
160 RCL 3
161 STO 4
162 LBL 5
163 RCL 0
164 RCI
165 -
166 ISZ
167 RCI
168 ÷
169 F? 0
170 GTO 7
171 RCL B
172 X
173 STO X 5
174 RCL 5
175 LBL 6
176 RCI
177 2
178 X
179 1
180 +
181 ÷
182 STO + 4
183 RCI
184 RCL 0
185 X > Y
186 GTO 5
187 RCL 4
188 RCL 2
189 X
190 RTN
191 LBL 7
192 CHS
193 STO X 5
194 CLX
195 STO 6
196 RCL 3
197 STO 7
198 1
199 STO 8
200 LBL 8
201 RCL B
202 CHS
203 STO X 8
204 RCL 8
205 1
206 STO + 6
207 RCL 6
208 2
209 x
210 +
211 ÷
212 STO + 7
213 RCL 6
214 RCI
215 X > Y
216 GTO 8
217 RCL 7
218 RCL 5
219 X
220 GTO 6
```

Discussion

T. Ersoy:

What is the length of the program, i.e., how many steps?

D.E. Nevel:

This will depend on the shape of the load (i.e., circular or rectangular). It may use up to 400 steps.

R. Frederking:

Do you assume a uniform pressure footprint or a rigid load?

D. Nevel:

The program assumes a uniform pressure distributed over a circular or a rectangular area.

USE OF ICE COVER AS AN AIRSTRIP IN THE THELON RIVER VALLEY BY THE CANADIAN ARMED FORCES

Lt. D.M. McCutcheon
1 Construction Engineering Unit
Canadian Armed Forces

Introduction

The Canadian Armed Forces have used airstrips built on both freshwater and sea ice in the past but not to such an extent that a large number of their pilots or engineers are familiar with their use. Although there are many conceivable instances where the construction and operation of an airstrip on an ice surface would be necessary for the Canadian Forces to carry out some of their roles, it has rarely been done unless an operational requirement arises. One such requirement occurred when a Russian satellite crashed, leaving potentially dangerous debris scattered across the Northwest Territories and the Canadian Forces had to conduct a search and cleanup program in this area.

On January 24, 1978, the Russian satellite COSMOS 954 re-entered the atmosphere after falling out of orbit. Much of the satellite disintegrated but parts of it fell across the Canadian North in a line running between Great Slave Lake and Frobisher Bay. Because the satellite had been powered by a small nuclear reactor containing about 45 kg of uranium, it was feared that some of the debris might be radioactive. A joint American-Canadian cleanup effort, called "Operation Morning Light," was launched to locate any dangerous fragments. The task force assigned, consisting of personnel from Federal agencies and private consultants from the United States and Canada, including the Canadian Department of National Defence, conducted aerial searches which located many such strikes. However, it was a group of naturalists from Warden's Grove in the Thelon River valley, in one of the most remote parts of the Northwest Territories, who reported finding a large crater in the ice on the river at a point about 530 km east-northeast of Yellowknife. This appeared likely to be a major strike location and the task force decided to establish a tented camp near the crater not only to support the cleanup work of this site, but also to act as a base camp for search and recovery helicopter operations in the surrounding area.

Initial deployment to the site was effected by helicopter but the support requirements for a base camp for up to 100 men and several helicopters demanded a more efficient means of resupply. For this reason, it was decided that an airstrip would be cleared on the surface of a small lake located near the campsite. The lake, later christened "Cosmos Lake", was located in a lowlying area adjacent to the Thelon River, (see Fig. 1). It was roughly circular in shape, with a maximum width of about 1600 m and a maximum depth of about 8 m. Initial inspections of the ice cover indicated that it appeared suitable for use as a landing strip and preparations for the construction of an ice strip were carried out during the first week of February 1978.

Construction

The selected site for the airstrip was on a line running roughly north-south from the south shore of the lake to within 50 m of the north shore. The snow cover on the lake was in hard-packed drifts ranging to more than one metre in depth and the snow clearance equipment required to move it could not be carried to the site by either helicopter or light aircraft. As a result, bulldozers had to be placed on the lake surface by means of LAPES (for Low Altitude Parachute Extraction System) drops, whereby the equipment was strapped to pallets which were pulled out of the rear cargo doors of low-flying Hercules aircraft by drag parachutes. Between 7 and 14 February, two light bulldozers brought to the site by this method cleared the snow to create an airstrip 30 m wide by over 1500 m long with turnaround areas at each end and two parking areas to the sides of the runway. Once removed from the runway, the snow had to be pushed back to form lower, wider snowbanks in order to avoid high embankments which would have produced higher loads on the underlying ice and greater chances of drifting problems on the runway surface. A layer of snow about 50 mm thick, packed down by the bulldozers, was left on the runway to facilitate steering control for aircraft and vehicles.

At the time of the runway's completion on February 14, the ice depth ranged from 0.87 to 1.06 m and consisted almost exclusively of clear or black ice. As a guide for safe usage of the ice strip, those responsible for its operation used Air Transport Command Publication 1409, Ice Strip Requirements for Hercules, Buffalo and Twin Otter Operations, (ATCP 1409. This was a military publication produced in 1971 as a user's manual for ice strip operations involving the types of transport aircraft currently flown by the Canadian Forces and its information was based upon a few theoretical works and some practical experiences. The most recent of these theoretical

works was published in 1963. Based on the guidelines presented in the pamphlet, the decision was made that the ice was of suitable depth and type to allow use of the airstrip by heavy transport aircraft.

Use of the Airstrip

The main type of aircraft used to resupply the camp was the Lockheed CC-130 Hercules four-engined turboprop transport. These were flown primarily out of Edmonton and Yellowknife. The aircraft were limited to a maximum total weight of 59,000 kg for any landing or takeoff on the ice surface. Although an effort was made to avoid having two aircraft on the ice at one time, this situation arose several times when one aircraft was delayed on the ground and another had to land to conserve fuel. The aircraft remained on the ice only long enough to off load and take on outgoing material; the time required to carry this out ranged from 70 minutes to over two hours. While the aircraft were parked, their two outboard engines were kept idling to facilitate quick movement in case such a need arose. At first, the aircraft was moved after being in one location for an hour and reparked at least 165 m from its original location. This distance was approximately twice the "load influence radius" calculated for ice of the observed thickness. In addition, the number of landings was initially restricted to three per day to avoid excessive fatiguing of the ice. The ice surface in the vicinity of the landing wheels was constantly watched while the aircraft was stationary in order to detect any cracking. Although no cracking was observed while the ice was under load, some deflections of the surface were reported a few times in the first week of the strip's use. There was no means of measuring these deflections available on site so that no quantitative evaluations of these were possible.

However, no deflections could be seen after the second week. The runway surface covering of hardpacked snow had been removed by vehicle traffic and aircraft propwash, leaving most of the airstrip with its ice cover exposed. This, coupled with the constant low air temperature, averaging at that time about -28°C, increased the ice thickness so that, by late February, no deflections in the ice surface could be seen regardless of the length of time the aircraft had been parked in one location. By mid-March, four weeks after the opening of the strip, the ice thickness averaged 1.25 m and at that time it was judged that the restriction in the number of flights onto the strip could be lifted to allow as many flights per day as was deemed necessary.

The strip remained in operation for 45 days from 16 February until the camp was closed out on April 2. By that time, 90 landings had been made on the airstrip by Hercules aircraft, with a maximum of five being made in one day. In addition, there were some landings made occasionally by medium transport aircraft and light helicopters.

Problems Encountered

Overall, there were no problems with the ice which were severe enough to curtail the use of the strip. The only noticeable effects on the ice due to the loads imposed by the aircraft were the deflections that were visible when the average ice thickness was about 1 m or less. Except for some short-term rapid temperature drops, the natural conditions of ice and weather were favourable for the operation of the ice strip although some cracking did occur.

With the loss of the wearing surface of hard-packed snow, it was evident that there were hairline cracks throughout the ice and the number increased daily. It was assumed that most of these were present before the airstrip was cleared or were the result of thermal effects caused by the removal of the insulating snow cover. It was noted that the cracks were more numerous at the points on the runway where most aircraft touched down on landing but it was judged that these were not of such a concentration that they constituted a weakening of the ice's capacity.

More serious cracking, first noticed to be forming while the strip was being cleared, was causing concern by the second week of the airstrip's use. A large split formed along the centre of the runway, running irregularly for about 600 m. Although the crack did not extend down to open water, it was typically 0.75 m deep and about 40 mm wide of the ice surface. This was assumed to be caused by thermal stresses plus the tension induced on the upper surface by the crowning of the ice along the centre of the runway. This crowning was pronounced enough to be noticeable to the eye and it was judged to have been the result of the removal of the snow loading and of the additional buoyancy created by the greater thickness of ice produced where the insulating snow cover had been removed. No load limit was placed on the ice strip because of this crack system because the ice thickness was thought to be great enough to compensate for the pressure of dry non-intersecting cracks. However, the cracks were undesirable because of the hazard they posed to the rolling aircraft.

Once the airstrip had been established, most of the snow clearing and runway widening was accomplished using a truck-mounted snowblower. As a result, the runway borders

consisted of the natural snow cover terminating with the vertical face cut by the snowblower instead of the low, wide snowbanks left by the bulldozers. The juxtaposition of the snowloaded and the unloaded conditions caused the ice surface to rebound sharply close to the runway's edge. The ice developed open dry cracks of 0.30 to 0.50 m depth parallel to the snowbank and about 3 m in from them in a zone where the surface could be seen as being curved convexly. Holes drilled through the ice close to the snowbank revealed that the upper surface was typically below the free water level whereas holes drilled 3 m to 4 m in from the snowbanks usually had about 50 mm of freeboard ice. As the runway was widened, the snow was cleared continuously out from the centreline and it was noted that cracks appeared at about the same distance in from the edge of the snow cover with each new location of the runway border.

For both the centreline crack and those found along the runway edges, repairs were effected by filling them with a snow and water mixture and, once filled, the cracks did not reopen.

According to ATCP 1409, the guide used for operation of the ice strip, a drop in average daily air temperature of 5.5°C per day or greater was considered to cause different thermal stressing to require the limitation of either the permitted maximum aircraft weight or of the number of landings daily. This condition occurred on several occasions but, because of the necessity to maintain all available flights, no restrictions were actually imposed. Although the suggested limitations, which called for a minimum ice thickness of 1.28 m or, alternatively, a 50 percent reduction in aircraft weight, were not met, the ice showed no signs of fatiguing due to the aircraft traffic.

1 Construction Engineering Unit was called in to advise on the airstrips use after it had been put into operation. Originally it had been anticipated that the base camp and therefore the runway would be in use into the spring season and the engineers responsible wished to establish a program of monitoring the ice performance, with measurements of deflections of the ice under static and moving loads, ice hardness, temperatures and ice thickness. Advice and assistance were provided from several sources, most notably the Transportation and Surface Water Engineering Division of the Alberta Research Council, but, by the time the program was ready to be started, the camp was starting to be closed out and the program was abandoned. Although no data on the ice performance was gathered on this venture, it is anticipated that the Canadian Forces will be better prepared to carry out such a program when a similar opportunity arises in future.

Summary

The airstrip built on Cosmos Lake utilized ice cover to successfully handle an average of two heavy transport aircraft a day for 45 days. Deflections of the ice surface under aircraft which had been parked in one location for one hour were noted with the minimum average ice thickness of about one metre, and hairline cracks were more numerous at touchdown areas on the runway, but otherwise the ice showed no signs of fatiguing. Although the ice formed open, dry cracks along the centre and edges of the runway and air temperatures sometimes dropped at rates likely to induce severe thermal stressing, the aircraft were flown onto the strip every day without curtailment of the number of flights or of weight of the aircraft. Despite this disregard for conditions which should have limited the capabilities of the runway, the ice strip continued to perform adequately, handling up to five landings per day of aircraft weighing up to 59,000 kg.

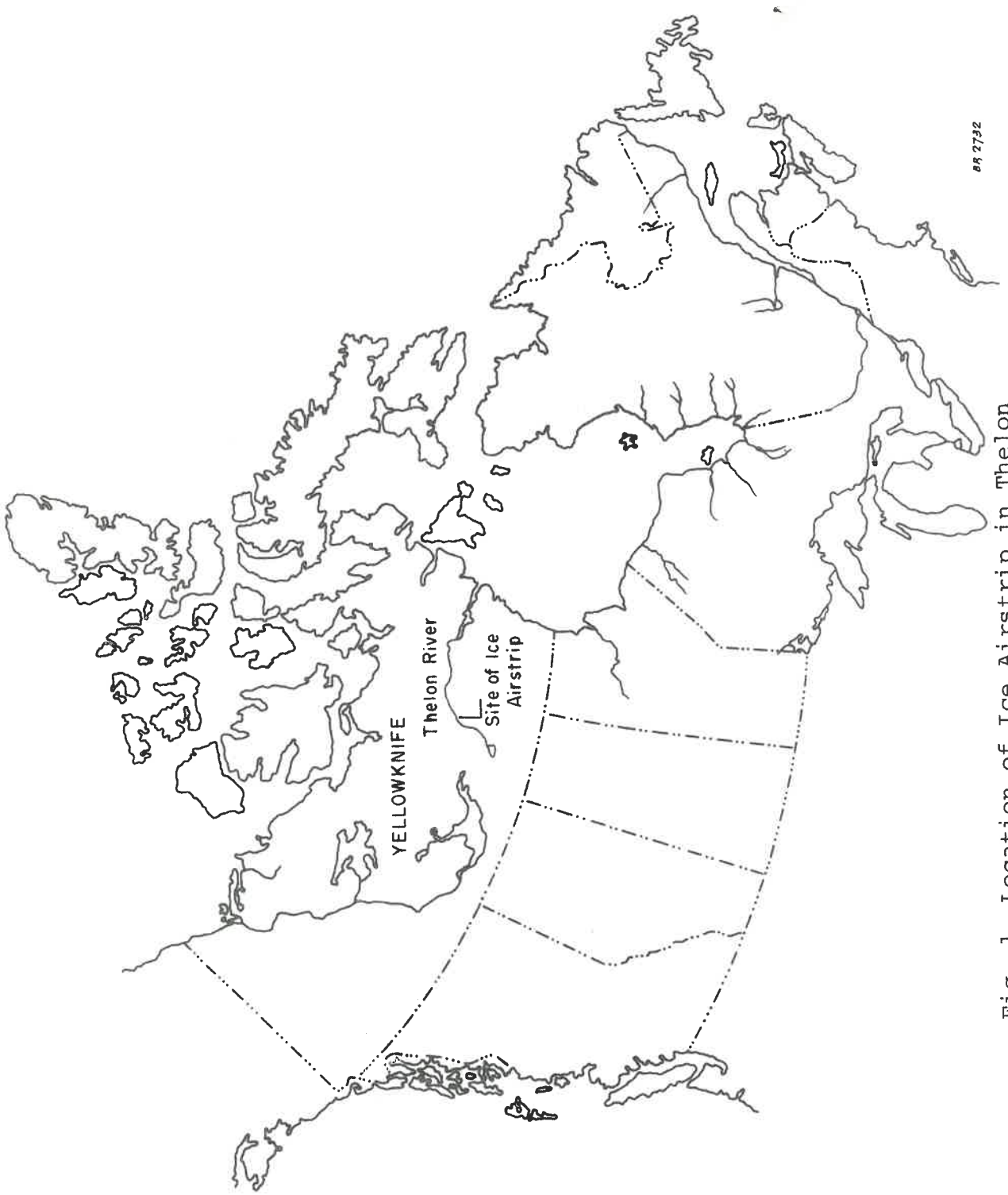

Fig. 1 Location of Ice Airstrip in Thelon River Valley.

Discussion

R. Kry:

Were all planes usually loaded to established maximum load?

D.M. McCutcheon:

In nearly all cases the aircraft were loaded to the stipulated maximum. In a few cases, the aircraft were carrying bulky materials which had the effect of reducing the weight of the cargo load, but the basic weight plus fuel load of the aircraft represents a considerable proportion of the imposed limit, being never less than about 41,000 kg in mass.

R. Gerard:

You said some deflection was noted during the first week. Could you give some idea of the magnitude of this deflection? Also could you comment on the response of the aircrew and others to this deflection and the use of the ice in general.

D.M. McCutcheon:

I was not on site during the first week and I had to interpret the reports I received. Those watching for the deflections were primarily the aircrew who tended to be hypersensitive and, since their knowledge of ice characteristics was limited, the aircraft were moved when the deflection became apparent to the eye but it was difficult to say how much that represented.

USE OF ICE AS STRUCTURAL SUPPORT IN THE CONSTRUCTION OF THE EAGLE RIVER BRIDGE

Lt. D.M. McCutcheon
1 Construction Engineering Unit
Canadian Armed Forces

From July 1976 to June 1977, combat engineers from 1 Combat Engineer Regiment of the Canadian Armed Forces from Chilliwack, B.C. erected a 90 m long through truss bridge across the Eagle River (see Fig. 1) in the northern Yukon Territory for the Department of Indian and Northern Affairs' Dempster Highway. Engineering assistance for this work, including the provision of the site engineer, was provided by 1 Construction Engineering Unit. The highway, now complete, connects Dawson and other southern communities with settlements in the Mackenzie River delta area on the Arctic Ocean. The bridge, 16 km south of the Arctic Circle and about 380 km from Dawson, was the last one to be completed on the highway. The bridge design, provided by the Federal Department of Public Works, had a clear span across the river course. Previous experience gained by the Armed Forces in erecting a bridge across the Ogilvie River farther south on the same highway showed that sudden flooding on the rivers in this region was not uncommon and could be serious enough to endanger any temporary or permanent support system located in the river channel. It was decided that, to overcome this problem, the work of erecting the main span would be carried out during the winter when the river flow would be at its lowest and there would be the least chance of sudden flooding. While the truss was being assembled, the sections would be supported by a wooden falsework system that would be placed on the riverbed. Because the river did not freeze completely but maintained some flow throughout the winter, some of the falsework would have to be placed over a channel carrying this flow. Over this gap, the falsework was to be supported by a short ice bridge.

Visits were made to the bridge site on the Eagle River in March 1974 and March 1976 to study the ice and flow conditions. It was determined that, with the flow that could be expected during the winter, the extent of the proposed ice bridge could be reduced by deepening the river channel along the north bank to handle the maximum expected seasonal flow where the natural channel depth was the greatest and by building an embankment out from the south bank as far as the edge of this channel. As a result, three of the eleven falsework supports would have to be placed above the new river channel that would be covered by the ice bridge while the remainder would rest on the embankment.

In March 1974, the river ice was found to be 1.3 m thick but had a one-metre high pressure ridge running through it parallel to the north bank in the area where the proposed ice bridge could be located. In March 1976, the river ice was in layers interspersed with water. From the literature on ice bearing capacity that was consulted, it was judged that the natural ice cover could not be counted upon to be satisfactory in thickness or quality to support the loads anticipated and it was decided to artificially produce ice to the desired thickness.

It was further decided to place reinforcement in the ice and to provide auxiliary support beneath the middle of the three falsework structures. This was not considered necessary for the other two supports. The one on the south side of the channel would be placed on ice that would extend to the channel bottom and the one on the north side of the channel would be placed close enough to the river bank that some of the load imposed by the support could be transferred there. The auxiliary support consisted of ten rock-filled 45-gallon drums which were placed on the channel bottom beneath where the middle falsework support would be located (see Fig. 2). The top half of these barrels, as well as a system of beams placed on them, would be embedded in the ice.

The ice surface was built up by daily flooding beginning on November 15, 1976. On December 4, sections of 10-gauge wire mesh were installed on either side of bridge's centreline, up and down stream of the supports, where moving cranes would be operating. This material was used as a reinforcement system under the working area primarily because it was available on site. On December 7, steel beams resting on timber sleepers were laid on top of the rock-filled barrels. It was found that there was no difficulty implanting the timber in the ice but that the steel disrupted the flooding because shell ice rapidly formed around it, which had to be removed to avoid producing air pockets with subsequent flooding. The flooding continued until January 16, 1977, with from 10 to 60 mm being added at a time until the ice cover was 1.6 m thick. The total extent of the reinforced and artificially-produced ice was 21 m in length and 15 m in width, with the built-up ice extending 20 m up and downstream from this section.

Steel erection began on January 19 and the timber falsework was in place from that date until March 11. The eventual load carried by each support was about 26 metric tons. In addition, the ice at times had to support the live loading of two mobile lifting cranes which weighed 30 metric tons each. These operated with one on either side of the bridge and lifted a maximum load of over three tons each. Therefore,

the ice had to support the continuous load imposed by one falsework structure and, occasionally, the combined live and dead load of about 90 metric tons.

Any deflection of the ice surface would have created difficulties in the assembly of the bridge's superstructure as it would have disturbed the vertical alignment. However, this situation did not arise. A hole drilled through the ice near the area where one of the cranes was operating showed that the surface of the ice was above the freewater level and, even when loaded by the cranes, the ice underwent no measureable deflection. The reinforced ice acted as a smooth working surface for the cranes and showed no sign of fatiguing throughout its use.

The ice bridge was nearly 1 m thicker than the natural ice adjacent to it and there was concern that, during the spring breakup, the ice bridge would cause a blockage of the river ice. To prevent this situation, which could have endangered the newly constructed bridge, the top half of the ice bridge was broken up using a ripping tooth. This proved to be an adequate solution as no problems of ice build-up occurred during the spring breakup.

Although the ice bridge was a small part of the temporary support system used, it was nevertheless an essential one for the economical erection of the Eagle River Bridge. Its use necessitated the completion of the truss assembly work during the winter, which complicated the construction and the living conditions with very low temperatures and short daylight hours. However, the advantages gained by having an economical support system during the time of low flow, which effectively eliminated the fears of possible flooding and washouts, more than compensated for these difficulties.

FIGURE 1

LOCATION OF EAGLE RIVER BRIDGE

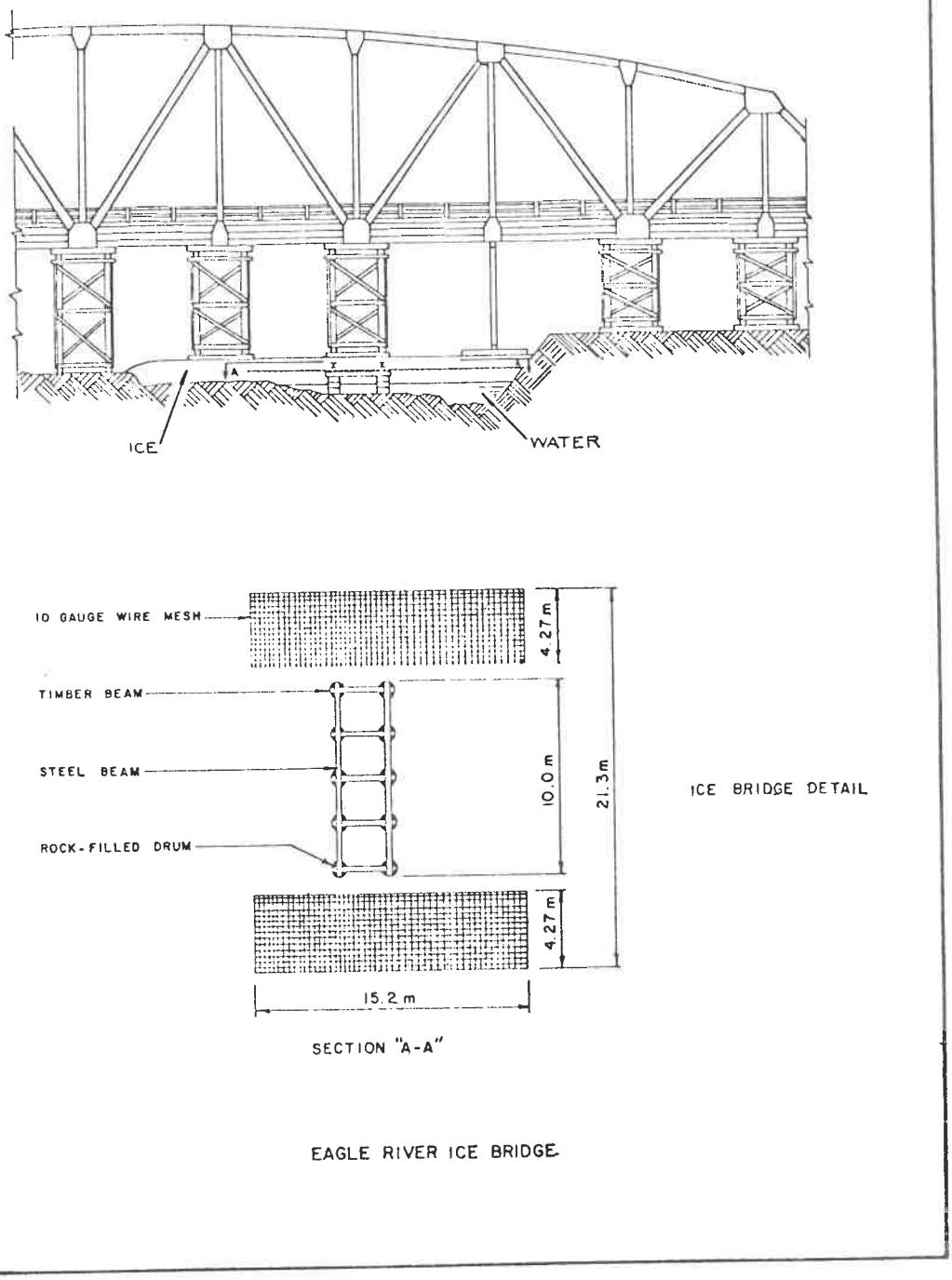

FIGURE 2

AUXILIARY SUPPORT OF FALSEWORK.

Discussion

R. Gerard:

You mentioned that, at the time of the first inspection, the ice was found to be alternate layers of ice and water. Could you comment on the reasons for this in an area that is presumably consistently cold during the winter? For example, was there a heavy snowfall that winter? I would also like to take this opportunity to thank Lt. McCutcheon for taking the trouble to present his experiences in this and the previous paper. Even if they are qualitative, such clear descriptions of events are extremely valuable.

D.M. McCutcheon:

Assuming that the weather was consistently cold that winter, the interspersed water and ice on the Eagle River would have to result from one or both of two conditions - a heavy snowfall, which would prevent full-depth freezing, and occasional flooding over top of the ice and snow. Without meteorological data of the specific area over the winter of 1976, it is impossible to know how each of these factors contributed to the observed conditions.

FLOODING OF SEA ICE ROADS

D. Favrat and P.R. Kry
ESSO Resources Canada Limited,
Production Research Division

Introduction

Exploration for hydrocarbons in the nearshore areas of the Beaufort Sea and between the Canadian Arctic Islands has provided large incentives for using ice as a building material. Artificially thickened platforms have been used for drilling exploratory wells (Masterson et al., 1975). Roads have regularly been constructed in the Mackenzie Delta over the last decade to support offshore drilling operations. Typically, loads involved are relatively heavy and usual practice is to wait until the natural landfast ice is sufficiently thick and construct the road by clearing accumulated snow.

In the winter of 1976/1977 Imperial Oil identified an incentive to move a drilling rig and camp from Atkinson Point to the articial Island Kannerk G-42 (Fig. 1) as early as possible in the winter. A relatively mild winter, relatively high salinity of ice, and the economic incentive for an early rig move dictated the desirability of artificially thickening portions of the road to ensure sufficient ice bearing capacity.

The Production Research Division assumed responsibility for advising on the road construction and monitoring the safety of the operation while Field Services was responsible for the road construction and the rig move.

Free flooding was used to artificially thicken the ice. This technique leads to flooded areas which are much wider than is necessary for a road. A particular advantage of this technique is the low level of residual stresses in the ice from the flooding. The theoretical basis for this is developed in this paper.

Flooding introduces a relatively high brine concentration at the top of the ice sheet. A potential strength deterioration would occur if this high brine concentration migrated through the thickness. Observations of the evolution of the ice salinity are presented which demonstrate no significant migration.

Flooding and Induced Stresses

Ice has a relatively low thermal conductivity so that the natural growth rate at the bottom of an ice sheet decreases with its thickness. An effective method used to artificially thicken an ice sheet is to spread and let freeze thin water layers on the surface of the ice cover to obtain direct heat transfer without the insulation effect of the ice cover itself.

In order to fully benefit from the increase of heat transfer, flooded layers need to be thin and freeze relatively quickly. In practice, layers of 20 to 90 mm are applied. These water layers represent a certain distributed load (0.5 kPa for a 50 mm layer) which causes the ice to deflect. Even after freezing, the hydrostatic equilibrium is still locally disturbed and bending stresses are generated. Even if the stresses introduced by one individual layer are low, they might not be totally relaxed under creep deformation before the introduction of the next layer. A buildup of stresses due to flooding is therefore likely to occur, resulting in residual stresses which could affect the bearing capacity of the ice cover.

There are two different ways to flood; either to let the water flow freely from the centre of the road (free flooding) or let the water flow to the road path by construction of small dikes (limited flooding). Limited flooding has the immediate advantage of thickening only the part of the road which will be required while limiting the amount of water, and thus the size of the pumps required to flood a certain road length. However, due to the width of a usable road (say 15 m) compared to the characteristic length of an ice beam as thick as the ice sheet, limited flooding induces the greatest stresses under the centre of the road. These residual stresses then add to stresses induced by loads on the road. Free flooding provides a thickened sheet some 50 m - 100 m in width and tends to limit stresses under the centre of the road.

Since flooding of a road is a relatively uniform process along its length, stresses and deflections across its width may be described by those of a unit width infinite beam on an elastic foundation. The stresses are induced by the weight of the flooding layer of thickness Δh on the ice sheet of thickness h. For purposes of discussion, the flooded layer will be assumed rectangular, covering a width B of the ice sheet. Assuming perfect elasticity the extreme fibre stress σ at the base of the ice sheet is given as a function of distance across the width x (Hetenyi 1971) as:

$$\frac{\sigma}{\sigma_o} = e^{-a}\sin a - \theta e^{-b}\sin b, \qquad (1)$$

where $a = (x + B/2)/\ell$

$b = \theta\,(x - B/2)/\ell$

$$\theta = \begin{cases} -1 & x \leq B/2 \\ +1 & x < B/2 \end{cases}$$

and

$$\sigma_o = \frac{3}{2}\,\Delta h k\,(\ell/h)^2 \qquad (2)$$

$$\ell = (Eh^3/3k)^{\frac{1}{4}} \qquad (3)$$

The normalizing stress σ_o is proportional to the vertical load per unit area due to the flooding and depends on the thickness. The quantity ℓ is the characteristic length of a unit width beam of Young's modulus E floating on water with a foundation modulus k.

Equation 1 is plotted for several widths of flooding in Fig. 2. Tensile stresses are taken to be positive. When the flooding is only over a very small width, the maximum stress is induced under the centre of the flooded area and is limited by the small weight of a limited width of water. As the width of flooded area is increased, keeping the flooded depth the same, the total weight of water increases, increasing the stress under the centre of the load until it reaches a maximum at a flooded width of $\pi/2$ characteristic lengths. As can be seen in Fig. 2, the central stress magnitude is not very sensitive to width of flooding between one and two characteristic lengths. For wider flooded areas, the location of the maximum stress moves from the centre of the road to the periphery where tensile stresses of the same order of magnitude exist in the bottom as well as in the top fibers. For very wide loads corresponding to a case of free flooding, the stresses are negligible in the centre of the road.

As a numerical example, on a 1 m ice sheet with a Young's modulus of 3 GPa, if a flooded layer 0.05 m thick were 28 m wide ($\pi/2$ times the characteristic length) a stress of 0.10 MPa would be generated under the centre of the road.

The deflection profile of the road under the flooding load is given by Hetenyi (1971) as:

$$\frac{\Delta y}{\Delta h} = \frac{1}{2}\,(1 - \theta - e^{-a}\cos a + \theta e^{-b}\cos b), \qquad (4)$$

where Δy is the deflection of the road flooded by a layer of thickness Δh. The parameters a, b, and θ are as given in Equation 1.

Equation 4 is plotted in Fig. 3 for several widths of flooding. This illustrates the reason for the transfer of maximum stresses from the centre of the road to its periphery. For a very wide flooded area, the ice sheet elastically deflects essentially the thickness of the flooded layer. The centre of a wide free flooded road reaches isostatic equilibrium whereas the centre of a limited flooded road has the maximum residual stress in the sheet directly under the anticipated heaviest loads. It is therefore recommended that the free flooding technique be used to cover areas wider than 3 to 4 times the characteristic length.

Salinity

The quick freezing on top of an existing ice sheet, which is one of the advantages of the flooding technique, implies that new ice formed will have a very high salinity content. The measurements in Fig. 4 indicate an average salinity of 20 ppt for a new ice layer 20 cm thick consisting of three flooded layers. The measurements were made by analyzing the conductivity and temperature of melted segments of a 7 cm diameter cylindrical core taken vertically with a CRREL ice coring auger. The same measurements were repeated 6 weeks later at the same location (within 2 m).

The freezing propagated almost as fast from the ice sheet as from the surface of the flooded layer. This resulted in a concentration of brine inclusions in the centre of each layer. These are visible in Fig. 5 which is a photograph of a portion of the flooded ice, three layers thick.

All the loads involved in a rig move are concentrated enough to generate the highest stresses immediately under them. In normal conditions the flooded layer is thus submitted mainly to compressive stresses. Since ice has a higher strength in compression than tension (Frederking 1975) the strong discontinuity of the salinity profile existing immediately after flooding does not significantly decrease the bearing capacity of the ice cover. It is only in the presence of intersecting open cracks and during a breakthrough phase that the top surface will be submitted to tension. Patterns of intersecting cracks are thus particularly dangerous on a flooded road.

Another source of potential concern is a gradual increase of salinity of the natural ice resulting from a migration of the brine pockets from the flooded layers towards

the natural ice. The saline migration is part of a macrosegregation process based on two main phenomena: a gravity effect, the concentrated brine being heavier than the pure water, and the existence of a temperature gradient implying a corresponding gradient of brine concentration in the brine droplet which tries to come into equilibrium with the ice. This gradient of brine concentration results in a melting at the base of the brine pocket. The direction of migration is always from cold to warm (Adams et al., 1960).

Based on these two phenomena we would expect the discontinuity of salinity gradient to smooth with time as most of the brine pockets make their way down to the natural ice and potentially weaken it. However, our measurements (Fig. 4) show a decrease in salinity over the entire thickness and do not demonstrate an important transfer from the flooded layer to the natural sheet over the life of the road.

Conclusions

Flooding is an excellent technique to artificially thicken an ice sheet. Free flooding should be employed to provide widths of 3 to 4 times the characteristic length of the natural ice cover to limit residual stresses.

Salinity migration does not increase salinity concentrations in the natural ice sheet over the life of the road. Therefore the bearing capacity of the road does not deteriorate due to brine migration. The high salinity concentration on the top surface of a flooded road increases the danger associated with the intersecting patterns of cracks.

Acknowledgments

We gratefully acknowledge permission of Esso Resources Canada Limited to publish this contribution. We thank Field Services of Esso Resources Canada Limited for their help and support in the field.

References

Adams, French, Kingery (1960). Solidification of Sea Ice. Journal of Galciology, Vol. 3, No. 28.

Frederking, R. (1975). Mechanical Properties of Ice and Their Application to Arctic Ice Platforms. Spring meeting, Society of Naval Architects and Marine Engineers, Montreal.

Hetenyi, M. (1971). Beams on Elastic Foundation. Ann Arbor. The University of Michigan Press.

Masterson, D.M., Baudais, D.J., and Wasilewski, B.R. (1975). Experience in Ice Platform Construction for Arctic Drilling. CIM Annual Western Meeting, Edmonton, paper no. 44.

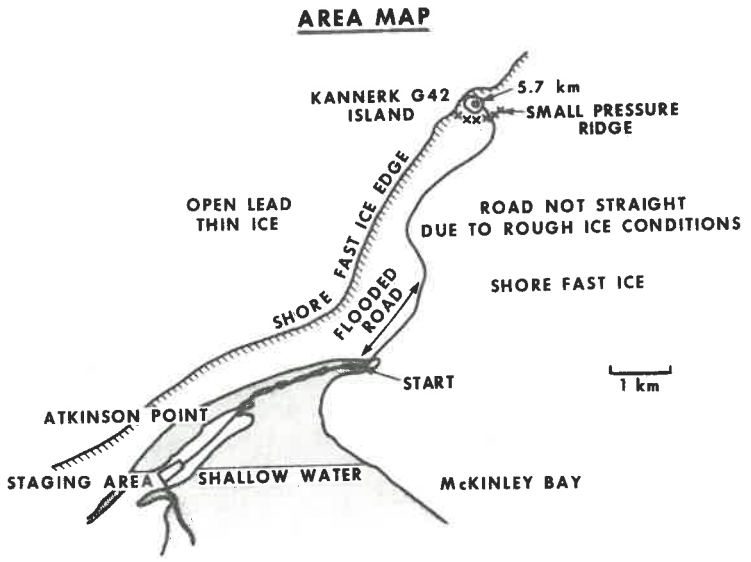

Fig. 1. Map of MacKenzie Delta area showing location of Kannerk Ice Road.

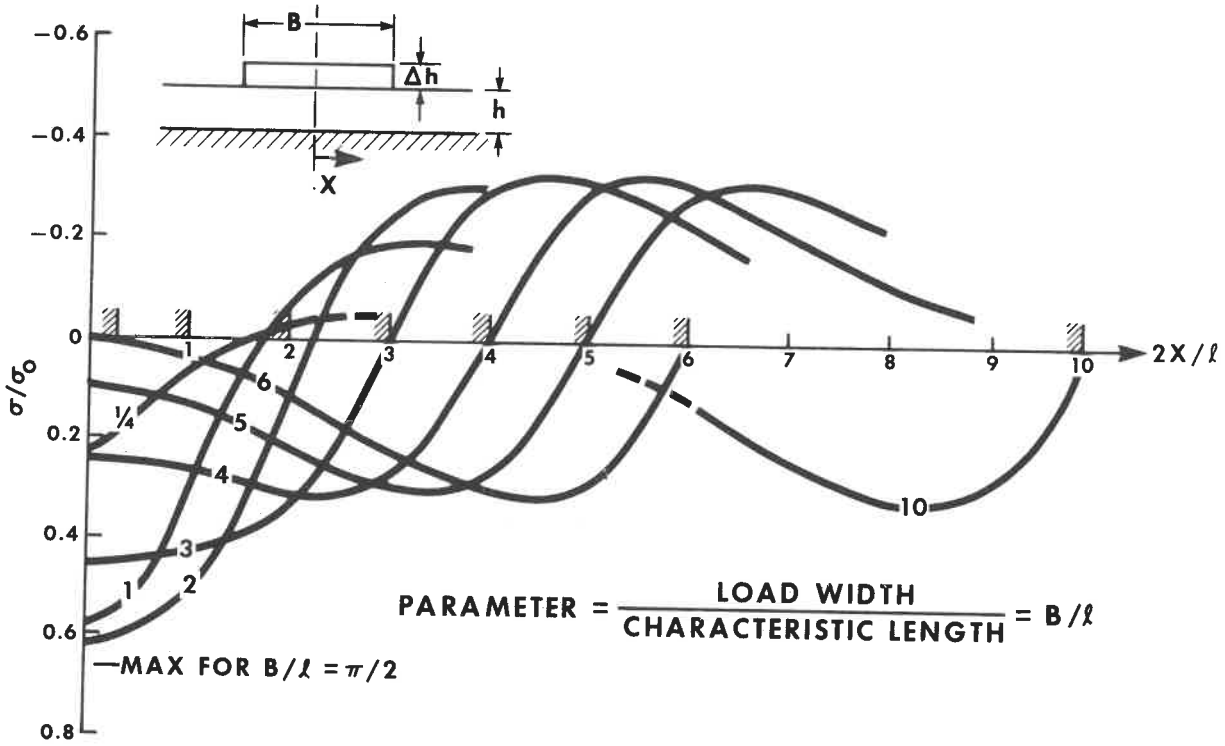

Fig. 2. Stress distribution across a road loaded by a uniform water layer.

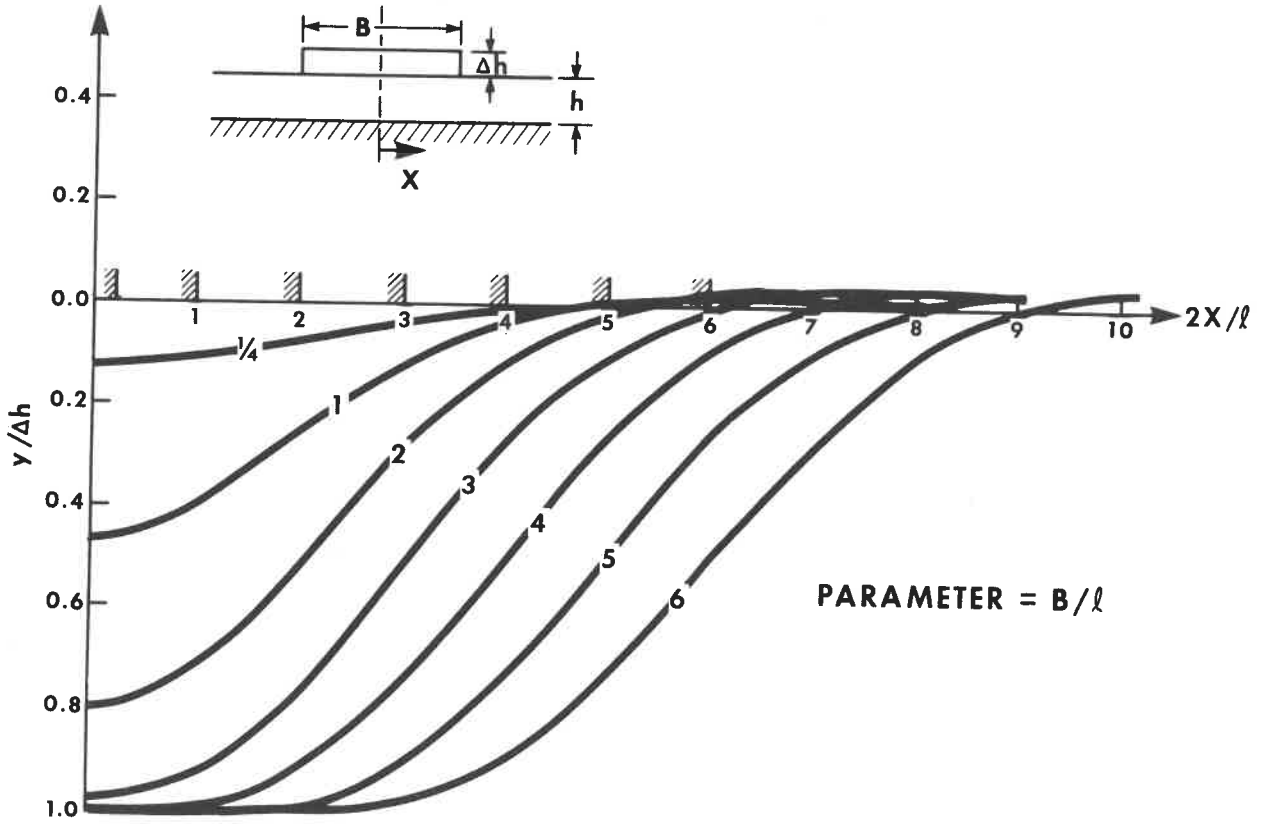

Fig. 3. Deflection profiles across a road loaded by a uniform water layer.

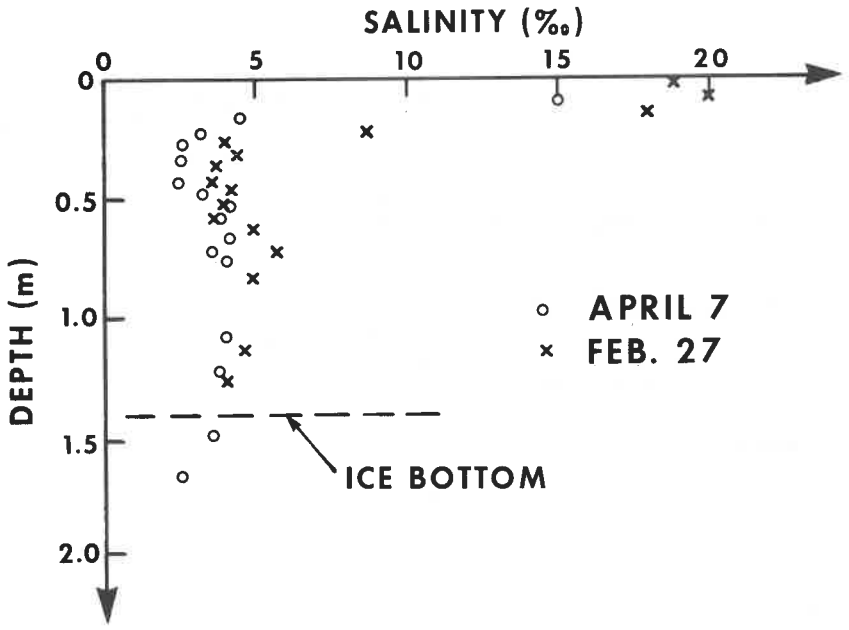

Fig. 4. Salinity profile with depth at one location on Kannerk Ice Road at two times.

Fig. 5. Sample of ice from flooded portion of ice road showing brine concentrations in centers of individual layers.

Discussion

B. Michel:

It is usually thought that there is a lot of brine migration in sea ice in temperate climates. Do you think that the small amount of brine drainage you had is due to the low prevailing temperatures and would you suggest this technique of ice build-up with sea water in other regions?

R. Kry:

I suspect that the cold temperatures during the life of the road (average April air temp of -20°C) did retard brine migration. Building sea ice roads in other regions should only be limited by the ability to freeze layers. Warm air temperatures in the spring would likely cause rapid deterioration of the surface layers. Flooded portions of the Kannerk ice road were observed to deteriorate faster in the spring than unflooded portions (after use of road was halted).

N.K. Sinha:

What was the salinity of water? If the water salinity was higher than the 20 °/₀₀ found in the flooded ice zone, where does the extra salt go?

D. Favrat and R. Kry:

The salinity of the water was not measured during flooding. Significant salinity variations occur in the region due to the Mackenzie River outflow. Water salinities near Kannerk were measured to be 30 ppt in November and 20 ppt in January.

D.M. Masterson:

You show a sharp discontinuity at the edge of flooding. Usually, flooded roads taper to natural ice. Does this not have a significant effect on stresses introduced by flooding? Also, did you measure the strength of the high saline ice?

D. Favrat and R. Kry:

The square profile for the flooded portion was used merely to simplify the theoretical analysis to demonstrate the point that wider roads are better for limiting central stresses due to flooding. In reality, flooding should occur with no special efforts made to limit water flow, resulting in a natural taper. Road width should be considered not to include such tapers.

We did not measure the strength of the high salinity ice. However it was noted this ice wore at least as well as natural ice under traffic.

K.R. Croasdale:

Although the salinity was high at the top surface, the temperature would be low. Did the authors plot the brine volume profile? Brine volume is generally accepted as being a better indicator of strength than salinity.

D. Favrat and P.R. Kry:

Salinity was chosen in Fig. 3 to emphasize the discontinuity due to flooding. While monitoring the road during the rig move, temperature profiles were measured to enable the calculation of the brine volume and establish the strength of the ice on the particular day of the move. Cold temperatures at that time reduced the brine volume at the top surface suggesting relatively strong ice. However, in general, should such a road be used in warm spring conditions, brine volumes due to warm temperatures and high salinities would suggest quite a weak ice for the flooded layers.

D.V. Reddy:

Can you comment on the effect of the parameter width/characterstic length on the validity of the 'beam on elastic foundation' concept used in your analysis? Would not a 'plate on elastic foundation' formulation be a more correct one?

P.R. Kry:

A plate on elastic foundation is the appropriate formulation to use when determining stresses due to a particular vehicle road. However due to the fact that a road is much longer than it is wide, a beam formulation is appropriate to determine stresses due to flooding.

Summary of Panel Discussion on Operational Experience

Regarding the stresses caused by flooding, it would seem that the Canadian Forces experienced some of the problems at Thelon River described by Kry. McCutcheon saw cracks about 3 m from the snow load centre at the airstrip edges.

A point was made regarding the use of the equations for elastic beams on an elastic foundation. As the beam becomes very wide, then for point loads it acts as a plate. Kry agreed with this and pointed out that he had only used the beam equations transverse to the road axis for analysis of the effects of flooding. Point loads were analyzed using plate theory.

Holes for flooding on the Esso road were spaced at about 200 m.

A rough guide for determining a proper road width is to make it 3 to 4 times the stiffness radius where the stiffness radius is 10 to 15 times the ice thickness. Traffic considerations must also be kept in mind.

Investigation of case histories indicates that failures are usually associated with people wandering off the road. Signs or guides are important.

Closing Session

The session began with a brief review of points raised to date in the Workshop. The Performance Measurements Session considered field measurements of strains in ice platforms and runways; deflection and strain measurements of ice covers with moving loads; field evaluation of creep properties of ice; and predictions of the effective modulus of ice. The time-dependent bearing capacity problem was approached via laboratory analog investigations and finite element analyses. Central to both approaches was the requirement for a constitutive relation and failure criterion for the ice. There was considerable discussion of failure criteria. An appropriate failure criterion has to be related to an acceptable level of performance, a limit established by the user. Operational experience dealt with prediction of bearing capacity; use of an ice cover as an airstrip and to support bridge erection; and characteristics of a flooded sea ice road. The value of documenting such operational experience was demonstrated and the need for further documentation emphasized.

The ensuing discussion evolved around forecasting the load bearing capacity of an ice cover. This was broken down into two aspects, ice quality and ice thickness. Ice quality can be inferred from indirect measurements such as temperature, salinity, etc., and a knowledge of mechanical properties measured in the laboratory. Ice thickness determination is both easy and difficult. Ice thickness at a point can be easily determined by drilling a hole through the ice cover. However when one considers an ice road extending over 10's of km the situation changes. Impulse radar systems are available which can remotely profile ice thicknesses over considerable distances. These systems work well on fresh water ice but have difficulties in sea ice. Further development is required to improve their reliability and reduce costs.

The use of reinforcement of ice covers was also discussed. To enhance the strength of an ice cover the reinforcing material should be below the neutral axis. However this is often difficult to achieve. Experience with ice bridges constructed on the James Bay Project using reinforcing below the neutral axis indicated ice thickness could be reduced by 30% and a safety factor of 2-3 could still be maintained. Even if the reinforcing material cannot be placed below the neutral axis, it does act as a "safety net" binding the ice cover together. The reinforcement to be effective must be rough so as to achieve a good bond with the ice. It was also pointed out that reinforcement is good for short-term loading, but that it does little to enhance long-term load bearing capacity. The environmental implications of using reinforcement must also be considered.

WORKSHOP ON THE BEARING CAPACITY OF ICE COVERS

PARTICIPANTS

ABDELNOUR, R.,
Arctec Canada Ltd.,
311 Leggett Drive,
Kanata, Ontario. K2K 1Z8

ADAM, K.M.,
Templeton Engineering Co.,
966 Waverley Street,
Winnipeg, Man. R3C 2Z1

ALLAN, A.,
C-CORE,
Memorial University of
Newfoundland,
St. John's, Nfld. A1B 3X5

BARR, Capt. G.L.,
MES CFSME,
CFB Chilliwack,
Vedder Crossing, B.C. V0X 1Z0

BAUDAIS, D.,
Panarctic Oils Ltd.,
P.O. Box 190,
Calgary, Alta. T2P 2H6

BELTAOS, S.,
Transportation and Surface
Water Engineering Division,
Alberta Research Council,
303 Civil-Electrical Bldg.,
University of Alberta,
Edmonton, Alta. T6G 2G7

BETTERIDGE, J.H.,
Esso Resources Canada Ltd.,
10025 Jasper Avenue,
Edmonton, Alta. T5J 1S6

BRUCE, D.,
Montreal Engineering Company
Limited,
P.O. Box 6088, Station "A",
Montreal, P.Q. H3C 3Z8

BUTT, K.,
C-CORE,
Memorial University of
Newfoundland,
St. John's, Nfld. A1B 3X5

CROASDALE, K.R.,
Esso Resources Canada Ltd.,
500 Sixth Avenue S.W.,
Calgary, Alta. T2P 0S1

DANYS, J.V.,
Marine Aids Division,
Ministry of Transport,
Transport Canada Bldg.,
Place de Ville,
Ottawa, Ontario. K1A 0N7

ERSOY, T.,
Head of Design & Construction,
Department of Public Works,
Government of the Northwest
Territories,
Yellowknife, N.W.T.

FREDERKING, R.,
Division of Building Research
National Research Council of
Canada,
Ottawa, Ontario. K1A 0R6

GAGNON, L.,
Département de Génie Civil,
Université Laval,
Québec, P.Q. G1K 7P4

GAJTANI, M.,
Canadian Marine Drilling Ltd.,
P.O. Box 200,
Calgary, Alta. T2P 2H8

GERARD, R.,
220D Civil-Electrical Bldg.,
University of Alberta,
Edmonton, Alta. T6G 2G7

GERBRANDT, R.,
Department of Highways,
Box 820,
North Battleford, Sask.
S9A 2Z3

GOLD, L.W.,
Division of Building Research,
National Research Council of Canada,
Ottawa, Ontario. K1A 0R6

GOODMAN, D.J.,
Department of Physics,
University of Cambridge,
Cavendish Lab.,
Madingley Road,
Cambridge CB3 0HE,
England.

HAJDO, L.E.,
Department of Mechanical Engineering,
University of Calgary,
Calgary, Alta. T2N 1N4

HILL, D.,
24 Pike Crescent,
Thompson, Manitoba.

ISMAILY, S.A.,
Public Works Canada,
Atlantic Regional Headquarters,
P.O. Box 2247,
Halifax, N.S. B3J 3C9

JARRETT, P.M.,
Department of Civil Engineering,
Royal Military College,
Kingston, Ontario.

KLEIN, J.,
Department of Highways,
Humford House,
1855 Victoria Avenue,
Regina, Sask. S4P 3T2

KRY, P.R.,
Production Research Division,
Esso Resources Canada Ltd.,
339 - 50 Avenue S.E.,
Calgary, Alta. T2G 2B3

LADANYI, B.,
Northern Engineering Centre (CINEP),
Ecole Polytechnique,
C.P. 6079, Succ. "A",
Montreal, P.Q. H3C 3A7

LAINEY, L.,
Département de Génie Civil,
Ecole Polytechnique,
C.P. 6079, Succ. "A",
Montreal, P.Q. H3C 3A7

LIPSETT, A.W.,
Research Council of Alberta,
303 Civil-Electrical Engineering Building,
University of Alberta,
Edmonton, Alta. T6G 2G7

MASTERSON, D.,
FENCO Consultants Ltd.,
301-805 8 Avenue S.W.,
Calgary, Alta. T2P 1H7

MICHEL, B.,
Département de Génie Civil,
Université Laval,
Québec, P.Q. G1K 7P4

MURAT, J.-R.,
Département de Génie Civil,
Ecole Polytechnique,
C.P. 6079, Succ. "A",
Montreal, P.Q. H3C 3A7

McCUTCHEON, Lt. D.M.,
c/o Commanding Officer,
1 Construction Engineering Unit,
CFB Winnipeg,
Westwin, Man. R2R 0T0

McMILLAN, J.D.,
Department of Highways,
Box 790,
Prince Albert, Sask. S6V 5S4

NEVEL, D.E.,
USA CRREL,
P.O. Box 282,
Hanover, N.H. 03755.

REDDY, D.V.,
Faculty of Engineering &
Applied Science,
Memorial University of
Newfoundland,
St. John's, Nfld. A1B 3X5

SINHA, N.K.,
Division of Building Research,
National Research Council of
Canada,
Ottawa, Ontario. K1A 0R6

TINAWI, R.,
Département de Génie Civil,
Ecole Polytechnique,
C.P. 6079, Succ. "A",
Montreal, P.Q. H3C 3A7

WATERS, Capt. G.F.,
c/o Commanding Officer,
1 Construction Engineering
Unit,
CFB Winnipeg,
Westwin, Man. R2R 0T0

WHYTE, R.J.,
Esso Resources Canada Ltd.,
10025 Jasper Avenue, Rm. 648,
Edmonton, Alta. T5J 1S6

A list of Technical Memoranda of the Associate Committee on Geotechnical Research may be obtained from the Secretary, Associate Committee on Geotechnical Research, National Research Council of Canada, Ottawa K1A 0R6.

La liste des Technical Memoranda (mémoires techniques) du Comité associé de recherches géotechniques peut être obtenue auprès du secrétaire du Comité associé de recherches géotechniques, a/s Division des recherches en bâtiment, Conseil national de recherches du Canada, Ottawa K1A 0R6.